CANADIAN THESES ON MICROFICHE

I.S.B.N.

THESES CANADIENNES SUR MICROFICHE

National Library of Canada
Collections Development Branch

Canadian Theses on
Microfiche Service

Ottawa, Canada
K1A 0N4

Bibliothèque nationale du Canada
Direction du développement des collections

Service des thèses canadiennes
sur microfiche

NOTICE

The quality of this microfiche is heavily dependent upon the quality of the original thesis submitted for microfilming. Every effort has been made to ensure the highest quality of reproduction possible.

If pages are missing, contact the university which granted the degree.

Some pages may have indistinct print especially if the original pages were typed with a poor typewriter ribbon or if the university sent us a poor photocopy.

Previously copyrighted materials (journal articles, published tests, etc.) are not filmed.

Reproduction in full or in part of this film is governed by the Canadian Copyright Act, R.S.C. 1970, c. C-30. Please read the authorization forms which accompany this thesis.

THIS DISSERTATION
HAS BEEN MICROFILMED
EXACTLY AS RECEIVED

AVIS

La qualité de cette microfiche dépend grandement de la qualité de la thèse soumise au microfilmage. Nous avons tout fait pour assurer une qualité supérieure de reproduction.

S'il manque des pages, veuillez communiquer avec l'université qui a conféré le grade.

La qualité d'impression de certaines pages peut laisser à désirer, surtout si les pages originales ont été dactylographiées à l'aide d'un ruban usé ou si l'université nous a fait parvenir une photocopie de mauvaise qualité.

Les documents qui font déjà l'objet d'un droit d'auteur (articles de revue, examens publiés, etc.) ne sont pas microfilmés.

La reproduction, même partielle, de ce microfilm est soumise à la Loi canadienne sur le droit d'auteur, SRC 1970, c. C-30. Veuillez prendre connaissance des formules d'autorisation qui accompagnent cette thèse.

LA THÈSE A ÉTÉ
MICROFILMÉE TELLE QUE
NOUS L'AVONS REÇUE

NL-339 (r. 82/08)

Canada

0-315-06023-9

National Library of Canada | Bibliothèque nationale du Canada

Canadian Theses Division | Division des thèses canadiennes

Ottawa, Canada
K1A 0N4

53943

PERMISSION TO MICROFILM — AUTORISATION DE MICROFILMER

- Please print or type — Écrire en lettres moulées ou dactylographier

Full Name of Author — Nom complet de l'auteur
Oldrich HUNGR

Date of Birth — Date de naissance Nov. 1, 1947	Country of Birth — Lieu de naissance Czechoslovakia

Permanent Address — Résidence fixe
95 E 20th Ave., Vancouver, B.C.

Title of Thesis — Titre de la thèse
Dynamics of Rock Avalanches and Other Types of Slope movements.

University — Université
U. of Alberta

Degree for which thesis was presented — Grade pour lequel cette thèse fut présentée
Ph. D.

Year this degree conferred — Année d'obtention de ce grade 1981	Name of Supervisor — Nom du directeur de thèse Dr. N.R. Morgenstern

Permission is hereby granted to the NATIONAL LIBRARY OF CANADA to microfilm this thesis and to lend or sell copies of the film.

The author reserves other publication rights, and neither the thesis nor extensive extracts from it may be printed or otherwise reproduced without the author's written permission.

L'autorisation est, par la présente, accordée à la BIBLIOTHÈQUE NATIONALE DU CANADA de microfilmer cette thèse et de prêter ou de vendre des exemplaires du film.

L'auteur se réserve les autres droits de publication; ni la thèse ni de longs extraits de celle-ci ne doivent être imprimés ou autrement reproduits sans l'autorisation écrite de l'auteur.

Date Sept. 15, 81	Signature

NL-91 (4/77)

THE UNIVERSITY OF ALBERTA

DYNAMICS OF ROCK AVALANCHES AND OTHER TYPES OF SLOPE MOVEMENTS

by

© Oldrich Hungr

A THESIS
SUBMITTED TO THE FACULTY OF GRADUATE STUDIES AND RESEARCH
IN PARTIAL FULFILMENT OF THE REQUIREMENTS FOR THE DEGREE
OF Doctor of Philosophy

Civil Engineering

EDMONTON, ALBERTA
Fall 1981

THE UNIVERSITY OF ALBERTA

RELEASE FORM

NAME OF AUTHOR Oldrich Hungr

TITLE OF THESIS DYNAMICS OF ROCK AVALANCHES AND OTHER TYPES OF SLOPE MOVEMENTS

DEGREE FOR WHICH THESIS WAS PRESENTED Doctor of Philosophy

YEAR THIS DEGREE GRANTED Fall 1981

Permission is hereby granted to THE UNIVERSITY OF ALBERTA LIBRARY to reproduce single copies of this thesis and to lend or sell such copies for private, scholarly or scientific research purposes only.

The author reserves other publication rights, and neither the thesis nor extensive extracts from it may be printed or otherwise reproduced without the author's written permission.

(SIGNED) ....

PERMANENT ADDRESS:

95 E. 20th Ave
Vancouver, B.C.
....

DATED Aug. 20 1981

THE UNIVERSITY OF ALBERTA

FACULTY OF GRADUATE STUDIES AND RESEARCH

The undersigned certify that they have read, and recommend to the Faculty of Graduate Studies and Research, for acceptance, a thesis entitled DYNAMICS OF ROCK AVALANCHES AND OTHER TYPES OF SLOPE MOVEMENTS submitted by Oldrich Hungr in partial fulfilment of the requirements for the degree of Doctor of Philosophy.

....
Supervisor

....

B. Simpson
....

....

....

....

....

....
External Examiner

Date....22 V. 81........

ABSTRACT

The subject of this research is the dynamic behaviour of slope movements, mainly after the initiation of failure. Two objectives have been followed. Firstly, a synthesis of published information was compiled in the form of a state-of-the-art review of the subject of landslide dynamics, covering all identified types of phenomena. Secondly, an enquiry was made into one of the current hypotheses proposed to explain the dynamic behaviour of large rock avalanches. This involved laboratory experiments of high velocity shearing of granular materials (sand).

The literature review included the collection of descriptive observational data concerning landslide movement. Velocities, volumes, descriptions of the mode of motion and of the material characteristics have been summarized.

Mechanical models have been identified with the various types of slope movements. These were organized into four basic groups: rigid particle movements (falls and topples), slides, distortional movements (creep), and flows. Methods of analysis for each of these models in their various geometrical configurations have been either reviewed or proposed. Material constitutive relationships in the form of stress-displacement laws have been reviewed, based on data from both landslide observations and from laboratory testing. This included information on the rate dependence of shearing in rocks and soils, the flow properties of clay slurries, dry and saturated granular materials and clay slurry- granular fragment mixtures.

Published calculations of landslide velocity and reach have been reviewed and others carried out, to illustrate the proposed concepts.

A major chapter has been devoted to the problem of the mobility of large rock avalanches, which tend to move further than could be predicted using frictional models without porepressure. Existing hypotheses have been critically reviewed in the light of information found in the literature and in a field study of the Frank Slide, Alberta.

Laboratory experiments have been made to investigate whether a reduction of the dynamic friction coefficient occurs in a granular material, when sheared at extremely high rates. The experiments included flume flow tests with velocities of up to 600 cm/sec, and ring shear tests with peripheral speeds of up to 100 cm/sec. The results were negative: no significant rate- dependent reduction of the frictional strength has been found, even at these ratesand at a range of normal stress levels. The conclusion was repeated for various materials, including rounded and angular uniform sand, dry or wet, sand and rock dust mixtures, and polystyrene beads.

It was concluded that the high velocity of rock avalanches is likely due to vibration near the movement base, or base lubrication by saturated soil. Circumstantial evidence indicates that the influence of air or steam pore

pressures is limited. Quite probably, various combinations of the above mechanisms contribute to the mobility of individual events.

Empirical approaches to rock avalanche reach prediction are recommended for practical use and have been reviewed in this thesis.

ACKNOWLEDGEMENTS

This work has been produced in the most stimulating, friendly and supportive athmosphere of the Civil Engineering Department, University of Alberta. Special thanks are due to Professor N. R. Morgenstern for the support given to the author throughout the course of this research.
Dr. Morgenstern suggested this topic, granted a generous amount of time and intellectual effort in problem- solving discussions, procured financial help on several occasions, and never failed to offer emotional help and encouragement. Many of the references reviewed were pointed out to the author by him.

Among many people who made valuable suggestions to this work are especially Professors G. Parker, P. Kaiser, D. Cruden, and Mr. S. Evans. Important comments were also made by Drs. Z. Eisenstein, F. Patton, J. Shaw, N. Rajaratnam and B. Stimpson.

Mr. Al Muir and his assistants were extremely helpful and competent in building experimental apparatus. Similar high level of assistance was offered by Mr. D. Sands in the field of cinematography. Messrs. G. Cyre, R. Howells, R. Gitzel and D. Wood helped in various tasks connected with the laboratory experiments and computing. Mr. G. Cyre further did a part of the drafting. Mrs. C. Whitehead typed all the tables, with exceptional speed and accuracy.

The excellent and well organized collection of engineering literature in the university library, and the competent assistance of the library staff, are highly appreciated.

Thurber Consultants Ltd. showed understanding in allowing the author to extend an agreed date of employment.

Financial support for this research was received from the National Scientific and Engineering Research Council of Canada, and from the Department of Civil Engineering, University of Alberta.

My wife, Klema Hungr and sons, Pierre and Nikolai sacrificed more to this thesis than could be described on these pages. I promise not to forget.

List of Figures

Figure..Page

1.1 Time history of landslides. (a) Concept by Terzaghi (1950) (b) soft clay excavation (da Silva, 1979) (c) Vajont rock slide (Mueller, 1964). ....

1.2 Correlation between response classes and the velocity spectrum. (Numbers refer to Table 1.1). ....

2.1 Path of a 60 cu.m boulder (Govi, 1977). ....

2.2 Rock fall safety angle suggested by the N.G.I. avalanche group (Lied, 1977). ....

2.3 Trajectory of a rock fragment after a fall on a shelf in the slope. ....

2.4 Kinematics of a full (a) and partial (b) cliff toppling failure. ....

3.1 Crossections of typical slides and slumps. ....

3.2 Analytical models for sliding. ....

3.3 Residual friction resistance of various clays: (a) vs. normal stress level, (b) vs. displacement rate (Kenney, 1967). ....

3.4 Strain rate effect on peak undrained strength of cohesive soils (Whitman, 1957). ....

3.5 Critical state friction in glass beads as a function of velocity of shearing and normal stress (Bridgwater, 1972). ....

3.6 Friction of a joint in granite at very high velocity and normal stress (data from Erismann et al., 1977). ...

3.7 Critical void ratio lines. (a) Concept, (b) actual results obtained in various types of test (Casagrande, 1976). ....

3.8 A family of critical state lines for clays (shown in terms of specific volume and first stress invariant, Schofield and Wroth, 1968). ....

3.9 Effective stress at peak strength in undrained traiaxial tests on sensitive clay as a function of w and of rate of testing (data from Crawford, 1969). .....

3.10
Back calculated variation of the mobilized effective friction angle. (a) Vs. strain rate in shear zone, (b) vs. displacement. Data from Gould (1960). ....

3.11
Typical crossection of an earthflow, demonstrating distributed strain (Sharpe, 1938). ....

4.1 Deep-seated creep in a glacial soil. (a) With depth, (b) with time. Slope angle = 30 deg. (After Wilson, 1970). ....

5.1 Roll wave: (a) during steady discharge from a reservoir, (b) at the front of a shallow flood, (c) at the front of the dam break wave (variable velocity). ....

5.2 Roll wave profiles for viscous and visco-plastic materials. ....

5.3 Flow front profile for a purely cohesive material. .....

5.4 Classification of the basic flow models. Flow regime criteria apply to the source depth h. H is the normal depth of a steady uniform flow. ....

5.5 Terminal state of a dam-break wave in a viscous material. ....

6.1 Viscosity vs. floc concentration for flocculated kaolin. (Michaels and Bolger, 1962). ....

6.2 Viscosity - concentration relationship for three clays with various pore water chemistry (Searle and Grimshaw, 1959). ....

6.3 Flow curve of a visco-plastic material: (1) no flow, (2) plug flow, (3) mixed flow, (4) general shearing (Searle and Grimshaw, 1959). ....

6.4 Bingham strength of clay slurries: (1) kaolinite (2) kolinite with sea water (3) montmorillonite (4) m. with sea water (Hampton, 1972). ....

6.5 Coaxial viscosimeter flow curves for a clay slurry at various concentrations (Yano and Daido, 1965). ......

6.6 Laminar flow of slurry and solid flakes. (a) Self-damming Poiseuille flow, (b) Flakes slowed down by side friction - sustained flow. ....

7.1 Grain flow profiles recorded by Savage (1979) (using polystyrene beads) 1, 2 and 3 refer to stations 33, 64 and 94 cm from flume entry. ....

7.2 Dimensionless velocity profiles for inertial grain flows with low and high porosities. ....

7.3 Variation of normal pressure and the coefficient a with linear concentration in the inertial regime (data from Bagnold, 1954, Fig. 4. Velocity term = 100). ....

7.4 Tangential pressure term. ....

8.1 Change of the grain stress ratio (friction coefficient) in the transitional regime. Data from Bagnold (1954). ....

8.2 Relative viscosity of uniform dispersions in the macro- viscous regime. ....

8.3 Relative viscosity of graded dispersions in the macro- viscous regime (Farris, 1968). ....

8.4 A crossection of the Vlietpolder flow slide (after Koppejan at al., 1948). ....

8.5 Viscosity change due to drainage in layers of different initial porosity. ....

8.6 Example, deceleration of a 1.1 m thick layer due to drainage. Initial porosity = 44 percent. ....

8.7 Pore air pressure generated by a soil structure collapse to a final porosity of 0.4 under undrained conditions. ....

9.1 Grain size distributions of debris flow materials. .....

9.2 Debris avalanches. (a) Hong Kong flow of fill (Lumb, 1975) (b) Modalen flow slide (Bjerrum and Jorstad, 1968). ....

9.3 Plan and section of the Aberfan flow slide of 1966 (after Bishop, 1973). ....

9.4 Correlation of the apparent viscosity of debris flows with water content.. (Modified form Jayapalan, 1980). ....

9.5 Frontal boulder accumulation in debris flow. (a) Steep slope, (b) flat slope, (c) schematic representation. ....

9.6 Dynamic equilibrium of a frontal boulder accumulation. ....

10.1
Rock avalanche initiating mechanisms. (a) Bedding slip : flat, with jump, convex, (b) slip across bedding or schistosity, (c) seismic collapse (Eisbacher, 1979), (d) collapse of a steep cliff. ......

10.2
Correlation between debris volume and thickness. ....

10.3
Correlations of (a) fahrboeschung (Scheidegger, 1973), and (b) mean travel angle with avalanche volume. ....

10.4
Frank Slide, Alberta, photographs. ....

10.5
Frank Slide, Alberta, aerial photo. ....

10.5a
Plan of the Frank Slide deposit. Overlay for Fig. 10.5. ....

10.6
Profile of the Frank Slide. (From contours by Daly et al., 1912). ....

10.7
The central portion of the CPR railroad cut through the Frank Slide debris. Base elevation is estimated. ...

10.8
Crossection of the examined outcrop, showing vertical sorting. ....

10.9
Vertical sorting of the Frank Slide deposit. Frame dimensions are 4 x 4 m. ....

10.10
Grain size curves in a vertical crossection of the debris. Sample numbers correspond to those in Figs. 10.8 and 10.9. ....

10.11
Change of characteristic grain sizes above the base of the railway cut (based on Fig. 10.9). ....

10.12
Correlation of the excessive travel distance and volume of large rock avalanches (Hsu, 1975). ....

10.13

Coefficients of friction and turbulence for rock avalanches (Koerner, 1976). ....

10.14
Friction coefficient (a) and vibro- viscosity (b) of a vibrated sand (Barkan, 1962). (c) Theoretical vibro- viscosity (Melosh, 1979). ....

11.1
Schematic diagram of the test flume. ....

11.2
An overall view of the flume apparatus. ....

11.3
Details of the flume apparatus. ....

11.4
Flow chart of the system of measurements. ....

11.5
Principle of the bed shear measuring device. ....

11.6
Examples form the camera records. ....

11.7
An example of the chart record. ....

11.8
Velocities of individual particles normalized with respect to the velocity of the group. ....

11.9
Bed friction coefficient, Ottawa sand. (a) From direct measurement, (b) from accelerations. ....

11.10
Bed friction coefficient, Polystyrene beads. (a) From direct measurement, (b) from accelerations. ....

11.11
Bed friction coefficient, angular sand. (a) From direct measurement, (b) from accelerations. ....

11.12
Flow classification versus bed slope angle and surface (maximum) velocity. ....

11.13
Velocity and flow thickness vs. time and position on the flume, Test No.9. ....

11.14

Velocity and flow thickness vs. time and position on the flume, Test No.10. ....

11.15
Velocity and flow thickness vs. time and position on the flume, Test No.15. ....

11.16
Velocity and flow thickness vs. time and position on the flume, Test No.16. ....

11.17
Density of Ottawa sand during flow. ....

11.18
Density of Polystyrene beads during flow. ....

11.19
Density of angular sand during flow. ....

11.20
Mean density vs. normal stress at two velocities, Ottawa sand. ....

11.21
Velocity ratio vs. mean velocity, Ottawa sand. ....

11.22
Velocity profiles measured through the side of the flume. ....

11.23
Idealized velocity profiles, derived from the relationship of Fig. 12.21, assuming linear velocity distribution. ....

11.24
Diagrams for flume test data processing. ....

12.1
Comparison of the design principles of the Imperial College - N.G.I. ring shear apparatus (Bishop et al., 1971) (a), and the present design (b). ....

12.2
Vertical section of the ring shear boxes. Dimensions in cm. Lower box rotating, upper fixed. ....

12.3
Ring shear apparatus photographs. ....

12.4
(a) Empty lower box, (b) sample in place, loading platten and membrane (right). ....

12.5
Strength envelopes of the dry 10–14 sand. ....

12.6
Strength envelopes of the 10–14 sand submerged in water. ....

12.7
Strength envelopes of the dry 8–10 sand (coarse). ......

12.8
Strength envelopes of the polystyrene beads. ....

12.9
Strength envelopes of the 4:1 sand and rock flour mixture. ....

12.10
Strength envelopes of the 4:2 sand and rock flour mixture. 168

A.1 Reference grid in perspective view. 168

B.1 Diagrams for the internal shearing model. ....

List of Tables

Table..Page

1.1 Slope movement classification according to Varnes (1978). ....

1.2 Examples of slope movement velocity and damage potential. ....

2.1 Summary of rigid particle motion formulas (after Goldsmith, 1960). ....

3.1 Typical failure velocities of sliding movements. ....

3.2 Main groups of sliding movements identified in the survey of literature. ....

3.3 Some laboratory- determined values of the Brittleness Index and velocity predictions using the simple model. ....

3.4 Investigations of the dependence of the constant volume friction angle on strain rate and stress level. ....

3.5 Some examples of observed shear zones. ....

5.1 Types of flow slides classified with respect to material. ....

9.1 Physical characteristics of some debris flows. ....

10.1 Dimensional parameters of rock avalanches. ....

10.2 Some estimates of rock avalanche velocities. ....

11.1 Dimensional analysis of the flume experiments. ....

11.2 Properties of test materials. ....

11.3 An example of the processed data. ....

11.4 Error analysis of the density and apparent friction coefficient determination. ....

12.1 Parameters of previous ring shear tests on granular materials. ....

12.2
Summary of residual friction angles measured in the ring shear tests. ....

PREFACE

Doctoral theses are usually intended to summarize a more-less narrowly focused research effort starting with a singular objective and ending with conclusions. This work also has such an objective, but beside it there is an attempt at a unified review of the entire subject of landslide dynamics. Such a review seemed timely, due to a somewhat unsatisfactory state- of- the- art.

Material relevant to landslide mobility is found scattered in the literature of several widely disparate fields of science, and furthermore often in a fragmentary form in papers devoted to different causes. It has therefore been attempted to bring all of this material together, to relate various hypotheses to each other, to review them critically from a central stance and to add new insights or proposals where possible. This was found to require somewhat more original thinking, and more effort in general, than is usually necessary for a literature survey. The review fills the bulk of the thesis (Chapters 1 to 10) and is presented as a contribution independent of the laboratory work reported in Chapters 11 and 12 which are largely self-contained and have an entirely different focus.

Table of Contents

Chapter Page

1. INTRODUCTION 1
   - 1.1 Purpose and Organization of this Research 1
   - 1.2 Basic Concepts and Definitions 7
   - 1.3 Classification, Principal Mechanisms. 12
   - 1.4 Velocity Spectrum 22
2. FREE PARTICLE MOVEMENTS 28
   - 2.1 General 28
   - 2.2 Rock Falls 28
   - 2.3 Topples 42
3. SLIDING MOVEMENTS 48
   - 3.1 Introduction 48
   - 3.2 Equation of Motion 62
   - 3.3 Predictions of velocity and reach 72
   - 3.4 Residual Friction. 78
   - 3.5 Pore pressure determination 91
   - 3.6 Determination of the resisting forces:Summary. . 101
4. DISTORTIONAL MOVEMENTS 110
   - 4.1 Description and Classification 110
   - 4.2 Theoretical Models, Failure Predictions. 118
5. FLOWS: GENERAL CONSIDERATIONS 125
   - 5.1 Introduction : Types of Flows 125
   - 5.2 Analytical models for flow sliding 127
6. FLOWS OF CLAY SLURRY 145
   - 6.1 Slow Earth Flows 145
   - 6.2 Rapid Earth Flows 153

6.3 Flow Properties of Clay Slurries 158
6.4 Analysis of Rapid Earth Flows 167
7. GRAIN FLOWS 173
7.1 Sand Flows, Talus Flows. 173
7.2 Experimental Observations 178
7.3 Theoretical Models 186
8. GRAIN FLOWS IN WATER 202
8.1 Subaqueous Flows of Granular Sediments 202
8.2 Turbidity Currents 213
8.3 Constitutive Relationships 218
8.4 Methods of Analysis and Considerations of Drainage 232
8.5 Air liquefied grain flows 241
9. FLOWS OF MIXTURES OF SOLID GRAINS AND SLURRY 246
9.1 Debris Flows 246
9.2 Debris Avalanches 259
9.3 Lahars 269
9.4 The Initial Conditions 272
9.5 Flow Analysis 276
10. ROCK AVALANCHES 297
10.1 Descriptive Introduction 297
10.2 Frank Slide, Alberta, Field Observations 329
10.3 Analysis- Energy and Friction 345
10.4 Analysis- Empirical Approach 353
10.5 Analysis- Physical Hypotheses 360
10.6 Conclusion 378
11. LABORATORY FLUME EXPERIMENTS 380

11.1 Introduction and a Statement of Objectives 380

11.2 Considerations of Similitude 382

11.3 The Test and the System of Mesurements 387

11.4 Results 403

11.5 Conclusions 428

11.6 Detailed Description of the Data Processing Techniques 431

11.7 Error analysis 436

12. HIGH VELOCITY RING SHEAR EXPERIMENTS 445

12.1 Introduction 445

12.2 Apparatus Design. 449

12.3 Results 460

13. SUMMARY AND RECOMMENDATIONS FOR FURTHER RESEARCH 469

14. REFERENCES 475

15. APPENDIX A, METHOD OF GRAIN SIZE ANALYSIS USED FOR FRANK SLIDE DEBRIS 497

16. APPENDIX B, FRICTIONAL ENERGY BALANCE OF LANDSLIDE ..502

1. INTRODUCTION

1.1 Purpose and Organization of this Research

Slope movements have always been of some importance in human lives. te But, the importance has perhaps not been very great in the past, compared with that of other natural hazards such as droughts, floods or earthquakes. This situation is changing rapidly with the recent dramatic increase in population in all parts of the world. Not only are mountainous areas being increasingly settled and exploited, but everywhere steeper terrain is being utilized for construction of dwellings, industrial plants and transportation routes. People are increasingly coming into conflict with slope movements. A single intensive storm in the Los Angeles area of California, for example, caused some 3 000 slope failures and $50 M damage in 1978 (Anon, 1979). Of the total predicted economic losses in California due to geological hazards from 1970 to 2000 about $10 billion (26 percent) is expected to result from slope movements (Schuster, 1978). There may have been hundreds of large postglacial rock falls or rock slides in the Canadian mountains (e.g. Cruden, 1976), but the only two known to occur in this century have both caused losses of life and property. A single event in Peru, the Huascaran rock avalanche of 1970, killed over 18 000 persons (Plafker and Ericsen, 1978).

But there is also an increasing awareness of landslide danger, as illustrated for example by the appearance of catalogues and maps of slope movements in Czechoslovakia and elsewhere (e.g. Spurek,1972), by the forming of a special "Avalanche group" at the Norwegian Geotechnical Institute (Lied,1977), or by the new California grading ordinances (Anon, 1979).

Prevention of landslide hazard poses two broadly defined engineering tasks. The first is to identify existing or potential slope movements and, as far as possible, prevent them from occurring. These are the questions of *stability*. Ever since the early years of Soil Mechanics, some 50 years ago, this has been a central subject of investigation and research. Enormous advances have been made in methodology, theory, experimentation and prediction, which are being periodically reviewed in professional meetings and publications.

There are cases, however, when potential slope movements are recognized but cannot be prevented from realizing themselves, due to technical or economic reasons. The second engineering task assumes primary importance in such cases: the analysis of *mobility*. Specifically, it is necessary to predict in such cases how destructive will the potential landslide be. It will be argued in Section 1.4 that destructiveness of slope movements depends on the area which they affect, their velocity and mode of motion. These are the elements that must be predicted.

In contrast to the stability questions, those of mobility or dynamics of slope movements have received very little attention in the engineering literature. An illustration of this is the fact that no major specialized review papers or publications on landslide mobility exist. The recently introduced volumes "Rockslides and Avalanches", edited by B. Voight (1978), contain a wealth of information, but without any attempt at organizing it systematically. Other reviews appear in summary articles biased strongly towards the stability aspects (e.g. Terzaghi, 1950, Skempton and Hutchinson, 1969). Besides these exceptions, one can only draw information from sporadic publications devoted to the analysis of specific events or from publications concerning slope stability, where the dynamic aspects have been treated as secondary topics (e.g. Conlon, 1966, Mueller, 1968).

Several branches of geological literature offer greater quantity of information concerning this topic. A complete, although unfortunately not very thorough, general review has been compiled by Scheidegger (1975). Reviews of specific categories of slope movements are relatively frequent (e.g. Johnson, 1970, Hsu, 1975). Works concerning the descriptive aspects of slope movements and their classification have, of course, always been numerous, since these questions constitute a branch of Geomorphology. But geological literature offers only limited answers to engineering problems because of its different emphasis. Even though physical theories are often developed, they are intended to *explain* the phenomena, not to analyze them with the purpose of predicting their quantitative effects.

The author admits that a large part of the present work also fails to cover the full distance between hypothesis and prediction, but this is to a fair extent a reflection on the present state of the art. An example may be given of debris flows and avalanches, discussed in Chapter 9. Theories are reviewed from several schools of analysis. Tens of articles have been read, many of them reviews. But the conclusion is that there is so far no rational universal procedure to predict the velocity and reach of these flows. The laws of their behaviour are known, but experimental parameters to be used in them are not, nor are the methods to measure them.

This research began with a double objective. Firstly, the author was to synthesize the available information concerning the dynamics of slope movements. The questions to be answered included: (1) what are slope movements, (2) what are their mechanisms and, (3) how far are we from being able to predict their mobility? This synthesis, which is covered by Chapters 1 through 10, is an attempt at a systematic general engineering review of slope movement dynamics which has, to the author's knowledge, not been done before. Stability aspects were not considered. It was assumed in each case that the dynamic analysis begins with the knowledge of the outline of material which is going to participate in the slope movement, as determined by a stability analysis.

A dynamic analysis consists of three equally important steps. The first step is to define the phenomenon by collecting any information which might serve as circumstantial evidence concerning its mode of motion. It would be fruitless to attempt to analyze a type of slope movement without knowing its general character. The circumstantial evidence helps to bracket the boundary and initial conditions, the type and condition of the material, the characteristic dimensions and velocities, special aspects of behaviour etc. It is collected mainly from field observations.

The second step is to formulate a boundary and initial value problem describing the motion. This is determined by its kinematic configuration, established in step one. Four basic kinematic models exist as described in Section 1.3, and a number of various boundary and initial conditions, which are treated in the appropriate chapters. The analytical models are based on the principles of conservation of mass, energy and momentum and generally derive from established concepts of the dynamics of solids and fluids. In some cases, physical modelling is substituted for mathematical treatment at this stage.

The last step determines the rheological constitutive relationship of the material, to be used in the equations of motion. It is determined on the basis of laboratory or field experiments such as shear tests or viscosity measurements, or by back-calculation from actual events monitored in the field.

The aim of the presentation was to place sufficient emphasis on each of these three steps. The material is divided according to three criteria: phenomenological (descriptive), kinematic and rheological. Each division is introduced by a description, then discussed in its kinematic and rheological aspects. In an exception to this system, the equations of motion and boundary conditions of all flows are treated in Chapter 5, although the subsequent five chapters divide flows further along rheological lines.

The second major task of this research was to investigate the problem of mobility of rock avalanches. These are large landslides from bedrock sources, exhibiting characteristic flow-like features in their deposits. Freshly fragmented rock is generally regarded as a frictional material, with relatively high friction angles. Rock avalanche debris cannot be fully saturated during its motion, due to the bulking effect introduced when the initially solid mass disintegrates. Nevertheless, large rock avalanches exhibit a degree of mobility that is not compatible with the assumption of frictional behaviour and zero pore pressure. Various hypotheses have been advanced to explain this. These include theories postulating discrete lubricating layers, gas pore pressures and rheological changes due to high shearing rates or internal vibration. Chapters 11 and 12 describe an experimental program designed to investigate one of these hypotheses, that of a rheological change at high shear rates. Comprehensive testing of granular materials in a sand flume and a high velocity ring shear apparatus showed that the hypothesis is unsubstantiated, i.e. that there is no change of frictional behaviour even at strain rate and stress levels comparable ot those expected in rock avalanches. The conclusions from this work are utilized in Chapters 7 and 10.

Throughout the thesis, "original" observations and deductions are mixed with those obtained from the literature, in order to present a unified picture. Emphasis is placed on a critical review, while it is attempted to make presentation of the obvious as brief as possible.

1.2 Basic Concepts and Definitions

This thesis is about *slope movements*, that is gravitational movements of earth materials on slopes, unassisted by a transporting agent such as flowing water or wind. Those movements triggered or promoted by human action, erosion or earthquake are included. An emphasis is placed on *landslides*, which are here understood to be movements of relatively large segments of slope material (over, say 25 sq. m in area) with significant present, past or future velocities (over 0.3 m/year, Terzaghi, 1950) and with at least some degree of detachment from the underlying "stable" mass. The use of the term does not mean that the predominant mode of motion is sliding; it is simply adopted as an established name for a slope movement of significant proportions and vigour. A review of other definitions can be found in Coates (1977), who adds that the movement of a landslide is "caused by factors that do not affect other (similar) slopes in the same manner". This is of course true as long as most of the similar slopes are not affected by landsliding at the same time. This occurs, for example, in the "landslide topographies" of Canadian Prairie river valleys. The author has taken the licence to replace the general term frequently by "slide, slip, fall, flow, flowslide or avalanche", all of which should be taken as synonyms for "landslide", intended merely to add some colour to the narrative. Rigorous definitions of kinematic movement models are given in Section 1.3.

The features of the time history of a landslide have been outlined by Terzaghi (1950), as shown in Fig. 1.1a. A "stable" slope is immobile or may move imperceptibly by a steady or periodic creep movement. At point A, a change in the equilibrium of the slope commences to take place; a slide producing agent begins to act. Gradual acceleration is observed, accompanied by signs of distortion and perhaps beginnings of detachment (tension crack). At point B the acceleration reaches a maximum and a period of rapid movement ensues, which is called *failure*. Gradual deceleration terminates it and a new "steady" post failure stage begins at C. A simple landslide may behave nearly

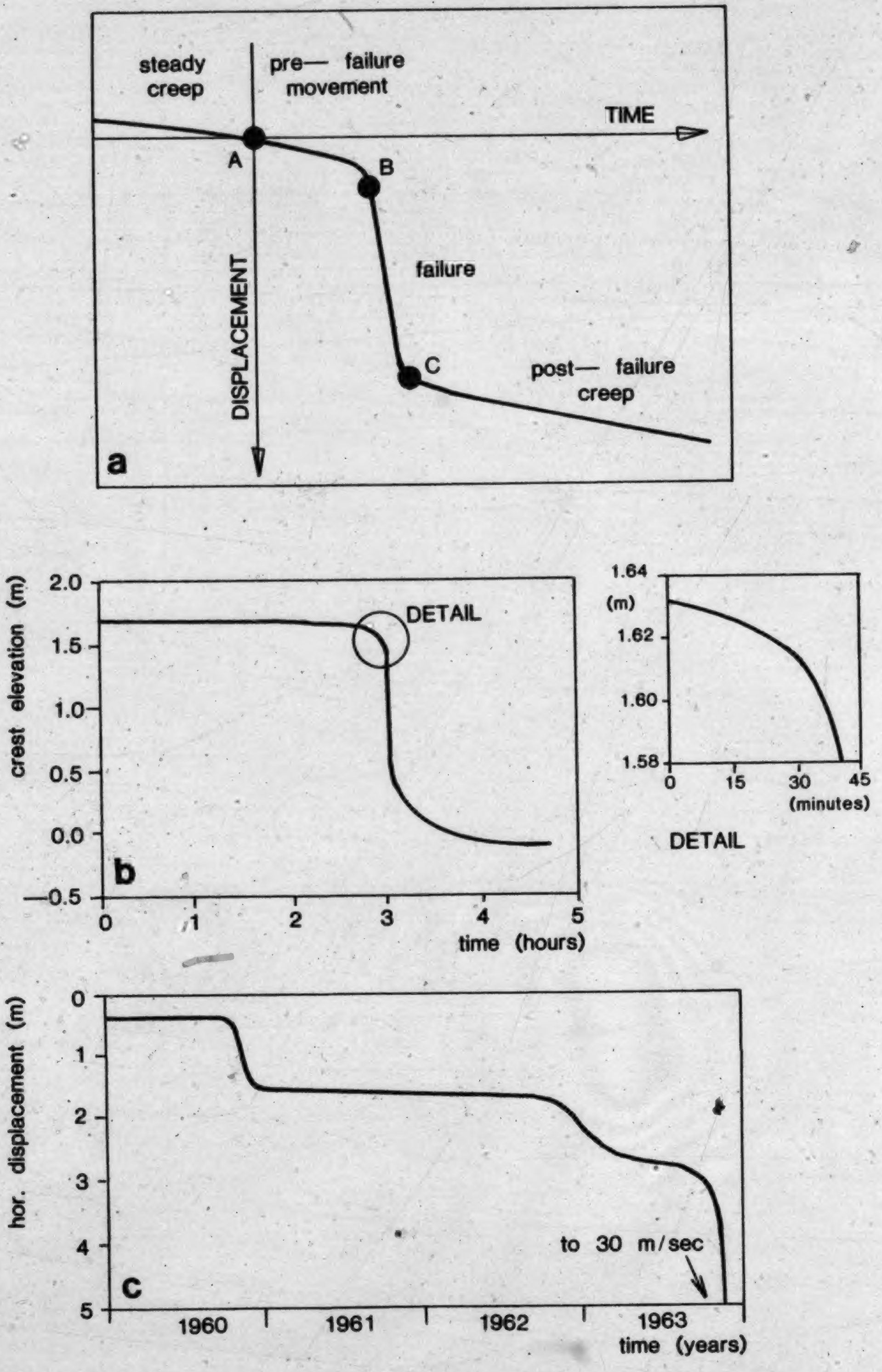

Figure 1.1 Time history of landslides. (a) Concept by Terzaghi (1950)
(b) soft clay excavation (da Silva, 1979)
(c) Vajont rock slide (Mueller, 1964).

exactly according to this scheme, as illustrated by the crest subsidence record of an experimental excavation failure in very soft organic clay of Itaipoo lagoon in Rio de Janeiro (da Silva, 1979, Fig. 1.1b). The excavation was approximately 4 m deep and the "slide producing agent" was rapid drawdown of water by pumping.

More commonly, however, the displacement history is much more complex as there are many factors influencing acceleration, most of which act neither uniformly nor steadily. The record of horizontal displacements prior to the catastrophic Vajont rock slide (Mueller, 1964 and Fig. 1.1c) appears as a sequence of three S- shaped curves. The first two periods of acceleration were brought about by temporary raises of reservoir level and amounted each to about 1 m of displacement. Although each has the characteristic shape, it cannot be called "failure" in comparison with the final acceleration which brought a displacement of 400 m and velocities of up to 30 m/sec. Some events, for example the Wind River landslide of Oregon (Palmer, 1977) move exclusively by a succession of random or roughly periodic accelerations, with no historical record of a major displacement. In such cases there is a difficulty in defining failure. This author would propose a definition as "the single most important episode of accelerated displacement over the entire history of the slope segment". It could thus be a major past displacement, which may have formed a crown scarp in pre- historic times, as in the case of many observed stiff clay slides. Or it could be a future catastrophic detachment, as in the case of Vajont when it was observed in 1962 and early 1963. In complex situations there might be separate failure episodes in various local parts of the moving slope.

The adjective *pre-failure* refers to the accelerating movement period immediately preceding failure. *Post-failure* movements occur in masses already distorted or displaced by failure. This stage of movements may be very complex and has been monitored more often than the others, for obvious reasons.

Velocity of a landslide is a vectorial quantity distributed nonuniformly in three-dimensional space and in time. But its complete distribution is generally unknown and is referred to only occasionally in connection with very thorough field observations or with theoretical results. More often, the term refers to estimates of mean velocity of the mass, spot velocity, or the speed of the leading front of the landslide. Also, reference is made to mean velocity obtained as the total displacement divided by the elapsed time, or to the maximum velocity of an acceleration episode. The term *creep* is meant to describe a very slow movement (less than .3 m/year).

Detachment generally occurs along a displacement discontinuity and may bound the moving segment fully or only partially. It may also occur along a strain discontinuity, as in the viscous flow of a mass of finite length.

Shear strain is understood in the engineering sense, i.e. as the normal gradient of displacement. *Shear strain rate* is the normal gradient of velocity. *Fluid* material is that which distorts under very low applied stresses. In other words, it has very low strength and its resistance to distortion is highly rate dependent. *Liquefaction* refers to a process of sudden decrease of shear strength, by which the material approaches the state of a fluid. *Fluidization* is reserved for the state of a granular material, in which effective stresses are nullified by upward seepage, leading to dilation and turbulence[1]. Grains are *suspended* if supported by turbulent fluid drag, and *dispersed* when supported by intergranular momentum transfer.

1.3 Classification, Principal Mechanisms.

The singleminded purpose of this research is to describe how landslides move: how far, how fast and in what manner. To do this systematically, it is necessary firstly to identify their various kinematic mechanisms, secondly to establish and classify the rheological nature of their materials. Besides this, it is necessary to have a working descriptive vocabulary to serve as a checklist of this diverse phenomenon and to maintain connection with other works on the subject. Consequently, the thesis is organized on the basis of three parallel classifications: (a) a descriptive one, (b) a kinematic classification of mechanisms, and (c) a classification of rheological models.

---

[1] Other definitions of these terms can be found in the literature of various engineering disciplines. The present definitions are convenient for the purposes of this research, however.

The descriptive classification was adopted eclectically, with the purpose of using comprehensive and well established terminology. A review of classification systems was therefore made, which is not described here. Excellent articles on landslide classification are those by Ladd (1935), describing systems in use prior to his time, and Coates (1977), summarizing more recent developments. The classification system selected is that of Varnes (1978). Its advantages are that it is well accepted on this continent, yet sufficiently general and free of regional bias. Further, it draws heavily from a number of older systems expecially that due to Sharpe (1938), and its terminology is therefore compatible with a large segment of the literature.

The classification system (Table 1.1) is based on three divisions, including the kinematics of movement, the character of the material and the rapidity of motion. In the first two aspects it apparently overlaps the classifications of kinematic and rheological models used in this thesis. But these do not attempt to describe the phenomenon by its external attributes. Instead, they refer to interpretative models to be used in its analysis. The descriptive classification also provides labels for distinct types of slope movements such as *rock falls*, *earth slumps* or *rock falls- debris avalanches*. Each of these is explained with a

TYPE OF MOVEMENT		TYPE OF MATERIAL		
		BEDROCK	DEBRIS (coarse soil)	EARTH (fine soil)
I	FALLS	rock fall	debris fall	earth fall
II	TOPPLES	rock topple	debris topple	earth topple
III SLIDES	ROTATIONAL	rock slump	debris slump	earth slump
	TRANSLATIONAL	rock block slide rock slide	debris slide	earth slide
IV	SPREADS	rock spread	-	earth lateral spread
V	FLOWS	bedrock flow (sackung)	debris flow debris avalanche block stream solifluction soil creep	wet sand flow rapid earth flow earth flow loess flow dry sand flow
VI	COMPLEX	rock fall - - avalanche	slump - earth flow cambering	-

RATE OF MOVEMENT SCALE:

extremely rapid
——3 m/sec——
very rapid
——0.3 m/min——
rapid
——1.5 m/day——
moderate
——1.5 m/mo.——
slow
——1.5 m/yr.——
very slow
——0.06 m/yr.——
extremely slow

Table 1.1 Slope movement classification after Varnes (1978)

definition and examples in Varnes' paper. In this thesis, the labels are italicized when first mentioned, and abbreviated definitions are given. The velocity spectrum proposed by Varnes is examined in the following section.

The classification was further subdivided in the case of sliding and slumping movements, to account for some fundamental differences in the brittleness of various soil groups. The proposed subdivision is shown in Table 3.2 and supported by the velocity data of Table 3.1. Another modification lies in the terminology used for subaquaous slope movements discussed in Chapter 8. Varnes only has one class, "wet sand or silt flow", which appears inadequate. Classification of subaquaeous landslides is briefly discussed in Section 8.1 and the class of turbidity currents is introduced in Section 8.2. The term *talus slips* is used in Section 7.1 for a phenomenon described therein. Flows of mining waste material are discussed under *debris avalanches*. The phenomena of *solifluction*, *soil creep*, *cambering* and *gravitational sagging* or *bedrock flow* are mentioned only briefly in Chapter 4; it is felt that their dynamics is of limited engineering significance. No frozen ground or glacial phenomena are treated, due to their special nature and because they have been well covered by previous work at the University of Alberta. Snow avalanches are mentioned only for the sake of parallels with landslide phenomena, e.g. in Section 10.4. Similarly with lahars (Section 9.3). Volcanic incandescent flows (nuees ardentes) are not dealt with.

The basic kinematic models have been recognized in the first known attempts at landslide classification. Baltzer (1875) found among Alpine landslides falls, slides and flows. Nemcok, Pasek and Rybar (1972) added "creep", a word which this author would prefer to replace by "distortion", when used in a kinematic sense. Varnes (1978) introduced topples and spreads, drawing on the work of Goodman and Bray (1976), Zaruba and Mencl (1969) and others. For the present purposes of dynamic analysis, it is thought that only four basic mechanisms need to be identified:

a. *Free rigid particle movements.* These are independent movements of largely nondeforming fragments with six degrees of kinematic freedom. They include free flight, rolling, impact and rebound. The word "nondeforming" has a strong exception in breakage and disintegration of such particles, which is reflected in changes of trajectory and impact conditions. A lack of interaction with other moving particles is implied, although each particle obviously interacts intermittently with the surface of the slope. Toppling movements are included in this category, although in this case the degrees of freedom are limited to one or two rotational ones.

b. *Sliding movements.* Sliding refers to translation of a body along a straight or curved displacement discontinuity or sliding surface. There are only two to three degrees of kinematic freedom. One block may slide independently, or several may slide with respect to the firm base as well as to each other. The sliding model is in many cases merely an idealization of a considerably more complex mechanism, as discussed in the introduction to Chapter 3.

c. *Distortional movements.* This term refers to displacements occurring without the creation of a displacement discontinuity and without a discernible change in the rheological character of the mass. In other words, the mass of the slope distorts under stress, but at the same time remains largely intact. Again, this is an idealization; displacement discontinuities may be found in observations carried out on a sufficiently small scale. Strain discontinuities may develop, but normally only at boundaries of different materials.

d. *Flows.* Flow movements are characterized, in the traditional sense, by distributed strains throughout a large part of the moving mass. This would not in itself differentiate flows from the distortional movements discussed above. Varnes (1978), in fact does not make a distinction between the two. But here it is assumed that a flowing mass is characterized also by a change in its rheological condition as a result of some process such as thixotropy, remoulding, formation of a flow structure (Casagrande, 1976), or general yielding ("critical state"). The boundary between the flowing material and the base is defined by a strain discontinuity or displacement discontinuity (basal shear) and the material outside it can be assumed rigid. Nondeforming, unstrained regions may be found within the flowing mass, which could be termed plugs or rafted blocks.

There is a smooth transition between flow and sliding, when the rigid blocks make up the major part of the mass and the flowing layer deteriorates into a thin shear zone. On the other hand, a sliding model would change gradually into a frictional flow, if the size of individual particles became too small and their number too great. In a macroscopic view one would obtain the picture of a flowing material, the rheology of which is determined by the existence of persistent shear zones.

The main reason for the above divisions is to facilitate the application of dynamic models. The free particle and sliding movements are amenable to the methods of rigid body mechanics, where a set of equations of motion is applied to each fragment individually at its center of gravity. The remaining two cases require treatment based on the mechanics of continua, because of the distributed strains. In the case of distortion, the equations would be applied on a domain consisting of the entire extent of the slope. In the case of flow, they would only be applied to the flowing mass limited by the rigid boundary of a channel or a bed. The boundary may change somewhat during the course of movement, as a result of erosion or deposition.

With these definitions, one is able to formulate a boundary and initial value problem for any actual geometrical configuration. The equations of motion (and continuity, where applicable) are the basis of the solution. The thesis is organized so that each chapter deals with phenomena dominated by only one of the kinematic classes. In fact, Chapters 2, 3 and 4 coincide with the first three classes. In each of these chapters there are paragraphs describing the equations of motion and boundary conditions, before discussing constitutive relationships. In the case of flows, the variety and complexity of the constitutive relationships is great. This is reflected in dividing the treatment of flows into 6 chapters (5 through 10). Chapter 5 deals with the equations of motion and the related boundary value problems for all flows. The remaining chapters deal with the varieties of rheological constitutive relationships identified in the corresponding landslide types.

The class of free particle movements has no rheology, but it does have constitutive relationships regarding impact conditions, which are discussed in Chapter 2.

Sliding is controlled by the rheology of shear zones. This is described at length in Sections 3.4 to 3.6. Under drained conditions, frictional behaviour appears predominant in rock joints and granular shear zones, and mildly dilatant (logarithmic with respect to the velocity) behaviour in clays. Undrained rheology of shear zones is very poorly known at the present time; only a limited amount of empirical data is available.

For the purpose of the discussion of rheology of flows, earth materials have been separated into a fine (colloidal) class and a coarse class referred to in general as "grains". The criterion for making this separation is the relative importance of electro- chemical and mechanical forces in particle interaction.

Chapter 6 therefore deals with the flows of clay (colloidal) substance alone. At a low water content and applied stress these flows may be plastic, i.e. relatively slow, with a tendency for strains to concentrate to narrow shear zones among relatively rigid blocks (Section 6.3). Such flows are transitional between sliding and flowing kinematics. The flow- like [2] character results from a high degree of disturbance of the moving mass, and may be due to numerous discrete slips. Nevertheless, distributed strain can often be assumed in the analysis of such phenomena.

At higher water contents or higher stresses, remoulded clay assumes viscous properties which may or may not be Newtonian. The motion tends to be faster and more fluid-like. (Section 6.4).

---

[2] Meaning with an appearance indicating distributed strain.

Masses of coarse materials (grains) are frictional when dry but also, under certain conditions, when saturated. Frictional flows of drained grain masses are referred to simply as *grain flows* and are treated in Chapter 7. This chapter thus deals with the flow of grains alone, where the dynamic influence of the pore fluid is only minor. When undrained, such masses assume a rheologically dilatant character, as described in Chapter 8. Increasing void ratios and high pore pressures cause saturated grain flows to lose their frictional character. There is a gradual transition to the "macro- viscous" regime (Bagnold, 1954), in which highly dispersed grain masses behave as viscous fluids. These flows are also discussed in Chapter 8, which is thus devoted to the flows of grain masses whose rheology is dominated by the influence of the pore fluid. *Turbidity currents*, which are flows of grains suspended by liquid turbulence, are also discussed in this chapter, as are flows of fine granular materials liquefied by high pore air pressures.

Chapter 9 introduces phenomena combining the properties of colloidal slurries with those of coarse grains. A full spectrum of materials exists from plain fine- grained slurries ("mudflows") to liquefied well graded coarse materials. In general, therefore, this chapter deals with flows of unsorted mixtures of well- graded materials. There is presently an ambiguity in separating the classes of slope movements referred to as *debris flows*, *debris avalanches* and *debris slides* (Blong, 1973). In this work, the term debris flows is used with respect to well channelled natural flows of long reach, which follow significant drainage courses in a mountainous topography. They may or may not be periodic in occurence. The term avalanche is used for all other flows of unsorted material which do not fall into this category because of their short reach, lack of channelling or unusual source materials (e.g. mining waste) or initiating conditions (e.g. rock fall impact). This division is purely descriptive; from the rheological and largely the kinematic point of view as well, these phenomena belong in the same class. A section on volcanic lahars is added, which are treated as a special kind of debris flows.

Rock avalanches are reserved a special chapter (Chapter 10), as they appear to have a unique character and importance as well as unusual, and so far poorly defined, rheology. Their definition and distinction from other phenomena is discussed in Section 10.1. The remaining two chapters present the description and results of laboratory testing conducted with the aim of discovering the rules of behaviour of granular materials during shearing at high rates. This is relevant to the question of the rheology of rock avalanches, as well as grain flows.

1.4 Velocity Spectrum

When first introduced to the landslide velocity scale shown in Table 1.1, the author had difficulty in visualizing its significance. Why should a certain range of velocities by defined as "rapid" and another "very slow". An outgrowth of this doubt was a realization that there is a lack in the slope movement literature of a unified scale of destructiveness, such as exists in the Mercalli scale of earthquake intensity. Some thought has therefore been given to the possibility of defining such a scale.

The Mercalli scale is defined on the basis of descriptions of local effects of an earthquake; degrees of damage that could be evaluated by investigating a small area such as a house and a section of a street. Yet, the intensity value can be correlated with the total energy release of the event. This implies that local damage is related to the magnitude of the earthquake and so is the area affected. The situation is different in the case of landslides. Small rapid debris avalanches of a few cu.m of material are known to have caused total destruction and loss of lives locally. On the other hand, a large slope movement of moderate velocity can have much less serious effects, as it can be avoided or structures affected can be evacuated or rebuilt.

This suggests that a landslide damage potential will require a two parameter classification, involving area affected and velocity. It may be noted that the product of these two parameters is approximately proportional to the power release of the landslide. A third parameter, which is difficult to quantify, is the degree of internal distortion of the landslide mass. This is relevant to structures standing on top of the mass which would be damaged in proportion to the internal distortion of their foundations. For example, the "Lugnez creep slope" in Switzerland (Huder, 1976) involves an area of 25 sq.km, moving steadily down a 15 deg. slope at velocities of up to 37 cm/year. The steady movements have been observed by surveying since 1887. Yet, there are six villages on the slope, with 300 years old stone houses and churches with bell towers. None of these structures suffer damage while displaced, because the creeping block is moving without distortion. But, as stated earlier, this aspect of damage potential is difficult to quantify and each case requires separate consideration.

Area, on the other hand, is a parameter easily described and demands no further discussion. Its connection with damage potential is clear.

Velocity alone is a parameter whose significance from the point of view of destructiveness may require a definition. Several case histories have been assembled, in which the effects of a slope movement on humans and their activities have been well described and where failure velocities are known as well (Table 1.2). These have then been sorted into the following five categories, according to the response which the people affected have been able to undertake:

1. No response possible. Catastrophe of major violence.
2. Some lives lost, velocity too great to permit all

persons to escape.

3. Escape evacuation only possible. Structures, possessions and equipment destroyed.
4. Temporary and insensitive structures maintained on or in front of the moving mass, others dismantled.
5. Remedial construction undertaken during movement. Permanent structures maintained.

As shown in Figure 1.2, there is an approximate correspondence between the response classes and the velocity spectrum suggested by Varnes. An important limit appears to lie between very rapid and extremely rapid movement, which approximates to the speed of a person running (3 m/sec.) Another important boundary is between moderate and slow classes (18 m/year), below which it appears feasible to maintain at least some structures on or in front of the landslide. No case history has been located for class 3.

LANDSLIDE,SOURCE,VELOCITY,EFFECT

---

1. Vajont, Mueller(1964), 25 m/sec, 1900 lives lost indirectly.
2. Frank, McConnell and Brock (1904), 28 m/sec, at least 70 lives.
3. Elm, Heim (1932), 70 m/sec, 115 lives.
4. Goldau, Heim (1932), 70 m/sec, 457 lives.
5. Aberfan, Bishop (1973), 4.5 m/sec, 144 lives, some buildings damaged.
6. St.Jean-Vianney, Tavenas et al. (1971), 7 m/sec, 14 lives, structures destroyed.
7. Ikuta, ENR (1971), 18 m/sec, 15 lives, equipment destroyed.
8. Jupille, Bishop (1973), 31 m/sec, 11 lives, houses destroyed.
9. Handlova, Zaruba and Mencl (1969), 2 300 m/year, 150 houses destroyed, complete evacuation.
10. Schuders, Huder (1976), 10 m/year, road maintained with difficulty.
11. Wind Mountain, Palmer (1977), 10 m/year, road and rlwy. require freq. maintenance, Girl Scout Camp bldngs. adjusted periodically.
12. Klosters, Haefeli (1965), 0.02 m/year, tunnel maintained, bridge protected by a slip joint.
13. Fort Peck Spillway, Wilson (1969), 0.02 m/year, movements unacceptable, slope to be flattened.
14. Little Smoky, Hayley (1968), 0.15 m/year, bridge protected by a slip joint.
15. Lugnez, Huder (1976), 0.37 m/year, six villages on slope undisturbed.

Table 1.2 Examples of slope movement velocity and damage potential.

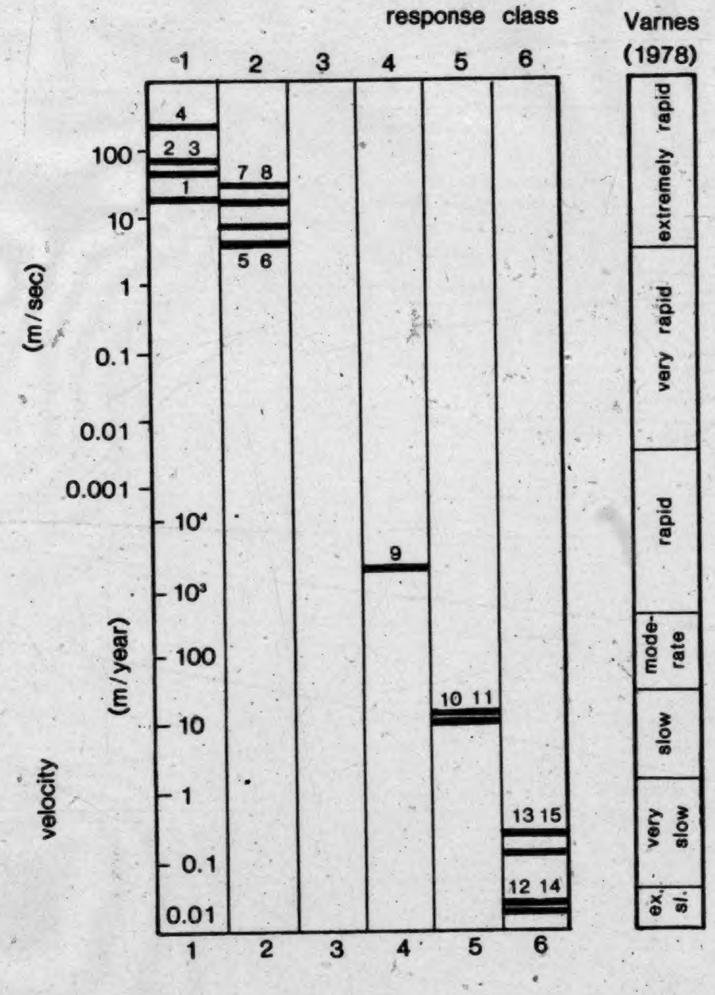

Figure 1.2 Correlation between response classes and the velocity spectrum. (Numbers refer to Table 1.1).

2. FREE PARTICLE MOVEMENTS

2.1 General

Failure of slopes built of sufficiently coherent materials occurs by separation and fall of discrete blocks which can, at least in the first approximation, be viewed as rigid particle movements. The specific modes of motion constituting this category include rotation, toppling, rolling, free fall and impact. The typical example is the *rock fall* which occurs either on its own, or as a (usually initial) part of a complex slope movement such as a *rock fall avalanche*.

Other slope movements involve rigid particle motions as components of their failure mechanisms, in conjunction with other processes such as sliding or distortion. Important among these are *topples* and combined *toppling- sliding* failures.

2.2 Rock Falls

Rock fall is ubiquitous in steep, rocky terrain. It is probably not the predominant transport agent even on steep mountain slopes, as shown by several comparative studies. For example, Rapp (1960) estimated that only about ten percent of the tonnage affected by slope movement in a northern Lapland locality could be attributed to rock fall, the remainder being snow and debris avalanche, debris slide and flow, while the average reach of rock falls was comparable or less than that of the other processes. But the significance of rock fall increases dramatically in local areas of steep gradient and fresh rock exposure and particularly in man-made cuts, where it becomes practically the only feasible type of slope movement if these slopes are stable overall.

Structures built on steep terrain, such as transportation routes, are subject to frequent interference by rock fall which causes damage either by direct impact or by creating obstructions which require to be cleared. The cost connected with such work is high. For example, the cumulative cost of maintenance of a highway cut may, over the life of the structure, exceed four times the cost of the initial excavation (Fookes and Sweeney, 1976).

The volume and weight of individual rock falls is inversely related to their incidence (Gardner, 1972) as is the case with many natural phenomena. While it is possible to prevent some of the larger instabilities in a given slope, others are too numerous to be treated individually and it is necessary to accept the risk of rock falls. Measures can then be undertaken to protect the endangered structure by stopping or diverting the falling blocks (Fookes and Sweeney, 1976, Peckover and Kerr, 1977), or by placing a sufficient distance between the structure and the cut wall. The effective design of such measures requires knowledge of the dynamics of rock fall movement, some aspects of which are discussed in the following.

It appears that the total horizontal reach of individual falling blocks generally increases with their size. This can be observed in rockfill dumps and talus slopes, where the largest blocks are usually found some distance beyond the toe of the deposit. Hadley (1964) mentions examples of large blocks which fell during the 1959 Hegben Lake earthquake and reached a valley floor highway far beyond the normal reach of talus debris.

Fig. 2.1 shows a typical profile of a rock fall triggered by the Friuli Earthquake in Italy (Govi, 1977). Large blocks (approx. 30 cu.m) travelled over the surface of talus, rolling amd bouncing, to reach a stable position at a travel angle of 28 deg. measured from the foot of the source cliff above. Photos show these blocks to lie quite isolated on the valley floor, since they reached considerably further than the smaller fragments composing the talus slope. On the basis of a number of similar observations, the Avalanche Group of the Norwegian Geotechnical Institute reports a provisional guideline for the estimation of the maximum reach of rock falls, shown as Fig. 2.2 (Lied, 1977). Although it is conceded that the actual distance travelled will depend on some terrain characteristics, the angles given should represent the maximum reach of single blocks in a fairly small rock fall.

Norwegian engineers counter the danger posed by large potentially unstable rock blocks by blasting them down with high fragmentation, so that the reach of the ensuing fall is

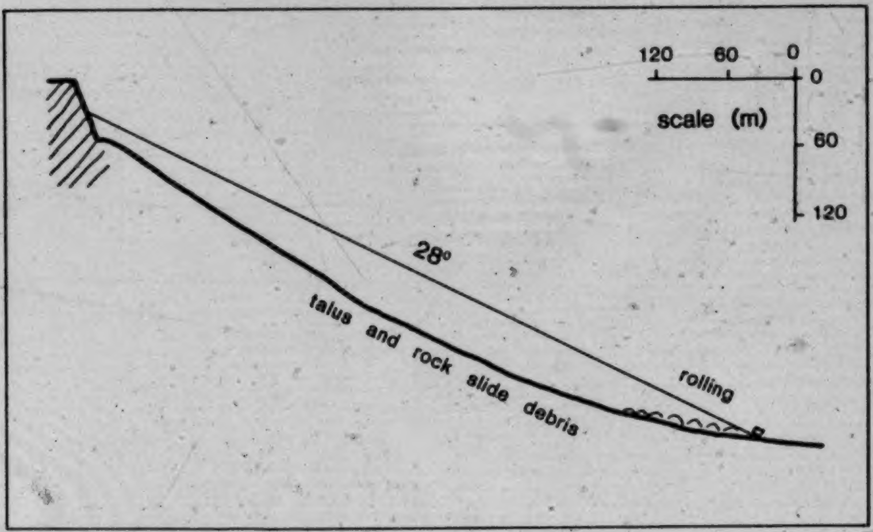
120
60
0
0
scale (m)
60
120
28°
talus and rock slide debris
rolling

Figure 2.1 Path of a 60 cu.m boulder (Govi, 1977).

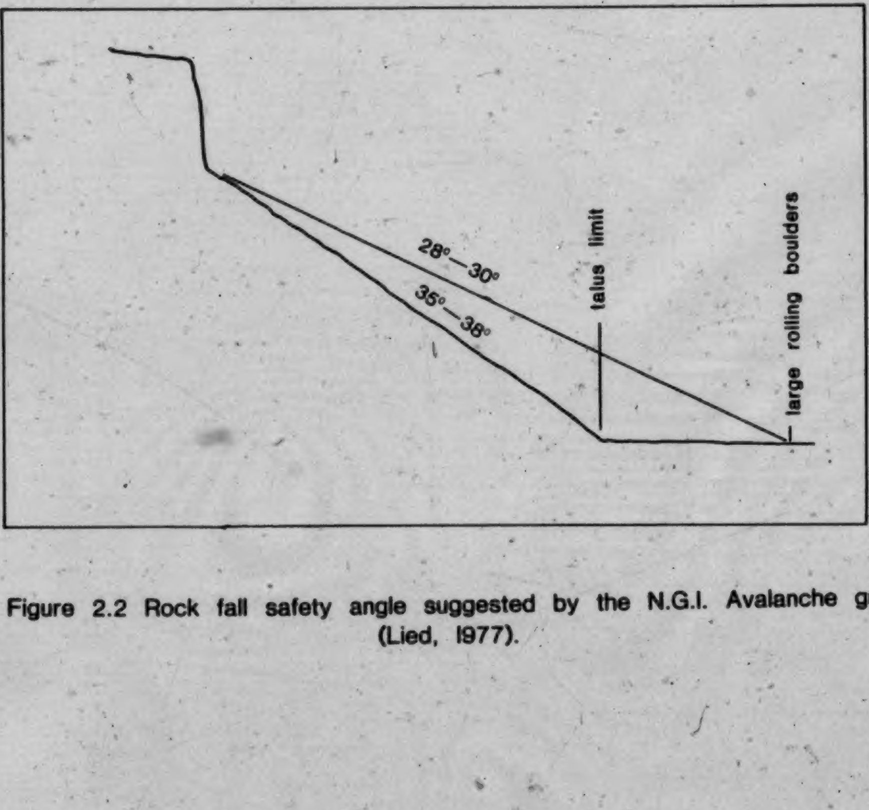
28°—30°
35°—38°
talus limit
large rolling boulders

Figure 2.2 Rock fall safety angle suggested by the N.G.I. Avalanche group (Lied, 1977).

less than if the block were to fall intact (Bjerrum and Jorstad, 1968).

This proportionality between size of blocks and length of travel is related to the mechanism of sorting of talus and it will be discussed further.

Ritchie (1963) conducted an extensive study of rock falls on quarry faces and highway cuts with the help of measurements and cinematography. A paraphrase of some of his general observations follows:

a. On steep slopes, rocks first begin their descent by rolling then, usually after one or two short bounces, continue by free fall in a trajectory.

b. Experience shows that most rocks will not accelerate in their rolling for a long distance on slopes flatter than 37 deg.

c. On impact, rocks seldom rebound very high but rather change their linear momentum into angular and begin to rotate and roll. An example is given of cliffs 27 - 40 m high and cut at 4 : 1 (76 deg.). Nearly all the rocks falling from this cliff made their initial impact within a 7 m wide fallout zone, but then rolled as much as 24 - 27 m from the base of the cliff. When intercepted by a 39 deg. inclined platform set at the edge of the fallout area, all the rocks were stopped.

d. Rocks that roll on 2 : 1 slopes (63 deg.) are given the greatest horizontal impulse.

e. Size and shape of a rock have little bearing on its falling or rolling characteristics, except in extremes of these two parameters. Larger rocks have a greater tendency to stay close to the cliff during their fall.

Some of these observations can be explained with the help of the theory of free fall and collision of rigid particles, the main formulas of which are summarized in Table 2.1.

If a nonrotating spherical particle impacts on a flat surface, over 70 per cent of its horizontal tangential velocity component will be preserved, even in a limited sliding impact (Eqn. 2.2, Table 2.1). Further, the first oblique impact of a particle on a rock wall will produce a negative angular velocity (Eqn. 2.5), which will help to conserve the horizontal velocity components resulting from subsequent impacts (Eqn. 2.2). Thus, it is concluded that 70 to 100 percent of the velocity component parallel with the surface will be preserved in any given impact.

As for the vertical component, however, this will be reduced in proportion to the coefficient of restitution, e. The rebound angle would therefore equal the incident angle, in a non-rotating impact, only if e was equal to 0.7.

Goldsmith (1960, p.258) reviews data showing that, for certain spherical stone particles, e might be approximately of that magnitude with initial velocities of up to 6 m/sec. Similarly, impact experiments carried out at ISMES in Italy

(A) FREE FALL TRAJECTORY EQUATION

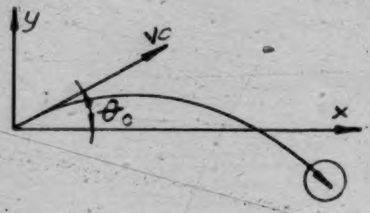

x, y	Cartesian coordinates
θ_o	initial travel angle.
v_o	initial velocity
g	granity acceleration

$$y = x \tan\theta_0 - \frac{g x^2}{2 v_0 \cos^2\theta_0} \quad \text{Eqn. (2.1)}$$

(B) IMPACT EQUATIONS (for a spherical particle)

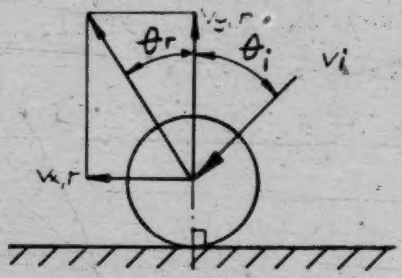

$$\tan\mu = \frac{2(v_i \sin\theta_i + R\omega_i)}{7(v_i(1+e)\cos\theta_i}$$

v_i	initial velocity
$v_{x,r}$, $v_{y,r}$	, x, y components of the rebound velocity
θ_i, θ_r	angle: incident, rebound
ω_i, ω_r	angular velocity: incident, rebound
R	particle radius
ϕ	angle of contact friction
e	coefficient of restitution
μ	controlling angle of sliding limitation

	limited sliding $\tan\phi > \tan\mu$	unlimited sliding $\tan\phi < \tan\mu$
$v_{x,r}$ =	$\frac{5}{7} v_i \sin\theta_i - \frac{2}{7} R\omega_i$ Eqn. (2.2)	$v_i \sin\theta_i - \tan\phi(1+e) v_i \cos\theta_i$ Eqn. (2.6)
$v_{y,r}$ =	$-e\, v_i \cos\theta_i$ Eqn. (2.3)	$-e\, v_i \cos\theta_i$ Eqn. (2.7)
$\tan\theta_r$ =	$-\frac{5}{7} \frac{\tan\theta_i}{e} + \frac{2}{7} \frac{R\omega_i}{v_i e \cos\theta_i}$ (2.4)	$-\frac{\tan\theta_i}{e} + \tan\phi\left(\frac{1+e}{e}\right)$ (2.8)
ω_r =	$\frac{2}{7}\omega_i - \frac{5}{7} \frac{v_i \sin\theta_i}{R}$ Eqn. (2.5)	$\omega_i - \frac{5}{2} \tan\phi(1+e) \frac{v_i \cos\theta_i}{R}$ Eqn. (2.9)

Table 2.1 Summary of rigid particle motion formulas.
(Goldsmith, 1960)

(Camponuovo, 1977) yielded e values in excess of 0.6 for rounded particles of "sound" rock some 20 cm in diameter. But it was noted that the same particles will break in such impacts when dropped from heights exceeding 1 - 2 m (corresponding to 4.5 - 6 m/sec. velocity), with a dramatic reduction in the restitution coefficient.

A further significant reduction results from irregular and especially angular shape of particles. Contact crushing, edge breakage and multiple point impact, all consume a large proportion of energy. This author would estimate that impacts of angular fragments on a solid rock surface have e values no greater than 0.1 to 0.3, even though rounded particles would reach 0.5 to 0.7 at moderate velocities and in small sizes that preclude breakage. In case of impacts on the surface of granular material such as talus or soil, e would of course be negligibly small.

The third of Ritchie's observations, stating that falling rocks tend to continue rolling rather than rebound very high, seems thus to be supported by impact observations and theory. Consequently, it would be reasonable to assume that the average impact of a rotationg rock fragment will conserve a large proportion of the tangential momentum component but only a small part of the normal one, with respect to the local orientation of the impacted surface (termed "impact shelf angle" in the rest of this section). The resulting motion of the particle will therefore occur nearly parallel to the impact shelf and include a large angular velocity, as shown in Fig. 2.3.

An example of the possible use of this collision model is given in the following: Eqn. (2.1) can be differentiated with respect to θ_0 in order to see which shelf angle will result in the longest trajectory for a given average slope angle. If it is assumed that a stone falls initially vertically and that after impact with the shelf a proportion c of its tangential velocity component is preserved (Fig. 2.3), it is found that the maximum trajectory length will result when θ_0 equals approximately $\alpha/2$ or if the shelf angle is about one-half of the average slope angle, irrespective of the actual value of c.

If such an optimal impact occurs, the horizontal trajectory length is given approximately as:

$$x = hc \tan\alpha \frac{\sin^2\alpha}{1+\cos\alpha} \qquad \text{Eqn. (2.10)}$$

where c is equal to, say, 0.8 on the basis of the previous discussion; and h is the height of the free fall preceeding the impact.

The vertical trajectory length:

$$y = x \tan\alpha \qquad \text{Eqn. (2.11)}$$

is found from Eqns. (2.10) and (2.11) to be equal to h for an angle α of 43 deg. It can further be shown from the trajectory equations that if optimal impact shelf angles continue to present themselves, each subsequent bounce of a stone falling at this particular average slope angle will

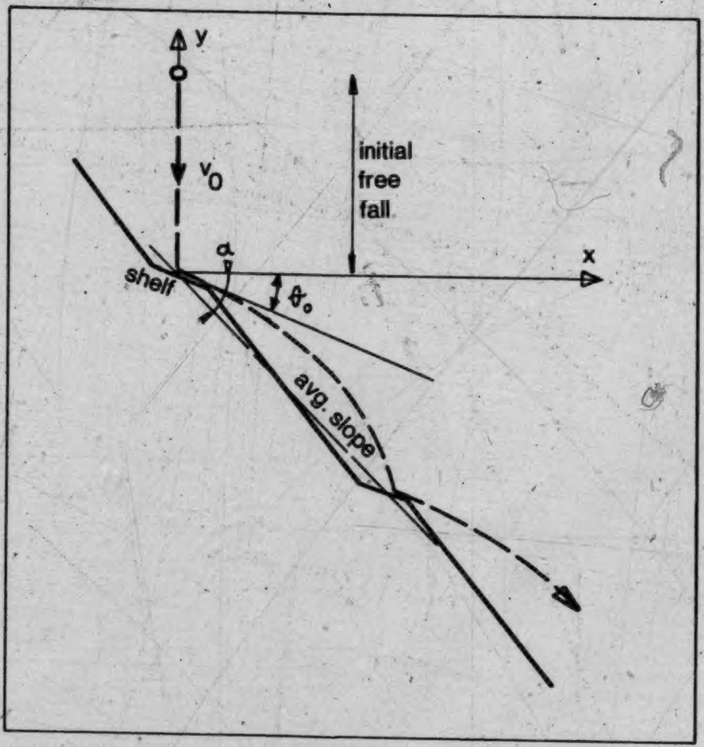
y
v_0
initial
free
fall
x
α
ϑ_0
shelf
avg. slope

Figure 2.3 Trajectory of a rock fragment after a fall on a shelf in the slope.

receive approximately the same amount of tangential impulse. Therefore, each trajectory will be nearly of the same length as the previous one, or shorter if the impact shelf angle is not optimal. The calculated value of 43 deg. is not much different from 37 deg. cited by Ritchie as the slope angle at which "most rocks stay put on the slope" and do not accelerate.

Further refinement of the theory of falling rock fragments can only be acheived by considering the statistical aspects of the phenomenon, i.e. the distribution of initial directions and velocities and especially the distribution of inclinations of asperities at the points of impact. This was considered by Piteau and Clayton (1977) who developed a computer model simulating rock trajectories on a slope of an arbitrary shape. In their model, impact conditions are approximated by equating the rebound and incident angles and there is a provision for perturbing the local asperity inclination (shelf angle) around the average slope angle. The output from the model is in the form of a histogram of stone landing frequency versus distance from the toe of the slope.

Hacar- Benitez et al (1977) described a similar computer model based on the impact equations given in Table 2.1, which can also account for an arbitrary slope shape but does not incorporate any statistical considerations. It is understood that comparisons of the results of such analyses with field experiments have been made. But so far none have been published.

An empirical approach was favoured by Kirkby and Statham (1975) who analysed the mobility of loose particles over the surface of scree slopes. The results of their measurements of travel distances of stones droped onto inclined surfaces covered by grains offer several further general observations:

The average length of downslope travel of a given stone is proportional to its height of drop. Thus, the downslope movement could be described in terms of a pseudo-frictional model, in which the resisting force is constant and independent of velocity. This model also assumes that the tangential (downslope) component of the free fall velocity is fully preserved, but the coefficient of restitution e equals to zero. This concurs with the foregoing discussion.

The travel distances for individual trials from a given height are distributed exponentially, indicating a constant probability for stopping at any interval of the inclined path.

The apparent dynamic friction angle controlling the motion of a stone down the slope increases in linear proportion with the increase of the ratio of diameters of the free particle to those which make up the inclined surface.

Eqns. (2.2) and (2.3) (Table 2.1) prove that, in a highly inelastic impact when e approaches zero, the loss of momentum increases sharply as the angle of the impacted surface becomes more perpendicular with respect to the direction of particle travel. When it is in fact perpendicular, all momentum is lost and the particle becomes trapped. A particle rolling over a slope of loose scree experiences an infinite variety of impact angles, and the probability of its being stopped in any given contact with the slope is constant, as evidenced by the second of the above observations. On the average it may take a certain number of contacts, n, before the trapping conditions are encountered. It could be assumed that the average n is independent of the height of drop. But the length of the trajectories between impacts increases linearly with height. Thus one finds on average a linear relationship between the height and downslope travel, as given by the first observation.

Finally, the dependence of the dynamic angle of friction upon diameter ratio is explained by the scale effect on slope roughness. A small particle rolling over a bed of larger ones will encounter a much greater range of impact angles than if the situation were reversed. A larger particle will have a tendency to travel over finer materials and lodge among fragments of its own size, causing grading of the deposit (Ritchie, 1963, Kirkby and Statham, 1975).

Statham (1976) also reports a weak shape sorting in some talus deposits, increasing average particle roundness being found at greater distances downslope.

A conclusion derives from the several foregoing paragraphs, that on scree slopes fragments which are larger and more round exhibit a greater mobility. This is in disagreement with observation (e) of Ritchie, stating that size and shape of stones have little effect on their motion. This is probably a result of the fact that the inherent range of asperity inclinations is much less on a solid rock face compared to a talus slope consisting of discrete fragments. The scale effect is therefore less strongly defined in the former case. Ritchie's observation that larger rocks tend to stay close to the cliff face, however, may be a reflection of the scale effect. The flat trajectory of such particles implies a small range of effective asperity inclinations. The resulting impacts have large tangential components and preserve much of the particle's momentum.

Large acceleration of falling stone movement may occur when a block rolling with a high angular velocity disintegrates. Theoretically, the resulting fragments may be catapulted at twice the velocity of the parent block. This is what may have caused the incredibly high launching velocities of boulders involved in the Huascaran rock avalanche of 1970, some of which had free flight trajectories 4 km long and moved at close to 1000 km per hour (Plafker and Ericksen, 1978).

2.3 Topples

Toppling is understood here as angular motion initiated from a stable condition, in contrast to rolling which refers to angular motion generated by a preceding fall or slide. Toppling motion of a discrete particle therefore requires an initiating impetus to occur, either in the form of a lateral thrust (by impact of another particle or by water, ice or wind forces) or of a loss of restraint through a foundation failure by shear or crushing. Thus, the pre-failure mechanism of toppling is usually connected with that of another process, which determines its rate.

For example, the observed movements of the 30 m high Threatening Rock in New Mexico (Schumm and Chorley, 1964) indicate a long period of drained creep of the shale foundation preceding the final catastrophic collapse of the sandstone cliff. The creep had been observed for six years, its average rate increasing exponentially with time. An extrapolation of this exponential trend into the past led the authors to estimate the time of onset of movement as about 2500 years before the final collapse, which took only seconds. Eyewitness description of the toppling failure comprises initial leaning out, rapid settlement, partial disintegration and a final pivoting movement on the outer edge of the block's base. All of these kinematic features suggest a classical circular shear foundation failure.

The failure phase of cliff toppling can be analyzed by the following simple model. It is at first assumed that the entire cliff topples on its foundation, as shown in Fig. 2.4a. The angular velocity of the rotational movement can be found by equating the terms for potential energy lost, E, and kinetic energy gained, K:

$$E = A\rho g \frac{h^2}{2} (1 - \sin\alpha) \qquad \text{Eqn. (2.12)}$$

$$K = \frac{1}{6} A h^3 \rho \omega^2 \qquad \text{Eqn. (2.13)}$$

where A and ρ are the base area and density of the block. From these two equations, the angular velocity ω equals:

$$\omega = \sqrt{3g(1 - \sin\alpha)/h} \qquad \text{Eqn. (2.14)}$$

Radial centrifugal acceleration at the top of the block is ω^2 h, which increases with the inclination angle There is a point where this acceleration will exceed the radial component of gravity acceleration, g sin α . At this point, the uppermost layers of the rock block will separate from the remainder along joints and pass into a free flight trajectory. The block is inclined at 48 deg. at this point. The detached mass has a horizontal velocity component equal to ω h, or $0.65\sqrt{gh}$ and a vertical component $0.75\sqrt{gh}$. Further vertical velocity increase, equal to about $1.4\sqrt{gh}$, will occur during the free flight prior to impact onto the lower slopes of the mountain (Fig. 2.4a). The tangential (downslope) component of the impact velocity will therefore

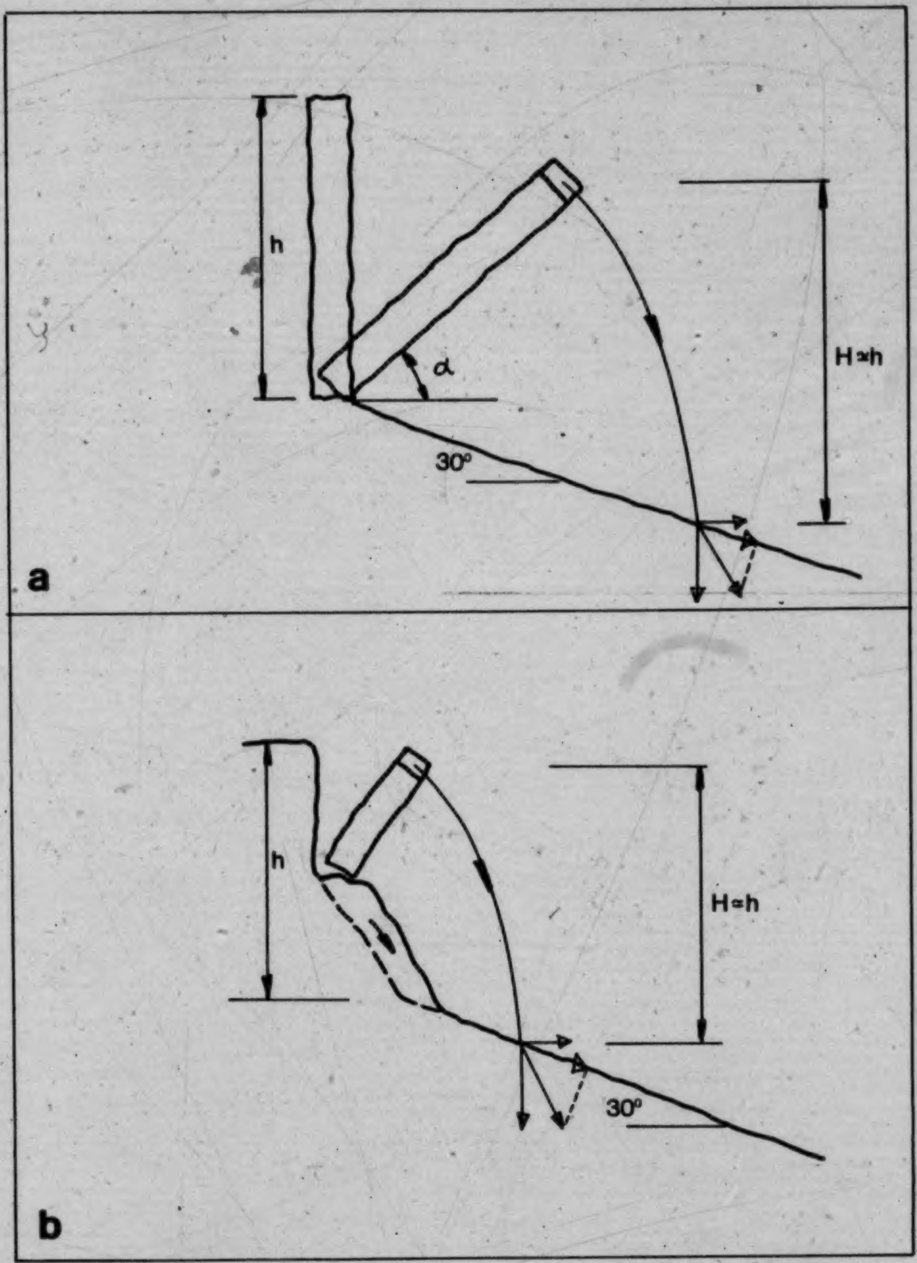
h
α
30°
H≈h
a
h
H≈h
30°
b

Figure 2.4 Kinematics of a full (a) and partial (b) cliff toppling failure.

equal $1.6\sqrt{gh}$, much of which may be conserved. It can be shown that the result would change little if only the upper half of the cliff toppled, as shown in Fig. 2.3b. The use of these formulas is illustrated in Section 10.1.

More complex mechanisms and geological configurations leading to the onset of toppling are listed and classified by Goodman and Bray (1976).

De Freitas and Watters (1973) stress examples in which toppling combines with sliding movement in the kinematics of a jointed rock mass. Within a failing slope they distinguish a rigid zone, where individual blocks do not move in relation to each other, a toppling-sliding zone where they rotate and slide and a sliding zone characterized by translatory motion which often forms a restraining block at the toe of a stack of toppling slabs.

The rate of such complex movements is obviously controlled by the time variation of stability related factors, such as pore pressures and strength of both the intact material and discontinuities. An important notion to consider, however, is that initial movements in a combined toppling-sliding failure carry the tilting blocks further out of their equilibrium position, thus increasing the propensity towards a sudden and rapid failure, without the need for a brittle decrease in shear strength. Citing the results of Ashby, De Freitas and Waters point out that in model experiments:

> "...toppling gradually developed over an initial rotation of a few degrees but at a certain angle a critical combination of angles and displacements can exist in the toppling mass which permits it to move very rapidly down the slope."

They mention examples of coastal slope movements in Devon, the development of which is measured in years, while the final "complete" failures occur within 24 hours. No specific records of the time development of velocities in a sliding- toppling failure have been found in the literature.

Hammett (1974) developed simple equations of overturning equilibrium for single and multiple rectangular blocks. Neglecting the weight of the blocks, he also notes that the toppling mechanism has a brittle character, in that the ratio of tangential to normal applied forces on the system decreases with increasing inclination of the blocks. For a single block, the ratio would diminish to zero when the inclination of the block exceeds the equilibrium value. When several blocks are in a frictional contact, however, the rotation is limited to the angle equal to the frictional angle of the intervening joints. At this angle, a stabilizing effect results and further motion would occur by direct shearing. But the mass overlying the system of tilting blocks may have acquired a significant amount of momentum by this time and a catastrophic failure may ensue. The brittle effect increases in importance with increasing height to width ratio of the blocks. It is inversely affected, on the other hand, by the number of blocks placed side by side. Consequently, kink bands composed of a large number of thin vertical laminae will not exhibit brittle behaviour, unless the joint frictional characteristic is brittleness. A shallow, ductile failure dominated by an extensive kink band in vertically laminated phyllite was observed in France (D.M. Cruden, pers. comm.)

Hammett's equations could be used to calculate the apparent shear strength of a band of toppling blocks, and its variation with displacement, which could be used as input into a conventional frictional block analysis to calculate accelerations and velocities. The same can be achieved for complex geometries using the computer-based "discrete element method" (Cundall, 1971, 1976) which is also capable of modelling some features of particle interaction, such as contact stiffness.

3. SLIDING MOVEMENTS

3.1 Introduction

The process of sliding is defined by Varnes(1978) as comprising

> "shear strain and displacement along one or several surfaces that are visible or may reasonably be inferred, or within a relatively narrow zone".

The presence of a displacement discontinuity is not implied in this definition and the character and thickness of the sliding zone is unspecified. For the purpose of a mechanical analysis it is sufficient to understand sliding as the movement of a relatively undistorted portion of the slope mass on one or several limited zones of concentrated shear straining. Thus the problem is kinematically simplified into one of rigid-body mechanics, coupled with the rheology of the shear zones. The latter aspect becomes increasingly important in the analysis when the sliding zone is thicker in proportion to the overall dimensions of the landslide, and the boundary between slides and flows is not quite distinct.

Nearly every slope movement includes an episode or element of sliding. Consider, for example, the combination toppling- sliding movements (De Freitas and Watters, 1973), *earth flows* which often move predominantly by marginal shearing (Skempton and Hutchinson, 1969) and *debris flows*, some of which initiate as surficial slides (Rodine, 1974).

Those types of slope movement that are dominated by the sliding mode of motion are commonly placed into the categories of *rotational slides* (slumps) and *translational slides* and occur in all types of material. In order to illustrate the variety of phenomena which may be characterized as sliding, the following review is presented of the classes of sliding movement proposed by Varnes (1978), with typical examples of failure and post- failure behaviour.

Rock slumps with rotational type of motion are uncommon, since rock sliding is generally controlled by planar weakness features or discontinuities. Rotational failures develop only where the discontinuities are favourably oriented for such a geometry to occur, or where the rock mass is so highly jointed or decomposed that it resembles a granular material in its mechanical character (Hoek & Bray, 1977). An example of the former case was described by Hamel (1972) from a location called Brilliant Cut in Pennsylvania. Here, a 50m high cliff separated along a deep vertical joint and slumped on a basal circular surface. (Fig. 3.1a). The movements built up over the period of at least three years, while the vertical crest joint opened gradually to approximately 0.4m. Then a sudden large movement developed overnight, (probably rapidly) and the head of the slide sank by 5 m and came to a stop. Excavation was carried out at the toe and the slide mass continued to

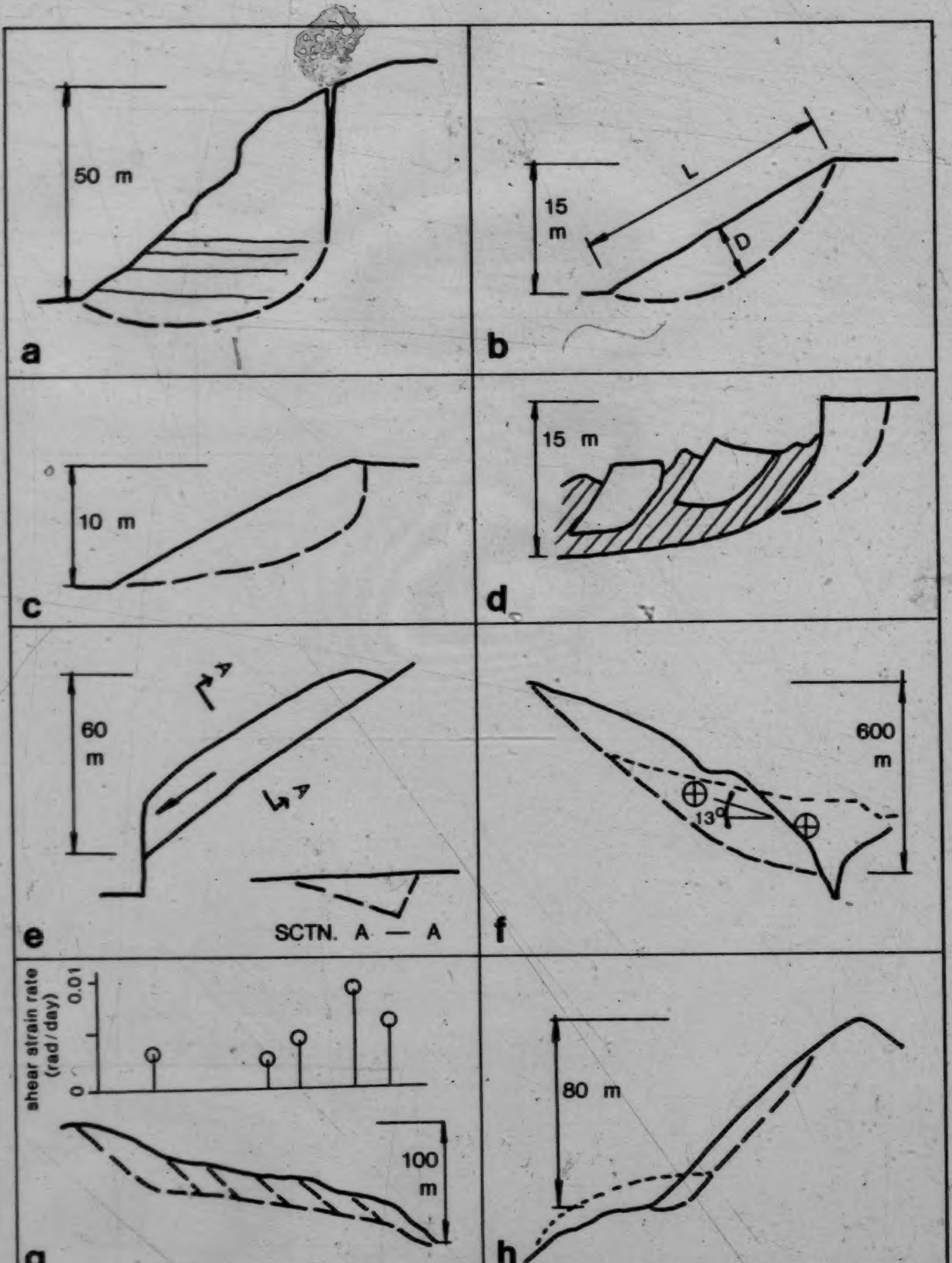
50 m
a
15
m
L
D
b
10 m
c
15 m
d
60
m
A
A
SCTN. A — A
e
600
m
13°
f
shear strain rate
(rad/day)
0.01
0
100
m
g
80 m
h

Figure 3.1 Crossections of typical slides and slumps.

move proportionately to the amount of material removed. Equilibrium was re-established after removal of 84 000 cu. m, or more than half of the total volume of the slide. Stability analysis carried out by Hamel indicated that peak frictional resistance must have been mobilized prior to the first movement. The initial acceleration was therefore probably due to the drop of the restraining forces to the residual condition. The steady movements experienced afterwards, on the other hand, involved constant residual friction.

Earth slumps, or rotational failures in fine-grained soils, occur in relatively homogeneous deposits such as deep clay layers or man-made fills. The depth of sliding is characterized by the depth ratio D/L (Fig. 3.1b and Skempton and Hutchinson, 1969). Experience shows that the depth ratio tends to be greater in soils of low consistency (Zaruba & Mencl, 1969), although this may be much affected by nonhomogeneity. The thickness of the sliding zone and the rapidity of movement are highly variable.

S. D. Wilson in his Terzaghi Lecture (1970) commented that he was unable to find complete observational data from a circular failure in a natural slope. Many case histories exist, but the bulk of the observed data relates to the stability aspects of the slides.

An example of a rotational slide in lightly overconsolidated, insensitive intact clay is the failure of the Lodalen railway cut (Sevaldson, 1956, and Fig. 3.1b).

The head of this slide is known to have sunk by 1.6 m in less than one hour, to find new equilibrium. The sliding zone consisted of less than 35 cm of highly remoulded clay of increased moisture content, surrounded by shear-generated fissures. The sensitivity of this clay is 3.

Slides in fissured overconsolidated clays tend to be noncircular, possibly due to the increased rate of softening in the back scarp (Skempton and Hutchinson, loc.cit.), although sometimes they retain a rotational character. An example is the Northolt cutting (Fig. 3.1c) described by the same authors. This is a delayed failure manifested by a very gradual slumping of the slope crest and bulging at the toe, which developed over a period of approximately one year, twenty years after steepening of the slope. The movement was halted by installation of drainage.

A radically different behaviour is displayed by rotational failures in highly sensitive clays. Small failures of this type rapidly slump on a highly curved surface far beyond their original equilibrium positon, leaving a steep exposed scarp prone to retrogressive sliding. This behaviour leads to the development of the extensive retrogressive "quick clay" sliding and subsequent flows of large quantities of remoulded material (Mitchell and Markell, 1974 and Fig. 3.1d). The behaviour and size of the initial slide is often unknown as all of its evidence is obliterated by the subsequent flow. There is little doubt, however, that it is a very rapid type of slope movement.

This is confirmed by eyewitness reports from Selnes, Norway (Kenney, 1969), which describe the initial slide as very rapid and accompanied by noise. This particular slide was preceded by a gradual development of tension cracks, over a period of at least three weeks. The subsequent retrogressive slides, which also have the character of rotational slumps, are equally rapid as described by eyewitnesses at St-Jean Vianney, Quebec who mentioned ground and houses "sinking" from sight, presumably in a matter of seconds (Tavenas et al.,1971).

Translational movements (slides) are more common than slumps in natural materials. *Block slides in rock* are characterized by simple geometry and mechanics and occur in naturally or artificially undercut cliffs where favourably oriented discontinuities exist. A typical wedge slide has been described by Hamel (1976) from the site of Libby Dam in Montana (Fig. 3.1e). A wedge of Precambrian argillite approximately 33 000 cu. m in volume slid on a bedding plane into an excavation. Its movements had been observed for four years prior to failure, using an extensometer. During this period approximately 5 cm of downhill displacement occurred. Of this 40 percent took place during the excavation, further 50 percent in three abrupt step movements and only less than 10 was due to steady creep. The failure movement took less than 41 seconds as determined by seismic records, but amounted to only 3.5 m as a result of restraint presented to the moving mass by the base of the excavation. The moved slab was only slightly broken.

The well known disaster at Vajont, Italy (Mueller, 1964, 1968), can be also classified as a rock block slide (Fig. 3.1f), although the bi-planar nature of the failure surface requires internal deformation during sliding (Mencl, 1966). The movement involved approximately 240 M cu. m of rock and occurred largely along bedding planes in Jurassic limestones with clayey intercalations.

According to Mueller (1964), the movements of this landslide developed mainly in three episodes, each corresponding to a period of raising the level of the Vajont dam reservoir. The movement was identified shortly after the first raising of the water level and reached an average of 3 cm per day but decelerated quickly when the level was lowered. The subsequent flooding substantially exceeded the previous maximum. Again, the movements decayed rapidly when the water level was brought down. The third period of filling exceeded the previous level only slightly. Movements again started in a similar manner to the previous two cycles and the water level was gradually lowered. But this time the movements quickly accelerated. The previous maximum rate was exceeded approximately a week before the failure and during the last few days about 20 cm per day was observed. Failure started when the total displacement on the sliding zone was close to 5 m. During the failure, the masses displaced up to 340 m horizontally and reached a velocity of 25 - 30 m per second according to estimates. The rock strata remained relatively undisturbed, although it contracted in length by 13 - 16 percent and expanded in thickness from 200 to 260 m (30 percent). The approximate angle between the centers of gravity of the displaced mass before and after failure is 13.5 deg. (measured on profiles compiled by Broili, 1964). Static limit-equilibrium analyses by various authors indicated that the average friction angle of the sliding plane must have been between 17 deg. and 28 deg. at the onset of failure. Dynamic equilibrium analysis based on calculation yielded a necessary friction coefficient of approximately 6 deg. (Jaeger, 1979), and based on model tests even 3 deg. (Mueller, 1968), to account for the estimated final velocity of the slide.

The category of *earth block slides* includes the translational failures in overconsolidated clays and clay shales, which are perhaps the most wide spread and best documented slope movements in temperate climates. They generally develop as delayed failures (Skempton. 1964) and are often compound or retrogressive (Mollard, 1977). Their movement histories are quite complex both in space and time. For example, Thomson and Hayley (1975) interpreted the Little Smoky River landslide in Alberta as consisting of a number of distinct blocks, separated by shear zones (Fig. 3.1g). The horizontal movement velocities vary with location within the slide as indicated by a velocity diagram shown in the illustration. "Intermediate" movements can be observed between individual blocks, both by inclinometer and on the surface. The main horizontal sliding zone is in clay shale and is approximately 3 m thick. The movements are obviously of ancient origin and are proceeding slowly enough (15 cm per year maximum) to permit minor periodical adjustments to a bridge abutment located adjacent to the toe of the moving mass. The existence of instability can be explained by calculating the equilibrium of each of the individual blocks, using residual friction values.

This type of landslides usually exhibits slow and intermittent movements. Most of the existing displacement records therefore relate to ancient events, while records of movement initiation in fresh ground are rare. An initial movement or a new retrogression extending into an undisturbed material may occur with considerable rapidity. For example, the Edgerton slide (Thomson and Tweedie, 1979) developed a 15 m high scarp and a graben within less then two days, thus initiating what may be a long period of slow movements.

The movements occurring after this initial rapid period should therefore be considered as post failure movements. Their velocity is often strongly controlled by the amount of precipitation. For example, the slide of highly weathered volcanics at a property of a zoo in Portland, Oregon moved a maximum of 57 cm in eight years, of which approximately 50 cm took place in eight step movements, each lasting less than a month and coinciding with a period of high precipitation (Radley- Squier and Versteeg, 1971). Sometimes a moving landslide of this type reaches a temporary equilibrium condition, but resumes movement in response to a very slight disturbance. A part of the very large Portuguese Bend Landslide in California was re- activated by the placement of a minor amount of fill near the crest and assumed a precipitation controlled movement regime with a maximum velocity of 2.5 cm per day (Wilson, 1970).

Slow, stable displacements also characterize slides in low grade schists. Huder (1976) and Zacas (1977) both reported cases of large scale movements in such materials, continuing at steady rates of less than 0.3 m/year for long periods of time. The Downie slide (Piteau et al., 1978) and several other cases in the interior of British Columbia appear to belong into the same category. The ductile behavior of these events is in contrast to the brittle failure of Vajont.

The translational geometry is not confined to overconsolidated clays and rocks. It occurs in the most rapid type of slope movements, associated with collapse or liquefaction of loose or sensitive soils. Some of the "quick clay" flows initiate as block slides. For example that at Furre, Norway displayed the usual retrogressive character, but moved in blocks on a thin layer of sensitive clay (Hutchinson, 1961). The total displacement of the central portion of this slide was 90 to 150 m and the movement lasted about 1 to 1.5 min on a slope of 1 : 4.

A similar mechanism characterizes a variety of *debris slides*. These originate in loose pervious soils upon sudden flooding, saturation or increase in pore pressure, which causes initial shearing followed by a contraction or collapse of the loose structure of the soil and consequent sharp decrease in effective stresses and rapid displacements. To this category belongs the important group of shallow slides in residual soil, exemplified here by the Canaleira slide near Santos, Brazil (Vargas and Pichler, 1957 and Fig. 3.1h). At this location a thin (approx. 5 m) mantle of residual soil slid on a 42 deg. slope over the underlying weathered igneous bedrock and moved to the base of the hill with sufficient rapidity to demolish completely several structures.

Even more mobile are shallow slides in colluvium blankets of mountain slopes. Such slides represent one of the alternative agents responsible for the origin of debris flows (Johnson, 1970). Sometimes, the material is in a sufficiently loose state to liquefy as a result of pore pressure increase during initial shearing, as observed in the head regions of small debris flows by Johnson. A similar phenomenon occurs in uncompacted mantle fills and will be further discussed in the chapter dealing with flows.

Skempton and Hutchinson (1968) presented tables of typical velocities of pre- failure and post- failure clay slides. A similar compilation is shown in Table 3.1, which lists average or peak velocities obtained in the course of

Case	dominant material	volume (m^3)	velocity estimate	basis for estimate	source
A. ROCK SLUMPS					
Brilliant cut	clay shale	150,000	0.4 m/h [6]	5 m slump overnight	Hamel (1972)
B. SENSITIVE CLAY SLUMPS					
Selnes	sensitive clay	140,000 [4]	1 m/sec [6]	some m in a few sec	Kenney (1967)
St.-Jean Vianney	sensitive clay	6,900,000 [4]	1 m/sec [6]	some m in a few sec	Tavenas et al (1971)
C. SLUMPS IN INTACT N.C. OR LIGHTLY O.C. CLAY					
Lodalen cut	clay	10,000	1.6 m/h [1]	1.6 m slump in 1 hour	Sevaldson (1956)
King's Lynn embankment	alluvial clay	20,000	0.3 m/h [1]	1.25 m slump in 4 hours	Wilkes (1972)
NBR embankment	soft clay	50,000	4 m/h [1]	2.1 m slump in 1/2 hour	Dascal et al (1972)
Itaipoo lagoon	organic clay	160	19 m/h [2]	measured slump	Sandroni (1980)
D. SLUMPS IN OVERCONSOLIDATED CLAY					
Northolt cut	O.C. clay	7,000	1 m/year [1]	some feet in 1 year	Skempton et al (1969)
Muirhead dam	boulder clay fill	100,000	18 m/year [2]	0.15 m in 3 days	Bishop (1973)
E. SLUMPS IN LOOSE SAND OR FILL (INITIAL TO FLOWS)					
Aberfan	shale waste	100,000	4-8 m/sec [3]	eyewitness	Bishop (1973)
Fort Peck dam	sand fill	8 M	2.4 m/sec [3]	1,400 ft in 3 min	Casagrande (1971)
F. ROCK BLOCK OR WEDGE SLIDES					
Libby dam (prehistoric)	argillite	2 M	21 m/sec [1]	analysis	Voight (1979)
Libby dam (1967)	argillite	33,000	0.4 m/sec [1]	4.5 m in 40 sec	Hamel (1976)
Vajont	limestone with clay seams	300 M	30 m/sec [2]	wave analysis	Mueller (1968)
G. SENSITIVE CLAY SLIDES (INITIAL TO FLOWS)					
Furre	sensitive clay	3 M	2.5 m/sec [3]	eyewitness	Hutchinson (1961)
Toulnoustonck	cemented silt	4 M	2.5 m/sec [3]	300 m in	Conlon (1966)
H. SLIDES IN OVERCONSOLIDATED CLAYS					
12 slides in California	tertiary clay	40,000 to 500,000	0.01 to 0.04 m/year [5]	inclinometer	Gould (1960)
Handlova	clay colluvium	14.5 M	0.25 m/h [2]	surveys	Zaruba and Mencl (1969)
Edgerton	clay shale		0.3 m/h [6]	16 m slump in 2 days	Thomson and Tweedie (1978)
I. SLIDES IN RESIDUAL SOIL OR LOOSE FILL (INITIAL TO FLOWS)					
San Mau Ping	res. soil fill	few thousand			Lumb (1969)
Ikuta	loam fill	570	20 m/sec [2]	analysis	ENR (1971)

NOTES: 1) average velocity
2) peak velocity
3) velocity of a flow subsequent to initial sliding
4) retrogressive slide
5) may not include any initial failure movements
6) lower limit estimate; movement was not observed

Table 3.1 Typical failure velocities of sliding movements

ONLY COPY AVAILABLE
SEULE COPIE DISPONIBLE

the initial failure motion. The table contains cases belonging into each of the various groups of sliding, defined by Varnes (1978) (Table 1.1). It has been divided according to this grouping, with an added subdivision to account for the fundamental differences in the mobility of slides in sensitive, soft and overconsolidated clays. The resulting categories, denoted by letters A to I in the table, appear relatively uniform in terms of velocities attained, while they are uniform by definition in terms of geometry and material character. In Table 3.2, they are correlated approximately with Varnes' classification, including a simplified mobility scale. The most mobile classes are connected with contractant material such as sensitive clay and loose granular soil. On the other hand, slides in dilatant material such as overconsolidated clay are among the slowest. This indicates that pore pressure changes during movement are a primary factor in determining slide mobility.

Some of the groups shown in Tables 3.1 and 3.2 have a strong regional significance, for example the sensitive clay slides initial to "quick clay" flows of Eastern Canada and Scandinavia. Others have a geographical context, such as the residual soil slides of humid, mountainous subtropical countries.

The suggested groups constitute a convenient framework for discussion of the analytical and quantitative aspects of sliding movements discussed below.

classification (Varnes, 1978)		VERY RAPID INITIAL TO FLOW	VERY RAPID	MODERATE TO SLOW	SLOW
ROTATIONAL SLIDES	ROCK			rock slumps	
	EARTH	sensitive clay slumps		slumps in intact N.C. clay	slumps in fissured O.C. clay
	DEBRIS	slumps in loose saturated sand or fill (mining waste)			
TRANSLATIONAL SLIDES	ROCK		rock block or wedge slides		
	EARTH	sensitive clay slides		slides in overconsolidated clays*	
	DEBRIS	slides in residual soil, colluvium and loose fill			

*including clay shales and weathered schists

Table 3.2 Main groups of sliding movements identified in the survey of literature

3.2 Equation of Motion

With the definition of sliding presented at the beginning of this chapter, it is possible to apply the equations of rigid body motion to either the whole or to individual parts of a sliding mass. The driving forces include the effects of gravity and minor phenomena such as water pressure in the tension crack or inertial forces due to earthquake acceleration. The resisting forces result from the frictional and cohesive resistance acting on the base or the mass.

The simplest geometrical configuration is that of a rigid block of a weight W, whose sliding on a planar surface inclined at an angle to the horizontal is resisted by a restraining force T (Fig. 3.2a). Assuming that the shear zone is well developed and has already been subject to a certain amount of displacement, the restraining force corresponds to the residual strength:

$$T = (W\cos\alpha - U)\tan\phi_r \qquad \text{Eqn. (3.1)}$$

where U is the uplift force due to any neutral pressure present in the sliding zone and ϕr is the residual friction angle as defined by Skempton (1966).

If M is the mass of the block and assuming gravitational driving forces only, the Second Law of Motion gives the acceleration:

$$a = \frac{1}{M}(W\sin\alpha - T) \qquad \text{Eqn. (3.2)}$$

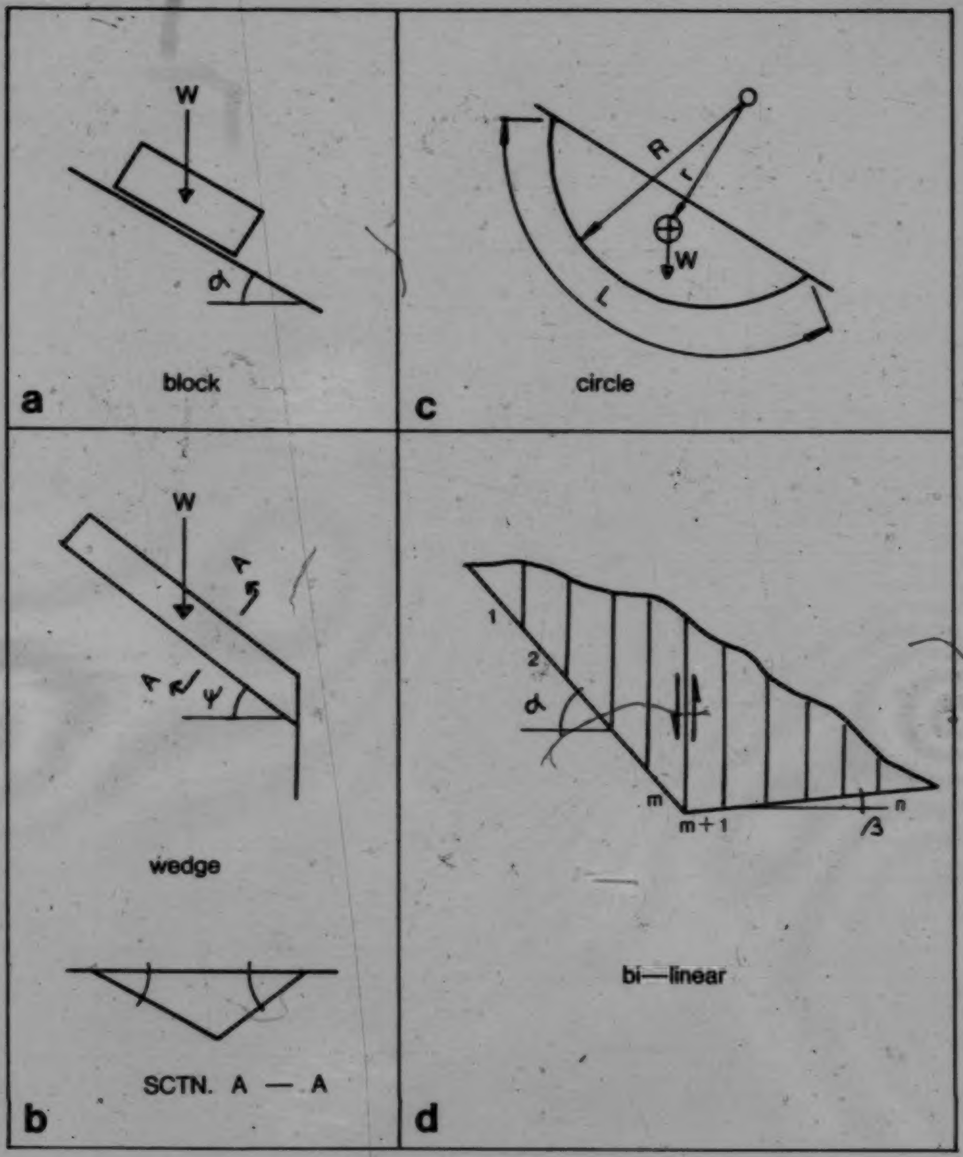
W
α
block
a
R
r
W
L
circle
c
W
A
A
ψ
wedge
SCTN. A — A
b
1
2
α
m
m+1
n
β
bi—linear
d

Figure 3.2 Analytical models for sliding.

or, substituting for T:

$$a = g\left[\sin\alpha - \left(\cos\alpha - \frac{U}{W}\right)\tan\phi_r\right]$$ Eqn. (3.3)

Alternatively, using total stress analysis based on the value of undrained residual strength, (Cu)r (Bishop, 1967):

$$T = A\,(c_u)_r$$ Eqn. (3.4)

(A is the base area of the block)

$$a = \frac{1}{M}\left[W\sin\alpha - A\,(c_u)_r\right]$$ Eqn. (3.5)

The onset of sliding is brought about by the reduction of the restraining force to the value corresponding to the peak strength of the shear zone, Tp. Thus, at this moment the driving force equals the restraining force:

$$W\sin\alpha = T_P$$ Eqn. (3.6)

Substituting into (3.2):

$$a = g\sin\alpha\,\frac{T_P - T}{T_P}$$ Eqn. (3.7)

If the slicing block is truly rigid and one can assume simultaneous mobilization of strength on the base, then it is possible to express Eqn. (3.3) in terms of shear stresses: $\tau_P = T_P/A$ and $\tau = T/A$. where A is the base area of the block. Then:

$$a = g\sin\alpha\; I_b$$ Eqn. (3.8)

where $I_b = \frac{\tau_p - \tau}{\tau_p}$ is the "Brittleness Index" defined by Bishop (1967) as a measure of the potential mobility of a given material under given loading and drainage conditions. Table 3.3 lists a few values of the index obtained from laboratory determinations of peak and residual strengths of various materials. For the sake of illustration, the table also shows the velocities which would be predicted by an integrated form of Eqn. (3.8)[3] for a block sliding for 10 m on a slope of 20 deg. The velocity is dependent on the square root of Ib and it therefore increases very rapidly with the smallest values of the index. In fact, according to this model, the given landslide would reach the "extremely rapid" velocity class in 10 m (3 m per second) with Ib equal to only 0.13. However, such direct application of the brittleness concept is not satisfactory for quantitative analysis for the following reasons:

a. the laboratory peak strength may by different from the strength mobilized in the field, due to the effects of scale, rate of testing, sampling disturbance or progressive failure

b. the residual strength is not a constant but a variable dependent on the magnitude and rate of displacement

---

[3] The integration was carried out assuming a full strength drop to residual immediately upon failure, to obtain

$$v = \sqrt{2 g d \sin\alpha \, I_b} \qquad \text{Eqn. (3.9)}$$

where d is the sliding distance.

material	drainage condition	I_B	slide velocity* (m/sec)
loose sand	drained	0.03	1.4
loose sand	undrained	0.65-0.94	6.6-8.0
London clay	undrained	neg. to 0.63	0 -6.5
boulder clay	undrained	0	0
"quick" clay	undrained	0.97	8.2
slate cleavage	dry	0.52	5.9
joints in porphyry	dry	0.1-0.46	2.6-5.6
sl. rough lim. bedding	dry	0.21-0.52	3.8-5.9

*calculated by Eqn. (4.9) for a 10 m long slide on 20 deg. slope.

Table 3.3 Some laboratory-determined values of the brittleness index and velocity predictions using the simple model

(Lab. data obtained from Bishop, 1973 and Goodman, 1970)

c. drainage conditions during sliding may be intermediate between "drained" and "undrained" and may change during the course of the movement.

The first of these arguments is a part of stability considerations and so lies outside the scope of this work. Here it is assumed that substantial accelerations result only when the process of sliding is so advanced that the entire shear zone has passed its peak displacement, and also that a stability analysis has outlined the extent of the moving mass and the shape and location of the shear zone. An understanding of the progressive evolution of the shear zone would be basic to the quantitative analysis of pre-failure movements, but it is not considered necessary for estimating the accelerations and velocities achieved during the failure (some amount of imprecision may result from this assumption in the case of slow moving slides).

The dynamics of a wedge- type rock slope failure (Hoek and Bray, 1977) can be analysed using th[illegible]me basic principles. It must be assumed, however[illegible]t the bounding discontinuities extend for a sufficient distance downslope from the limits of the wedge itself, to preserve the geometry of the sliding mass during movement. If this is not the case, the wedge sliding model would only be applicable temporarily and the rock mass would probably break up upon issuing from the bounding discontinuities and continue moving over the slope surface in the form of a flow of fragments (Chapter 10).

The wedge geometry is described by three angles, including the angle ψ of the line of intersection of the bounding discontinuities to the horizontal (Fig. 3.2 b) and the two angles β and ξ characterizing the attitude of the bounding planes in the plane normal to the intersection. During motion, which occurs in the direction of the line of intersection, the wedge is propelled by the force of gravity, $W \sin\psi$ and restrained by the frictional restraining force:

$$T = [W \cos\psi \sin\beta / \sin(\xi/2) - U] \tan\phi = (W \cos\psi K - U) \tan\phi$$

Eqn. (3.10)

where K is the wedge factor defined by Hoek and Bray and presented by them in a graph. U is the total normal component of the uplift force due to pore pressure activity on the base of the wedge. Assuming a simple linear distribution of pore pressure (Hoek and Bray, 1977) from a maximum p max at the centre point of the intersection line to zero everywhere at the surface of the rock, the force U can be calculated:

$$U = \frac{1}{3} P_{max} A$$

Eqn. (3.11)

where A is the total area of the bounding discontinuities. The pressure P max would be equal or less then the hydrostatic pressure at the centre point of the intersection line, due to a head extending to the crest of the slope.

The equation of motion then is:

$$a = g\left[\sin\psi - \left(k\cos\psi - \frac{U}{W}\right)\tan\phi\right]$$

Eqn. (3.12)

which reduces to (3) for the case of $k \leq 1.0$, when planar failure occurs.

An equation of motion for a rotational slide with circular geometry (Fig. 3.2c) is given by Nisbet*(1973) as follows:

$$a = \frac{R}{r}\left[g\cos\theta - \frac{LR\,(c_u)_r}{M}\right]$$

Eqn. (3.13)

where a is the arc acceleration at the level of the circular slip surface; R is the radius of the slip surface; r is the radius of gyration of the slipped mass about the center of rotation; 0 and L are defined in Fig. 3.2c.

The equation again considers gravity driving forces only, neglects energy losses in internal distortion and is formulated in terms of total stress. An equivalent effective stress formulation suitable for drained analysis is not presently available.

The three models presented so far assume that motion is kinematically feasible without internal shearing or distortion of the sliding mass. This is however not the case in many examples of noncircular slides. A simplified analysis of sliding on a bi-linear surface has been suggested by Romero and Molina (1974), as shown on Fig. 3.2d and is presented here in a slightly modified form. They divided the slide into a number of vertical slides and assumed that internal forces among the slices are everywhere in static equilibrium, except at the intersection of the two straight segments of the sliding surface, where vertical shearing between two adjacent slices occurs. The problem is analysed by calculating an energy balance through a number of horizontal displacement steps, each of which has a length d, equivalent to the horizontal width of each of the elementary slices. There is a total of n slices, numbered from the crown down, and the slice positioned just above the intersection in any given step is number m. The upper and lower segments of the sliding surface are inclined at angles α and β respectively, measured clockwise from the horizontal. The energy changes associated with each displacement step are calculated by summing across the sliding mass:

potential energy change:

$$\Delta E_p = \sum_{1}^{m} \gamma h d \tan\alpha + \sum_{m+1}^{n} \gamma h d \tan\beta$$

Eqn. (3.14)

external friction:

$$\Delta E_e = \sum_{1}^{m} \left(\gamma h - \frac{u}{\cos^2\alpha}\right) \tan\phi \, d^2 + \sum_{m+1}^{n} \left(\gamma h - \frac{u}{\cos^2\beta}\right) \tan\phi \, d^2$$

Eqn. (3.15)

internal friction:

$$\Delta E_i = \frac{c}{2} \gamma h^2 d \tan(\alpha - \beta) \tan\phi_i$$

Eqn. (3.16)

Kinetic energy:

$$\Delta E_k = \frac{1}{2g} (v^2 - v_o^2) \left[\sum_{1}^{m} \frac{\gamma h}{\cos^2\alpha} + \sum_{m+1}^{n} \frac{\gamma h}{\cos^2\beta} \right]$$

Eqn. (3.17)

In the above equations, γ is the density of the material, u the pore pressure, h and d are the height and width of each slice, ϕ and ϕ_i are the angles of friction of the sliding surface and of the material in the interior of the sliding mass respectively. The current horizontal velocity is v and vo represents the horizontal velocity of the preceding step. The coefficient c in Eqn. (3.16) accounts for the unknown magnitude of the horizontal interslice forces as well as for the degree to which the internal shearing resistance is actually being mobilized. It must be estimated more-less arbitrarily, with regard to the sharpness of the intersection angle and the kind of material.

At each step, the current horizontal velocity can be calculated by combining the above equations into an energy balance:

$$\Delta E_p = \Delta E_e + \Delta E_i + \Delta E_k \qquad \text{Eqn. (3.18)}$$

and solving for v. The final distance of travel is obtained when the velocity becomes zero.

The simple analysis is capable of further refinements such as adding external water pressure and more than one intersection so that in the limit one could consider a different segment angle under each slice to represent a continuously curving surface. Furthermore, the residual frictional angle of the sliding surface and /or the pore pressure, can be considered as a variable dependent on the distance travelled, the velocity or both.

More complex geometries can be modelled by the Distinct Element Method (Cundall, 1974) which is based on the same equation of motion but is capable of simulating the interactions of a large number of rigid blocks.

3.3 Predictions of velocity and reach

This section reviews published accounts of attempts to use theoretical means to predict or explain the behaviour of sliding movements. Very few of such accounts can be found, which is perhaps a reflection on the difficulty of obtaining suitable data to use in the differential equations summarized earlier.

The simple sliding block model, modified to account for a bi-planar sliding surface, was used in perhaps the only published attempt to predict *a priori* the velocity of a potential landslide, by the US Corps of Engineers at Libby Dam in Montana (Banks and Strohm, 1974). The analysis conservatively neglected the energy losses associated with internal shearing and displacement of water in the reservoir. Yet, it was necessary to assume extremely low frictional resistance values in order to match observed displacements of prehistoric slides in the area. The expected sliding surface consisted of an inclined wedge intersection of a bedding plane and a joint, a horizontal valley bottom surface and a portion of the opposite valley wall. The dynamic analysis assumed constant residual frictional angles of the order of 20 deg. to 26 deg. on the discontinuities forming the wedge. On the valley bottom and the opposite side, however, it had to be assumed that the frictional resistance would be reduced to zero on account of high neutral pressures. The actual mechanism which could cause such dramatic reduction in strength remained unspecified. Similar cases are discussed in Chapter 10.

The sliding block model has also been used in attempts to explain the high velocity of the Vajont slide (Jaeger, 1979). Neglecting internal energy, the average dynamic frictional angle would need to be as low as 10 deg. to achieve the estimated maximum velocity of 25 m per sec. This is perhaps not surprising, as the sliding surface appears to have been coated by montmorillonitic clay (F.D. Patton, pers. comm.)

The high mobility of the Vajont slide inspired the development of theories suggesting that excessive pore pressures may develop in rapidly moving shear zones as a result of the heat of friction. P. Habib seems to have originated the idea in the sixties ,pointing to the possibility of vaporization of pore or cleft water (cf. Habib, 1975 and Section 10.4). The feasibility of this hypothesis with respect to Vajont was shown by Romero and Molina (1974). Recently, it has been suggested that high pore water pressures may result even if vaporization does not take place. Heating of a saturated soil under undrained conditions produces an increase in pore pressure , due to the greater thermal expansion coefficient of water with respect to that of minerals. Lachenbruch (1980) treated this process theoretically, making allowance for energy balance, dilatancy and heat and fluid escape away from the shear zone. One should note that this process would not be feasible, except in a fully saturated shear zone. The process should also be expected to occur somewhat intermittently in natural shear zones, where large scale roughness must cause frequent shifting of stress concentrations and changes of discontinuity opening. The quantitative predictions are therefore likely to be highly imprecise.

Rock slides and slumps can be analysed using the simple frictional models of the preceding section. A proof of this is that the "travel angle" [4] corresponds to the average dynamic friction angle of the sliding plane, which is about 30 deg. for many rocks. This was first observed by Heim (1932) and later recapitulated by Scheidegger (1973).

The frictional model only applies to relatively small rock slides, or those that are very slow on account of a low brittleness (e. g. the weathered schist slides). Large, rapid events tend to be more mobile, as discussed in Chapter 10. The limiting value appears to be approximately 1M cu. m.

---

[4] The vertical slope of a line connecting the centres of gravity of the landslide before and after failure (Sctn. 10.1)

Experiments in post-failure analysis of clay slopes were carried out by Nisbet (1973). He integrated Eqn. (3.5) numerically, with the general assumptions of circular geometry and zero internal shearing. Two typical failure configurations of a 10 m high cutting were considered, namely a deep seated and a shallow failure. The resulting integrals represented acceleration, velocity and displacement as functions of time and of the resisting forces quantified by the undrained residual shear strength, which could in itself be a function of displacement and/or velocity. For undrained Brittleness Index values of between 0.25 and 0.5, he found maximum velocities generally exceeding 1 m per sec and slide duration times of less than 20 seconds, even though he assumed that the full drop to the residual strength would not be achieved until 1 to 8 m of displacement. Such velocities are too great for slopes in insensitive clays in comparison with the observed behaviour. They are not so unrealistic in the case of sensitive clays and loose sands, although much larger values of Ib would need to be used there. Nisbet concluded that the discrepancy lies in the dependence of undrained residual strength on the rate of shearing, of which little is known as discussed in the following sections. In the absence of other information, he assumed that undrained residual shear strength of clay varies with velocity in a manner analogous to the strain rate dependence of undrained peak shear strength as reviewed by Bishop (1954). The experimental data was fitted by a function:

$$(C_u)_r = C_{ref}\left[1 + 2\left(\frac{dx}{dt}\right)^{0.2}\right] \qquad \text{Eqn. (3.19)}$$

where cref is the residual strength at some reference displacement rate.

Numerical solutions of Eqn. (3.5) were made using the viscous relationship of Eqn.(3.19) and the same geometrical and strength parameters as before. Computational difficulties made it necessary to neglect the inertial terms in the equation. The resulting velocities ranged between 0.01 m per min and 3 m per min for an Ib of 25 to 50 percent and the predicted slide durations exceeded one hour, which is in the order of observations for landslides in insensitive clays.

An alternative method of analysis of sliding problems utilizes physical models. For example, Reik and Hesselman (1977) carried out model studies of sliding of gypsum blocks on a bi- planar surface, resembling that on Fig. 3.2d. Their results confirmed the validity of the simple sliding block analysis, but also illustrated the quantitative effect of internal shearing. Because of the loss of energy by internal deformation of the mass while moving through the "knee" of the sliding surface, the measured velocities reached only 80 to 90 percent of those calculated using the block model. The final displacements were between 65 and 90 percent of those calculated. Neither the reach nor velocity changed when blocks of weak material were used, indicating that energy losses connected with intact material crushing may not be very important. The experimental block masses deformed and dilated by up to 25 percent in terms of volume. These internal deformational effects could, however, be regarded as extreme since few natural slides have to conform to such sharp changes in angle.

The state-of-the-art of predictions of sliding movement behaviour may thus be summarized so that:

a. it is possible to predict the velocity and reach of small rockslides (up to approximately 1 million cu.m), although in case of large events the frictional theory appears to underestimate the results;

b. slides in overconsolidated and insensitive clays tend to move slower than expected on the basis of frictional theory coupled with undrained residual strength values and it appears necessary to take the rate-dependence of this parameter into an account;

c. the frictional theory and laboratory values of undrained Brittleness Index do seem to be able to account for the high velocity of sliding initial to flow slides in sensitive clays and loose saturated sands. But it is probable that the precision of such results will not be very high, unless rate effects are also considered.

Evidently, the chief difficulty in applying the equation of motion towards predictions of reach and velocity of sliding lies in the evaluation of the resisting forces resulting from the shear resistance of the sliding zone. The failure process implies large displacements and therefore the key factor in its analysis is the *residual shear strength*. Most geotechnical materials, when sheared to the residual condition exhibit little or no cohesion and therefore the residual strength is generally characterized by the drained or effective *residual friction angle*, (Skempton, 1964). The residual shear strength then equals:

$$\tau = (\sigma - u)\tan \phi_r \qquad \text{Eqn. (3.20)}$$

where σ is the normal stress acting on the sliding zone and u the *neutral pressure*.

Neither ϕ, nor u are in general constant, rather, each is a function of several other variables. Therefore, a separate section is devoted to each of these parameters, with a view towards establishing their functional form suitable for input into the equations of motion.

3.4 Residual Friction.

The residual friction angle of soils and rock discontinuities depends on mineralogy, grain shape, size or roughness, normal stress level and velocity of shearing.

In some cases, such as in granular materials derived from soft rocks or in rough rock discontinuities, the displacements required to reach true residual strength are very large, possibly of the same order of magnitude as those attained in large scale slope movements. It is then necessary to deal with strength values intermediate between peak and residual and to consider them as being dependent on displacement. The term *ultimate strength* has been proposed for similar situations by Krsmanovic (1967) and Krahn and Morgenstern (1979).

Effective residual strength is measured by direct shear tests in a reversing shear box (Skempton, 1964), by direct shear or triaxial tests on samples cut from a natural sliding zone, or by ring shear tests. Bishop et al (1971) concluded that the last method is likely to produce the most reliable results. They showed that direct shear values of the residual friction angle may be up to 50 percent higher for some clay soils than indicated from the ring shear results, presumably due to the discontinuous nature of movement in the former type of test [5]. The other two methods of testing appear mutually compatible , provided that the natural sliding zone samples are fresh and well preserved.

In further discussion of residual strength and its controlling factors it is convenient to consider cohesive soils, cohesionless soils and rock discontinuities separately.

Kenney (1967) and Skempton (1964) showed that the drained residual friction coefficient of clays at slow rates of shearing (not exceeding 0.1 mm per min) is primarily a function of mineral composition of the sample and its clay content. It is independent of the degree of the initial disturbance, water content or stress history. It is slightly affected by the magnitude of the normal stress and by pore water chemistry, as indicated in Fig. 3.3. Normal stress dependence of the residual strength of some clays and clay shales has also been noted by Bishop et al (1971) in the form of slight convexity of the residual strength envelopes. The same authors also confirmed its independence on stress history by doing stage shear tests in a random order of normal stress steps and by obtaining the same results from both normally consolidated and overconsolidated remoulded samples of the same soil.

---

[5] In the case of Cucaracha Shale from Panama Canal, however, the ring shear values were higher.

Ring shear tests indicate that the true residual strength of clays and clay shales is reached within a displacement of 10 to 40 cm, which is very little on the scale of slope movements. There is a difficulty in applying this conclusion to the analysis of actual slides, as will be discussed in Section 3.6.

Rate of displacement or strain influences residual strength of clays, but the relationship has not yet been satisfactorily explored. Generally, it is found that drained friction angle increases very gradually with increasing rate. Kenney (1967), for example, found less than 10 percent increase for a range of minerals subjected to shearing rates increased by five orders of magnitude. De Beer (1967), on

ONLY COPY AVAILABLE
SEULE COPIE DISPONIBLE

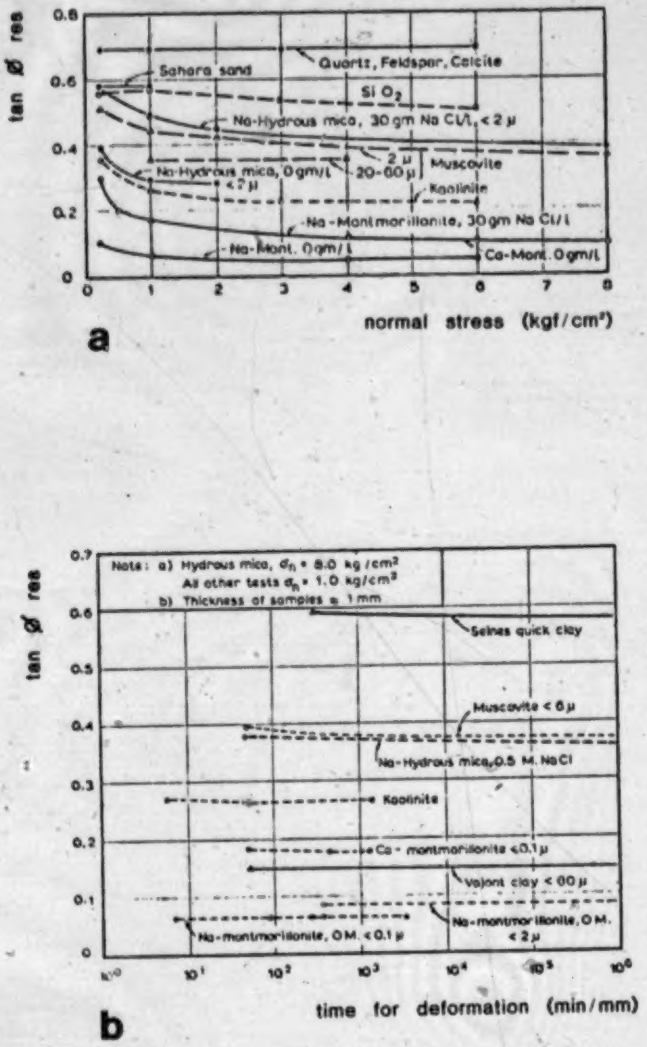

Figure 3.3 Residual friction resistance of various clays:
(a) vs. normal stress level,
(b) vs. displacement rate (Kenney, 1967).

the other hand, found an opposite influence while testing "Boom Clay". Petley (1966) obtained a 5 percent increase in drained residual shear strength for a rate increase of three orders of magnitude, and defined a semi- logarithmic relationship between the two variables.

While the rate influence found by these and other authors is relatively minor, it must be noted that their tests have not been done at sufficiently high displacement rates to approximate those encountered in actual landslides. The standard rates of displacement in drained laboratory tests generally do not exceed 0.1 mm per min or 2 to 5 orders of magnitude less than rates occurring in slope movements. The author is not aware of undrained direct or ring shear tests having been run on clays at much higher rates and to large strains.

Rate dependence of peak undrained strength is a well known phenomenon. In general, the strength increases approximately with the logarithm of strain rate (e.g. Whitman, 1957 and Bjerrum, 1971, Fig. 3.4), by an order of 10 to 20 percent over two orders of magnitude of rate increase for normally consolidated clays or up to 50 percent for overconsolidated clays. It appears that this is due to three factors:

1. rate dependence of the effective strength parameters
2. rate dependence of volume changes during failure
3. internal moisture migration.

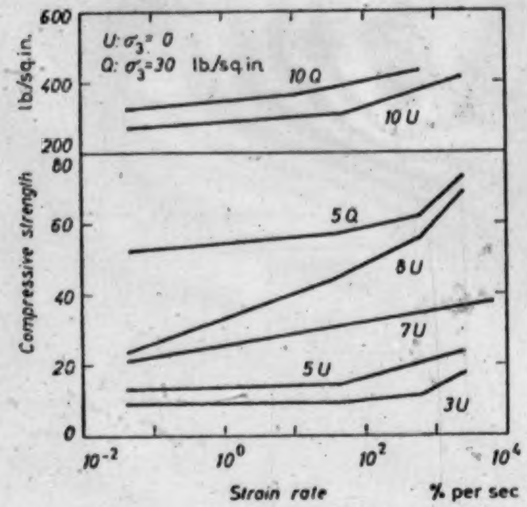

No.	Description	Plasticity index *PI*	Plastic limit *PL*	Water content *w*	Unconfined strength[1] $(\sigma_1-\sigma_3)f$	Strain-rate effect[2] *S–R*
1	*Normally consolidated sensitive ocean sediment, undisturbed*	63	49	92	0·3	2·0(4)
2	*Very plastic clay, remoulded*	27	38	48	7	1·6(6)
3	*Plastic clay loam, remoulded*	17	11	16	10	1·7(6
4	*Medium soft slightly sensitive clay, undisturbed*	24	26	27	10	2·0(4
5	*Slightly plastic clay loam, remoulded*	23	22	21	13	1·4(3)
6	*Plastic clay, remoulded*	27	38	44	15	1·7(6
7	*Moderately sensitive silty clay undisturbed*	21	22	35	22	1·6(3)
8	*Impervious compacted fill*	17	11	12	25	1·8(4
9	*Tough compacted fill*	41	21	26	35[5]	2·0(3
10	*Stiff dry clay, undisturbed*	23	30	20	250	1·3(4

Notes:—(1) Unconfined compressive strength in standard slow test.
(2) *True* strain-rate effect between strain rates of 0·03 and 1000 per cent per second.
(3) Determined from triaxial tests.
(4) Determined from unconfined tests at small strains.
(5) Strength with σ_2 = 42 lb./sq. in.
(6) Determined from unconfined tests on plastic soils.

Figure 3.4 Strain rate effect on peak undrained strength of cohesive soils (Whitman, 1957).

Richardson and Whitman (1963) showed that in a particular plastic clay the first of these factors is predominant at low strain levels (approx. 1 percent) while the second one becomes important close to peak strain (approx. 5 percent). The third factor is of major importance in overconsolidated dilatant clays.

Richardson and Whitman also found that, in a normally consolidated clay, the rate effect can be fully demonstrated even if the loading rate is increased after a considerable amount of strain has been achieved at a slower rate. Thus, at least in this type of clay, undrained strength appears to be uniquely related to strain rate, irrespective of the loading rate history. Therefore, one could presumably in this case extrapolate the rate effect to the residual condition. This is not likely to be possible in the case of overconsolidated clays, since the internal moisture migration effect is cumulative through the development of strain before and after peak. In the residual condition, a different amount of strain rate influence would be obtained in a sample which was failed rapidly than in one which was failed slowly allowing redistributed pressures to equalize.

Under normal circumstances, the residual shear strength of cohesionless soils is synonymous with the strength at the critical void ratio as defined by Casagrande (1936). The critical void ratio is reached after a substantial shear displacement and remains constant during subsequent shearing, being a function only of the effective normal stress. An effective friction angle øcv is associated with this condition and is generally regarded as a material constant (Lambe and Whitman, 1979).

The achievement of the critical condition requires typically over 15 percent of axial strain in triaxial tests or 80 to 100 percent of nominal shear strain in ring shear tests (Healy, 1963). For this reason, direct shear tests are unsuitable for the determination of øcv.

Healy further reports that nominal shear strains of up to 10 000 percent are required in ring shear tests to reach a condition of zero volume change, although he explains this as being the result of a gradual growth of a shear zone in the sample. In his interpretation, while the thickness of the shear zone increases between nominal strains of approximately 10 and 1 000 percent, its localized void ratio and frictional resistance is constant and consistent with the critical condition. The final thickness of the shear zone apparently depends on sample thickness.

Once established, the residual strength of granular materials with strong grains appears to be little changed through a range of conditions. Several authors investigated its dependence on strain rate and generally found it to be negligible (Tab. 3.4). An exception was suggested in tests by Bridgwater (1972) who used unusually high rates of shearing combined with relatively high normal stress. A summary of his results is replotted in Fig. 3.5. Three distinct types of rate dependence are evident. At low normal

AUTHOR	material type	TEST	nominal strain rate range (%/sec)	normal stress range (kPa)	variation in ϕ_{cv}
Healy (1963)	Ottawa sand	ring shear 2	3 to 1,130	10 to 60	increase 5%
Castro (1969)	Banding sand (quartz)	undrained triaxial 3	up to 200 ^{1}	up to 400	negligible
Novosad (1964)	glass beads	ring shear 2	up to 5,000	up to 2	negligible
Bridgwater (1972)	glass beads	ring shear 2	up to 5,000	0.6 to 25	complex (see text)
this work (Ch. 12)	coarse quartz sand	ring shear 2 & 3	4 to 4,000	0 to 200	negligible

NOTES:
1) axial strain rate
2) dry test
3) test in water

Table 3.4 Investigations of the dependence of ϕ_{cv} on shear strain rate and stress level

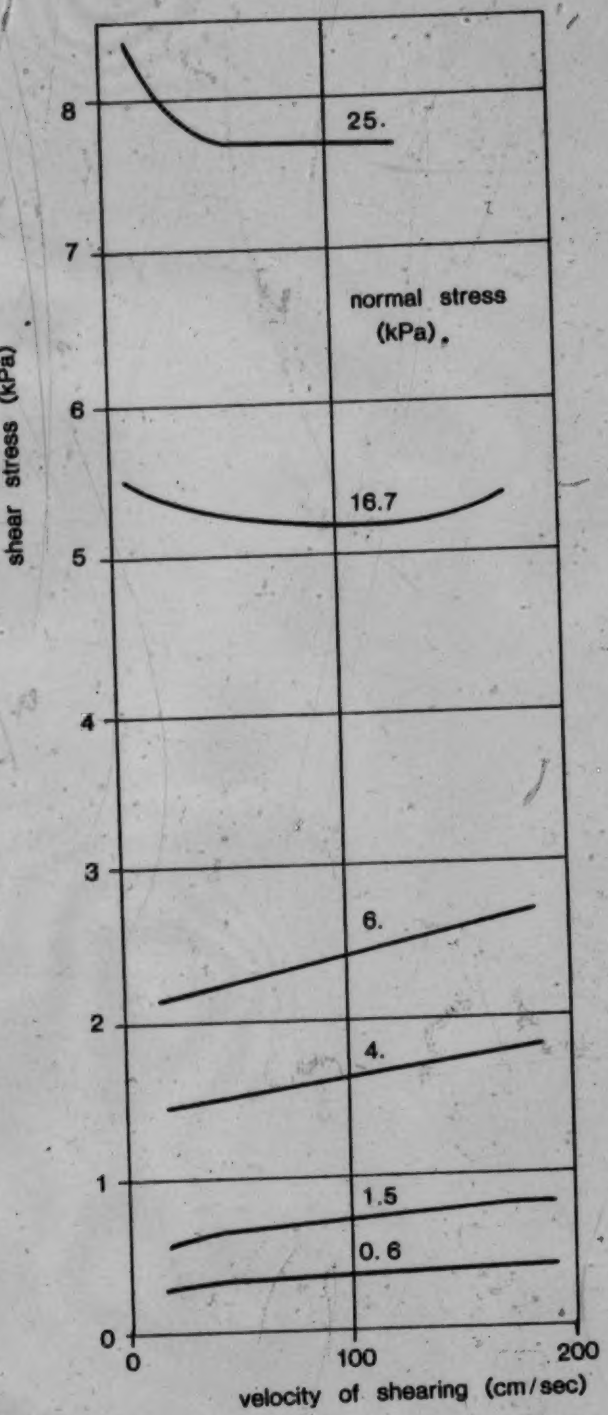

Figure 3.5 Critical state friction in glass beads as a function of velocity of shearing and normal stress (Bridgwater, 1972).

stress level, the frictional resistance is nearly constant over a range of shearing velocities of about 0.2 to 2.0 m per sec. At high stress level there is a gradual increase in ocv with rate, perhaps comparable with that reported by Healy (1963) [6]. At a still higher stress level, commencing at about 15 KPa, the tests indicated a rapid fall of strength with increasing rate of shearing. The maximum normal stress applied in Bridgwater's experiments corresponds to an overburden of only approximately 1.5 m. If the trend towards decrease of ocv with fast rate of shearing continued to develop at higher normal stresses, this would have an important influence on the mobility of large slides in cohesionless debris. This possibility is further explored in Chapters 10 to 12.

In granular materials derived from shales or other soft rocks, such as mining waste, progressive deterioration of grains may continue during displacements of hundreds of metres. Bishop (1973) mentions ring shear tests on colliery waste (mudstone from Aberfan) which originally contained less than 10 percent fines and had a drained peak friction angle of 37 deg. This material deteriorated into a cohesive plastic soil with a residual friction angle of 20 deg. after a displacement of 270 m. It appears that an even greater reduction occurred during shearing in the field, after a displacement of only somewhat more than 20 m (Bishop et al,

---

[6] There is a possibility, suggested by Healy, that the increase is due to growing side friction in the ring shear box.

1969).

Residual shear strength of rock discontinuities is measured by direct shear testing and is usually identified with the more or less constant stress level achieved shortly after a drop from the initial peak. A list of results obtained in 140 such tests by various investigators has been compiled by Goodman (1969). These results, derived from a number of rock and discontinuity types, reveal a range of only approximately 0.5 to 6 cm for the displacement required to reach the "residual strength", which is 1 to 4 times lower than the corresponding peak shear strength. Krsmanovic (1967), among others, commented that displacements of several cm that are usually obtainable in shear box tests may not be sufficient to reach the true residual strength of rough joints and suggested the term ultimate strength to be used for results of such tests. The ultimate strength is often found to fluctuate with continuing displacement in a number of secondary peaks and change on reversal of displacement direction, indicating that the ultimate sliding plane has measurable roughness. The sliding plane in brittle rock is coated at this stage by fragments of crushed rock and rock flour which roll and shear between the walls of the discontinuity.

Krahn and Morgenstern (1979) found that the ultimate shear strength of joints as measured in the direct shear test is by no means independent of the initial roughness of the tested discontinuities. Testing Turtle Mountain

Limestone from the site of the Frank Slide in Alberta, they found ultimate friction angles which varied between 10 and 33 deg. for artificial joints with different surface preparation and between 15 and 32 deg. for natural discontinuities of different types, ranging from rough bedding planes to slickensided joints pre-sheared by flexural slip. They were of the opinion that the differences among these measured friction angles could not be eliminated by shearing at stress and temperature levels characteristic of even a large landslide.

This conclusion seems to be substantiated at least for some rock types by the rotational shear tests reported by Kutter (1974). Fine grained sandstone and plaster specimens with discontinuities were tested at a circumferential speed of 5.9 mm per min, under normal stresses of up to 1.12 MPa. The measured coefficients of friction in both types of sample fluctuated cyclically during each rotation, even after a total displacement of more than 4 m, confirming the existence of a residual roughness. Aside from this fluctuation, the average residual friction angle of the sandstone was between 31 and 33 deg. for both initially smooth and rough discontinuities. This constant average stress level was reached in both cases after a displacement of approximately 80 cm. The amplitude of the fluctuations around it was approximately 5 deg., but it is not certain how much this may have been affected by the compliance of the loading system. Doubling of the displacement rate apparently had no affect on the frictional resistance.

Schneider (1976) found negligible influence of velocity on residual friction of plaster samples over the range of 0.01 to 200 mm per min. When testing saw cut discontinuities in limestone, however, he found a 5 percent increase in the residual strength upon reduction of the displacement rate from 1.5 to 0.1 mm per min.

The influence of high velocity and stress levels on the ultimate resistance of rock discontinuities was studied by Erismann et al.(1977). They conducted short- duration torsional tests on small samples of granite (diameter aprox. 6 cm). At an average circumferential velocity of about 10 mps they found a progressive decrease of the frictional coefficient beginning at normal stresses exceeding 4 MPa (Fig. 3.6). According to the authors, the coefficient of friction decreases under these extreme conditions as a result of frictional melting at the contacts of the test pieces. Fragments of molten rock were actually produced during the experiments in increasing quantity with rising normal stress.

3.5 Pore pressure determination

Casagrande's concept of critical void ratio of sand is based on a unique relationship between void ratio and effective confining pressure in the ultimate state (Fig. 3.7a). If the void ratio during sliding is known, as is the

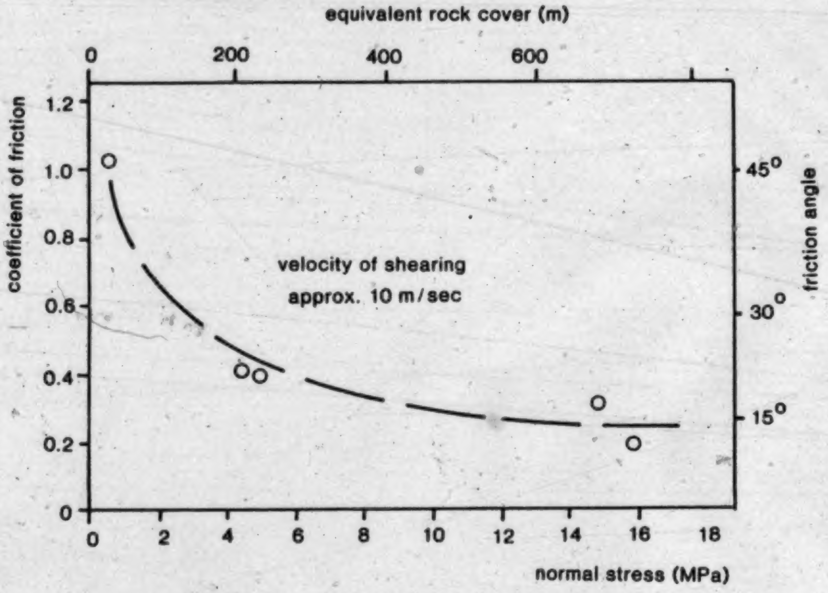

Figure 3.6 Friction of a joint in granite at very high velocity and normal stress (data from Erismann et al., 1977).

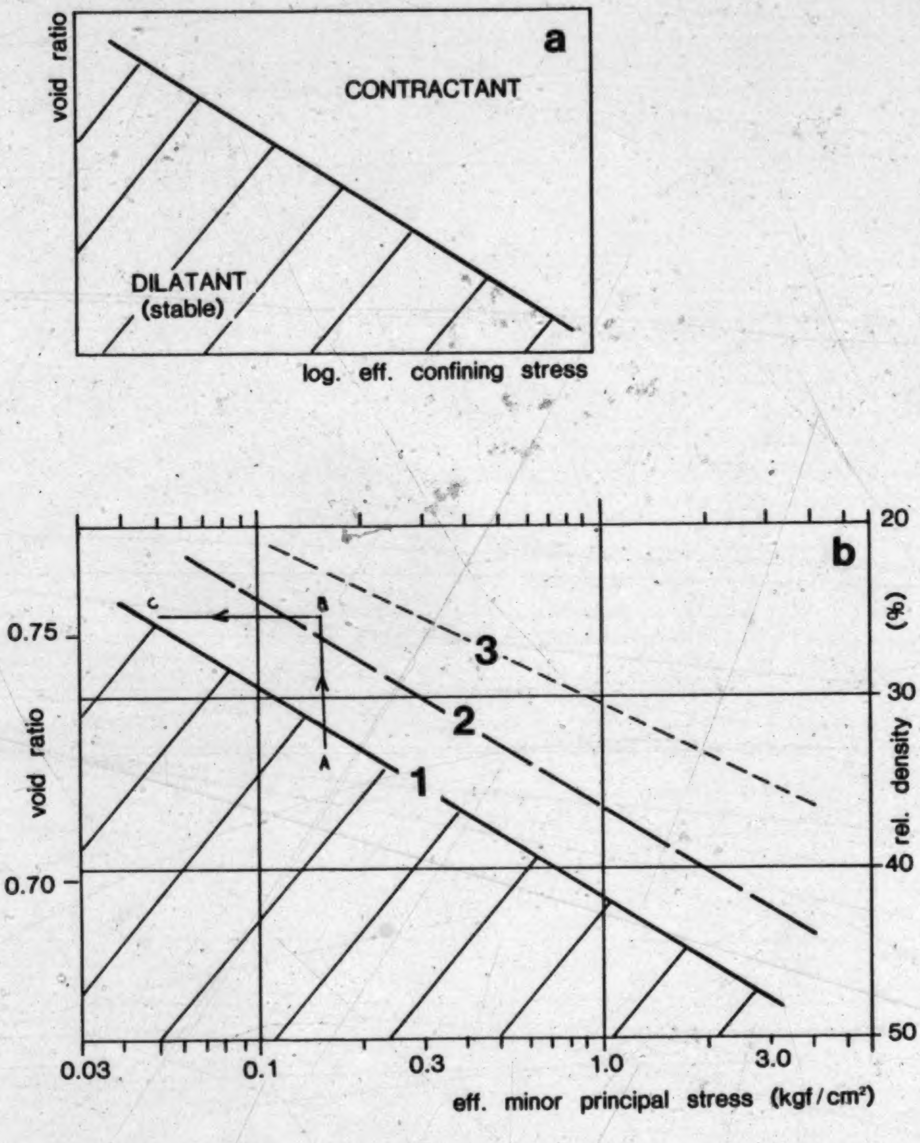

Figure 3.7 Critical void ratio lines. (a) Concept, (b) actual results obtained in various types of test (Casagrande, 1976).

case under undrained conditions, the corresponding effective stress can be predicted from the critical void ratio diagram, as shown by line AB in the figure. In a fully drained situation, on the other hand, the effective stress can be calculated directly.

The third possibility is the partially drained situation (Bishop, 1973), common to some flow slides. This occurs when loose saturated material is allowed to strain slowly in a drained fashion, until a point is reached near the peak strength when the rate of drainage can no longer keep up with the accelerating rate of straining and volume change. At this point pore pressures build up and undrained rapid failure ensues. The failure of the Aberfan waste tip occurred in this way, the rapid flowage being preceded by a relatively slow slumping which developed during the preceding night (Bishop, 1973). A similar process is illustrated by the development of movements and tension cracks weeks before the onset of the rapid sensitive clay flow slide at Selnes (Kenney, 1967) and elsewhere (Mitchell and Eden, 1972). In such situations it is necessary to predict the void ratio corresponding to the peak drained strength condition, which applies at the initiation of failure. This is then used to enter the critical void ratio diagram and predict the effective stress prevalent during the undrained sliding.

The preceding discussion suggests that predicting effective stresses or pore pressures in sliding zones in sands is a simple matter. A considerable difficulty, however, lies in the reliable determination of the critical void ratio line. Fig. 3.7b shows three such lines corresponding to three different types of triaxial tests on the same sand, obtained by Castro (1969): rapid stress-controlled tests (1), strain- controlled undrained tests (2), and slow drained tests (3). Casagrande (1976) proposes that the difference among the three results primarily from the different rate of strain. That is, at a given effective confining stress, the critical void ratio is less in faster tests than in slow ones. This conclusion is diametrically opposite to that reached by Healy (1963) based on triaxial and ring shear tests on a dry sand. Further, Castro (1969) cautions about the possible effects of boundary conditions in small scale triaxial tests as well as of the limited amount of strain which is attainable in these tests. Obviously, proper selection of testing procedure used to determine the critical void ratio line is highly important. Perhaps the consolidated undrained triaxial test with stress control on loose specimens as developed by Castro (1969) is most realistic, although it is not a technique that could easily be adopted by standard laboratories.

The difference between drained and fast-undrained critical void ratio lines in Figure 3.7b has another consequence, as pointed out by Casagrande (1976). A sand stratum existing in a relatively dense condition represented by point A in the figure may be subject to slow initial drained deformation. Since it is dilatant, it absorbs moisture gradually to reach a considerably looser saturated state at point B. A subsequent increase in load may then cause acceleration and an undrained rapid failure accompanied by liquefaction. In this case again, the initial condition should be taken as that found at reaching the drained peak strength.

The concept of a unique critical state at large strains is equally valid for clays. It is the basis of "Critical State Soil Mechanics" ,the textbook of which (Schofield and Wroth, 1968) contains a collection of critical state lines representing the relationship between effective confining pressure and specific volume analogous to the critical void ratio line (Fig. 3.8). But again, for the purpose of estimating the neutral pressure useable in a dynamic analysis, the concept is incomplete in ignoring the effect of strain rate.

The strain rate effect upon effective stresses at undrained failure has been mentioned in the preceding section. Based on the work of Richarson and Whitman (1963), it was concluded that the effective stress depends on the current strain rate only in the case of normally consolidated clays and probably on this as well as on the previous rate in the case of overconsolidated clays, where significant pore pressure redistribution must be accounted for. The nature of the dependence is illustrated in Fig. 3.9a, derived from data obtained in consolidated undrained

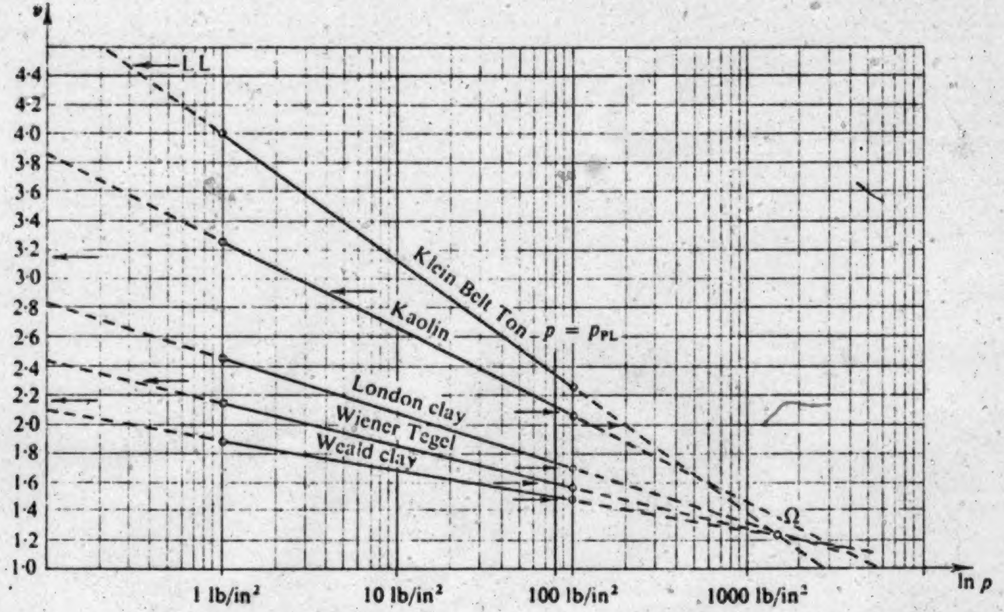

Figure 3.8 A family of critical state lines for clays (shown in terms of specific volume and first stress invariant, Schofield and Wroth, 1968).

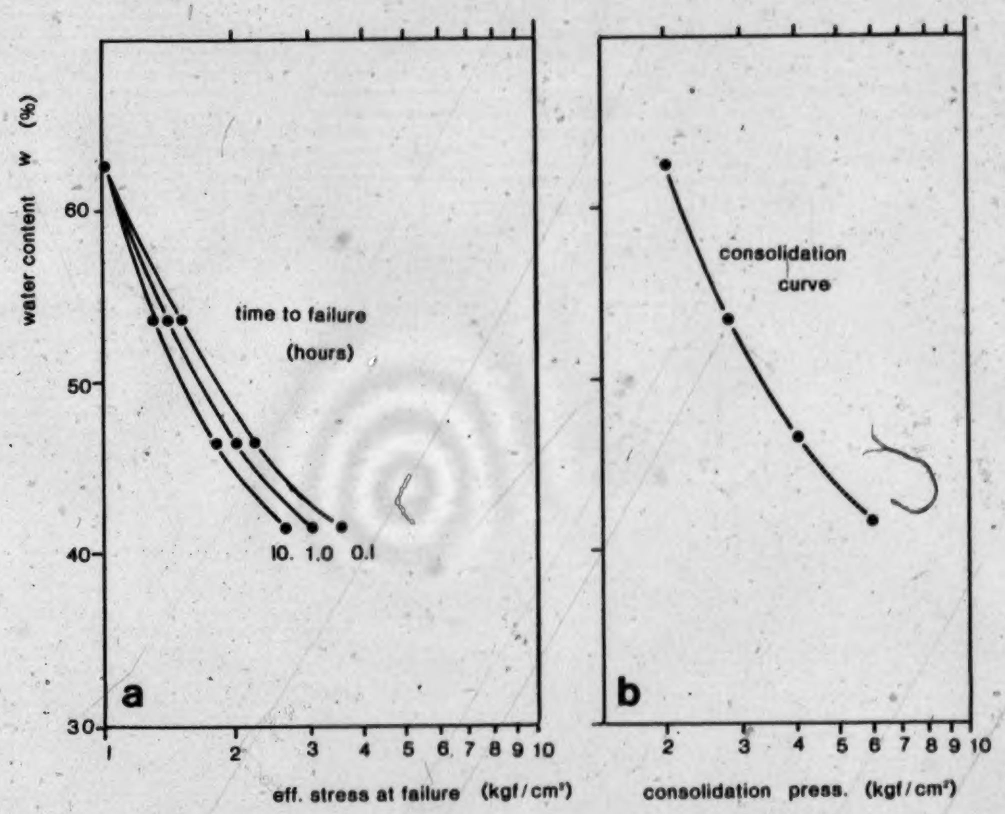

Figure 3.9 Effective stress at peak strength in undrained triaxial tests on sensitive clay as a function of w and of rate of testing (data from Crawford, 1969).

triaxial tests on the extra sensitive Leda Clay by Crawford (1959) [7] The figure has been plotted in a similar form as Fig. 3.8 and relates to the condition at maximum deviatoric stress which, admittedly, is not synonymous with critical state in these highly structured soils. It shows that the "critical state line" tends to move up with the logarithm of strain rate in a trend opposite to that noted by Castro (1969) but corresponding to that reported by Healy (1963) for sands. The lines are curved similarly to the isotropic consolidation curve shown in Fig. 3.9b.

At a given constant water content, one could alternatively express the relationship of Fig. 3.9a as:

$$\sigma_3' \simeq a + b \log \dot{\epsilon}$$

Eqn. (3.21)

or:

$$\sigma_3' \simeq a\,(\dot{\epsilon})^b$$

Eqn. (3.22)

where $\dot{\epsilon}$ is the strain rate, or inverse of the time to failure and a and b are constants. The power relationship of Eqn. (3.22) seems to fit the data somewhat better of the two.

Of course, the discussion of the preceding paragraphs related to the condition at failure and the validity of extending its conclusions to the residual state is uncertain. This is due to the major structural changes that must occur in the material before the latter is reached (Morgenstern and Tchalenko, 1967). A dilemma exists in laboratory testing, as it is impossible in triaxial tests to obtain large enough strains for the residual condition to be established, while in direct or ring shear tests one can neither measure nor control the distribution of strain and pore pressure.

---

[7]. Similar data from less sensitive Norwegian clays has been reported by Bjerrum et al (1958).

The situation is more complex still in the case of overconsolidated dilatant clays. In this author's opinion, the problem of internal pore pressure redistribution in the vicinity of a localized shear zone is presently intractable in laboratory testing. Also, as pointed out by Bishop (1973), negative pore pressures may not be sustained across a displacement discontinuity, in which case "u" effective within the sliding zones of shallow undrained slides in dilatant materials may by limited to some cavitation pressure.

In view of the above arguments it is concluded that the most reliable method of estimating the dynamic shear resistance in clays is to assume the total stress approach and to measure the resistance directly in a ring shear apparatus. The test should be conducted at stress levels and displacement rates closely approximating those expected in the field. Or, perhaps preferably, the test should be stress controlled similarly as in the case of loose sands. If a drained failure is expected in the field, the pre-peak part of the test should be conducted slowly to allow drainage.

In slow moving landslides (post-failure movements), the neutral pressure in the sliding zone is determined by seepage conditions. Hence the dependence of accelerations on precipitation and drainage in such landslides.

3.6 Determination of the resisting forces:Summary.

An attempt will now be made to summarize the foregoing discussion in such a way as to suggest what functional form should the resisting force term assume in the equation of motion, for the various materials. The independent variables considered are displacement and velocity, since the numerous other factors controlling the magnitude of the resisting force, such as water content or total stress level are reflected in the initial condition of the material prior to shearing.

1. *Granular materials* - sands, gravels, rock fall debris, coarse mining waste:

   The effective friction angle is constant with shear strain, beyond some fairly small limiting value (80 to 100 percent in the case of Ottawa sand). In granular materials composed of weak grains (shale, mudstone, coal), a gradual, probably exponential decrease with large displacements may be expected, as a result of grain crushing. It appears constant with strain rate, except at very high rates combined with moderate effective confining stresses (about 1 000 percent / sec and 25 kPa in case of Ottawa sand). The relationship under the latter conditions is unknown.

The effective stress at the critical state is a function of void ratio, but the dependence of this function on strain rate is undetermined. It appears that reasonable results obtain from stress controlled triaxial tests and, if the above function is determined from such tests, the undrained effective stress could be assumed constant in calculations.

2. *Clays* - intact or remoulded.

The effective residual friction angle appears to develop after less than 1 m of displacement and remain relatively constant with further displacement. It tends to increase with the logarithm of displacement rate by a small amount. This conclusion derives from tests run at limited velocities only.

The effective stress at the residual condition may also increase approximately with the logarithm of the strain rate (Eqns. 3.21 and 3.22), although this is concluded merely by analogy with the peak strength triaxial condition. The conclusion therefore does not account for the structural change associated with the development of residual strength. The laboratory measurement of the above dependence, even at peak, is made extremely difficult in the case of dilatant clays where strong pore pressure gradients develop inside the sample.

Undrained residual shear strength appears to be the preferred parameter for use in the equation of motion. It would probably be constant after less than 1 m of displacement. Analogy with peak strength relationships suggests that it may be dependent on the logarithm of strain or displacement rate (or use Eqn.3.19). It should preferably be measured in ring shear tests simulating the development of velocity in the actual landslide

3. *Rock joints* acting as shear planes in block or wedge slides:

The ultimate friction angle of rock joints develops in less than 1 m of displacement and remains constant therafter, at least in strong rock. The angle, however, incorporates some residual roughness, which may deteriorate further in weak rocks.

There is little evidence of it being dependent on velocity, except at extremely high velocities combined with very high normal stresses (in excess of 10 mps and 4 MPa in granite).

These conclusions derive from laboratory testing and it is now necessary to consider whether and how can they be applied to the behaviour of actual shear zones in the field. It will have been noted that the previous discussion used the terms strain and displacement or strain rate and velocity indiscriminately. The reason for this is that in most types of laboratory tests both are strictly nominal parameters, since the actual distribution of strain within the sample is nonuniform and often unknown. Exceptions to this last statement are, on one hand, triaxial tests on loose sands or soft clays which tend to develop fairly uniform axial strains at least in the middle third of the sample (Taylor, 1948) and, on the other hand, rocks which generally fail in shear along a discrete displacement discontinuity. In remaining types of material, the failure zone may be of a finite thickness and consist of a complex of several strain and displacement discontinuities. It is likely that the thickness of the shear zone would be affected by the boundary conditions and would thus be different in different types of test, in samples of different sizes and in the field.

The problem of relating post-failure data from laboratory tests to the field was faced by Lo (1972) in his work on progressive failure. After a review of published observations on shear zone geometry he concluded that the assumption of a discrete displacement discontinuity immediately after peak in drained failure was reasonable in clays.

A survey of literature with the same purpose has been carried out in the course of this work (Table 3.5). No shear zones were found thicker than about 1 m. This is an upper limit estimate since, as pointed out by Lo, inclinometer casings conform only with difficulty to greater strains. On the other hand, the collected data is somewhat biased in favour of dilatant materials, in which one would expect thin

Case	material	shear zones	depth (m)	displacement rate (max.)	total displacement	nature	source
Fort Peck	clay shale[3]	two, "a few inches thick"	6 & 12	0.02 m/year each	0.6 m	steady	Wilson (1970)
Seattle freeway	O.C. silt & clay	0.6 m[1]	16	1.2 m/year	some m	accel.	Wilson (1970)
Minneapolis freeway	clay shale[3]	5 cm[1]	5	0.05 m/year	some m	accel.	Wilson (1970)
Columbia river	contact of talus and mudstone	1 m[1]	45	1.2 m/year	"large"	prec.[4]	Wilson (1970)
Point Loma	shale	0.6 m[1]	25	0.04 m/year	"large"	prec.	Wilson (1970)
12 sites in California	O.C. clay	1.2 m avg.[1]		0.01 to 0.4 m/year	large	prec.	Gould (1960)
Little Smokey	clay shale	1.6[1] [2]	50	0.01 m/day	large	steady	Thomson & Haley (1975)
King's Lynn	soft clay	1 m[1]	8	0.3 m/h	1.25 m	trans.	Wilkes (1972)
NBR embankment	soft clay	none[2]	10	4 m/h	2 m	trans.	Dascal et al (1972)
Furre	quick clay[3]	a few cm[2]	16	1 m/h	some m	trans.	Hutchinson (1961)
Khosta	clay	a few cm[1]	4	2.5 m/h			Ter-Stepanian (1965)

NOTES:
1) monitored by inclinometer
2) observed in borehole
3) probably stratigraphically controlled thickness
4) movements variable with precipitation

Table 3.5 Some examples of observed shear zones

shear zones to develop. Also, several of the cases have stratigraphic control.

Skempton (1966) and Morgenstern and Tchalenko (1967) show that most shear zones in clays eventually develop displacement discontinuities (called displacement shears by Skempton). It is necessary to answer several questions: 1) how much displacement does it take in the field, before displacement shears develop from the initial strain discontinuities and oblique shears. 2) Do displacement shears develop in soft clays and loose sands? 3) When displacement discontinuities develop , they may still occur in groups, sharing simultaneous movements.

Such questions appear substantiated by the findings of James (1971) and Gould (1960). Their back- analyses of pre- and post- failure geometries of slow moving landslides in clays indicated that considerably greater displacements are required in the field to reach residual strength than would be expected on the basis of laboratory tests (Fig. 3.10). Further, it is known that undrained shear straining in loose saturated sands or sensitive clays tends to incorporate rapidly large volumes of material, in creating a flow slide. Slumps in soft clays develop a characteristic S-shaped earthflow crossection (Fig. 3.11), which reveals distributed, flow-like strains. These probably co-exist with a displacement discontinuity in this case.

Before considerably more information is assembled about the geometry of shear zones, or before theoretical means of

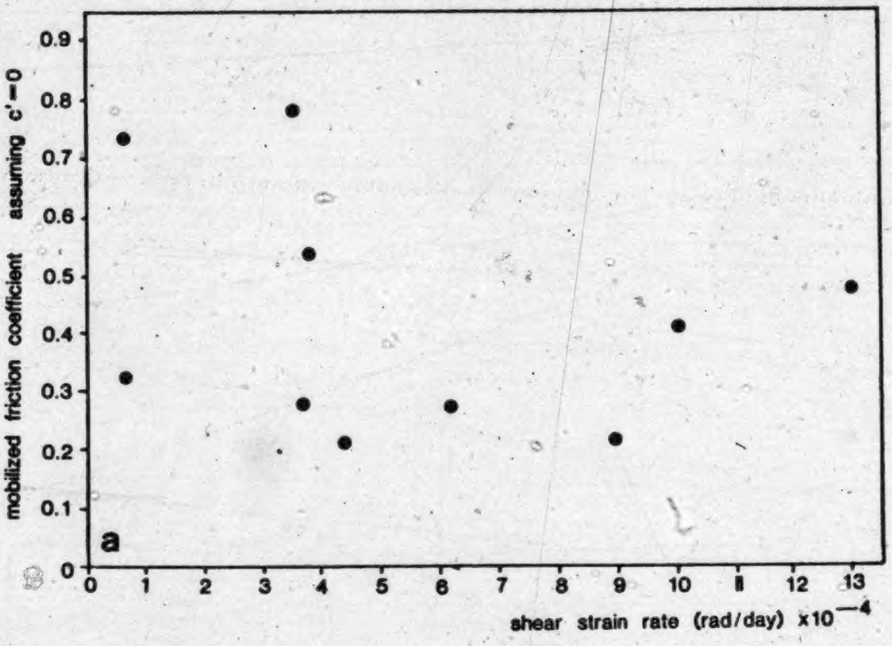

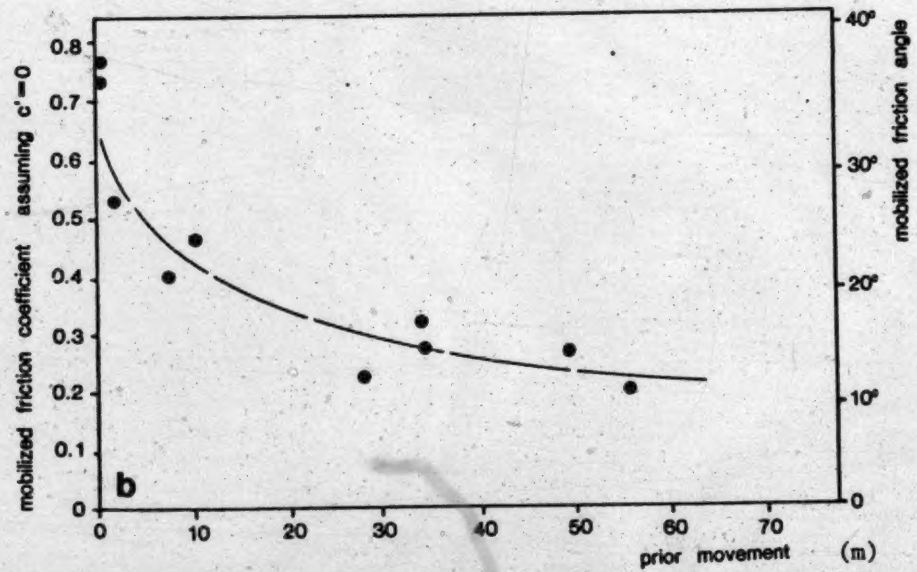

Figure 3.10 Back calculated variation of the mobilized effective friction angle. (a) Vs. strain rate in shear zone, (b) vs. displacement. Data from Gould (1960).

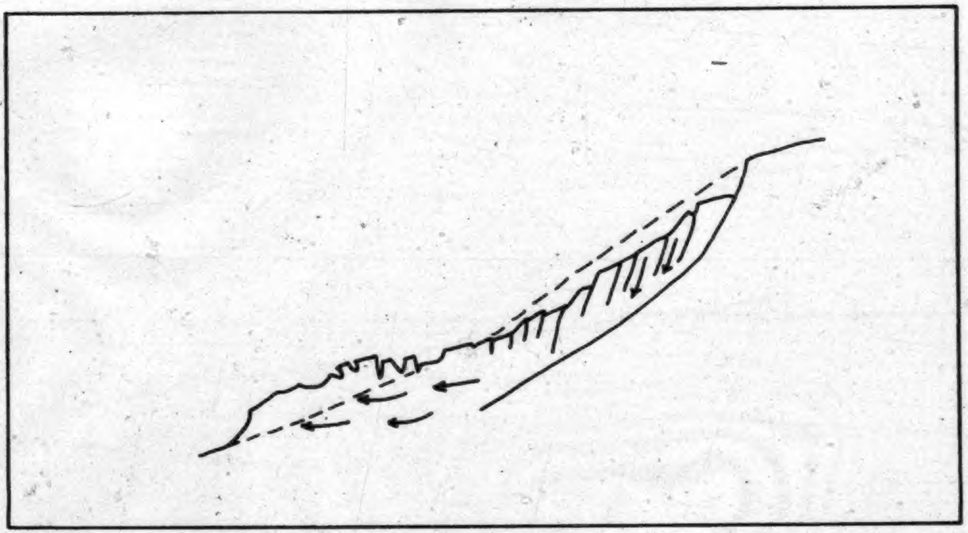

Figure 3.11 Typical crossection of an earthflow, demonstrating distributed strain (Sharpe, 1938).

their estimation become available, it will be necessary to guess at their thickness. Fortunately, for the purposes of dynamic calculations, the knowledge is only required for those materials where the restraining forces vary with respect to strain or strain rate. According to the preceding review, this can presently only be accounted for in clays. If one then assumes as Lo (1972) did that relationships determined in the laboratory are applicable to the field conditions in case of overconsolidated clays, the only materials affected by the uncertainty are soft clays. The author would suggest the assumption of uniformly straining shear zones 0.1 to 1.5 m thick as a first estimate, to be used in the analysis of a typical case.

4. DISTORTIONAL MOVEMENTS

4.1 Description and Classification

This is the only chapter dealing with slope movements which do not comprise a failure episode. The term was defined in the Introduction as acceleration of a slope segment to a velocity exceeding 0.3 m/year, accompanied by a substantial detachment of the failing mass from the stable part of the slope. Distortional or "creep" movements are those that do not fulfill these prerequisites; either they do not accelerate, or if so then not to large enough rates, or they do not produce a sufficient degree of detachment such as a crown scarp or tension cracks. Creep movements are usually divided into two rather distinct groups: *surficial* (seasonal) and *deep- seated* (continuous). Varnes (1978) defines two corresponding classes, "bedrock flow" and "soil creep". The term flow has been somewhat more restricted in the present work. Further, Varnes' division does not aknowledge the presence of deep- seated creep in soils. Therefore, this chapter makes an exception in not using his terminology.

Surficial creep has been recognized by the geomorphologists of the previous century as a major agent of hillslope evolution by mass movement. It is the slow downhill displacement of near- surface soil, resulting from a number of rather subtle seasonal processes including expansion and contraction due to temperature changes, wetting and drying, frost cycles, animal burrowing and treading and plant root activity. Since all of these agents weaken with depth and the rate of movement is cumulative upwards, its expected vertical distribution is exponential with a maximum at the surface (Kirkby, 1967). A table of published records of displacement and mass movement rates has been assembled by Brunsden (1979). The velocities vary between 0 and 50 mm/year, and average about 9 mm/year, at 18 locations in moderate climates (California to Scotland). Depths are approximately 0.5 m. Schumm (1967) established at one Colorado location a linear dependence between the movement rate of soil creep and slope inclination, up to 50 mm/year at a slope of 40 deg. The slope consisted of a relatively fine sandstone talus over shale base. Some authors (e.g. Hutchinson, 1968) recognize talus creep as a separate class of slope movement.

The surficial movement is considerably more important in periglacial regions, because of strong freeze- thaw cycles and inhibition of drainage by permafrost. The slow seasonal flowage of the active layer above frozen ground is termed *solifluction* or *gelifluction*. Brunsden's table cites rates of up to 450 mm/year. These movements generate characteristic lobate features, and may occassionally assume the dimensions of a slope failure named *skin flow* by McRoberts and Morgenstern (1974). This last article should be consulted for further information concerning permafrost slope movements.

Detached blocks of bedrock seated on inclined bedding surfaces also travel slowly downhill, as a result of temperature expansion cycles or, in cold climates, ice wedging (e.g. Simmons and Cruden, 1980).

Deep- seated creep is distinguished easily, as it extends at least an order of magnitude deeper than surficial creep. It is also not the result of a host of external agents, but a manifestation of the time dependent properties of the material. Both rock and soil masses are capable of distorting, slowly and steadily, as a result of sustained gravitational shear stresses. The prosess is manifested in the appearance of distortional structures in areas where they cannot be accounted for by regional tectonics. Radbruch- Hall (1978) compiled an extensive summary of the literature of deep- seated creep in rock masses. She describes six types of geological setting in which this process has been evidenced:

a. Squeezing of soft layers from beneath rigid caps (cambering of strata and valley bulging).

b. Creeping and buckling of rigid inclined layers on soft bases (example: Goldau slide, prior to failure, Section 10.1).

c. Localized distortion in uniform material (example: California clay shale landslides described by Gould, 1960, see Section 3.1).

d. Incremental movements on rough- surfaced inclined discontinuities. Dodds (1966) measured intermittent downhill movements of massive conglomerate blocks at a dam site in Iran. Typically, they were measured in thousandths of a mm. But sometimes their rates increased to over 2 mm/day and catastrophic sliding then usually ensued.

e. Bending and folding of strata on high slopes, deduced from certain structures found in the Alps, assumed to be of gravitational origin (Zischinsky, 1966).

f. Spreading of mountain ridges, bulging of slopes, based on similar evidence as (e). This process is thought capable of triggering landslides by gradual steepening of mountain slopes.

These classes do not differentiate between movements of steady nature and those that occur prior to or after a landslide (b and c). Such a division would appear essential from a practical point of view.The potential for a failure, or the fact of its previous occurrence, are more important than the creep movements in themselves. One would be interested to know whether significant creep movement rates are possible in a stable rock mass, independently of a landslide. On examination of Radbruch- Hall's summary and other publications reviewed by this author, the answer is that such independent rock creep appears to be known only from circumstantial evidence. That is from interpretation of geological structures which are assumed to be its end products. It has never been measured in motion.

All gravitational bedrock movement measurements reviewed refer to movements of failed masses, or those about to fail. This includes all of the examples given by Radbruch- Hall: Vajont (Section 3.1), Northern California Coast Ranges, Point Firmin, Cal. Only one case of steady movement without acceleration and without a reported sign of detachment is known to the author. This is the Lugnez slope described by Huder (1976), which has been observed for nearly 100 years (Section 1.4). Here, the creep distortion appears concentrated to a thin shear zone of schist, 60- 200 m beneath the 25 sq. km moving plate. The publication of course does not give all the details, but it appears possible that this slope movement is in fact a sliding failure, whose velocity is restricted by a buttressing effect of the toe. Displacement occurs only in response to the gradual erosion of the toe by a stream which flows in front of it. The Klosters creep slope, where rates of about 7 mm/year had been recorded inside a tunnel 200 m deep in schist, is identified by Huder as an old landslide area.

It would consequently appear reasonable to conclude that bedrock creep takes place at rates too slow to be measurable by standard techniques. Where significant movements of bedrock are indicated, one should assume that a failure has occurred in the past, or might possibly occur in the future.

Deep seated creep has been somewhat better documented in soils. But the distinction between steady movements and those associated with failure has again been neglected. Ter-Stepanian (1965) reports creep measurements from colluvial slopes in Caucasus. The typical measured depth- velocity profiles consist of an accelerated (surficial) creep zone less than 1 m thick, an unstrained rigid block, followed by a distributed shear zone extending between the depths of 2 and 4 m. The movement rate is about 10 cm/year. In some cases, a shear zone only a few mm thick may develop, while the overlying soil continues deforming slightly. Some of these movements therefore also do not represent true creep, but appear similar to the behaviour of earth flow complexes (Section 6.1).

A good example of deep- seated creep is given by Wilson (1969). This was measured by inclinometer on a 30 deg. slope of glacial soil in Western Washington (Figure 4.1). The rate is apparently steady at the surface, where surficial creep is superimposed (8 mm/year). At a depth greater than 1 m, however, the rate appears to decay with time (Fig. 4.1b). Similar decreasing rate of creep was measured by Fleming and Johnson (1975) in a layer of highly plastic montmorillonitic clay, in response to the excavation of a pit. The clay layer was only 1.5 m thick over claystone bedrock and the slope angle about 10 deg. The surface displacement rate began at about 0.2 mm/day immediately after excavation, and decayed logarithmically to a negligible rate within about 3 days.

Kojan (1968) measured creep displacements ranging up to several cm/year, and resulting from strains distributed to

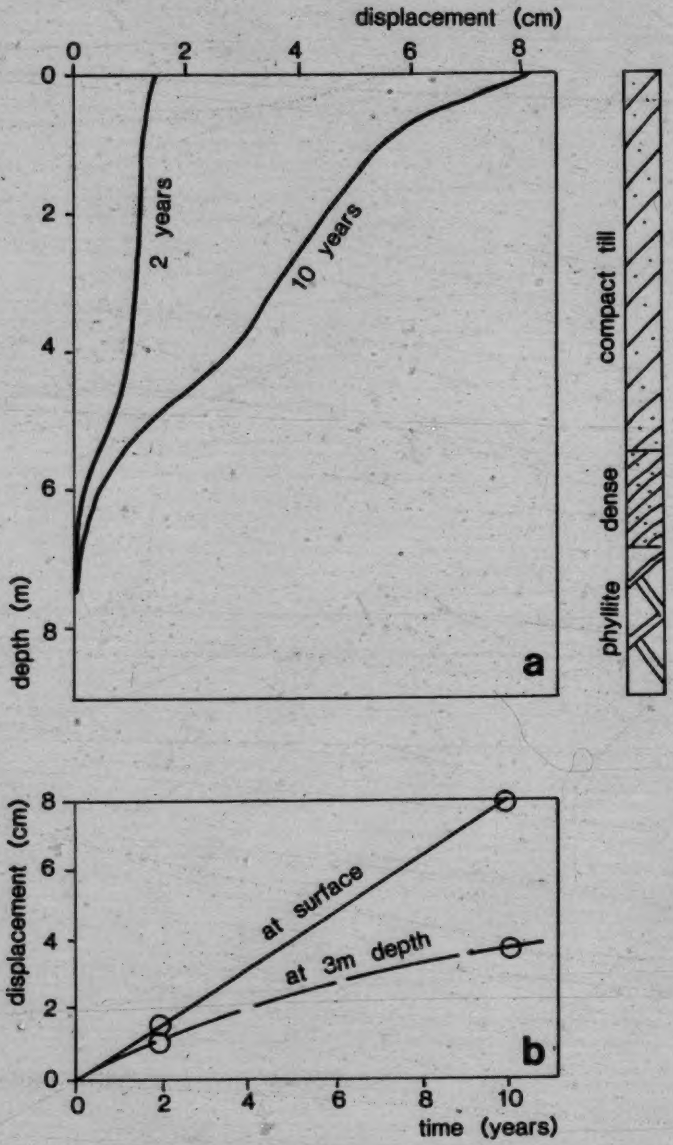

Figure 4.1 Deep—seated creep in a glacial soil. (a) With depth, (b) with time. Slope angle = 30 deg. (After Wilson, 1970).

the depth of 10 m. His observations are the same as Ter-Stepanians' , that is some distributed strains combined with displacements on confined shear zones. In addition, a crown scarp of a landslide can be observed above the measuring locations.

Gould (1960), having made measurements in Tertiary clay slopes in California, stated:

> "No case of continuous creep was observed in intact slopes, and movements of intact materials were so small as to fall within the range of instrument error or else where accelerated and then slowed."

To this author's knowledge, no one has so far produced field evidence to contradict the general validity of this statement. In summary, therefore, it appears that "continuous" creep carrying on at steady rates without change in applied or resisting forces exists only in the surficial layers of soil. At depth, only a decaying creep has been measured, in response to some specific equilibrium change. Again, steady movements occur only on failure-generated shear zones, or in material that is approaching failure. Soil appears entirely different from snow and ice in this respect.

An exception is the steady creep of ice rich permafrost, measured by Savigny (1980). But the rates appear to be very slow, only 2.5- 3 mm/year in a layer 40 m thick sloping 18 deg. on average.

4.2 Theoretical Models, Failure Predictions.

For the surficial creep process of soils there is a theoretical model due to Kirkby (1967), which may be used to explain the distribution of velocity with depth.

Numerous attempts have been made to fit theoretical models to deep- seated creep observations in soils. Most have adopted some modification of the Bingham model as the constitutive relationship. That is, the soil was considered rigid while stressed to a shear stress level below some yield strength or flow limit. It was then assumed to flow under high stress as a fluid of a constant viscosity. The infinite (one- dimensional) slope has invariably been adopted as the kinematic model. Examples of such derivations have been presented by Stroganoff (1961), Ter- Stepanian (1963 and 1965) and Yen (1969), with minor variations. The last two presented attempts to analyse actual field observations. Ter- Stepanian (1965) applied his equations to the case from the Caucasus mentioned in the previous section. Yen (1969) analysed the same case and one of the landslides monitored by Gould (1960) in California. Yen found disagreement while attempting to calculate the Caucasus movements using his theory and a soil viscosity value back- calculated by Ter- Stepanian. The two theories are thus mutually inconsistent which is surprising, as both are based on the same simple constitutive relationship. Emery (1978) also re- analysed this same case history using his finite element model, and found a satisfactory agreement with Ter-Stepanian.

The case histories so far analysed by these methods are quite obviously post-failure movements, under conditions resembling those of slow earthflows described in Section 6.1. But arguments presented in that section are in favour of other constitutive models. Further, it is shown there that the slow flow-like movements of earth flows are strongly controlled by processes difficult to quantify, especially groundwater fluctuation and horizontal load transfer between adjacent sections of the flowing mass. These models are therefore unlikely to gain much practical value. No successful predictions have ever been reported based on laboratory creep test data or on backcalculated parameters.

An analysis of the true transient deep-seated soil creep, two examples of which have been mentioned in the previous section, has not yet been attempted. It might be done with the advantage that a well substantiated creep law exists for normally-consolidated clays, derived from controlled laboratory tests. It has the form (Mitchell, 1976):

$$\dot{e} = Ae^{\alpha D}\left(\frac{t_1}{t}\right)^m$$

Eqn. (4.1)

where e is the strain rate (axial or shear), D the deviatoric or shear stress, t time and t1 time datum. The remaining three parameters are material constants. The equation is supported by both drained and undrained test data.

Creep of rock slopes has received less attention from analysts. Scheidegger (1973) presented equations for the vertical velocity distribution in an infinite slope, assuming a logarithmic creep law. The resulting displacement distributions resemble the shape of the "sackung" structures described by Zischinsky (1966). Many other forms of creep equations have been derived in the rock mechanics literature, as reviewed for example by Afrouz and Harvey (1974), but they cannot be tested against actual cases until the velocities of gravitational creep in rock masses can be measured.

A most important practical branch of creep research is concerned with the possibility of predicting failure from pre- failure creep measurements. The task amounts to predicting ahead of time the development of the Sshaped curve shown in Fig. 1.1. Theoretical solution of this problem is exceedingly difficult and is the subject of much current research, under the label of progressive failure. The difficulty lies in the necessity to model gradual growth of shear bands or sliding zones within the continuum, with localized changes in the constitutive laws. Existing solutions require advanced iterative numerical techniques. The author is not aware of the existence of a successful prediction of the time- displacement curve of an actual landslide. But solutions are being obtained and success is probably not far away (e.g. Lo, 1972, Simmons, 1981).

An empirical approach is used in practice. It is most useful in the control of open pit mine slopes. The advantage there is that continuous long term monitoring of the slopes results in a large body of data or at least qualitative experience being assembled, against which new observations can be judged. A well-known example is that of the Chiquicamata copper mine in Chile, described by Kennedy and Niermeyer (1971). Surface target monitoring of an unstable part of the mine slope plotted a curve of characteristically accelerating displacement. The curve was extrapolated graphically to yield an accurate prediction of the day and hour of failure, approximately a week before it took place. Voight and Kennedy (1978) discussed the extrapolation technique in great detail and concluded that no rational generalization can be made; the extrapolation was simply the "best guess" of the shape the curve was about to take during the final days before the failure.

A more specific generalization was made by Broadbent and Ko (1972). They observed movements of a periodic nature in a stable mine slope. Typically, a sudden acceleration of displacement would coincide with a major blast near the monitored wall. The slope would move for some time at a new, relatively rapid velocity. But a gradual decay of movement rate would take place, tending to a very slow approximately constant velocity. The authors were able to fit a viscoelastic relationship similar to the Kelvin Body to the individual cycles of acceleration and decay. The length and total displacement of a cycle could now be predicted from the fitted equation, as soon as the initial velocity became known. If the measured displacements in any cycle did not conform with the prediction, then there was a danger of failure developing. This requires a long record of observations and relies on the assumption that no change of external conditions is taking place, such as a rise in the groundwater level, which could modify the displacement cycle without leading to a failure.

Another attempt at a generalized method of failure prediction has been developed in Japan (Saito, 1965). It is claimed that the failure process in slides of various kinds of soils follows a characteristic pattern:

a. slow or zero strain rates exist in a stable slope;
b. the approaching failure is preceded by a sudden acceleration to a higher constant strain rate at some of the observation points;
c. a new sudden acceleration brings about the failure.

The time period between b) and c) is called "creep rupture life" and is found by Saito to correlate closely with the accelerated pre- failure strain rate measured immediately after b). Thus, when a sudden acceleration of strain appears in a potentially unstable mass, the time to failure could be estimated using the new strain rate in the given correlation. According to Saito, the same pattern occurs also in laboratory tests.

Unfortunately, the sudden acceleration to a new strain rate noted in b) generally does not appear in pre- failure records. Instead, the displacements and strains usually tend to increase gradually, as shown in Fig. 1.1. Perhaps, the suggested patern has some regional limitation.

The main difficulties in such predictions are firstly to recognize the scale of acceleration required to cause failure, and secondly to be able to isolate fluctuations of displacement caused by external agents but not leading to failure. The scale of pre- failure velocities ranges from 2 mm/day recorded prior to the sliding of rock blocks by Dodds (1966) to 14.6 m/day measured by Campbell (1978) prior to a failure on the face of a 200 m high rock waste pile. Some other pre- failure velocity data are given by Skempton and Hutchinson (1969) and in Section 3.1. Often, a locally developed criterion is most reliable. For example, Mitchell and Eden (1972) found that toe displacement rates in extra-sensitive Leda clay slopes exceeding 4 cm/month led to failures, while slower rates did not. Size scaling should be used in such criteria, to take into consideration slope height.

The elimination of harmless fluctuations of velocity (those due to factors other than the onset of failure) must be done with caution, since they may be superimposed on accelerations due to the onset of failure. This is what happened at Vajont, as described in Section 3.1. If an acceleration occurs without some obvious change of external parameters, it is safe to assume that failure will occur. If on the other hand, the observed acceleration has "a good explanation", e.g. in a rise of the water table, change of slope geometry or similar, it still cannot be automatically assumed that the slope is stable and consideration must be given to the scale of the acceleration.

5. FLOWS: GENERAL CONSIDERATIONS

5.1 Introduction : Types of Flows

Earth materials that are uniformly weak in resisting internal distortion move as flows. Among such materials are mixtures of gases (air, steam), fluids (water), colloidal suspensions (clay slurry, mud) and granular solids (silt to boulders) [8]. Characteristic types of slope movement result from various combinations of these materials, coinciding with the descriptive classes of Varnes (1978). They are listed in Table 5.1.

At one end of the spectrum are flows of slurries; slow if plastic or more rapid if liquid as in the case of *quick clay flows*. These flows are governed by the laws of plasticity and visco-plasticity. At the far end of the spectrum are flows of granular solids alone, which are frictional at small scale but change their behaviour in large scale events such as the catastrophic *rock debris avalanches*. Flows of solid particles suspended in a carrying fluid are intermediate in character and conform to the laws of two phase flow. The carrying fluid might be clay slurry, as in the widespread semi-arid or alpine *debris flow*, water as in *quick sand flow* or air as in the flow of fine dry silts or ash.

Each of these three kinds of physical behaviour will be considered in a separate chapter. The next one deals with

---

[8] Snow, ice, lava and volcanic incandescent spray flows are not within the scope of this review.

Flows of plastic clay:

slow earth flows (temperate mudflows)

Flows of liquid clay:

quick clay flows

fine grained debris flows (mudflows) and lahars

Flows of solid particles in clay slurry:

semi - arid and alpine debris flows

debris avalanches (residual soil, colluvium, fill and waste)

volcanic lahars

Flows of solid particles in water and air:

minor subaqueous sand flows

quick sand flows

turbidity currents

dry silt and ash flows

loess flows

Flows of granular solids:

dry sand or gravel run

rock debris avalanche

Table 5.1 Types of flow slides classified with respect to material (based on Varnes, 1979).

University of Alberta

the flow of clay slurries alone. Chapter 7 will introduce the major subject of this thesis, that of flow of granular solids. Chapter 8 is concerned with the flow of granular materials suspended or dispersed in water or air. The flow of clay slurry and solid grains mixtures is treated in Chapter 9. Finally, Chapter 10 discusses the special characteristics of rock debris avalanches.

The present chapter reviews the general solutions of the equations of motion for flows, which are applicable to all types of flow slides, regardless of their constitutive behaviour.

5.2 Analytical models for flow sliding

By definition, the theory of flow slides belongs to the domain of fluid mechanics and, more specifically, to the hydraulics of open channels. There are three aspects which make the fluid mechanics of mass movements somewhat different from that of stream flow. Firstly, this is because of the diverse constitutive relationships encountered in flowing earth materials. Those which are reviewed in this and the three following chapters include viscous, visco-plastic (Bingham), pseudo-plastic (power law) and frictional behaviour. Even in cases where the Newtonian viscous model is applicable, the viscosity is usually high so that laminar flow is prevalent in most situations, contrary to the experience from stream flow where turbulent flow is dominant (Chow, 1959). Further, earth materials tend to be nonhomogeneous and thixotropic, so that fluid behaviour is often restricted only to a part of the flowing mass, while the rest is being rafted in the solid state.

Another characteristic of mass flows is the prevalent importance of unsteady flow. Typically, slope movements issue from sources of limited volume and the point of greatest interest is the unsteady motion of the flow front.

This section is devoted primarily to a review of this last aspect, i.e. to the models of unsteady flow. This will establish a point of reference for the discussion of the individual types of slope movement in the other chapters, which will then be focused mainly on the constitutive behaviour as reflected in the equations of steady, uniform flow.

The general equations of unsteady, nonuniform flow of fluid in open channels include the equation of motion:

$$\frac{\partial H}{\partial x} + \frac{\alpha v}{g}\frac{\partial v}{\partial x} + \frac{1}{g}\frac{\partial v}{\partial t} = S_o - S_f \qquad \text{Eqn. (5.1)}$$

and the equation of continuity:

$$\frac{\partial Q}{\partial x} + B\frac{\partial H}{\partial t} = 0 \qquad \text{Eqn. (5.2)}$$

where H is the flow depth measured normal to the bed slope, x is the downslope distance, v is the mean flow velocity, So and Sf bed and friction slope respectively, α a velocity distribution factor, Q is the flow rate, B the surface width and t time. Eqn. (5.2) assumes constant density. For flows on steeply sloping beds, which is the case for many landslides, the bed slope should be calculated as the sine of the horizontal slope angle α , while the frictional slope equals:

$$S_f = \frac{\tau}{\rho g H} \qquad \text{Eqn. (5.3)}$$

ρ g being the unit weight of the fluid and τ the bed shear stress.

In a uniform, steady flow, all of the terms on the left hand side of Eqn.(5.1) are zero and:

$$\sin \alpha = \frac{\tau}{\rho g H} \qquad \text{Eqn. (5.4)}$$

The large majority of published work concerned with the theory of flow sliding stops with deriving the equation of steady, uniform flow appropriate to the chosen constitutive relationship. Considerations of the more complex aspects of flow slide movement are rare. Morgenstern (1967) presented equations describing the motion of a sloping layer of infinite extent and constant thickness, composed of a Coulomb - viscous material characterized by a frictional shear strength and a constant plastic viscosity. The solution includes the inertial terms and is thus capable of modelling the gradual increase of velocity of a flow sheet of constant thickness before the steady state normal condition is reached. Such a model may be applicable to flow slides which develop spontaneously over a large area and immediately enter a prismatic channel without constrictions.

Furthermore, the steady state flow at the full thickness must be subcritical, so that the flowing mass would not thin out during its motion. Possibly, some types of very rapid debris avalanches may behave in this way. The method will be designated here as the infinite layer method, or Model A. (For a classification of the basic models, see Figure 5.4.)

The dam break problem (e.g. Chow, 1959, pp 534 and 568) has been applied by Jeyapalan (1980) to the analysis of debris flows generated by the failures of mine tailings dams. This analysis calculates the progress of waves generated by the sudden failure of a dam retaining a reservoir of still fluid in a section of a prismatic channel (Figure 5.1c). In an inviscid (frictionless) fluid on a horizontal bed, an upstream wave travels at a constant velocity equal to the celerity of a shallow - water wave away from the dam location. A pointed downstream wave proceeds in the opposite direction at the same time, at twice the velocity. The frictional resistance of the real fluid affects only the tip region. The motion of the upstream wave is therefore unaffected. The downstream wave develops a bulging front, the velocity of which decreases progressively and steadily, on a horizontal bed. Jeyapalan (1980) reviews solutions with turbulent frictional resistance and develops a new solution considering laminar flow in the front, which is more applicable to the highly viscous materials such as clay slurries or tailings. He further derives a solution of the dam break problem in a

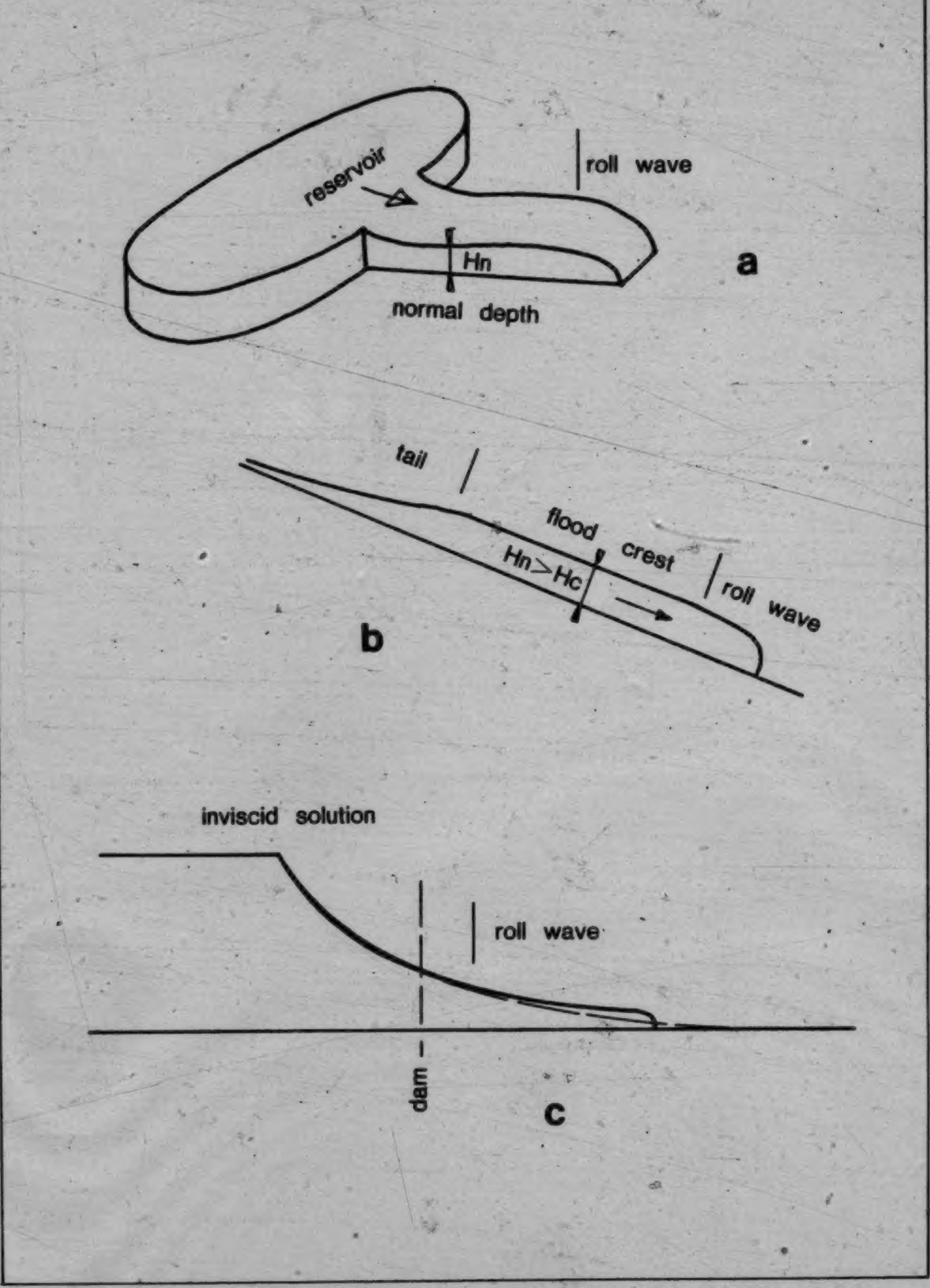
reservoir
roll wave
Hn
normal depth
a
tail
flood crest
Hn>Hc
roll wave
b
inviscid solution
roll wave
dam
c

Figure 5.1 Roll wave: (a) during steady discharge from a reservoir,
(b) at the front of a shallow flood,
(c) at the front of the dam break wave (variable velocity).

visco-plastic (Bingham) material and on a slope. In those solutions, the front thickness decreases gradually to a limiting value, at which the shear resistance of the fluid overcomes the driving forces and the flow "freezes". The solutions are very complex. The resulting charts presented by Jayapalan indicate that greater flow distances should result at flatter bed slope angles, which does not appear correct. The dam break problem will be referred to as Model D.

One simple model useful for the analysis of flow fronts of elongated and relatively shallow landslides is the uniformly progressive flow (Chow, 1959, p 528). Under this condition, the flow front moves forward in the form of a wave (called roll wave) which does not change its shape with time or distance. This forms typically when the flow at some point behind the wave front achieves normal (uniform and steady) velocity and depth, due to a constant supply of material from behind. For example, a roll wave would develop in a long relatively narrow channel, emptying a large reservoir at a constant rate (Fig. 5.1a). Alternatively, it could form the flow front of a flood of large total volume as shown in Fig. 5.1b, where the long crest approximates to a subcritical normal depth.

The first important property of the roll wave is that it moves with a velocity equal to the mean normal velocity of the flow. This forms a justification of the frequently used concept of calculating slide front velocities from some uniform flow (or "infinite slope", in case of frictional materials) analysis. The second property of the roll wave which greatly simplifies calculations is that both of the acceleration terms in Eqn.(5.1) are zero, so that one has a simple relationship in which the depth gradient of the wave equals the difference of the bed and friction slopes:

$$\frac{dH}{dx} = S_o - S_f \qquad \text{Eqn. (5.5)}$$

In the case of a turbulent flow of a Newtonian fluid, the friction slope is given by the Chezy equation:

$$S_f = \frac{V^2}{c^2 H} \qquad \text{Eqn. (5.6)}$$

where v is the mean velocity, H the local depth and C the Chezy coefficient. An expression for the normal depth can be obtained from:

$$H_n = \frac{V^2}{c^2 S_o} \qquad \text{Eqn. (5.7)}$$

where So is the bed slope, sin α. Combining Eqns. (5.6) and (5.7), subsituting into (5.5) and integrating, one obtains the equation of the surface profile of the roll wave:

$$\frac{x}{H_n} S_o = \frac{H}{H_n} + \ln\left(1 - \frac{H}{H_n}\right) \qquad \text{Eqn. (5.8)}$$

A dimensionless plot of this equation is shown by the dashed line in Fig. 5.2. The calculation has been carried out for a slope angle of 30 deg. but results for other slope angles could easily be obtained from the figure by

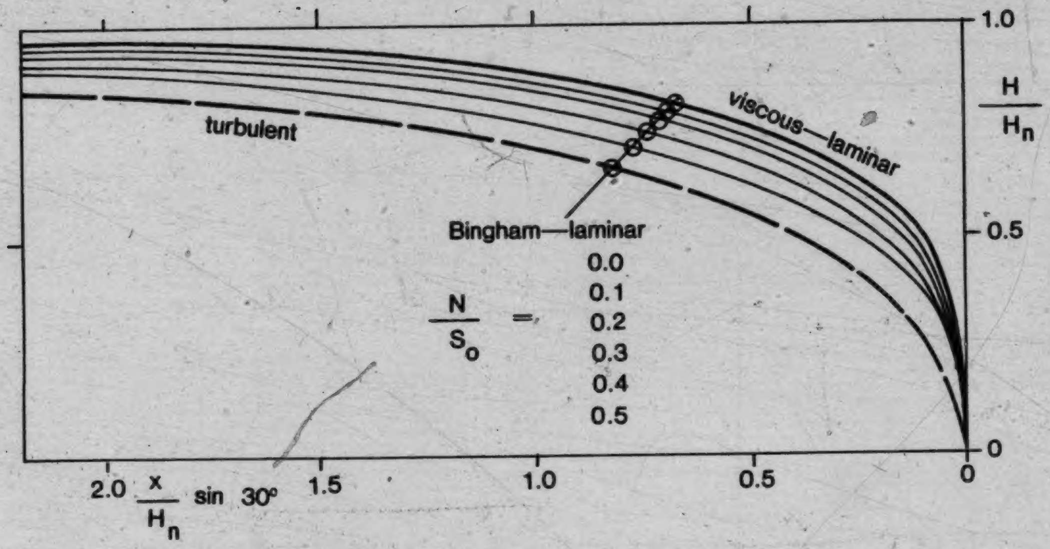

Figure 5.2 Roll wave profiles for viscous and visco—plastic materials.

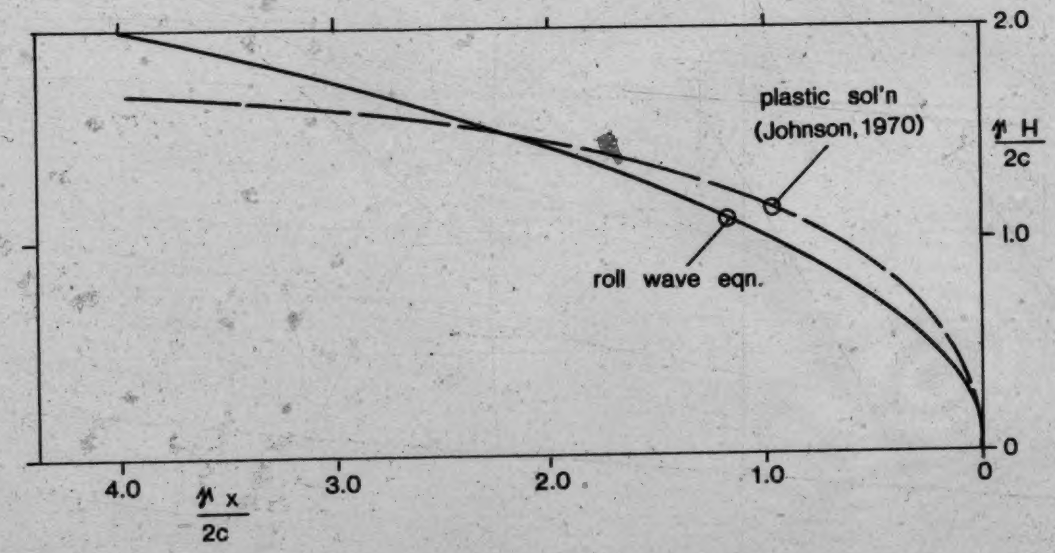

Figure 5.3 Flow front profile for a purely cohesive material.

multiplying the abscissa by the ratio between the sinus of the sought angle and sin 30 deg. The slope of the roll wave does not depend on the Chezy coefficient, although it does depend on the bed slope, the wave being longer and flatter at steep angles.

The same method of analysis can be applied to the viscous laminar flow:

$$S_f = \frac{3 v \eta}{\gamma H^2} \qquad \text{Eqn. (5.9)}$$

where η and γ are the viscosity and unit weight of the fluid respectively. The roll wave equation is in this case:

$$\frac{x}{H_n} S_o = z + \frac{1}{2} \ln \left(\frac{z+1}{z-1} \right) \qquad \text{Eqn. (5.10)}$$

z is the ratio H/Hn . The dimensionless equation is again independent of the fluid properties and is plotted by the heavy line in Fig. 5.2.

A visco-plastic(Bingham) material is characterized by a shear strength, c as well as viscosity. The friction slope is calculated as:

$$S_f = 2 \left(\frac{1.5 v \eta}{\gamma H^2} + \frac{c}{\gamma H} \right) \qquad \text{Eqn. (5.11)}$$

The same procedure yields a somewhat cumbersome expression, which reduces to Eqn. (5.10) for c=0. It is plotted in Fig. 5.2 for several values of the ratio N/S where:

$$N = \frac{2c}{\gamma H_n}$$

Eqn. (5.12)

These results indicate, that the shape of the roll wave is quite insensitive to material properties and even the constitutive relationship adopted, although both would of course affect the normal depth and with it the relative size of the wave.

It is interesting to note that Eqn.(5.5) can be applied realistically even to problems of quasi - static shearing. For a purely cohesive material, for example, one has by integration of (5.5):

$$\frac{H\gamma}{2c} = \sqrt{\frac{x\gamma}{2c}}$$

Eqn. (5.13)

which is compared in Fig. 5.3 with a solution from the Theory of Plasticity, derived by Johnson (1970). The curves are slightly different, because the hydrodynamic equation does not assume the existence of general shearing as the plasticity solution implicitly does. An application to the shearing of a frictional material is even simpler:

$$\frac{dH}{dx} = S_o - \tan\phi$$

Eqn. (5.14)

The predicted shape of the roll wave in this case is a straight line, inclined at an angle equal to the difference between the bed slope and the internal friction angle of the material. Such shapes have actually been observed in the sand flume experiments (Chapter 11). Of course, the roll wave theory is not strictly valid for the frictional case, since uniform velocity can only be achieved at a bed slope equal to the friction angle (Chapter 12). But it appears to be a reasonable approximation for slopes that are near this value.

The estimate of the size and velocity of the roll wave requires the knowledge of the normal depth, which is controlled by the discharge at the crest of the wave. The roll wave theory thus constitutes a complete predictive model only if combined with a determination of either discharge or normal depth by some other means. This can be accomplished relatively simply in several important instances, classified in Fig. 5.4:

Many landslides are characterized by an extensive but shallow source area, from which the liquefied material flows out through a narrow opening and a drainage channel. This configuration is typical of the large retrogressive flow slides in extrasensitive ("quick") clays or loose saturated sands. The flow in the drainage channel (Fig. 5.1a) assumes a normal depth fronted by the roll wave after a certain small initial distance. The normal depth is controlled by one of three factors, namely rate of production of disturbed material, rate of outflow through the opening or the normal discharge in the channel.

The first mechanism occurs in retrogressive landslides with relatively slow rate of retrogression, R, measured in m/sec. The volume of flowing material produced in the source area per unit time is:

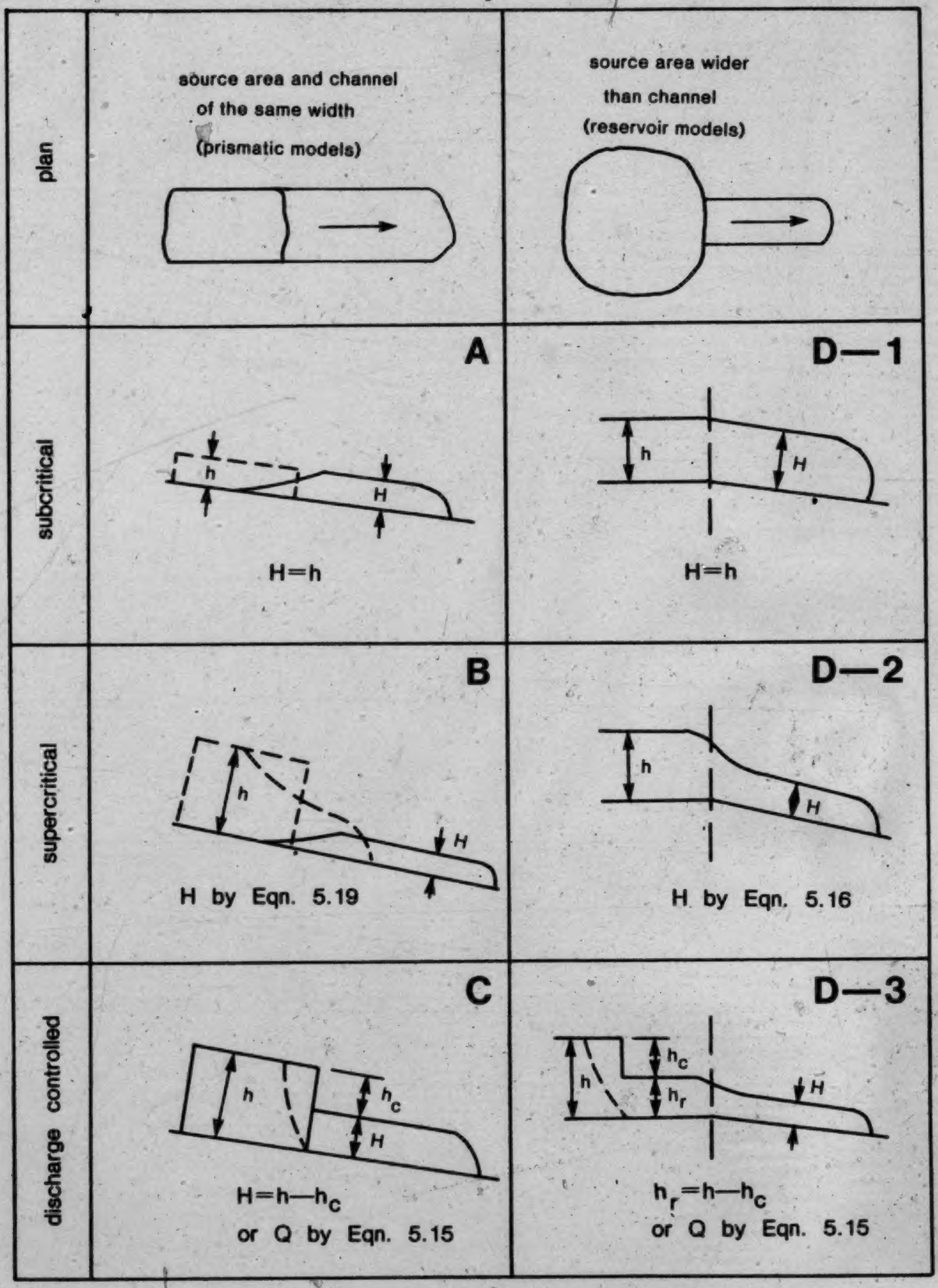
plan
subcritical
supercritical
discharge controlled
source area and channel of the same width (prismatic models)
source area wider than channel (reservoir models)
A
h
H
H=h
D—1
h
H
H=h
B
h
H
H by Eqn. 5.19
D—2
h
H
H by Eqn. 5.16
C
h
h_c
H
H=h—h_c
or Q by Eqn. 5.15
D—3
h
h_c
h_r
H
h_r=h—h_c
or Q by Eqn. 5.15

Figure 5.4 Classification of the basic flow models. Flow regime criteria apply to the source depth h. H is the normal depth of a steady uniform flow.

$$Q = RLh \ (m^3/sec.)$$

Eqn. (5.15)

where L is the length and h the height of the retrogression front. This discharge can be used directly in a standard equation of uniform steady flow, to calculate the normal depth and velocity. This mechanism is designated as Model D-1 (Fig.6.4). The retrogression rate as well as the dimensions of the potential source area are not easy to predict, and recourse must be taken to empirical observations. Mitchell and Markel (1974) give a correlation of scar dimensions with stability number which might be used for quick clay slides, although one should also consider local conditions, such as the extent of forestation and topographic relief. The rate of retrogression may be highly variable. For quick clay flows, slide durations of between a few seconds and a half an hour have been reported (Meyerhof, 1957). Subaqueous slides in loose sands have similar retrogression rates (Bjerrum, 1971a). Thus, it would generally be advisable to expect the retrogression rate to be very high.

In such a case, the landslide scar transforms almost instantaneously into a "lake" of liquid material (a term actually used by Tavenas et al, 1971, to describe a large quick clay failure). The hydraulic analysis then depends on whether the channel slope is steep or flat. If the slope is subcritical,then the normal depth equals the initial depth at the entrance of the channel. The velocity calculation is then simple, using the uniform flow formula (Model D-2). If the normal velocity is supercritical, then the depth in the channel will be less than that in the reservoir and must be determined by a formula for the discharge over a broad-crested weir:

$$Q = CBh^{3/2} \qquad \text{Eqn. (5.16)}$$

where C equals approximately 2.7 to 3.0 and h is the depth at the channel entrance. This constitutes Model D-3.

The situation is more complex in cases where the flow occurs in a width equal, or at least comparable to, the width of the source area. Here again, one should consider whether the flow initiates spontaneously or retrogressively. Spontaneous initiation is probably restricted to flows resulting from earthquake liquefaction or to thin debris avalanches starting on steep slopes. In these cases, the spontaneous acceleration implied by Model A would be approximately applicable. A roll wave would develop at the front of such flows on subcritical slopes but a general thinning should be expected on supercritical ones (Model B) with a front resembling the dam break wave.

If the failure develops retrogressively, the discharge could again be controlled by the rate of retrogression. This could, in such a case, be estimated by considerations of equilibrium. Rapid retrogressive failure develops basically under undrained conditions. In such a case, the strength of the soil is characterized by an apparent cohesion, c, and there is a critical stable slope height associated with it.

For a vertical slope:

$$h_c = \frac{2.5c}{\gamma} \qquad \text{Eqn. (6-17)}$$

It could then be assumed that a new retrogressive failure will occur at the crown scarp of a flow slide when the remoulded material at its toe has flown away in a sufficient quantity, so that the exposed height of the scarp equals the critical height. Assuming further that the flow develops its normal depth within a short distance, then the latter depth will equal the total height from the base of sliding to the crest of the scarp, minus the critical height. The normal velocity and thus the velocity of the roll wave at the flow front can again be calculated by standard formulas and this constitutes Model C.

The dam break problem (Model B) is applicable to the sudden failure of actual dams retaining reservoirs of liquid matarial or to the situation of spontaneous liquefaction of thick deposits standing on gentle slopes. Even there, the unsteady flow would be only episodic. After some time, the dam break wave profile flattens considerably and a point may be reached, when the crest of the variable roll wave at the tip of the flood approximates to the normal depth given by the uniform discharge through the "dam" location, given by the inviscid solution [9]:

---

[9] This neglects the slope of the source area and might be inaccurate on steeper angles.

$$Q = \frac{8}{27}\sqrt{g}\,h^{3/2}$$

Eqn. (6-18)

(Henderson, 1966), where h is the depth above the "dam" crest. By combining Eqn.(6-18) with the equations of the steady uniform flow for different fluid types, one can obtain formulas for the ratio between the depth of a flowing slug and the original depth of the source area. For example, for a viscous Newtonian liquid:

$$\frac{H}{h} = 0.96\left(\frac{\eta\, q^{1/2}}{S\gamma}\right)^{1/3}\frac{1}{\sqrt{h}}$$

Eqn. (6-19)

where η is the viscosity and S the slope. This relationship is plotted in Fig. 5.5 and can be used to estimate the terminal thickness of flow sheets generated by spontaneous liquefaction on gentle slopes. An equivalent could easily be derived for Bingham flow as well.

The simple models developed here and classified in Fig. 5.4 can be used in practically any situation to obtain a first estimate of the roll wave velocity and height, in its steady - state terminal stage. This can then be supplemented and modified using standard rules for uniform flow to take into account channel sinuosity, changes in angle and crossection etc. For a more refined analysis, one could obtain a numerical solution to Eqns. 5.1 and 5.2 using a flood routing computer program. Existing stream flow programs are generally developed for turbulent flow on the basis of Manning's formula and would have to be modified for other constitutive relations. Jeyapalan (1980) developed a computer program for flood routing of Bingham material in

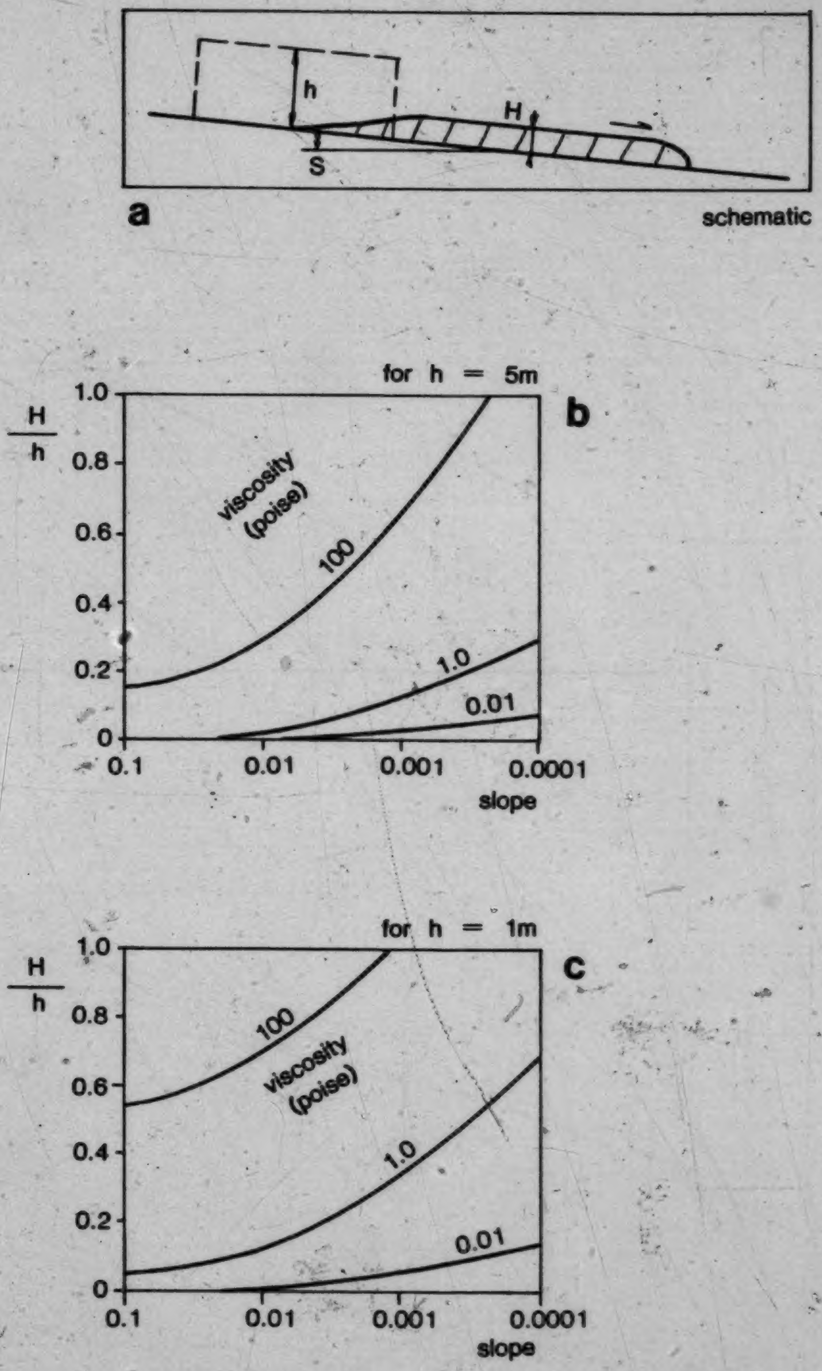

Figure 5.5 Terminal state of a dam—break wave in a viscous material.

prismatic channels. It should be pointed out, however, that uncertainties connected with constitutive behaviour, which are to be discussed in the following sections, do not justify the use of very complex analytical models.

6. FLOWS OF CLAY SLURRY

6.1 Slow Earth Flows

Slow earth flows are transitional in character between slides and flows, since they combine mass displacement along discrete shear zones with internal distortion.

Characteristic examples of small, earth flows have been described by Sharpe and Dosch (1942) in the upper Ohio valley. Surficial creep results in the movement of cohesive debris downhilland in its deposition in layers up to 3 m thick, on slopes of 17 deg. The disturbed colluvial materials easily saturate by infiltration, as they are underlain by more impervious materials, and become sources of flows.

The individual flows are on average 30 m wide, 60 m long and a maximum of 3 m thick. In cros- section they exhibit tear- drop shaped frontal lobes, the curved surfaces of which are thrust up above the general slope surface (Fig.3.11). In the early stages of development, the lobes are smooth. Often, the original turf covering them remains untorn. Later, minor thrust faults and ridges develop. The head areas contain concentric crack systems and detached slump blocks in front of a well defined sub- vertical scarp. Each flow develops initially in a single, moderately rapid movement during several days. Afterwards, the movements remain intermittent and slow (4m/year). The main (basal) sliding surface is difficult to define in the frontal area.

Keefer (1977) observed similar basic features in earth flows of the San Francisco Bay area. In addition, he noted the presence of slickensides on both basal and lateral shear planes. He measured average velocities of 12 to 44 m/year and maximum (temporary) velocities of up to 140 m/year on well developed flows. All of the movements had been taking place during the wet winter months. Earthflow material increased in water content and became noticeably soft and plastic during the period of activity.

Earth flows are capable of surges, during which they may achieve destructive velocities and proportions. A well known example is the Handlova earth flow in Czechoslovakia (Zaruba and Mencl, 1969). This flow, ultimately more than 20 M cu. m. in volume, developed in colluvial deposits of periglacial origin, on a slope of 7 to 13 deg. At first, a large earth flow developed in the upper part of the 1800 m long slope. This surged and rapidly dumped a large quantity of material on the deep colluvial deposits of the lower slope. These were thus brought into motion, generating a flowing sheet 1 km wide. The initial rapid motion period lasted for about a month and achived a maximum velocity of 6.3 m/day. One hundred and fifty houses were evacuated and subsequently destroyed.

The previous examples illustrated "spontaneous" development of earth flow out of previously stable debris, generally on account of a temporary overloading of the head or rise in water level. An alternative type of earth flow develops as a transporting link between a source area where material is fed by some other process, and a toe area subject to active erosion. Such earth flows have been thoroughly investigated by Hutchinson (e.g.1970) in the coastal cliffs of south-eastern England. The source areas were couloirs and gullies in the steep upper slopes of the cliffs, where desiccated London Clay debris was supplied by minor slumps and falls. Several minor "feeder flows" converged on central "accumulation flows". The tongues of the latter overode the sandy beach some 30 m below and extended to within the range of storm wave erosion. The central parts comprised channels inclined less than 10 deg., with slickensided shear planes. The material consisted of lumps of intact clay suspended in a soft remoulded matrix. The flow at Beltinge moved irregularly at an average rate of 15 m/year (100 m/year maximum).

Hutchinson et al. (1974) described distinct surges in the history of a coastal earth flow at Minnis North, North-East Ireland. The geometry of the earth flow is similar to that described earlier. Sudden movements of several metres (surges) occurred between periods of stability at intervals of one week to four months. Each surge initiated abruptly, without much previous creep, and reached a velocity of up to 8 m/min on the accumulation flow. The total displacement in a large surge is believed to be capable of exceeding 100 m. An eyewitness to a major surge noted temporary water flow stoppage in surface runoff channels on the earth flow ,followed by a rapid movement of the feeder flows, accumulation of material on the top part of the trunk flow and a surge of the latter, the entire process occupying about 10 min.

A similar description applies to the alpine Slumgullion earth flow (Crandell and Varnes, 1961), except for scale. The active part of this earth flow is 4 Km long, 300 m wide and moves on an average slope of 7.6 deg. at a steady rate of 5 m/year. There is no record of surges in this earthflow. The source materials are hydrothermally altered Tertiary volcanic rocks, rich in montmorillonite.

Earth flows appear generally to develop in previously disturbed colluvium or fill. Keefer (1977) summarized information indicating that the grain size composition of many flows comprises 10 to 50 percent clay, 25 to 65 percent silt and 5 to 50 percent sand. He also determined, by laboratory shear testing and conventional stability analysis, that the basal shear zones of the earth flows he studied had been sheared to reach the residual strangth. Both Hutchinson (1970) and Keefer (1977) measured vertical velocity profiles, showing that nearly all the shear strain in the central portion of the flows is concentrated at, or in the immediate vicinity of, the basal shear plane. Basal scouring or "inclusion" is common. On the other hand, the frontal parts of earth flows are known to deform strongly internally, so that they often overrride the ground ahead without disturbing the underlying topsoil. Surface velocity profiles are usually quite uniform across the flow indicating that, again, much of the strain is concentrated in the lateral shear surfaces. Longitudinal velocity profiles, however, are highly nonuniform, suggesting kinematic waves (Keefer, 1977).

The slow, intermittent nature of earth flow movements is caused by a balance between the gravitational driving forces and the residual frictional resistance of the basal shear plane. Accelerations result, when the balance is disturbed by an increase in groundwater pressure, due to added infiltration or to undrained loading. Hutchinson and Bhandari (1971) measured the water pressure in the interior of an accumulation deposit at the head of an earth flow. The pressure changed from hydrostatic to geostatic level with addition of fresh material to this location. Keefer (1977) noted visible softening of the active parts of earth flow complexes, accompanied by a rise of water level in cracks to the ground surface.

The assumption that earth flows are in stable balance during dry periods and mobilize in response to an increase in pore pressure at the basal plane is not sufficient to account theoretically for the observed velocities. This is because frictional theory would predict excessively large velocities. As an example, consider a flow 2 m thick, with a density of 1.73 g/cu.cm and standing on a 7.2 deg. angle. If the residual friction angle of the material were equal to 15 deg. and the pore pressure at the base plane level were equivalent to water table 0.2 m beneath the ground surface, the flow would be marginally stable. If now the pore pressure rose to the ground surface level, i.e. by 20 cm, Eqn.(3.3) (Section 3.2) would predict an acceleration of 0.14 m/sec2 and catastrophic velocities within seconds. There are two reasons why earth flows do not accelerate like this. Firstly, as had been discussed in Section 3.4, residual friction angle increases with the logarithm of velocity. Keefer (1977) investigated this in a single test on a sample cut from a basal shear plane of an earth flow, but found in that case that the increase was relatively minor, only about 5 percent for a velocity range of from 0.1 to 200 cm/day. Nevertheless, he did suggest using a Coulomb power law material to model changes of velocity due to water pressure fluctuations:

$$\begin{gathered}(\tau - \sigma' \tan\phi - c)^n = A\dot{\epsilon}_s \\ \tau > \sigma' \tan\phi + c\end{gathered} \qquad \text{.Eqn. (6.1)}$$

and

$$\begin{gathered}0 = A\dot{\epsilon}_s \\ \tau = \leq \sigma' \tan\phi + c\end{gathered} \qquad \text{Eqn. (6.2)}$$

where $\dot{\epsilon}_s$ is the shear strain rate in the deforming zone, τ and σ' are the shear and effective normal stresses respectively c, and ϕ are the Coulomb strength constants applicable within the deforming zone.

The velocity profile can be obtained easily by integration of these equations. But the validity of such an approach is questionable, since Keefer himself notes that the major part of the movement occurs on the slickensided discrete basal shear plane. Perhaps a better model could be obtained by using the sliding block equilibrium equation with a viscous term based on the friction angle - log. velocity relationship. The latter can be written approximately as:

$$\tan\phi = r + s\log\left(\frac{v}{v_o}\right) \qquad \text{Eqn. (6.3)}$$

where v is velocity, v_o a reference velocity and r and s are constants.

Steady-state motion with no acceleration implies that the driving and resisting forces must be equal. In such a case, from Eqn. (3.1):

$$\tan\phi = \frac{\sin\alpha}{\cos\alpha - \frac{u}{w}} \qquad \text{Eqn. (6.4)}$$

and the stable velocity can be calculated by subsitituting into:

$$v = v_o\,10^{\left(\frac{\tan\phi - r}{s}\right)} \qquad \text{Eqn. (6.5)}$$

It is now possible to recalculate the previous example on the basis of this model. In addition to the previous parameters, it is necessary to know r and s. If the direct shear test yielding ϕ were conducted at a speed vo =0.1 cm/day, then r=tan 15 deg. = 0.268. The coefficient s is assumed as 10 percent in four log cycles (or twice the value suggested by Keefer's and Petley's (1966) experiments). By introducing these values into Eqns. (6.4) and (6.5) one obtains a velocity equal to 100 m/day for the 20 cm rise in water pressure, which is still much too high. Therefore, this theory, although it derives directly and simply from laboratory tests and field observations, is still insufficient to explain the low velocities observed in earth flows. Perhaps, the answer lies in the geometrical complexity of the phenomenon. Thickness, water level, slope of the basal plane, channel width and a number of other parameters vary from place to place in an earth flow. It is clear that all locations within the earth flow area do not mobilize simultaneously. The material that does become unstable tends to move, but it thrusts into other material that is quite immobile. An example of the latter is the relatively well drained material in the front of the flow, which furthermore lies on the flattest slope. Internal distortion and thrusting therefore occurs, and the mobility of the whole is much reduced. Surges occur, when the rise in water pressure is great enough that the mobilized areas are more extensive. To make a quantitative prediction of velocity resulting from a given change of conditions, one would need to integrate the mobility equations across the area of the earth flow, assuming that the controlling parameters can be reliably estimated everywhere. This appears to be exceedingly difficult, expecially in view of the fact that velocity estimates resulting from the semi-logarithmic relationship represented by Eqn.(6.3) are extremely sensitive to the accuracy of strength data.

There seem to be some exceptions to the above discussion. For example, the Slumgullion earth flow in Colorado (Crandell and Varnes, 1961) moved at a steady rate for 13 years without at all reflecting the seasonal climatic variations. It was therefore mobilized uniformly. Possibly, as suggested by the authors, the flow moisture levels were constantly at optimum throughout the year in the entire area of the flow.

Hadley (1964) describes a re-activation of the Kirkwood earth flow in Idaho caused by the Hegben Lake earthquake of 1958. The earth flow, stagnant for many years, began moving about five days after the earthquake and displaced 30 m during the following several weeks. Rise in water levels due to vibrational compaction and slight increase in the slope angle may have been responsible for the renewed movement, which can thus be explained in a conventional way.

6.2 Rapid Earth Flows

The extrasensitive postglacial marine clays of Eastern Canada and Scandinavia are subject to spectacular flow slides known as *quick clay flows*. These failures are of a retrogressive nature, starting from minor bank slumps and extending in concentric steps to generate wide, roughly circular or elongated craters. The mechanics of the initiation and retrogression are those of slumping or sliding of a very brittle material and have been discussed in Chapter 3. The subsequent events, however, must be considered in this chapter dealing with flows. The rapid slumping movements remould a substantial portion of the clay, which then flows out of the crater through a narrow opening and may follow a natural drainage course for a considerable distance.

Meyerhof (1957) summarized case histories to show that these landslides develop on river terraces with gently sloping banks adjoined by extensive plateaus underlain by the marine deposits. The slide volumes are usually in the range of 0.5 to 1.0M cu.m, although the largest historical event at Vaerdalen in Norway comprised 55M cu.m (Holmsen, 1953) and even larger prehistoric flows are witnessed by scars. Velocities of translation (presumably within the crater) are quoted by Meyerhof as well as Skempton and Hutchinson (1969) as varying between 2 and 5 km/hour. The velocities of the subsequent flow through the drainage channel may be considerably faster. At Vaerdalen, the flow front arrived 5 km down the valey 45 min. after the initial slide, but at one point the debris is said to have resembled "a wave of water, travelling faster than a horseman". The Kenogami flow of 1924, in Canada, travelled at about 15 km/hour in a valley with a gradient of 6 deg. (Terzaghi, 1950), while that at St.Jean-Vianney (Tavenas et al, 1971) developed an estimated average speed of 26 km/hour on a sinuous course 3 km long .

The material involved in these landslides is typically soft to firm clay of low plasticity, silty or varved clay, or silt (Meyerhof, 1957). Its chief characteristics in the unweathered state are natural moisture contents equal to or exceeding the liquid limit (25 to 60 percent) and a sensitivity greater than 10 and often as high as several hundred. Some of the materials possess cementing bonds in the undisturbed state, which help to increase their brittleness (Conlon, 1966). Nearly all authors writing about quick clay describe its conversion by remoulding into a "viscous liquid" state.

Another important aspect of quick clays is the presence of a desiccated crust. The upper 2 to 4 m of the clay stratum, where exposed the ground surface, have different properties from the underlying parent material. The most important differences are a decrease in natural water content below the liquid limit, increase in peak strength and a drop in sensitivity. Desiccation effects are accentuated by the action of tree roots (Crawford, 1968),so that forested areas are often more stable.

The character of quick clay flow motion has been described in several eyewitness accounts: The Selnes flow (Kenney, 1967) had a volume of 140 000 cu.m and moved out of a roughly rectangular area of 1.8 ha. The clay was soft and had a sensitivity exceeding 100. After a quick series of retrogressive failures, occupying only a few minutes, the debris flowed out of the crater and for 400 m down the stream valley, where it became "dammed against a growth of small trees at a sharp bend of the river". Several persons were carried down with the flow, riding on flakes of undisturbed ground and inside a building located on one large flake. An eddy current was observed in the flow. The longitudinal profile of the surface of the debris after the flow was inclined at not more then 1 degree. The flow eroded the bottom and sides of its channel.

The South Nation River landslide near Ottawa (Eden et al, 1971) had an area of 28 ha. Its material consisted of extrasensitive clay (sensitivity 10 to 100) overlain by 1.8 to 6 m of silty sand. The crater was again rectangular, open to the river in its full width of 640 m. Within it are preserved the individual retrogression strips in the form of backtilted and subsided terraces, separated by ridges and pinnacles of undisturbed clay. The river channel was filled without much overflowing to a maximum depth of 11 m for a total length of 2450 m, including both the upstream and downstream branches of the flow. The surface of the clay flow in the river is not steeper on the average than the original flat gradient of the channel. It is covered by solid debris, including many large flakes of ground surface with trees standing upright. The existence of such firm flakes on the surface of a rapid clay flow has also been described in a vivid eyewitness report from the Kenogami slide in Quebec, quoted by Terzaghi (1950).

The St.Jean- Vianney clay flow of 1971 had an estimated volume of 6.9M cu.m, resulting from an area of 27 ha. It formed within a crater of a much larger prehistoric landslide. Approximately 80 percent of the soil involved in the slide left the area of the crater through a wide opening and travelled down the Petit Bras and Aux Vases river valleys for a distance of 3 km. Its velocity had been estimated from superelevation in meanders as 26 km per hour, which seems to match the timing of the events. The maximum depth of the flow was about 18 m near its origin and 9.5 m at the lower end of the channel, where the flow issued into the large Saguenay River. This latter depth decreased rapidly with time after reaching its maximum , and 2 hours after the slide the Aux Vases river valley was completely evacuated of debris and back to its original level. The sides of the valleys show signs of intensive erosion, including horizontal scour marks left by solid debris carried by the clay slurry. Several houses, cars and a bus, washed away from the far side of the crater, have all been carried down all the way to the Saguenay River. The authors suggest that a dam of solid debris delayed the flow temporarily near the mouth of the scar, creating a "lake of liquid clay", before releasing it into the river.

Two significant conclusions emerge from these descriptions. One is that remoulded quick clay slurry is indeed capable of almost purely viscous (Newtonian) flow behaviour, without any significant shear strength. This is demonstrated by the extremely low angles of debris surfaces achieved shortly after the flow and, even more strongly, by the capacity of the flow to evacuate completely a flat drainage channel within a few hours after the event. A plastic (Bingham) flow would leave a stagnant residue of finite thickness. Even nonlinear (pseudo- plastic) material would leave such residue, although only temporarily. The evacuation would occur with some time delay. Bentley (1979) carried out viscosimeter tests on clay samples from the St.Jean- Vianney site and indeed found them to approximate relatively closely to the ideal Newtonian behaviour, although with a slight dilatant curvature.

The second conclusion involves the apparent importance of solid debris carried by the flow. Obviously, much of the desiccated crust is strong and insensitive enough to resist remoulding and thus is carried on top of the underlying slurry in the form of large solid flakes, reinforced by timber, root systems and turf.

A method of analysis of quick clay flows is proposed in Section 6.4, after a review of the flow characteristics of clay slurries.

6.3 Flow Properties of Clay Slurries

Clay slurries, or mixtures of clay mineral particles and water, may behave as viscous, visco-plastic or nearly perfectly plastic substances, depending upon water content, strain rate and a number of other factors. The ideal objective of this section would be to delineate quantitatively the range of conditions corresponding to each of the three types of behaviour. Due to the complexity of the phenomenon, however, this has not been possible and the following discussion is therefore largely of qualitative nature, stressing the influence of the main factors.

Clay particles submerged in water or other fluid form flocs, the size and density of which is controlled by the electro-static forces associated with the particular mineral-electrolyte combination. The flocs themselves are not entirely electrically inert and in suspensions of higher concentration they form weakly-bonded aggregates. It is the interaction between the fluid and the flocs that largely controls flow behaviour of slurries (Michaels and Bolger, 1962). The behaviour is therefore determined by the following primary factors:

- clay mineral type
- electrolyte type (i.e. salt content in pore water)
- concentration of solids

Further factors, which are derived from the three basic ones are:

- floc concentration
- floc size
- floc shape
- electrostatic fields between flocs

At very low solids concentration, slurries retain the Newtonian character of clear water. Their viscosity is independent of the strain rate and given by the Einstein's equation which discribes the effects of solid particles that do not interact with each other (e.g. Searle and Grimshaw, 1959). In terms of relative viscosity, i.e. the ratio of slurry viscosity to that of water, the Einstein's equation is

$$\frac{\eta}{\eta_w} = 1 + kC$$

Eqn. (6.6)

where C is the volume concentration of solids and k a constant, equal to 2.5 for spherical particles, but up to 4.9 for elongated aggregated flocs (Lewis and Nielsen, 1968).

The simple relationship breaks down at greater concentrations, as the motion of the clay particles begins to be restricted, either by direct contact or through electro-static forces. Various corrections then exist adding higher terms or changing the form of Eqn. (6.6) (Ford, 1960), but none has been accepted as universally valid for all types of clays. The major factor determining the viscosity at this stage appears to be the floc concentration, as shown in Figure 6.1. Due to the entrapment of water inside the flocs, this latter concentration may be as much as 10 times the total concentration of solids (Michaels and Bolger, 1962), although it may also equal only to 2 (Takahashi, 1980). Thus, the ratio between floc

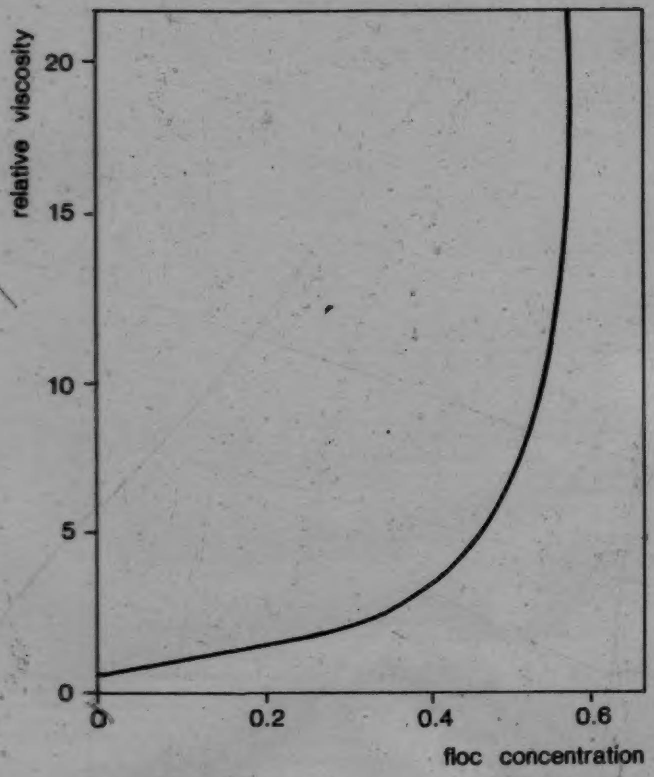

Figure 6.1 Viscosity vs. floc concentration for flocculated kaolin. (Michaels and Bolger, 1962).

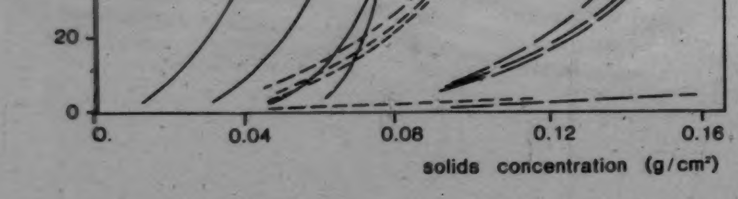

Figure 6.2 Viscosity — concentration relationship for three clays with various pore water chemistry (Searle and Grimshaw, 1959).

concentration and clay concentration is a critical parameter controlling the flow behaviour of a clay slurry and, in general, flocculated clays are much more viscous than dispersed ones. This is why a great range of viscosity-concentration relationships can be found for different mineral - electrolyte combinations (Fig. 6.2).

At a critical solids concentration which corresponds to a floc concentration of about 0.6, the viscosity rises almost asymptotically. Even prior to this, however, the suspension loses its Newtonian flow character and develops a pseudo-plastic curvature and, at higher strain rates , a linear Bingham viscosity relationship (Fig. 6.3). For a flocculated Kaolin suspension, Michaels and Bolger (1962) found that the Bingham yield strength in dynes/ sq. cm equals about hundred times the square of the floc concentration. Hampton (1972) determined Bingham yield limits for four types of clay slurries, which are given in Fig. 6.4 in relation to water content. If one assumes 100 dynes/ sq. cm as the lowest significant strength value for a clay slurry involved in a gravitational flow, this is seen to correspond to a water content of 70 percent in the case of Kaolinite and 85 to 100 percent in the case of bentonite.

The pseudo-plastic nature of flow behaviour of clay slurries is important at low shear strain rates, typical of full scale gravity flows that occur in slope movements. Figure 6.5 shows flow curves determined from an unspecified clay slurry by Yano and Daido (1965). The curved

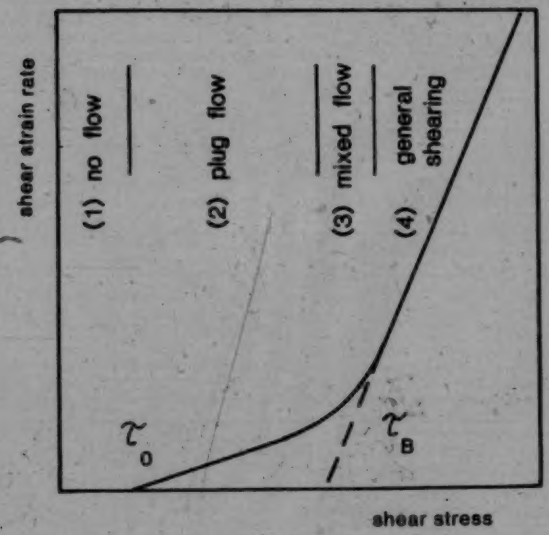

Figure 6.3 Flow curve of a visco—plastic material: (Searle and Grimshaw, 1959).

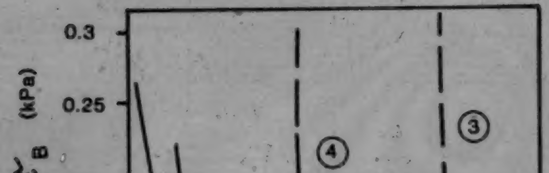

Figure 6.4 Bingham strength of clay slurries: (1) kaolinite (2) kolinite with sea water (3) montmorillonite (4) m. with sea water (Hampton, 1972).

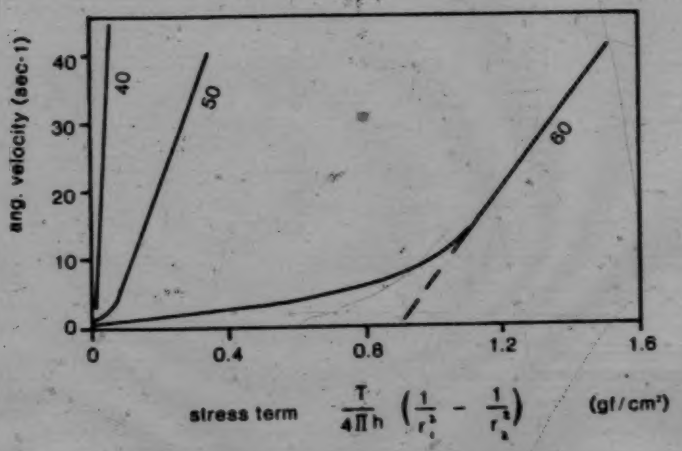

Figure 6.5 Coaxial viscosimeter flow curves for a clay slurry at various concentrations (Yano and Daido, 1965).

relationship at low strain rates could possibly be regarded as a linear one up to a certain limit, at which the curvature becomes important. From Figure 6.3 it would appear that this first limit would correspond to the Bingham yield value. At a higher stress or strain rate, it would be necessary to use the pseudo-plastic power relationship of Eqn.(6.1). At still higher stresses, a point is reached called the upper yield limit, beyond which a linear relationship between strain rate and stress is again recovered. The flow is then controlled by the Bingham's equation:

$$\dot{\gamma} = \eta(\tau - \tau_B)$$

Eqn. (6.7)

where η is the plastic viscosity, $\dot{\gamma}$ the shear strain rate, and τ_B Bingham's yield limit.

The apparatus most often used to measure the flow propertis of clay slurries in ceramic and chemical industries is the coaxial cylinder viscosimeter (Searle and Grimshaw, 1959). For design of industrial slurry pipe transport systems, the capillary viscosimeter is also used. Either of the two types of instruments would therefore be suitable to determine the potential mobility of earth materials involved in landslides, if the appropriate water content could be predicted.

When a suspension of flocculated clay particles is stagnant, weak electro-static forces bind groups of flocs into aggregates and the latter among themselves. In some concentrated suspensions, this process may build up a fairly strong network which must be broken up if shearing is to take place. Thus, the suspension behaves thixotropically. The above described viscosity changes at low strain rates are due to the gradual breakdown of the aggregates (Michaels and Bolger, 1962). Hampton (1975) observed that the ability of a clay suspension to support solid particles decreases dramatically while the suspension is being sheared.

When a thick clay slurry is being extruded through an orifice under gradually increasing pressure, three different types of flow are observed (e.g. Searle and Grimshaw, 1959). At first, there is no flow, before the initial yield strength of the slurry is exceeded. When flow starts, it takes first the form of a plug flow, shearing along discrete shear planes. Near the Bingham limit stress, a mixed flow regime appears, with both discrete and internal shearing. Finally, at pressures above the upper yield limit, the streamlined internal (flow) shearing begins to predominate. Thus, thick slurries can be regarded alternatively as plastic solids or viscous fluids, depending on the magnitude of the forces, the boundary between the two models being determined approximately by the Bingham limit which in turn depends on water content (Fig. 6.5). The distinction between these two flow regimes has an equivalent in the natural division of clay slides and flows, slow earth flows belonging to the intermediate category.

6.4 Analysis of Rapid Earth Flows

No one has attempted to analyse quick clay flows from the point of view of fluid dynamics in the published literature. Therefore, a simple analysis is offered here. The sudden outflow of liquid clay from an extensive crater into a narrow river channel resembles the situation when the sluice gate of a reservoir is suddenly open, or when a dam impounding a reservoir at the head of a narrow channel bursts. Thus, models D-1,2 or 3, developed in Section 5.2 and illustrated in Fig. 5.4 appear directly applicable, provided that the supply of material is large and that the channel is approximately prismatic.

To obtain the velocity of the wave, it is necessary to calculate the velocity in the channel corresponding to the normal depth, H. According to arguments presented earlier, the shear strength of the clay slurry in the typical case can be neglected, and the flow treated as Newtonian. Further, in view of the high viscosity of the slurry it is at first assumed that the flow is laminar, although it is recognized that local eddies may result from major irregularities of the geometry. For a wide, rectangular channel, the Poisseuille equation gives:

$$V = \frac{\gamma S H^2}{3 \eta} \qquad \text{Eqn. (6.8)}$$

where η is the dynamic viscosity of the clay and γ the bulk unit weight.

It is now necessary, however, to consider the behaviour of the flakes of solid material carried on top of the flow. If they moved with the surface of the laminar flow as shown in Figure 6.6a, they would constantly overtake the fluid slurry and concentrate at the front. Thus, the flow would dam itself within a very short distance down the channel. But there are two other factors. Firstly, the solid flakes develop high friction with respect to the sides of the channel and are thus slowed down. Secondly, as any given flake moves forward towards the flow front and begins to become grounded, the slurry, immediately backing up behind it, will tend to lift it up again and bring it back into motion. One could then conceive that the velocity of the flakes will be at the most equal to the *mean velocity* of the liquid slurry. Of course in many instances it will be less than that, due to high side friction resulting from irregular banks or sinuous channels. Often, the flow will indeed become dammed at a channel irregularity, as occurred in the case of the Selnes flow slide. But while such effects are analytically intractable, the above assumption is a conservative one. It can be implemented by re- deriving the Poiseuille relationship so that the mean velocity of the fluid will equal the surface velocity. (Fig. 6.6b). Using the parabolic velocity distribution, it is found that this occurs when the depth of the liquid, h , equals 1.5 times the depth h of the velocity maximum as shown in the figure. Under such conditions, the mean velocity, equal to the

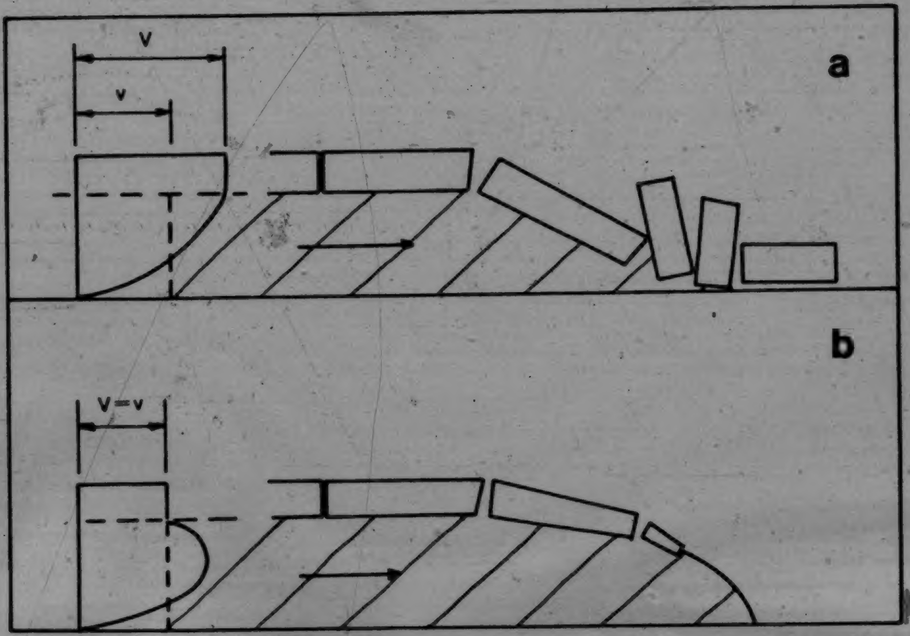

Figure 6.6 Laminar flow of slurry and solid flakes. (a) Self—damming Poiseuille flow, (b) Flakes slowed down by side friction — sustained flow.

velocity of the flakes is:

$$v = \frac{\gamma S H^2}{6\eta} \qquad \text{Eqn. (6.9)}$$

and the Reynolds' number:

$$R_e = \frac{2}{3}\,\frac{vH\rho}{\eta} \qquad \text{Eqn. (6.10)}$$

The thickness of the solid raft does not enter into the equations, since its weight is offset proportionately by its side friction.

The above relates to a wide, shallow channel. The flow in a confined channel will have a velocity:

$$v = \frac{\gamma S H^2}{k\eta} \qquad \text{Eqn. (6.11)}$$

where k is some coefficient. In case of a semi-circular channel, k equals to 8. If the semi-circular channel carries a raft under the same conditions as considered above, a simple solution is not possible. But it may be sufficient to estimate that the raft will increase k about 1.5 times, i.e. to 12. The Reynolds' number for the semi- circular channel with raft equals approximately one- half that given in Eqn.(6.10).

Turbulent flow would occur, if the Reynolds' number exceeds 500 to 1000 (e.g. Chow, 1969). In that case, normal velocity could be estimated using the Darcy- Weisbach equation:

$$v = \sqrt{\frac{8gRS}{f}} \qquad \text{Eqn. (6.12)}$$

where R equals H in a wide channel flow, 0.67H in a wide channel with a raft, 0.5H and 0.33H in a semi- circular channel without and with a raft respectively. The friction coefficient f could be estimated from a standard flow resistance diagram.

The St.Jean- Vianney landslide can serve as an example, although the author does not have detailed information concerning the geometry of the flow. Bentley (1979) measured the viscosity of this clay as approximately 0.3 poise at a water content of 74 percent, which is probably close to the field value. The clay was dispersed ultrasonically prior to the experiment , which could have lowered the viscosity considerably. The flow front velocity was 7 m/sec, in a narrow channel sloping approximately 10 m per km. The channel crossection is assumed to be semi- circular, with a liquid depth of 8 m beneath the raft. The Reynolds' number would equal about 1M, indicating a fully turbulent regime. Estimating f from the Manning's formula with n=0.04 as f=0.04, Eqn.(6.12) yields a mean velocity of 7.3 m/sec. This is certainly fortuitous, considering the lack of reliable data. Nevertheless, the identification of turbulent regime is positive in this case. If the viscosity were to be back-calculated from the viscous flow equations for any reasonable geometry , it would be of the order of 1000 poise, which is much too high for a clay with a water content of 70 percent. The observed scouring of channel walls also attests to the existence of turbulent flow.

Considering the high speed and steepness of the flow front, and the low permeability of the clay, it is possible to estimate that the water content of the flowing slurry is not different from the average water content of the parent clay. Therefore, viscosity data from tests conducted on remoulded samples without adding water could be directly used to make estimates of velocity.

Reach of the flow slide is more difficult to predict. Since the crater floor can be expected to lie somewhat above the floor of the channel, it is reasonable to assume that the roll wave will progress with undiminished velocity for as long until its volume, combined with the volume of the wave proceeding upstream, equals the volume escaped from the crater i.e. up to 80 percent of the slide volume. At that point, the crest of the roll wave will tend to subside and damming is likely to occur.

7. GRAIN FLOWS

7.1 Sand Flows, Talus Flows.

Flows of fine grained slurries were seen in Section 6.3 to be significantly affected by electro - chemical forces acting between the microscopic solid particles. In the case of coarser nonplastic materials, the importance of these forces lessens and the flow behaviour becomes dominated by mechanical effects. Carrigy (1970), testing dry crushed quartz, found the last observable vestiges of electro - static attraction to disappear at a grain size of 0.074 mm, corresponding approximately to the silt - sand boundary. More commonly e.g. Fisher, 1971, the limits of colloidal behaviour are identified with the boundary between medium and fine silt sizes (0.008 mm).

The mechanical forces acting between coarse mineral particles include normal static intergrain pressure and friction and their dynamic impact equivalents, and the viscous or turbulent drag forces contributed by the pore fluid. Bagnold (1954) proposed a division of the granular flow into three regimes. The intergrain forces dominate in the *inertial regime* which occurs at high solid concentrations and high shearing rates. The fluid drag forces control in the *macro- viscous* regime at high fluid contents. A transition regime occurs at intermediate concentrations, when both groups of forces are important. The criteria for delimiting the three regimes will be discussed in Section 8.3.

This chapter considers flows of granular materials conforming to the inertial regime. Such flows may occur both in air and in water and, at least in concept, with any value of pore pressure equal to or different from the hydrostatic. The effect of pore pressure, other than simple submergence, are left to Chapter 8. Especially, liquefied "quick" flows are now excluded, since their initiating mechanisms, volumes and speeds set them apart from the phenomena described below.

Inertial grain flows occur on all slopes built of granular materials at angles approximating the angle of repose. A characteristic example is sliding on the slip face of a sand dune. Bagnold (1941) described the process by which the lee side of a dune becomes progressively oversteepened in its upper part by vertical settling of wind-borne grains. When a limiting angle of about 34 deg. is reached, an avalanche of sand moves down the slope, cutting into its upper part and depositing below, to establish a new straight slope face standing at some lower angle. The process can be easily simulated at small scale in two dimensions by the rotating drum experiment (Carrigy, 1970). If a transparent cylinder containing a small amount of sand is rotated slowly around a horizontal axis, avalanches will descend periodically down the surface of the sand layer. The surface will remain approximately planar, but its angle will vary from a maximum , just prior to an avalanche, to a minimum just after. For dry Ottawa sand, the respective angles are 35.6 and 30.9 deg. For a moist sand of the same kind, they are 43.4 and 28.0 deg. The angles further depend on grain size (directly) and roundness (inversely). There is some evidence that the difference between the two angles is proportional to the value of either one of them, although the proportionality coefficient may depend on the length of the slope and, possibly, other factors (Evans, 1979). The volume of the avalanches per unit width is the product of the difference between the two angles and the square of the length of the slope involved in sliding (Allen, 1970).

The actual dynamics of these minor sand flows have never been described in detail in the literature. This author has made some observations on dry Ottawa sand in a rotating drum 30 cm in diameter. Despite the straightness of the sand face prior to avalanching, only the upper one - third to one half of the slope participates in movement, if initiated by a slow, careful rotation of the drum. The flow, which in this case was no more than one cm thick, quickly develops a slightly elevated bulbous front, indicating general shearing rather than a slip on a discrete surface. It descends at a velocity of some 5 cm/sec and gradually decays in convexity, so that by the time the bottom of the slope is reached and the flow stops, the surface resumes a straight crossection. Thrust shearing and development of a flatter slope angle near the toe, described from natural sand dunes by Bagnold (1966), was not observed in this case.

Velocities of sand avalanches on desert dunes have been reported in the range of 13 to 120 cm/sec. Some of these avalanches emitted loud booming or roaring sounds during the later stages of their descent (Bagnold, 1941).

Similar dry surficial flow of particles has been pointed out as an important mechanism in shaping surface angles of talus cones and gravel or rockfill storage piles (Carson, 1977). Scheidegger (1975) applied circular arc analysis to the problem of stability of talus faces. This appears inappropriate, since the circle is by far not the critical failure surface shape in drained frictional materials. On the other hand, the model of periodical oversteepening by deposition and avalanching does not seem realistic either for long natural talus slopes, since it would imply the frequent occurrence of very large flows which has not been reported. Allen (1970) suggests that oversteepening only occurs in the upper slopes of talus cones, and avalanches from there travel only a short distance downslope. They deposit load there which in time avalanches again, on a limited scale, and so on. Of course, the interaction of the discrete rockfall process (Statham, 1976) and avalanching is probably complex on most talus slopes.

The dynamic nature of talus avalanches is again lacking detailed description in the literature. The author is familiar with them from climbing trips in the Rocky Mountains of Alberta. A typical occurrence is described in the following: A talus slope over a hundred metres long, composed of uniform angular fragments with a median size of about 5 cm was crossed by two climbers at mid - height. Their crossing caused a local instability and slight initial movement. The movement quickly spread out both downslope and up, so that in a few seconds a train of talus about 3 m wide and 15 or 20 m long was moving. It accelerated briefly and moved steadily for a few more seconds at a speed of approximately 20 - 30 cm/sec, then began to decelerate gradually. The end of the movement was an almost imperceptible creep. The movement was accompanied by a low rumbling noise which seemed to issue from the depth of some dm beneath the surface. The surface itself gave little indication of general shearing and the surficial grains were neither rotating nor moving with respect to each other. The front of the movement was pointed and indistinct, as was the tail. The total displacement during this episode amounted to about 2 m.

Similar flows observed by the writer on the face of a large coarse mine waste pile during dumping at the crest were similar in character, although larger in size. They moved at estimated steady velocities of up to 1.5 m/sec and exhibited slightly more surficial disturbance in the form of rolling, especially of the larger fragments.

Presumably, greater velocities and flow thicknesses can be achieved by talus flows initiated by some external impact such as that of a large rockfall. It must be pointed out, however, that dry talus flows, even when very large, almost never overrun the toe of the cone by very much [10]. For example, the 100 000 cu. m rockfall of December, 1978 from the Barrier in Garibaldi Park, B. C. (Hardy et al., 1978), propelled coarse debris not much further then the toe of the existing cone. Highly mobile flows on the surfaces of debris cones would deposit tongues of debris extending beyond the limits of the slopes. Such tongues have almost never been reported except in a few cases, where fluidizing action of interstitial mud cannot be ruled out (see Section 9.2). It can therefore be concluded that the displacement angle of dry talus and sand flows is certainly not much greater than the lower angle of repose (30 deg. in case of sand and 35 deg. in talus).

Inertial sand and talus flows occur on submerged slopes as well, for example on underwater dunes, on the distal faces of deltas, or on the walls of submarine canyons. Dill (1964) observed a range of slope movements, from sediment creep to initial turbidity current in the head of Scripps Canyon, California.

7.2 Experimental Observations

A number of experimental studies of dry grain flow have been reported by sedimentologists and by mechanical engineers concerned with the movement of bulk solids and powders. The purpose of these investigations has generally been to find experimental substantiation for proposed theories of granular flow, but also to provide data for possible future development of the theories.

---

[10] Although large, individually rolling fragments will do so, cf. Chapter 2.

Most investigators studied grain flow directly in inclined flume experiments, some of which are described below. Others concentrated on examining constitutive relationships in ring shear tests; their results have been reviewed in Section 3.4. A unique approach was taken by Bagnold, (1954) who derived constitutive laws for coarse granular dispersions in concentric cylinder viscosimeter tests on mixtures of fluid and hard wax grains of the same density. The details of his investigation are described in Section 8.3 and the theory deriving from it, as it applies to the inertial regime, is discussed in Section 7.3.

One of the earliest programs of flume experiments was reported by Takahasi (1937), who measured the velocity of sand flow on a 1.5 m long rectangular flume of various inclinations. The velocity was calculated from the shape of the trajectory of particles leaving the end of the flume. It was noted that sand flow could attain considerably greater velocities than water flow of the same thickness at flume inclinations greater than about 35 to 40 deg. The sand flow velocity was proportional to the flume inclination up to a certain velocity limit. At velocities below this limit, the sand flowed in a partial profile, forming a stagnant layer on the bed of the flume. Beyond the limit, however, the flow took place in full depth and attained a turbulent character. Velocity was again proportional to the inclination, but with a lower proportionality constant. The limiting velocity was approximately 1 and 2 m/sec in a narrower and a wider channel respectively. The paper gives no information concerning the degree of uniformity of the flow and roughness of the channel surface.

Roberts (1969) studied flow of seed in a smooth - surfaced flume with a high speed camera. At steady flows about 1 cm high and with an average velocity of up to 2 m/sec, he found that the bulk of the shearing occurs at the wall contact, although there is a slight, nearly linear velocity gradient throughout the depth of the flowing bed. The steady flow conformed to a simple sliding block analysis (such as Eqn. 3.3, Section 4.2), being uniform (free of accelerations) at a flume angle equal approximately to the residual friction angle of the material - wall interface.

Suzuki and Tanaka (1970) performed similar experiments with sand, using flow thicknesses less than 1 cm on a rough base. Their conclusion that shear strain rate at the base of the flow is directly proportional to shear stress (i.e. Bingham fluid) is based on the assumption that base slip velocity is independent on flow thickness and that the bulk density is uniform throughout the depth of the flow. Neither one of these assumptions has been substantiated.

A density distribution with depth was derived from experiments with sand by Augenstein and Hogg (1974). Their flows were also less than 1 cm thick, with a rough base. Vertical velocity profiles were derived by catching the sand into a row of compartments placed so as to differentiate the various trajectory lengths of layers travelling at different speeds. The rough data therefore consisted of percentage weight fraction versus velocity relations. To derive flow thickness vs. velocity diagrams from this, the authors had to assume vertical density destributions. They concluded that a thin layer immediately above the bed had a density of about 22 percent of the loose random piling density, compared to 78 percent for the bulk of the flow. Their method is questionable because firstly, the trajectories of the lowermost layers may be affected by the release of the dispersive pressure (cf. Sections 7.3 and 8.3) existing in the flowing layer upon leaving the channel. Secondly, the existence of stagnant corners in the flow, that have been observed in the present work, would further distort this analysis. Nevertheless, upward density increase above the bed of a granular flow was reported by others as well.

Velocity profiles with respect to depth have been recorded by Savage (1979) using a sophisticated measuring technique based on fiber optics. His test flume was 1.22 m long and 3 cm wide, with glass walls and a base lined with a rough rubber sheet. Surface velocities of up to 150 cm/sec were achieved. The experimental flows of polystyrene beads were approximately 1.5 cm thick. Nonaccelerating flows of nearly constant thickness were observed at flume inclinations between 32 and 39 deg., for a material with an estimated angle of repose of 24 deg. Dimensionless velocity distributions obtained by measuring through the glass side of the flume are shown in Fig. 7.1. These are likely to be somewhat distorted by side friction as pointed out by Savage. In another experiment, Savage (1979) established the existence of a normal depth in the flow of glass beads over a 6 m long flume with smooth base. The same flow depth resulted from two flows with different initial depths. But it must be pointed out that the maximum flow depth in this experiment was only 4 mm. When the experiment was repeated with a greater mass flow resulting in greater depths, an accelerating flow was found with progressively decreasing thickness.

An extensive program of flume experiments was carried out in the course of the present research, as reported in detail in Chapter 11. In contrast to much of the previously reported work, these experiments were designed to achieve large velocities and substantial flow rates. The velocity range achieved was 1 to more than 5 m/sec. Flow thicknesses (depths) varied between 3 and 13 cm. The measuring flume used was 20 cm wide and 150 cm long, with Perspex side walls and a base lined with the particular test material. Materials used included Ottawa sand, Polystyrene beads (probably the same as used by Savage, 1979), a crushed coarse angular sand and a mixture of angular sand and rock flour. Direct measurements were made of surface velocities

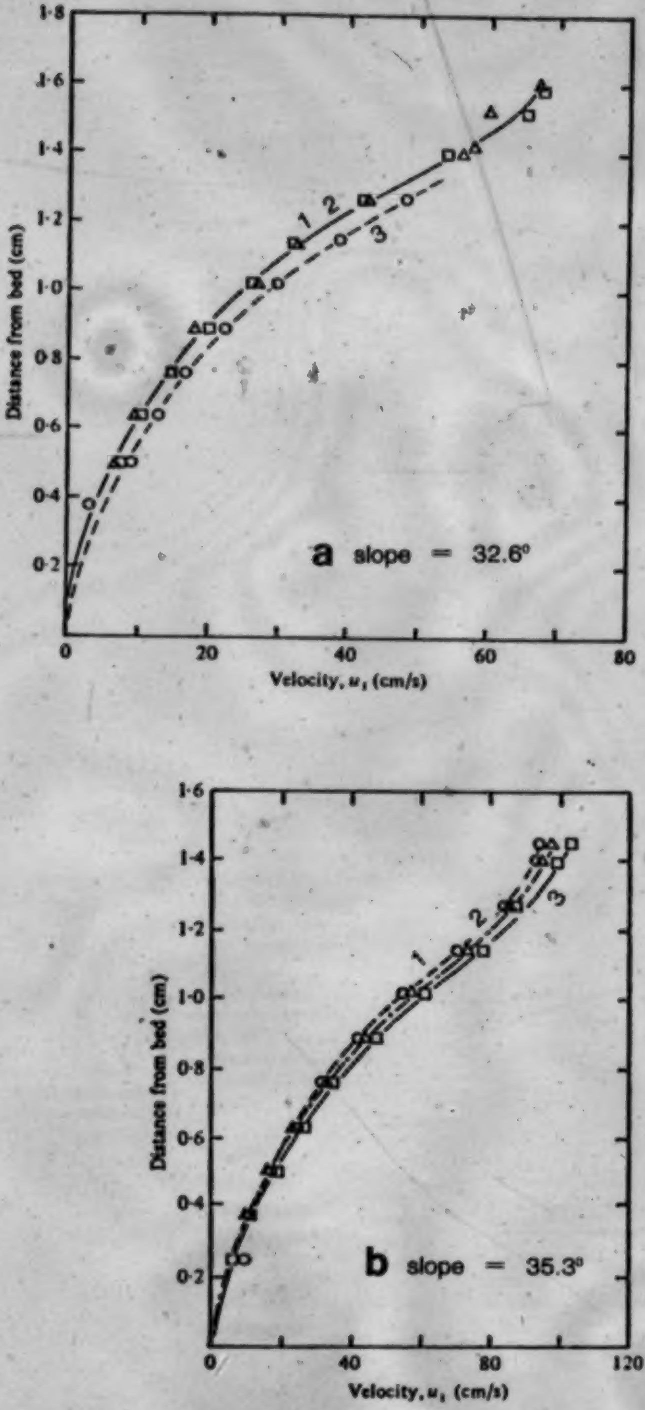

Figure 7.1 Grain flow profiles recorded by Savage (1979) (using polystyrene beads) 1, 2 and 3 refer to stations 33, 64 and 94 cm from flume entry.

and accelerations, side velocity profiles, mass flow rates, flow thicknesses, mean bulk densities of the material during the flow and the base shear resistance. The main conclusions, detailed in Sections 11.4 and 11.5 can be summarized as follows:

a. Base frictional resistance was practically constant over the entire range of velocities and therefore independent of the shear strain rate.

b. The apparent angle of internal friction, as derived alternatively from the base resistance values and from an equation of motion based on surface accelerations, was constant at all velocities although somewhat less in magnitude than the quasi - static lower bound angle of repose of the material.

c. Nonaccelerating flows were only obtained at slope angles approaching the above angle of internal friction, with the exception of very thin flows (less than 3 cm). They could be made to travel at various velocities and depths, indicating the nonexistence of a normal depth.

d. Bulk density showed a slight linear decrease with velocity. It was practically unaffected by flow thickness, except in flows thinner than about 3 cm.

e. Nearly linear vertical velocity profiles were observed at lower speeds. At mean velocities exceeding about 1.5 m/sec, significant base slips were both directly observed and derived from velocity ratios. At velocities approaching 5 m/sec, virtual plug flows were observed. It is probable that these changes in velocity profile are at least partly due to the flow not being completely developed in the faster experiments. A considerably longer flume would be required in order to study the fully developed velocity profile at high speeds.

f. At low speeds, the flows invariably developed stagnant corners, sometimes as much as 3 cm thick. At low velocities and angles flatter than the apparent friction angle, the flows deposited stagnant layers on the bed.

g. Flow surfaces of even the fastest experiments were relatively smooth and quiet, free of turbulence or mixing. Surface velocities were practically unaffected by side friction and were constant across the entire width of the flume.

An important suggestion arises from this summary, that thin flows (less than approximately 20 or 30 times particle diameter) behave somewhat differently at high speeds than thick ones. Their degree of bulk dispersion is greater. They may move without acceleration on slopes exceeding significantly the internal friction angle, although thicker flows are unable to do so, as confirmed by Savage (1979). Therefore, their dynamic frictional resistance appears to be higher, in general, and probably dependent on velocity, which it is not for thicker flows. This can be observed to some extent in Figures 11.9 to 11.11, Section 11.4, although the trend is somewhat obscured by the fact that thin flows have the greatest margin of error (Section 11.7). The author feels that some of the results of the previous researchers derive from using extremely thin flows. This explanation can be applied to the break in the line correlating slope angle and velocity in experiments by Takahashi (1937), as well as to the fact that Savage (1979) was able to produce uniform flows at a range of slope angles. The results of the present experiments are in agreement with Roberts' (1961) conclusion that uniform flows are only to be expected at one particular slope, equal to the constant dynamic internal friction angle. Flows travelling on a flatter slope will decelerate to the point where they will begin to deposit a stagnant mass at the base and cease to flow, if they cannot establish a steeper angle. On steeper slopes, flows will accelerate and thin out because of continuity requirements. Eventually, they will reach some low terminal thickness, with an associated velocity and degree of dispersion which may lead to the establishment of a uniform flow.

7.3 Theoretical Models

The theoretical aspect of the inertial grain flow category of slope movements constitutes basically the theory of open channel flow of granular materials. This seems to have received little attention in all of technical literature. Even the literature of powder mechanics and bulk solids transport generally lacks reference to this class of problems, probably because prismatic chutes generally do not represent critical points in the design of solids transport systems.

A practical theory applicable to smooth - based chutes of various shapes has been proposed by Roberts (1969). On this basis of his experiments, mentioned earlier, Roberts assumed that energy dissipation in such flow occurs predominantly by friction at the base and at the walls of the chute and that dynamic particle interaction during the flow is minimal, so that density is constant. A direct outcome of this assumption is the possibility to apply the equation of volume continuity and the simple equation of motion for a frictional sliding block (Eqn. 3.3). The steady- state flow in a straight wide channel can be described by the velocity equation:

$$v = \sqrt{2xg\,(\sin\alpha - f\cos\alpha) + v_o} \qquad \text{Eqn. (7.1)}$$

which is derived from Eqn.(3.3) by integration, considering an initial velocity vo and a dynamic base friction coefficient f. The continuity equation gives the flow thickness:

$$H = \frac{v_o}{v}\,H_o \qquad \text{Eqn. (7.2)}$$

The integration of the equation of motion can easily be done for curved flow paths or for narrow channels, with a consideration of the side friction. The theory is, however, not applicable to flows on rough base which tend to develop a vertical flow profile as a result of internal shearing.

Bagnold (1954) obtained two basic conclusions concerning the flow of granular material in the inertial regime:

a. The shear stress is proportional to the square of the shear strain rate, as in the case of the turbulent flow of liquids.

b. The ratio of shear to normal stress is constant and probably similar or related to the angle of repose (or rather the dynamic angle of internal friction, *viz* Bagnold, 1966).

In quantitative terms the normal (P, or dispersive) and shear (T) stresses within the flowing material are related by the equation:

$$P = a_i \rho_g \lambda^2 D^2 \left(\frac{du}{dy}\right)^2 \cos\alpha \qquad \text{Eqn. (7.3)}$$

and

$$T/P = \tan\alpha \qquad \text{Eqn. (7.4)}$$

where ρ_g is grain density, λ linear concentration (defined by Bagnold as the inverse ratio of the clearance between particles to particle diameter, D, in an idealized tetrahedral packing), dU/dy is the shear strain rate, α is an angle identified by Bagnold (1966) with the dynamic coefficient of internal friction and ai is a constant . (The angle α will further be refered to as ϕ .) The equation of motion of the uniform, steady gravity flow of any material, irrespective of its constitutive flow relationship, can be reduced to the form:

$$T/p = \tan\beta$$

Eqn. (7.5)

Comparing the last two equations, one finds that they are satisfied as long as $\beta = \alpha$. Therefore, steady uniform flow can only occur at one slope angle, equal to the dynamic angle of internal friction. Further, it means that velocity is dependent on concentration only and independent of slope or stress level. As long as the flow bed has the one required slope, steady uniform flow can exist at any given velocity or depth; the faster flows will merely be more dispersed. This is in accord with the experimental observations made in the course of this research. Eqn.(7.3) can be used to derive a velocity distribution in uniform flow. Equating the bed slope with the dynamic friction angle and substituting the tangential gravity stress component for T:

$$T = g \sin\alpha \int_y^0 \rho \, dy$$

Eqn. (7.6)

where ρ is the bulk density above the point in consideration, which lies y beneath the free surface of the flow. Combining (7.3) and (7.6) and solving for the velocity gradient:

$$\frac{du}{dy} = \left(\frac{g \int_y^0 \rho \, dy}{a_i}\right)^{1/2} \frac{1}{\lambda D}$$

Eqn. (7.7)

which could be integrated to obtain a velocity profile, if the distribution of the linear concentration was known. Bagnold (1954) and Lowe (1976) chose to assume the linear concentration to be constant and equal to 17. This choice is entirely arbitrary, being merely equal to the highest concentration used in Bagnold's experiments. Its use leads to the velocity profile equation (Bagnold, 1954):

$$U = 0.11\sqrt{g \sin\beta}\ \frac{y'^{3/2}}{D}$$

Eqn. (7.8)

where y' is measured upwards from the bed. The boundary condition used in the integration is zero bed slip, and the material is assumed to have a bulk density corresponding to random static piling (porosity=0.4). The equation produces a velocity profile sketched in a dimensionless form by the full line in Fig. 7.2. The shape of the profile is correct, insofar as the assumption of uniform concentration is valid. The absolute value of velocity derived from Eqn. (7.8), however, is not much more than an arbitrary number; a given grain flow may assume a range of uniform velocities with various associated concentrations, greater or smaller than 17.

Such a value of λ severely limits the possible level of effective stress and thus, for a drained flow, the material thickness. Consider, for example, a 2 m thick flow of medium sand, with a velocity distribution according to Eqn. (7.8) and a surface velocity of 5 m/sec. The value of

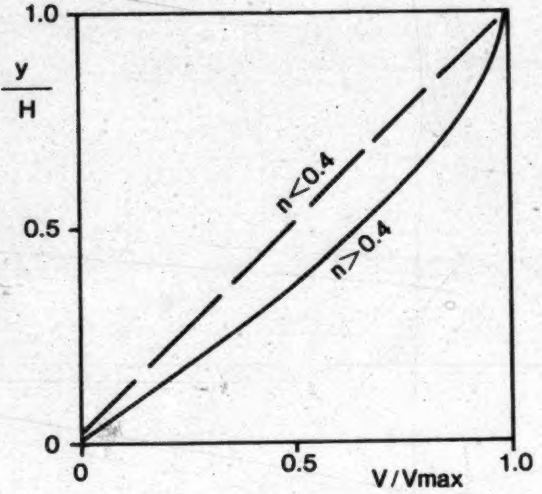

Figure 7.2 Dimensionless velocity profiles for inertial grain flows with low and high porosities.

$a_i \lambda^2$ required in Eqn. (7.3) to balance the weight of the flowing material would equal 930 000. If the highest measured value of $a_i = 0.2$ were accepted, λ would have to be more than 2000. But a_i must vary strongly with the concentration in this range. Taking guidance from Figure 7.3, one could regard a and P as proportional. From Fig. 4 of Bagnold (1954), P= 30 dynes/sq.cm and $a_i = 0.2$ at $\lambda = 17$. Therefore, the proportionality constant is 0.2/30= 0.007. Substituting into Eqn. (7.3), one obtains $\lambda = 21.5$ which is close to the limiting value of 22.5 at which shearing of a tetrahedral packing would not be possible. But this is a tenuous extrapolation of Bagnold's results. Also, the relationship between the volume and linear concentrations for natural materials would certainly be different from the ideal Eqn. (8.4). It is suggested here that Eqn. (7.3) should not be used as a basis of a constitutive relationship for the calculation of velocities, although it is the only available means for predicting velocity profiles. Eqn. (7.4) is more suited to velocity prediction, as it is confirmed experimentally over a range of conditions (Chapters 11 and 12).

A refinement of the velocity profile derivation can be made on the basis of Bagnold's (1954) data. Equation (7.7) can be rewritten using Equations (7.5) and (7.6) in terms of the normal stress P:

$$\frac{dU}{dy} = \sqrt{\frac{P}{a_i \cos\phi}}\,\frac{1}{\lambda D} \qquad \text{Eqn. (7.9)}$$

Thus, the velocity gradient at different depths within the flow is seen to depend on, besides the normal pressure and constants, the coefficient a and the linear concentration λ . P is known at any given depth within the flow, but there is only one equation for the remaining two variables, i.e. the velocity gradient and concentration. The difficulty can be removed by considering that variation in the velocity gradient due to the second term in the right hand side of Eqn. (7.9) is likely to be insignificant, the relationship between the linear concentration and P being logarithmic. The main source of variation must be the first term, or:

$$\frac{dU}{dy} \simeq \text{const.}\sqrt{\frac{P}{a_i}}$$

Eqn. (7.10)

Figure 7.3 has been plotted on the basis of data presented in Bagnold's Figures 4 and 5. The coefficient a is seen to be constant for all linear concentrations less than 14 (corresponding to volume concentrations less than 60 percent or porosities greater than 40 percent). Therefore, in highly dispersed state at high speeds, the velocity gradient varies with the square root of the normal stress, and Eqn. (7.8), as well as the full line profile in Fig. 7.2 derived from it, are valid. At higher concentrations, constant a cannot be assumed. Fig. 7.3 shows a line tracing the relationship between P and the linear concentration for one arbitrary constant value of the velocity gradient. This line is approximately parallel to the other diagram in Fig.

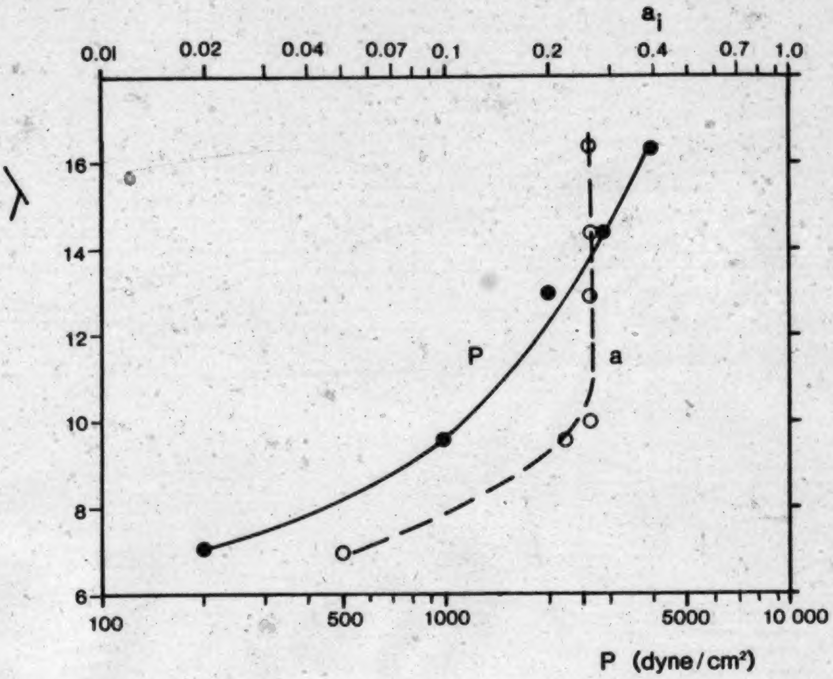

Figure 7.3 Variation of normal pressure and the coefficient a_i with linear concentration in the inertial regime (data from Bagnold, 1954, Fig. 4. Velocity term = 100).

7.3 suggesting that, in this more concentrated region, the ratio P/a is constant. Therefore, from Eqn. (7.10), the velocity gradient is constant and velocity varies linearly with depth, as shown by the dashed line in Fig. 7.2.

Thus, Bagnold's data apparently do not contradict the observation of approximately linear velocity profiles made in the course of this study. Nevertheless, Bagnold's theory is semi - empirical and does not reveal a fundamental reason for the predilection of the material to forming a velocity profile of a given shape. In fact, it is surprising that granular material should have such a tendency, since in transition from a static piling to the critical state of shearing it behaves thixotropically, i.e. an additonal expenditure of energy is required to effect such a change for every unit of volume involved (e.g. Rowe, 1962). If a plug flow is initially forced, as in the case where a sand sheet slipping on a smooth chute is suddenly introduced onto a rough - based section, it is difficult to see why the region of shearing should grow in thickness, while shearing on a discrete plane produces no greater frictional resistance than general distortion. But this is what was observed in the experiments. One might venture a hypothesis, that normal impacts sustaining the dispersive pressure at any level within the flow excite neighbouring static layers in a similar way that a single vibrating spring in a series of many would induce the vibration of the whole assembly. There might, of course, be limits to such a chain reaction, in which case the flow would tend to form a non- deforming plug above the shear zone. It is almost certain that this is the case at least in larger flows, exceeding the scale of the laboratory experiments. Further, the propensity of a grain flow to form a particular velocity distribution is certainly not as strong as that, for example, of viscous laminar flow. Many flows will therefore move long distances without forming fully developed velocity profiles. The only prediction that can be made at present concerning such flows is that their velocity distribution will lie between constant and linear.

A recent series of publications attempts to derive the constitutive behaviour of flowing granular materials from the basic relationships of continuum mechanics. The original work (Goodman and Cowin, 1971) was based partly on an assumption of a viscous relationship between shear stress and strain rate and is said to have contained other inconsistencies (Savage, 1979). A subsequent re-derivation of the theory by Savage and Cowin (Savage, 1979) introduces Bagnold's square stress - strain rate relationship. The theory divides the stress tensor into an "equilibrium" part which conforms to the Mohr - Coulomb criterion at zero strain rate, and a "dissipative" part which is proportional to the square of the strain rate as prescribed by Bagnold. A further assumption, parallel to an original argument by Goodman and Cowin (1971) stipulates that the "equilibrium stress" should be proportional to the gradient of volume concentration. Savage admits a lack of definite substantiation for this assumption. One may also question the validity of splitting the stress tensor into two mutually independent parts without an empirical or theoretical basis for such a hypothesis.

The theory predicts velocity profiles which vary between Bagnold's profile (Fig. 7.2) and a nearly linear profile with a stagnant base layer about 0.3H thick, depending on the assumption of volume concentration near the base. Absolute prediction of normal velocity again cannot be given, unless the concentration was known. Savage points out a similarity between the predicted velocity profile and those he measured in flume experiments, but acknowledges that the latter are distorted by wall friction. This author is of the opinion that the theory is yet to be substantiated by experiment or more fundamental theoretical considerations, either at the point of the original assumptions, or in terms of the final predictive results. Both the original and revised versions predict concentration decrease with height above the base of the flow. This is in variance with the limited direct observations mentioned in the previous sections, with the observed calmness of flow surface in flume experiments, with the probabilility of the existence of non- shearing surface plugs and with Bagnold's findings of increasing dispersion with a higher shear strain rate.

For practical purposes, analysis of granular flows can be conducted with the use of adapted general equations of open channel flow, which do not depend on the constitutive relationship. A basic form of the equation of motion for unsteady nonuniform flow in a prismatic open channel is (Chow, 1959):

$$\beta v \frac{\delta v}{\delta x} + \frac{\delta v}{\delta t} = g \sin\alpha - \frac{\tau}{\rho H} - g \cos\alpha \frac{\delta H}{\delta x}$$

Eqn. (7.11)

the terms of which from left to right include: the convective and local acceleration, the bed slope, bed friction head and pressure head. The factor β is the velocity distribution coefficient, derivable from equating kinetic energy expressed in terms of an integral to that in terms of mean velocity v and flow thickness H:

$$\int_0^H \frac{v^2}{2g} = \beta \frac{v^2}{2g} H$$

Eqn. (7.12)

From this equation, β equals to 1.0 for a plug flow , 1.33 for a linear velocity distribution and 1.25 for the Bagnold's distribution. The bed friction term can be expressed using the constant dynamic friction coefficient designated earlier as the stress ratio T/P. The pressure term should be modified for the possibility of non-hydrostatic stress state within the flow. The normal stress must, from equilibrium, equal the normal component of gravity. If an assumption of tangential confinement is made, the stress acting parallel with the bed will equal the normal stress times the lateral pressure coefficient k which probably varies between 0.5 and 1.0. With reference to Fig. 7.4, the unbalanced force on normal planes, deriving from the depth gradient equals approximately

$$\frac{\Delta P}{\Delta x} = \frac{H}{x}\gamma k$$ Eqn. (7.13)

With these modifications, assuming that k = 0.75, the equation of motion can be rewritten as:

$$\frac{\beta}{g\cos\alpha}\, v\frac{\delta v}{\delta x} + \frac{\delta v}{\delta t} = \tan\alpha - \frac{T}{P} - 0.75\frac{\delta H}{\delta x}$$

Eqn. (7.14)

In the case of a steady flow, when the local acceleration term is zero, this can be directly integrated to yield the Bernoulli equation in terms of slopes:

$$\frac{\beta\,\Delta(v^2)}{2g\,\Delta x\cos\alpha} = \tan\alpha - \frac{T}{P} - 0.75\frac{\Delta H}{\Delta x}$$ Eqn. (7.15)

The equation of continuity must also be satisfied, so that between two stations 1 and 2:

$$\frac{\rho_2}{\rho_1}\,\frac{H_2}{H_1} = \frac{v_1}{v_2}$$ Eqn. (7.16)

where the density and mean velocity could be interrelated by some empirical relationship such as described in Chapter 11.

This theory was applied to the results of the laboratory flume experiments with moderate success. It was easy and relatively precise to back - calculate friction factors from known acceleration values but rather unreliable

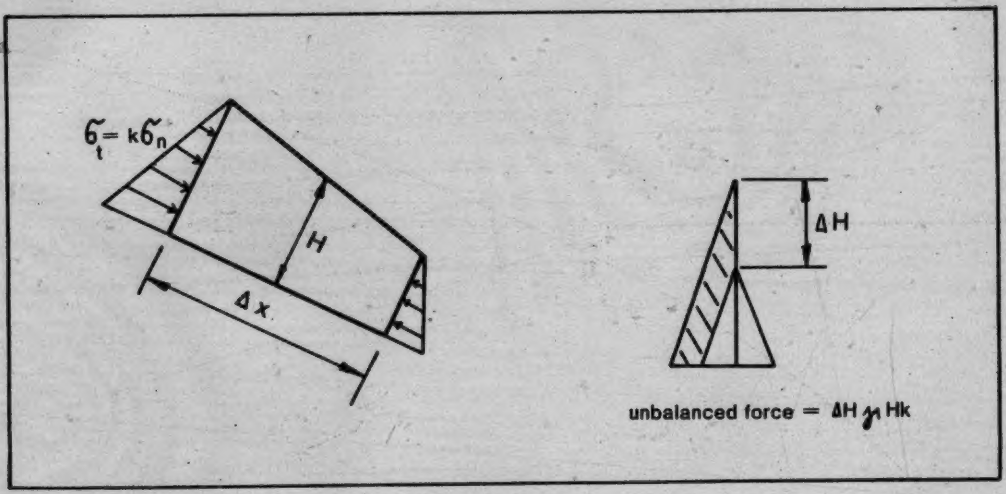
$\sigma_t = \kappa\sigma_n$
H
Δx
ΔH
unbalanced force = $\Delta H \gamma_n Hk$

Figure 7.4 Tangential pressure term.

to do the opposite. In contrast to the equations describing water flow, the two terms describing bed slope and friction slope are dominant in granular flow. Therefore, one calculates acceleration on the basis of a small difference between two large numbers; a situation conducive to the magnification of error. Further, the theory is so far incapable of describing the effects of either gradual deposition of stagnant layers at the base of the flow, or bed erosion. Since the previously discussed question of the uniform velocity distribution affects only β (and that only between the value of 1.0 and 1.33), it is of a minor practical importance related to these other problems.

For the prediction of the reach of minor slips in dry granular material, one can easily take advantage of the basically frictional nature of their behaviour. The travel angle (Section 10.1) of flows in shallow prismatic channels will exactly equal the coefficient of kinetic friction, which is a few degrees less than the lower angle of repose. Allowance for lateral spreading can also be made by the method of Appendix B, if the geometry of the final deposit can be estimated.

8. GRAIN FLOWS IN WATER

8.1 Subaqueous Flows of Granular Sediments

Slopes built of dense, saturated cohesionless soils are usually stable, with failure restricted to minor sloughing of the face, erosion, or to the rare cases where strong upward seepage forces exist. The resulting type of movement is probably an inertial grain flow of the type discussed in Section 7.1. Slopes of loose saturated sands and silts, on the other hand, tend to produce voluminous and violent failures which result in quantities of water and solid grains mixtures flowing for large distances. Most saturated slopes in granular material are under water or adjacent to bodies of water and, consequently, these flow slides are usually subaqueous.

The sediment flow slide, although perhaps the best documented, is not the only type of underwater slope movement. It is therefore appropriate to put it into context by mentioning a few of the many classifications of such movements. Terzaghi (1957) distinguished slides in coarse sediments, in fine granular sediments with loose metastable structure and in clays. The first two categories correspond roughly to those introduced in the first paragraph of this section. The clay slides would produce coherent slumps, slurry flows or debris flows which do not differ from their subaerial counterparts in the basic mechanical attributes.

Morgenstern (1967) outlined a progression of stages of mobility in gravity sediment movement. Each of the stages may either fully describe a given event or relate only to an episode in its development. The stages include coherent (block) slumping, incoherent slumping with internal shearing and mixing, laminar gravity flow and turbidity current. Only the last two stages involve the physical aspect of flow of grain- water mixture, relevant to this chapter. The first two stages again describe slope movements that are not fundamentally different from subaerial events discussed elsewhere in this thesis.

One of the most recent classifications (Middleton and Hampton, 1976) adopts Terzaghi's three classes, adding a fourth for turbidity currents which Terzaghi did not discuss. It is noted that these categories represent four alternative methods of sediment support (i.e. of transfer of vertical normal stress within the flow): by matrix strength in cohesive mud or debris flows, by mechanical grain interaction in inertial grain flows, by upward fluid drag in fluidized (or liquefied) sediment flows and by turbulence in turbidity currents. A somewhat similar classification has been offered by Carter (1975), adding categories for surficial sediment creep and underwater rock fall.

Direct observations of subaqueous slope movements are limited to the initial events at the shoreline (e.g.Bjerrum, 1971) and to some minor sloughing of sand on steep underwater slopes (Dill, 1964). Most of the information that can be used to describe these phenomena is therefore inferred from evidence such as the generation of waves, sudden changes of seabed topography and breakage of submarine cables. Even more of the published information is deduced from the character of sedimentary rocks. Consequently, the very existence of some types of movements is debatable and uncertain, e.g. the dense turbidity current (Menard, 1964) or the submarine debris flow (Hampton. 1975). Fortunately, there are only two types of subaqueous slope movement which require separate discussion from similar subaerial phenomena within the framework of this study. These are the liquefied sediment flows, which form the content of this section, and turbidity currents covered in Section 8.2.

Natural sediment deposits can become liquefied in three ways. Firstly, it is conceivable that, in some circumstances, rapid consolidation of coarser sediment may force significant upward flow through an overlying finer bed, giving rise to a case of true fluidization similar to the processes used in industry (Lowe, 1976). This mechanism is a hypothetical one and has apparently never been described yet. Of course, upward flow does occur in consolidating layers and may even approach quite close to the critical hydraulic gradient condition in some fine deltaic sediments (Morgenstern,1967)

A more important mechanism is the collapse of the loose structure of some (fine- grained) recent sediments which possess a loose, unstable structure formed during deposition (Terzaghi, 1957). The collapse may be brought about due to the disturbance by an initial sliding failure. This phenomenon of spontaneous liquefaction (Casagrande, 1969) has been discussed in Section 3.5. An alternative mobilization mechanism in the same type of soil is liquefaction caused by earthquake (Seed, 1968).

The spontaneous liquefaction events usually, but not always, initiate in the form of a retrogressive slide (Andresen and Bjerrum, 1967). A limited initial slump appears at a location which may be oversteepened or over loaded by fill. Since the failure, however started, proceeds in a fast undrained manner, the slump crater is quickly emptied, leaving steep unsupported scarps at its head and sides. These fail in turn, and thus the slide retrogresses rapidly in concentric slices. The speed of retrogression may vary from 50 m to several km per hour (Andresen and Bjerrum, 1967). There is, therefore, a steady supply of material into the ensuing flow, for a period of several minutes.

Flow slides of this type are characteristic of the Dutch province of Zeeland (Koppejan et al., 1948). The region consists of numerous islands divided by estuaries filled by recent fine sands. The banks of the islands are protected by dykes against high tide and storm flooding. In many places, the dikes have to be doubled because of their frequent breaching by flow slides. In some locations, recent slide scars extend in an uninterrupted line along the shore for several km. The pre- slide topography usually includes slopes of 15- 20 deg. below the water line, while the dry land is flat. The slides initiate at a steep submerged slope section scoured out by tidal current. There may be as many as fifty retrogressions within a few minutes, leaving a fan-shaped crater extending some distance behind the water line and often encroaching on the dykes. A volume of up to two million cubic m of sand flows under water and settles a few hundred metres from the shore at angles of 3 to 4 degrees. Flow velocities have not been observed; Terzaghi (1956) estimated them in the order of 5 m/sec. Triaxial testing of dry samples of the fine sand involved in these slides (Koppejan et al., 1948) indicated contractant behaviour during shearing for initial porosities more than 44 percent. These laboratory results should of course be viewed with caution, in the light of the findings of Castro (1969) as outlined in Section 4.5.

Similar events have been repeatedly observed in the heads of some Norwegian fjords, where granular sediments are being accumulated from the discharge of rivers (Bjerrum, 1971 and others). The peculiarity of these fjord landslides is that they often seem to involve connected series of events. For example, the flow slide of 1930 in Orkdalsfjord was manifested as three separate slumps occurring at different sides of the head of the fjord and over a km apart. The slides were observed to occur within a period of 15 minutes and were estimated to have involved about 25 M cu. m of nonplastic silt, with an in situ porosity of about 49 percent (Andresen and Bjerrum, 1967). Eight minutes after the initial slide, a submarine cable broke 3 Km down the fjord and two hours later another cable failure occurred in the main branch of the fjord, 21 Km from the site of initiation. Thus, the sediment flow appears to have travelled at an average speed of 25 Km per hour over the first 3 Km of its path and 10 Km per hour over the next 18 Km. THe bed slope was about 6 degrees for the first Km, 1.4 degrees over the next 3 and considerably less than 1 degree for the rest of the path. During another slide in Follafjorden, a dredge was towed by its anchor caught in the flowing sand masses, for 300 m at a speed of 15 Km per hour. The direction in which it was towed was perpendicular to the axis of the 1000 m wide fjord, indicating that this was perhaps a side failure of material undercut by the main slide travelling along the axis from the head of the fjord. Such side failures, and erosion of the flow path in general, undoubtedly add considerably to the volume of subaqueous flow slides.

There are many similarities between these liquefied sand flows and the quick clay flows described in Section 6.2. One of them is the ability of the disturbed material to flow through a narrow gap at the mouth of the failure crater. This is illustrated by two cases of flow failures of hydraulically placed fill. About 6000 cu. m of silty sand liquefied during placement in Helsinki Harbour in 1936

(Bjerrum, 1971). The material began to flow on a base angle of about 2.5 degrees, emptied through a 20 m wide gap and deposited on the bottom of the harbour as an essentially horizontal bed. During the flow, the sand did not erode the underlying soft clay. A similar case took place in Chicago, in 1946, where over 400 cu.m of liquefied fine sand flowed through a 75 cm wide gap in a sheet pile wall in 30 minutes (Peck and Kaun, 1948). The hydraulic fill from which this flow originated had a Standard Penetration Resistance of one blow per 22 in (56 cm).

Another example of a flow of sand placed as hydraulic fill is provided by the failure of the Fort Peck Dam (Casagrande, 1965). The nearly completed dam section containing a large proportion of fine sand failed, probably as a result of sliding in the underlying clay shale. About 3.9 M cu. m of the fill and 3.6 M cu. m of foundation alluvium liquefied and spread out over underwater slopes of 2.9 degrees to a maximum distance of 500 m The entire movement took place in 10 minutes, indicating a minimum front velocity of 1 m/sec. The deposit widened and thinned during its flow and came to a rest with an average surface slpe of 1.9 deg. Large blocks of undisturbed material from parts of the dam shell were rafted in the disturbed matrix, which remained in a "quick" condition for 10 days after the event and exhibited sand volcanoes.

Submarine sediment flows triggered by earthquakes have a similar character, except that they are often larger. The

Valdez landslide during the 1964 Alaska earthquake, for example, involved 75 M cu. m of deltaic material and extended 150 m inland from the shoreline (Seed, 1968. It seems to have occurred almost instantly, without a record of gradual retrogressions. The toe of the flow deposits in the bay could not be found after the earthquake. Previous earthquakes in the Valdez region coincided with submarine cable breaks, suggesting the possibility that turbidity currents resulted from these sediment flows. The same earthquake triggered failures also at Lakeview and other deltas in Kenai Lake, Alaska (Seed, 1967). Some of these had a retrogressive character, the retrogressions taking place throughout the duration of shaking. The dry ground above the crests of these failures was intensely cracked and deformed. Some of the cracks spouted sand and water from liquefied layers beneath.

Evidence of submarine slumping due to earthquakes or other causes has been compiled by Menard (1964) and Morgenstern (1967), mostly from the results of bathymetric surveys. The largest of these events had volumes of up to 7 x 10^{22} cu.m. Many were followed by submarine cable breaks at considerable distances away within a few hours of occurrence, indicating that they triggered, or changed into turbidity currents.

A very unusual and spectacular example of liquid sand flow was observed near Sept- Isles, Quebec, by Dredge and Thom (1976). A flat terrace of estuarine sands and silts rose 30 m above the level of Moisie River. Its surface was relatively featureless and heavily forested. A raised bog existed on it some 1.5 km from the river. The soil profile consisted of horizontally bedded sands, silty sands and sandy silts overlying clay. After a strong rainfall in the summer of 1959, a small water spout was observed on the river bank, ejecting water and mud to a height of 10 m. Shortly afterward, the soil of the river bank at that location began to flow, creating a V shaped gully which quickly expanded back into the terrace deposits and later branched into a dendritic pattern. Within five hours, the gully system grew to a total length of about 1500 m and discharged 200 000 cu.m of sediment into the river, creating a temporary dam. No further mass movement took place until the fall of 1966, when after an intensive rainstorm another catastrophic expansion of the gully system took place. This time some 10 km of gullies were generated within a few hours, affecting an area of 2 sq. km and discharging 3.5 M cu. m of sand. This appears to be the only recorded case of a similar phenomenon and the difference from the usual pattern of development of flow sliding is striking. There is some correlation in the location of the major gullies with cleared paths on the surface of the terrace. The pattern of failure resembles the behaviour of channelling beds, known in industrial fluidization prosesses (Kunii and Levenspiel, 1969). The fluidizing medium chooses preferred escape paths, while the surrounding material remains undisturbed. A heterogeneous grading in the terrace deposits would promote such a selective flow process.

Liquefaction occurs also in sand or silt layers or lenses overlain by beds of cohesive material. This results in rapid spreading failures, when intact blocks of clay subside, tilt and move forward floating on a layer of liquefied soil beneath. The Turnagain Heights landslide at Anchorage, which was also caused by the 1964 earthquake, involved approximately 12 M cu.m of material from a 20 m high bluff rising above the shore line. The landslide affected horizontal layers of soft to stiff sensitive clay. At the base level of the initial sliding, corresponding to the depth of 20 m, there was a string of loose fine sand lenses. Evidence reviewed by Seed and Wilson (1967) indicates that the spreading movement initiated when the sand lenses liquefied as a result of earthquake shaking. The overlying clay was separated into blocks which subsided on average by 10 m and moved outwards into the water for a maximum distance of 600 m. The motion was very rapid, having been completed in a period of several minutes. In a few locations, liquefied sand rose up in the fissures between the clay blocks and deposited ridges and sand boils.

Several events of similar character have been reviewed by Seed (1968), involving continuous layers of sand which liquefied beneath cohesive overburden. Thes type of landslide could be viewed as a combination of the clay block slide (Section 4.1) and a sand flow, where the flow properties and thickness of the liquied sand layer can be substituted for those of the conventional shear zone. In the case of a failure passing through sand lenses, of course, the load sharing between quick sand and sheared clay must be taken into the consideration.

Several authors presented criteria for recognition of sands susceptible to liquefaction. Terzaghi and Peck (1948), in the first edition of their textbook, suggest that such sands should have a relative density of less than 0.4 or 0.5 (loose to compact), an effective size less than 0.1 mm (fine sand), a uniformity coefficient less than 5 (uniform to well graded), and rounded grains. These are very wide criteria. In the revised edition of 1968, they are replaced by a qualitative criterion stating that the sand must possess a metastable structure, which may form by either deposition in a moist condition or by underwater sedimentation of sand including a small fraction of cohesive particles such as clay, silt or organic matter. Andresen and Bjerrum (1967) concur with the above. From laboratory test results they found that susceptible sands had porosities exceeding 44 percent and failed in undrained shear at extremely low strain.

Liquefied sand flow deposits are characterized by some typical structures (Lowe, 1975). Firstly, the existence of low shear strength before deposition is manifested by a mixing and gross distortion of the primary sedimentary structures of the bed. In a fully fluidized bed, complete homogenization usually takes place. Normal grading may develop as large particles sink to the base of the bed through the fluid matrix, and small particles are elutriated upwards. Dish- shaped laminations occur in some sands, separated by vertical pillar structures which mark locations where liquefied sediment extended through coherent zones in "weak" locations. Sand volcanoes with craters and raised rims are found at the surface.

8.2 Turbidity Currents

Turbidity currents are flows of water carrying significant quantities of sediment, held in suspension by tubulence (Middleton and Hampton, 1976). They move on subaqueous slopes by virtue of their greater density with respect to the overlying clear water. An experimental current has been described as "a slowly boiling cloud, pushing its way through surrounding quiet water". Thus, the sediment is being held in suspension by water movement, which is itself being maintained by the weight of the sediment. The process was called "autosuspension" by Bagnold (1961) and lies on the border between mass movement and mass transport phenomena. The definition is conceptual and is difficult to apply in border cases. The distinction and relationship between subaqueous grain or slurry flows and turbidity currents is still somewhat controversial. In general, the latter are distinguished by lower densities and higher fluidity, which is reflected in large extent, low thickness and normal grading of deposits.

Direct observations of turbidity currents are limited to lakes and reservoirs, where they derive from the turbid inflow of sediment- bearing rivers, and to experimental events created in the laboratory (for a review see Menard, 1964 and Middleton, 1970 respectively). Inferential evidence for their existence on the ocean floor, also reviewed by Menard, includes wide distribution of coarse sediment on abyssal fans and plains, displacement of shallow water fauna and the already mentioned cable breaks.

On the basis of this evidence it appears that turbidity currents originate at the crest of the continental shelf, travel down the continental slope at angles of 1 to 10 degrees and the negligibly sloping sea floor beyond. A fairly well established hypothesis states that the currents erode submarine canyons. On the continental rise or submarine fan, they tend to move through U- shaped channels hundreds of km long, bordered by deposited levees. It has further been deduced that the currents thicken considerably some distance past the toe of the continental slope and that their geometry is remarkably elongated. Some may have been 350 km long and only several km wide.

Velocity estimates have been derived from the data on progressive breaking of submarine cables in a few cases. The Grand Banks current of 1929 (Heezen and Ewing, 1952) maintained a steady velocity of between 19.1 and 28.3 m/sec.

(by different interpretations) for distances of over 400 km.

Density of the turbulent sediment suspensions is generally regarded as low. Those observed in lakes and reservoirs had not exceeded 1.1 g/cu.cm and in fact were often as low as 1.01. "High density" turbidity currents (exceeding 1.1 g/cu.cm according to Middleton, 1970) have been postulated to account for the transport of some coarse sediment sizes, but their existence is still debatable.

It is now fairly well established that submarine slumps produce, or convert into, turbidity currents (Morgenstern, 1967). The mechanism by which this conversion takes place has not yet been unequivocally established, although several hypotheses have been advanced. Hampton (1972) stresses mechanisms of water incorporation into slumping masses, which have been observed at the source sites of subaerial debris flows (see Section 9.1). The initial movement has the character of sliding, grain flow or slurry flow. When an initially coherent slump is somewhat diluted by jolting and mixing and accelerates to a substantial velocity, other processes may come into action.

Firstly, the upper interface of the moving sediment and water may be unstable and mixing may take place across it (Keulegan, 1949). Secondly, two mechanisms of mixing at the head of the flow have been postulated. The head of an experimental turbidity current has a bulbous shape with a rounded tip, whose leading part is raised somewhat above the bed (Middleton, 1966a). The head tends to be thicker than the main body of the current following behind. Mixing has been observed on the frontal upper part of the head (Hampton, 1972). Allen (1971) collected evidence indicating that a part of the water displaced before the head is forced into tunnels or pipes in the body of the current, where it probably dissipates by mixing with the sediment. Menard (1964) suggested that further mixing may occur at the toe of the continental slope, where enormous hydraulic jumps may develop. There are, therefore, at least four possible mechanisms of dilution of the turbidity current during its travel, although only the first two have been actually observed in experiments. Some authors argue that the entrained cloud above the main body of the sediment, created by mixing at the upper interface, may separate from the denser flow below and travel at a slower speed for a longer distance. But this hypothesis has not yet been substantiated.

Predictions of turbidity current velocities have been made using conventional open channel flow formulas and empirical equations derived from laboratory experiments. The Chezy formula for steady flow in open channels, corrected for the effective density $\Delta\rho$ of a turbidity current is:

$$v = C(RS\Delta\rho)^{1/2} \qquad \text{Eqn. (8.1)}$$

where v is the mean velocity, R the hydraulic radius and S the slope of the energy line (equal to the bed slope for a uniform flow). Kuenen (1952) estimated the Chezy coefficient, C, as 400 on the basis of back calculation from reservoir data, and $\Delta\rho$ as 0.6 g/cu.cm, to arrive at estimates of the thickness of the Grand Banks turbidity current. At one location, he calculated the thickness as 270 m, for a velocity of 28 m/sec. He assumed equal friction both on the bed and on the upper face of the current, so that R is equal one half the depth. Menard (1964) criticized both this assumption and the selection of the effective density. He also introduced the modified Darcy- Weisbach expression for the Chezy coefficient:

$$C = \left(\frac{8g\,\Delta\rho}{f\,\rho_c}\right)^{1/2} \qquad \text{Eqn. (8.2)}$$

where ρ_c is the density of the current and f is the Darcy- Weisbach resistance coefficient dependent on slope and roughness in the rough- turbulent regime. The selection of f both for the bed surface and for the interface between current and water is difficult due to the absence of detailed field data against which the formulas could be calibrated. Middleton (1966b) found, from his flume experiments with salt solutions, that the resistance coefficient of the bed can be estimated roughly from pipe flow diagrams. That of the interface is generally smaller but difficult to quantify, as it depends both on Froude and Reynolds' numbers of the flow. Bagnold (1961) chose to use the semi- empirical rough channel law dependent on the characterictic bed roughness k:

$$f = 2\log\left(\frac{14.8R}{k}\right)^2$$

Eqn. (8.3)

Bagnold also derived conditions for maintaining a steady, uniform turbidity current flow from the point of view of energy balance. Energy losses result from flow resitance and from lifting the suspended grains against their natural fall velocity by turbulence. These losses must be equal to the change of potential energy caused by the motion of the suspension down the slope of the bed. The resulting balance equation determines the minimum slope for a given velocity, thickness, density, roughness of bed, and grain size of the turbidity current. An application of the equation (with parameters estimated by Bagnold) to the Grand Banks current yields a maximum attainable velocity of 25 m/sec for a fine sand suspension, which is a reasonable result. If the equation is applied to the empirical velocities and other data reported by Middleton (1966a), a minimum slope angle of the test flume of 2.7 deg. is obtained. This cannot be checked against experiment, because Middleton tested suspensions only in a horizontal flume.

8.3 Constitutive Relationships

The behaviour of subaqueous flows described in the previous sections contrasts strongly with that of the dry sand or talus flows discussed in Chapter 7. The one factor best illustrating this difference is the travel angle, which is equal approximately to the constant volume internal friction coefficient in the case of the latter phenomena, while it is only a negligible fraction of the same in case of the former. It was also mentioned that small subaqueous slides deriving from slopes of relatively dense sand behave in a similar way to dry sand slides. Therefore, these differences in the character of the same material are not due merely to the presence of water, but rather to the role of pore pressure and effective stress.

The Einstein's equation introduced in Section 6.3 implies that solid particles, added to a viscous liquid in small quantities, do not alter the Newtonian character of the system, even though they change its viscosity. Thus, one can identify two limiting types of behaviour of flowing granular materials, depending mainly on solids concentration but also on other factors. On one side of the spectrum is the frictional (Coulomb) behaviour of the type dealt with in Chapter 7. On the other side is the Mewtonian viscous behaviour of dispersions of particles having very low concentrations. Between these two limiting states, there is a transitional link.

R. A. Bagnold published, in 1954, an account of experimental work designed to investigate the character of this transitional region. His experiments were essentially coaxial cylinder viscosimeter tests on dispersions of solid spheres in liquid. The test material consisted of spherical droplets of a mixture of parafin wax and lead styrate, with a constant diameter of 0.132 cm and a density almost precisely equal to that of water. The apparatus and test procedure were so designed as to enable the direct observation of normal and tangential pressures on the surface of the inner cylinder due to the presence and activity of the solid particles, i.e. apart from the normal pressure and drag of the interstitial fluid. The shearing annulus was closed to keep the concentration constant. Tests were carried out with a variety of concentrations and shear strain rates. Further tests were conducted using fluids with higher viscosities than that of water.

The presence of solid particles in the water really did create normal stress on the surface of the inner cylinder during motion. Bagnold called this the dispersive pressure, P. It was found to increase with the square of the linear concentration[11], particle diameter and the shear strain rate, at high test velocities. At lower velocities the square dependence on the strain rate gradually changed towards a linear one. The presence of solid particles was also manifested by a shear stress, T, called grain shear stress, additional to the fluid drag. This shear stress was related to the dispersive pressure by a ratio:

$$T/P = \tan\phi \qquad \text{Eqn. (8.5)}$$

---

[11] The linear concentration as defined in Section 7.3 correlates theoretically with the volume concentration, C, and the volume concentration at the maximum static density, Co by the formula:

$$\lambda = \left[(C_o/C)^{1/3} - 1 \right]^{-1} \qquad \text{Eqn. (8.4)}$$

(Bagnold, 1954)

which, as already mentioned in Section 7.3 was found approximately constant in the fully inertial range (at high concentrations and velocities), but different in the more dilute or slower ranges.

In an attempt to evaluate the relative influence of hydrodynamic and mechanical forces, Bagnold defined a dimensionless number analogous to the Reynolds' number, equal to the ratio of the inertial stress to viscous stress. The inertial stress is given by Equation 7.3. The viscous stress was found in the low velocity region of the experimental data to vary approximately with the 1.5 power of the linear concentration. Therefore, the dimensionless number N (later called Bagnold number by some authors) equals:

$$N = \frac{\lambda^{1/2} \rho_g D^2 \, dU/dy}{\eta} \qquad \text{Eqn. (8.6)}$$

where D is the particle diameter, ρ_g particle density, dU/dy the shear strain rate and η the fluid viscosity. The test results indicated that both the grain shear stress and the dispersive pressure were only influenced by the fluid viscosity while N was less than about 40. On the other hand, the square relationship between grain stresses and shear strain rate only fully developed at N greater than approximately 450. Thus, the Bagnold number is confirmed as an indicator that can be used to delineate the boundaries of the macro- viscous (Newtonian), transitional and inertial (frictional) regimes.

It was shown in Section 7.3 that the ratio T/P is the critical parameter required for the analysis of grain flows in the inertial regime, where it represents directly the friction slope in the energy equation. The same thing must be true in the transitional regime as well since Bagnold's data show that, at least for concentrations exceeding some 40 percent, the plain fluid drag is less than one- tenth of the grain stress.

From Bagnold's data, it appears that the stress ratio exhibits a unique variation with N, from approximately 0.75 at the boundary of the macro- viscous regime to about 0.25-0.35 within the inertial regime, as shown in Fig. 8.1. It has been suggested by Bagnold (1961), and confirmed in Chapter 11, that the stress ratio in fully inertial flows should equal the approximately constant kinetic friction coefficient. Thus, the value of 0.25- 0.35 in Fig. 8.1 reflects the low internal friction angle of the wax beads. On the other hand, the value 0.75 found at the other limit of the transitional region, is unlikely to be affected much by the frictional properties of the material, since the grain stress at this condition derives mainly from local turbulence of the interstitial fluid. For a given material, therefore, such as Ottawa sand, one may correct the relationship of Fig. 8.1 by drawing a smooth line across the transitional region from T/P=0.75 to the stress ratio corresponding to the kinetic friction angle of that material.

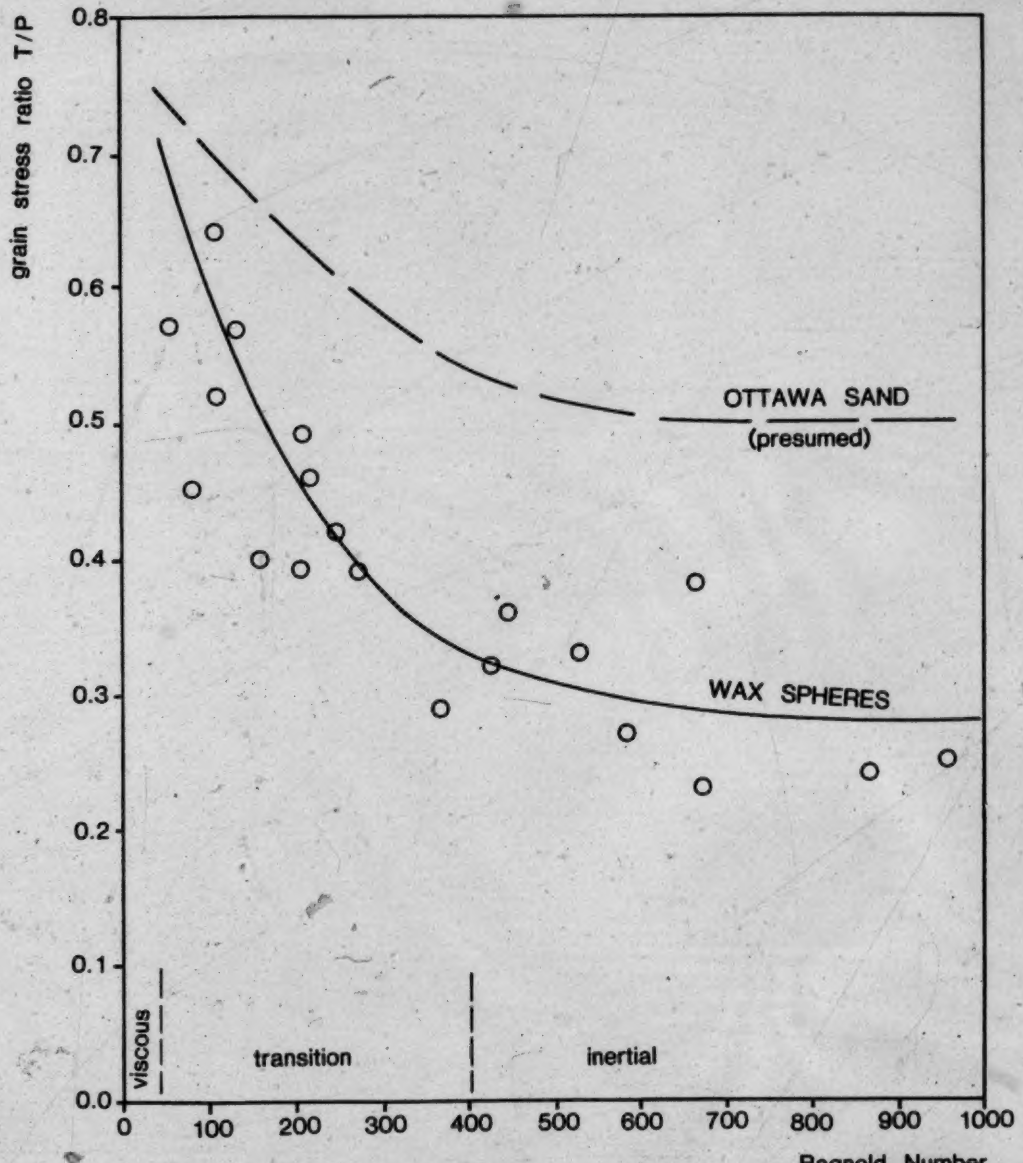

7

Figure 8.1 Change of the grain stress ratio (friction coefficient) in the transitional regime. Data from Bagnold (1954).

If one could estimate the value of the effective stress P at any point within the flow sheet, T would be given by this set ratio and the simple frictional analysis of Chapter 7 would be applicable. This is in fact the case in dry flows of coarse materials, since one can assume the interstitial air pressure to be zero. The same argument could be applied to completely drained subaqueous flows which dilate with acceleration, but whose interstitial water is immediately replenished by seepage, leaving effective stress P at the level of the submerged overburden. This is not the case, however, in most rapid sand flows and probably even dry flows of fine materials such as silt and ash, which are undrained. The fluid movement in such undrained flows is delayed and the tendency for dilation at higher velocities is translated into a dispersive pressure exceeding the static effective stress level. But the magnitude of the dispersive pressure defined by Eqn.(7.3) is very strongly dependent on concentration and thus difficult to evaluate. It is therefore suggested here that in flows which are not fully liquefied, the effective stresses should conservatively be assumed to equal the pseudo- static value as determined by an undrained shear test. The frictional analysis of Chapter 7 would then apply, using effective stresses.

It is interesting now to approach the transitional region from the other limit. A large number of publications in the field of chemical engineering refers to viscosimeter experiments on dispersions of granular materials. The results are usually presented in terms of (constant) relative viscosities; most of these researchers do not even address the possibility of non- Newtonian behaviour. Metzner and Whitlock (1958) review five independent research programs, all of which concluded that granular dispersions in liquid behaved as Newtonian fluids. Particle sizes varied from 1 to 160 microns (up to medium sand), volume concentrations up to 64 percent, shear stresses of several kPa and strain rates of over 1 000/sec. The liquid viscosities were relatively high, equal to 80 cp for the largest particles. Therefore, despite the high shear strain rates applied, all of these testing programs were conducted within the macro- viscous regime, with N less than 40. Their findings are thus in agreement with Bagnold's. A typical relative viscosity- volume concentration curve is shown in Fig. 8.2 (Farris, 1968). Its shape is said to depend little on particle size (up to medium sand rage), although it would likely be affected by grain shape and grain size distribution. Viscosity rises relatively slowly at first, being equal to only 10 times that of clear water for volume concentrations of up to 0.5. Between a concentration of 0.55 and 0.60 (porosity of 40 to 45 percent), the viscosity rises dramatically, reaching a nearly vertical tangent, on a semi- logarithmic plot within a few percentage points of concentration increase. This must be the limit at which grain stresses develop and the transitional regime is

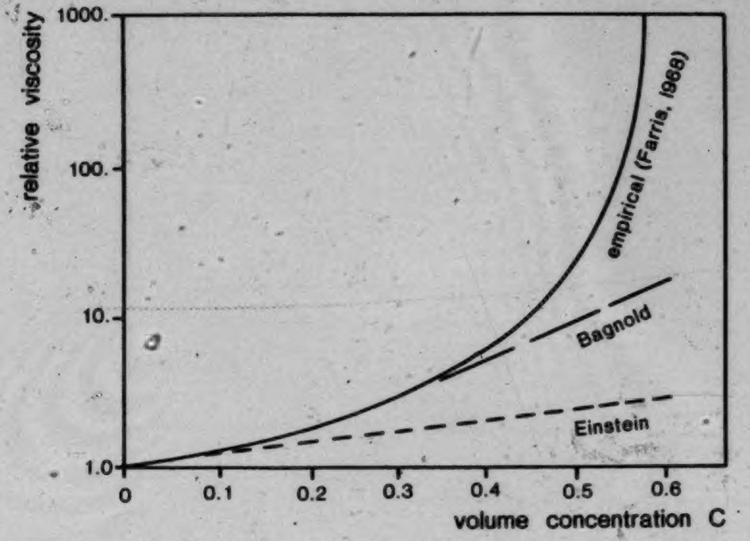

Figure 8.2 Relative viscosity of uniform dispersions in the macro— viscous regime.

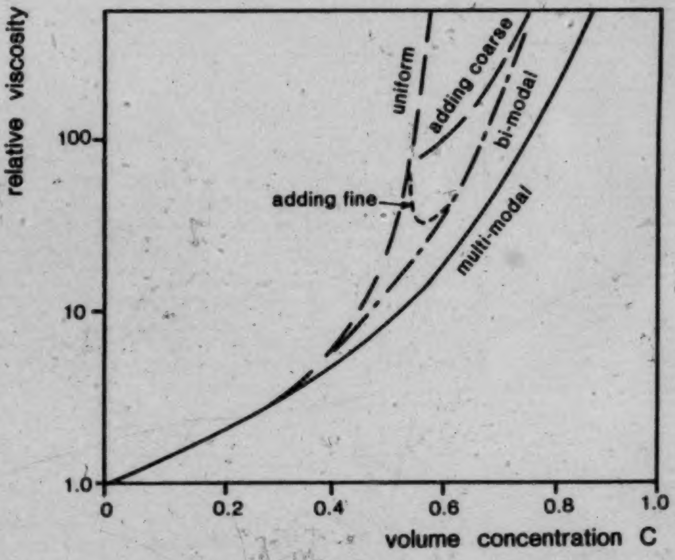

Figure 8.3 Relative viscosity of graded dispersions in the macro— viscous regime (Farris, 1968).

reached. A relationship proposed by Bagnold (1954) for the relative viscosity in the macro- viscous regime is shown by the dashed line in Fig. 8.2. It agrees very closely with the other curve up to a concentration of 0.5.

The above discussion relates to the problem of the dynamics of subaqueous slides. It must firstly be pointed out that natural saturated flows may exist in the macro- viscous regime. This is substantiated by the observed high fluidity of such flows as described in Section 8.1. If one assumed a laminar flow of fine sand 5 m thick and with a surface velocity of 5m/sec; the maximum velocity gradient would equal 2 sec . Assuming further that D = 0.1 cm (fine sand), ρ_g = 2.7 g/cu.cm, viscosity of water = 1 cp and porosity is 40 percent, corresponding to a linear concentration equal to approximately 14.5, the Bagnold number would be 0.20, which is well below the limit for the macro- viscous regime. Secondly, it appears that natural sand flows would not be far from the regime boundary in terms of concentration. Since the boundary is reached very abruptly as the concentration increases, this explains the "freezing" of quick sand flows as they slightly consolidate during their motion.

The limits of the macro- viscous regime as given by the sudden upturn of the viscosity curve in Fig. 8.2 agree remarkably well with the porosity values found in Norwegian and Dutch flowing sands, as reported in Section 8.1. But the curve of Fig. 8.2 cannot be applied as a universal criterion of liquefaction danger. All of the preceding discussion is in terms of uniform grading. Fig. 8.3 shows qualitatively the influence of grain size distribution on the viscosity curve. Farris (1968) quoted an accepted rheological concept of scale: if a mixture is formed of two very different grain sizes, one may consider two separate levels of dispersion. The fine fraction dispersed in water forms a fluid in accord with the relationship of Fig. 8.2. This then becomes the base fluid for a dispersion of the large fraction and the whole remains mobile at a considerably increased total concentration. Fig. 8.3 shows the viscosity curves for such bimodal dispersions, formed by adding fine to coarse or coarse to fine fractions. A theoretical multi- modal dispersion appears capable of considerable mobility at total concentrations of over 0.7 to 0.8 (porosities of only 20- 30 percent). The important conclusion from this is that well graded sands should be susceptible to liquefaction at smaller porosities than uniform ones, although they would also necessarily have to possess the metastable structure required for structural collapse. There appears to be a possibility of assessing liquefaction susceptibility by viscosimeter tests run close to the field concentration. Some means of preventing settling of particles in the viscosimeter would have to be invented, perhaps by using a heavy pore fluid of known viscosity.

A summary of the preceding discussion, and that of Chapter 7, yields a classification of flow relationships for saturated granular materials, depending on the Bagnold's number and on the degree of drainage:

a. *Drained inertial fluid.* In fully drained flows, the fluid pressure remains near the ambient static level. The material is free to reach a degree of dispersion suited to the strain rate and the effective stresses are in equilibrium with the submerged overburden weight. The sand then behaves as the frictional medium of Chapter 7, in terms of submerged densities. The same equations are valid in the transitional regime, except that the ratio T/P changes as in Fig. 8.1. Drained macro- viscous fluid probably cannot exist, except if the specific gravity of the solids was low.

b. *Undrained inertial (Bagnold) fluid.* If there is no time for pore fluid movement, the solids concentration (or porosity) remains constant as it was in Bagnold's experiments. The resisting shear stress is then given directly by the grain shear stress equation (Eqn. 7.3 and 7.4) and it is not necessary to know the effective stresses in order to write the equation of motion. Only the total normal pressure in the flow sheet remains constant:

$$\sigma = \gamma y \cos \alpha \qquad \text{Eqn. (8.7)}$$

where γ is the bulk density y depth below the free surface and α the slope angle. At the onset of motion, the pore pressures are controlled by the initial quasi- static volume changes. At higher velocities, the effective stress must approach the value of the dispersive pressure given by Eqn. (7.3). Because water is incompressible, the initial pore pressures are "erased" by the dispersive stress and replaced by a value dictated for a given material exclusively by concentration and velocity:

$$u = \sigma - P$$

Eqn. (8.9)

The driving force per unit area of an undrained flow is given by the tangential component of the total weight of the flow sheet:

$$\tau_d = \gamma y \sin\alpha$$

Eqn. (8.10)

Combining this with Eqn. (7.3):

$$a_i \rho_g \lambda^2 D^2 (dU/dy)^2 \sin\phi = \gamma y \sin\alpha$$

Eqn. (8.11)

Bagnold (1954) used the same equation, but he worked in terms of submerged weight, being concerned with a drained flow. Solving (8.11):

$$\frac{dU}{dy} = \left[\frac{\gamma}{a_i \rho_g \lambda^2 D^2} \, \frac{\sin\alpha}{\sin\phi}\right]^{1/2} \sqrt{y} = \xi \sqrt{y}$$

Eqn. (8.12)

which can be integrated over a depth H with a condition of zero bed slip to obtain the surface velocity:

$$V = \frac{2}{3} \xi H^{3/2}$$ Eqn. (8.13)

From which the mean velocity:

$$v = \frac{4}{15} \xi H^{3/2}$$ Eqn. (8.14)

These equations constitute a method of total stress analysis in the inertial regime. But it is exceedingly difficult to evaluate ai and λ for conditions which lie greatly outside the range of Bagnold's experiments, i.e. for effective stresses greater than about 0.4 kPa. Possibly, the approximate proportionality of ai and P (Fig. 7.3) could be used together with Bagnold's assumption that λ is unlikely to be less than 22.5.

Or, the conventional approach could be taken of equating the effective pressure with the effective stress obtained from some empirical "critical state" relationship as shown in Fig. 3.7. The velocity determination could then follow the frictional flow approach of Chapter 7, in term of effective stresses. This would amount to neglecting the influence of strain rate on the effective stress and relying on a sufficiently high rate of testing.

c. *Undrained viscous flows* are similar to the preceding class except that, by virtue of their low concentration, they belong into the macro- viscous regime (N<40). They could be analyzed using the standard theory of viscous flow, with the viscosity estimated either from Figures 8.2 or 8.3 or from experiments.

Neither of the models reviewed here approximates to the often used visco- plastic or Coulomb- viscous model. In fact, granular dispersions would classify rheologically as dilatant, not plastic. Plastic behaviour thus appears to be restricted to materials with colloidal particles.

8.4 Methods of Analysis and Considerations of Drainage

Bagnold's work did much to clarify the constitutive behaviour of granular materials under any conditions. Nevertheless, the prospect of rational analysis of undrained sand flows is not very encouraging. Even in the viscous regime (Figs. 8.2 and 8.3), density and grain size distribution has so overwhelming an influence on the viscosity that it does not appear feasible to predict it better than to an order of magnitude. A difference in porosity of mere 3 percent would change the viscosity by a factor of 10. Porosity of natural or compacted sand deposits is unlikely to be constant to less than plus or minus 3- 5 percent. This is why undisturbed blocks are often found in flow slide deposits, which did not participate in the general shearing, but were rafted within the more mobile material (Casagrande, 1965). This is the only analytical approach feasible, however, and so it must be used, although it should be checked by empirical observations to the greatest possible extent.

The Vlietpolder flow slide, reported by Koppejan et al. (1948) can be used as an example. Its crossection is shown in Fig. 8.4. The mean thickness of the source area is 20 m. It is 400 m long and probably similarly wide. The initial slope beneath the toe of the source area is 5 deg. The depositional area begins about 200 m beyond the toe, sloping at 1 deg. The material is a fine sand with an in situ porosity of at least 44 percent and an estimated saturated unit weight of 1.8 g/cu. cm. It will at first be assumed that the failure spread out almost instantaneously, as in the dam break model (B in Fig. 5.4). The material will be assumed to behave according to the viscous regime. Fig. 8.2 yields a viscosity of about 200 cp for the given porosity. From Eqn. 5.19, the height of the terminal roll wave would be 4.3 m on the 5 deg. slope and 6.8 m in the depositon area. The corresponding velocities would equal 18.7 and 11.8 m/sec respectively.

An alternative method of analysis could be based on the average rate of retrogression for the coastal flow slides, reported by the authors as being equal to approximately 50 m/hour (Model C). From Eqn. 5.15, the total outflow rate from the source area is 111 cu.m/sec. If one expects a narrowing of the flow tongue from the source width of 400 m to 300 m, this would correspond to a unit outflow of 0.37 cu.m/sec (200 times less than that which would result form the dam break wave, Eqn. 5.18). The resulting roll wave

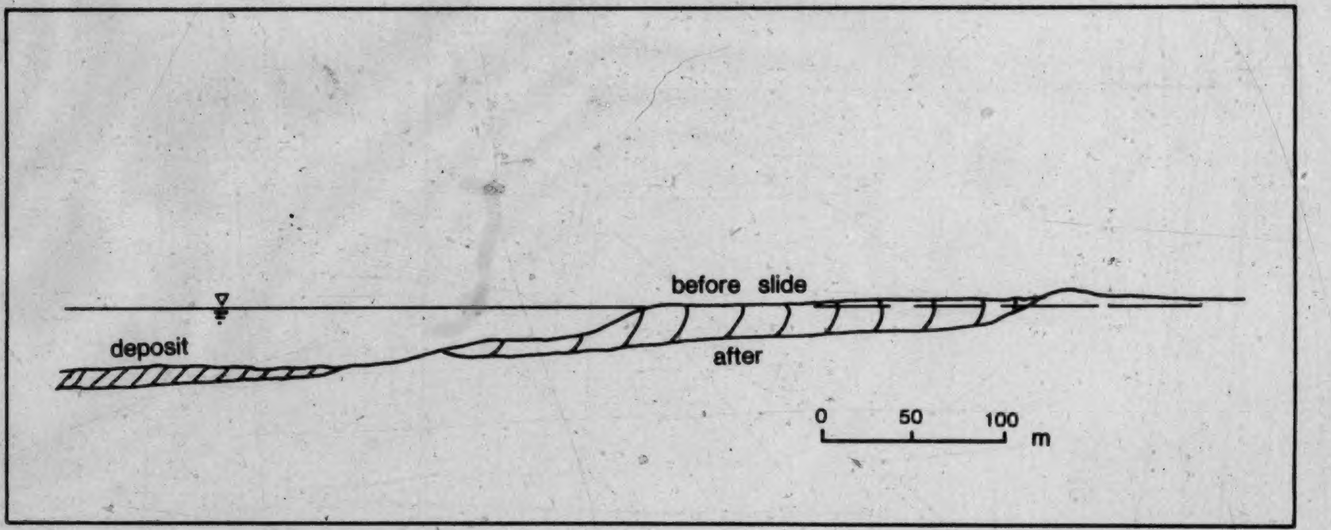
before slide
after
deposit
0
50
100
m

Figure 8.4 A crossection of the Vlietpolder flow slide (after Koppejan at al., 1948).

height and velocity in the depositon area would be 1 m and 0.3 m/sec respectively. This thickness is about 10 times less than the thickness of the actual deposit which could, however, have been built up in successive layers. Using a mean particle diameter of 0.1 mm, the Bagnold number is found to equal only 0.1 , confirming the assumption of Newtonian behaviour. The difference between the two solutions is striking and it indicates the importance of the rate of retrogression. The dam break solution is certainly conservative for flows that were not liquefied by an earthquake, and represents an upper limit estimate. The second solution, while more realistic, is based on what could be a subjective observation.

One may also try to back- calculate the retrogression rate from a known velocity. The Norwegian slide at Follafjorden, described earlier, was completely submerged and thus its development could not be observed. But a flow velocity of approximately 5 m/sec was registered by the motion of the dredge which the slide towed by an anchor. If one assumed, for lack of better information, an overall geometry similar to that of the Vlietpolder flow, a reversal of the procedure of the preceding paragraph would yield a predicted retrogression rate of 0.8 m/sec or a slide duration of over 8 minutes, which corresponds reasonably with descriptions.

It remains now to consider the problem of drainage of flowing sand masses. Neither the inertial or viscous *undrained* model would predict "freezing" or stoppage of the flow front, except on a zero or negative slope. But drainage must occur with time and, as the flow consolidates it will always ultimately convert into a drained inertial (frictional) state and stop [12].

Hutchinson and Bromhead (1981) applied the consolidation theory in order to predict the loss of pore pressure with time. But it was shown in the preceding section that liquefied sand flows with porosities exceeding 40 percent have initially only negligible effective stresses. The concept of consolidation, which assumes a measurable drained stiffness of the grain skeleton, is therefore inapplicable. The theory of "hindered sedimentation" (Lowe, 1976, McRoberts and Nixon ,1976) is to be preferred in this case. This assumes the effective stress to be zero and visualizes a process similar to the settling of a grain bed out of a concentrated suspension. The key parameter is the settling velocity of grain aggregate in the fluid for which there is a relationship due to Richardson and Zaki (1954) for uniform grain sizes:

$$V_a = V_s (1 - C)^n \qquad \text{Eqn. (8.15)}$$

where vs is the settling velocity of a single grain, C is the concentration and n a constant equal to 2.4 to 4.7

---

[12] Unless turbulent mixing produces a self- sustaining turbidity current, cf. Section 8.2.

[13].

The single particle velocity can be calculated by a formula (Massey, 1970):

$$V_s = \sqrt{\frac{4}{3}\,\frac{D}{\rho}\,\frac{\gamma'}{C_D}}$$

Eqn. (8.16)

where D is the diameter of a particle and γ' its submerged unit weight, ρ fluid density. Also:

$$C_D = \frac{24}{R}\left(1 + \frac{3}{16}R_e\right)^{1/2}$$

Eqn. (8.17)

and

$$R_e = \frac{v D \rho}{\eta}$$

Eqn. (8.18)

where η is the viscosity of water. Laminar flow regime persists for $Re < 0.1$. The empirical drag coefficient equation (Eqn. 8.17) is valid well into the turbulent range, for Re exceeding 100.

The sedimentation time, during which the concentration of the bed decreases from C to C is given by a mass balance formula (Lowe, 1976):

$$t = \frac{H(C - C_o)}{C V_a \cos\alpha}$$

Eqn. (8.19)

where H and α are the bed thickness (initial) and slope, respectively. Lowe (1976) used this equation to calculate times required for various flows to reach a concentration of 0.6, at which he expects "freezing" to occur. Assuming initial concentration of 0.54 (n = 46 percent), he obtained flow times ranging from 0.6 sec per cm of bed thickness for coarse sand to 11.9 sec per cm for fine sand. Using his formulas, the 1.1m thick flow obtained earlier using the discharge flow condition would travel for about 150 m.

---

[13] With respect to single particle velocity.

A more refined analysis of the process can be made by considering the gradual increase of viscosity with concentration as shown in Fig. 8.2. The relationship shown in the figure can be fitted empirically by a polynomial (Ford, 1960):

$$\eta_r = 1 - a\,C + b\,C^5 + d\,C^7 \qquad \text{Eqn. (8.20)}$$

where the coefficients a, b and d equal respectively 2.5, 20.6 and 41.1 to fit the data of Fig. 8.2. Neglecting the flat slope angle, the concentration C can be expressed as a function of time from Eqn. (8.19):

$$C = \frac{C_o}{1 - \frac{t\,V_a}{H}} = \frac{C_o}{1 - T} \qquad \text{Eqn. (8.21)}$$

where T is a dimensionless time factor. The solution of Eqn. (8.20), which shows the change of viscosity with increasing time, is plotted in Fig. 8.5. It is obvious from the figure that the initial porosity influences the time required for "freezing" of the flow even more strongly than it does the initial viscosity. Figure 8.6 shows the decay of flow velocity with distance for the 1.1 m thick flow. This was obtained by calculating the average uniform velocities for several equal time intervals, reading the appropriate viscosity value in each interval from Fig. 8.5. This

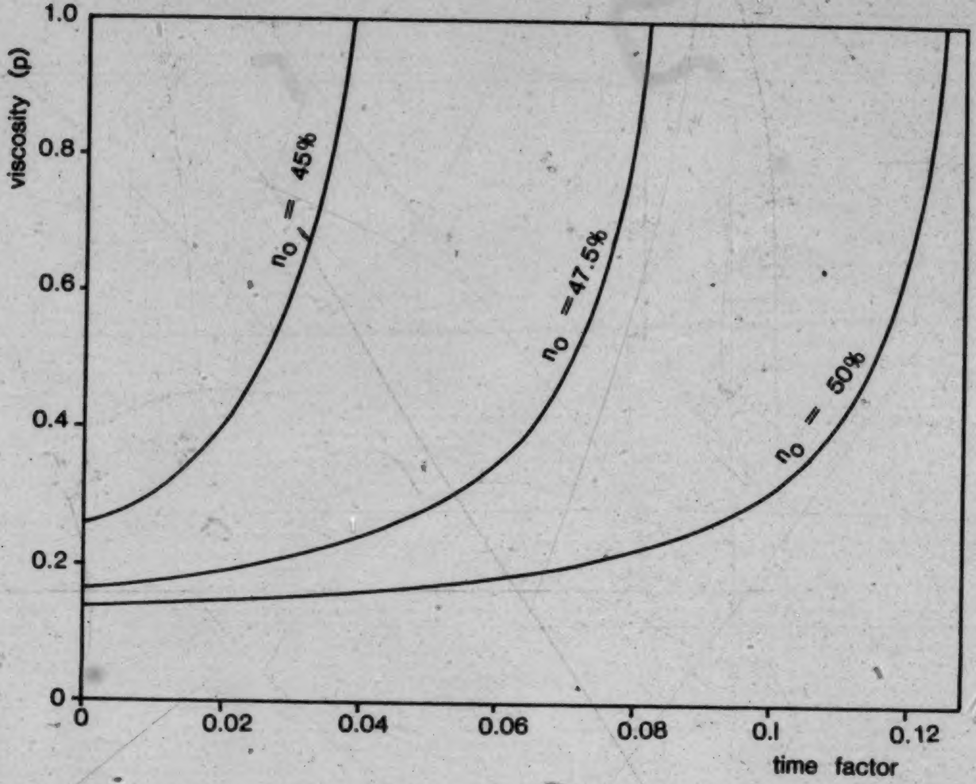

Figure 8.5 Viscosity change due to drainage in layers of different initial porosity.

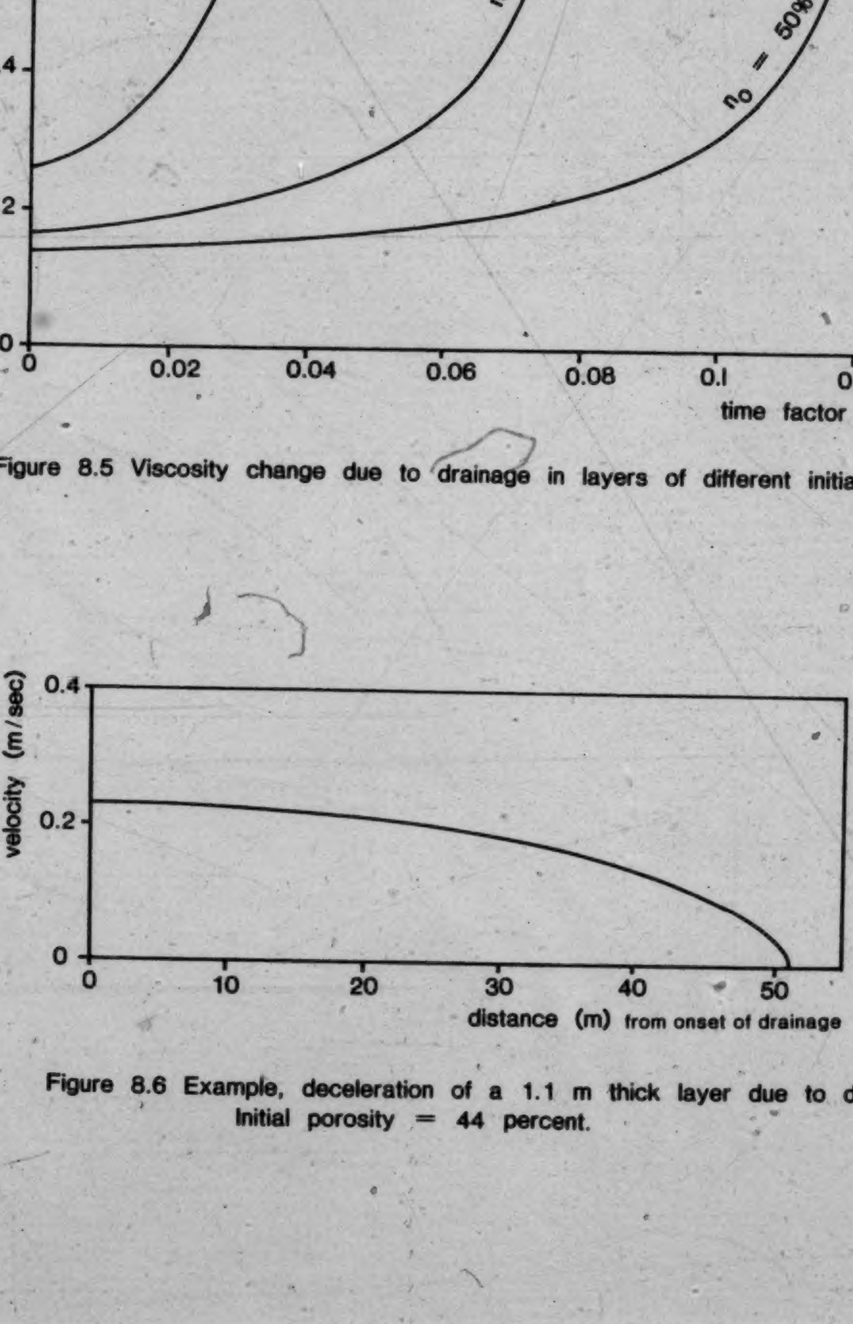

Figure 8.6 Example, deceleration of a 1.1 m thick layer due to drainage. Initial porosity = 44 percent.

predicts a travel distance of only slightly over 50 m after the start of drainage, stressing the importance of viscosity increase before "freezing" of the flow. The result shows that the retrogression rate of this flow must have been greater than assumed, in order to produce a thicker flow sheet. The above method of analysis makes several implicit assumptions:

a. That the effective stresses are negligible. this was confirmed by a calculation of the magnitude of Bagnold's dispersive pressure. This is only a very small fraction of the total stress in full size flows, for linear concentration values less than about 100.

b. That drainage occurs simultaneously in a long stretch of the flow sheet, which thus decelerates uniformly without a change in thickness or distortion due to thrusting of the less well drained material behind. This is nearly true when the flow front has advanced some distance beyond the toe of the slide and a long uniform tongue has developed behind the frontal roll wave. Prior to this, while the flow thickness is larger and variable as in the dam break model, drainage could probably be neglected. ; Thus, it is suggested that the total reach of the landslide as shown in Fig. 8.6 should be increased by about 3 to 5 times the height of the slide scarp to account for this episode of undrained motion.

The drainage of inertial flows, which have significant effective stresses, could be analysed using conventional consolidation theory, as was done by Hutchinson and Bromhead (op. cit.).

8.5 Air liquefied grain flows

Several examples exist in the literature of rapid flow slides wich were apparently either dry or incompletely saturated. All of the better documented cases involve material of silt size or finer. Varnes (1978) shows a photograph of a small silt flow (only some 2m wide) wich resulted from a steep fall of a block of dry silt, but continued in an apparently liquid state over a flat surface for some meters. Bishop (1973) (quoting Calembert and Dantinne, 1964) described a flow of fly ash from a storage pile in Jupille, Belgium. Over 100 000 cu. m participated in the flow slide and travelled at a velocity of over 30 m/sec on a slope of 18 deg. The material was placed at an initial water content of 25 percent and was saturated at the base of the pile. But the bulk of the flowing mass was apparently dry. The thickness of the flow was about 7 m.

The extremely destructive and large loess flows of Kansu Province in China are frequently mentioned. Unfortunately, the only detailed reference is a popular account by Close and Mc Cormick (1922) which gives little technical information. Especially, the degree of saturation of the flows cannot be reliably estimated. The article makes an impression of the flows having been partly coherent, since people and structures were transported on top without damage. The flows were triggered by an earthquake. Varnes (1978) suggests that they were dry.

Air liquefaction could occur by air entrapment into the soil material during an initial steep or vertical fall. This is what probably occurred in the minor flow already mentioned. The mechanism might be important in large rock avalanches and will be further discussed in Chapter 10. Flows that do not involve a fall episode can only liquefy by a structural collapse similar to that in saturated sands. The compressibility of air must be taken into consideration. Assuming rapid adiabatic compression, it can be shown that the pore pressure resulting from an undrained change in porosity from no to n is:

$$P = P_o \left\{ \left[\frac{n_o}{n} \, \frac{(1-n)}{1-n_o+\frac{S}{1-S}\left(1-\frac{n_o}{n}\right)} \right]^{\gamma} - 1 \right\} \qquad \text{Eqn. (8.22)}$$

where po is the original (athmospheric) pressure, S is the degree of saturation defined as the fraction of the pore space occupied by water and γ is a constant equal to 1.40 for air. This formula neglects air solution, which should not be significant at low saturation. The porosity after the collapse is limited to the value of :

$$n \geq \frac{n_o S}{1-n_o+n_o S} \qquad \text{Eqn. (8.23)}$$

at which the material approaches full saturation. The typical loose porosity of dry silt and natural, undisturbed loess is approximately 0.5. After collapse, the nonplastic soil would tend to compact to a porosity of about 0.4. Using these two values, Eqn. (8.22) would predict pore pressures equal to 76, 128, 365 kPa and infinity for saturation values of 0, 0.25, 0.5 and 0.67 respectively (Fig. 8.7). In case of thin layers, the pore pressure would of course be limited by the magnitude of the total stress and Eqn. (8.22) could then be used to predict the final porosity.

The value of 76 kPa suggests that a dry layer of quartzose silt about 6 m thick could fully liquefy by the collapse and could therefore flow in the macro- viscous regime. Thicker layers would be only partially liquefied and would need to be analysed as undrained inertial flows. The frictional analysis could be used to advantage, since the effective stresses can be predicted. For example, assume that the Jupille ash flow was indeed mostly dry and that it mobilized by a structural collapse caused by a saturation and failure of its foundation. The material had a saturated water content of 58 percent. Assuming its specific gravity to be 1.8, the initial porosity is found to be 0.5. The 7 m thick flow would have a base total pressure of 75 kPa and could thus be fully liquefied, with effective pressures close to zero. The frictional analysis (with zero friction) would therefore give a very conservative result and one should attempt to estimate the viscosity of the flowing

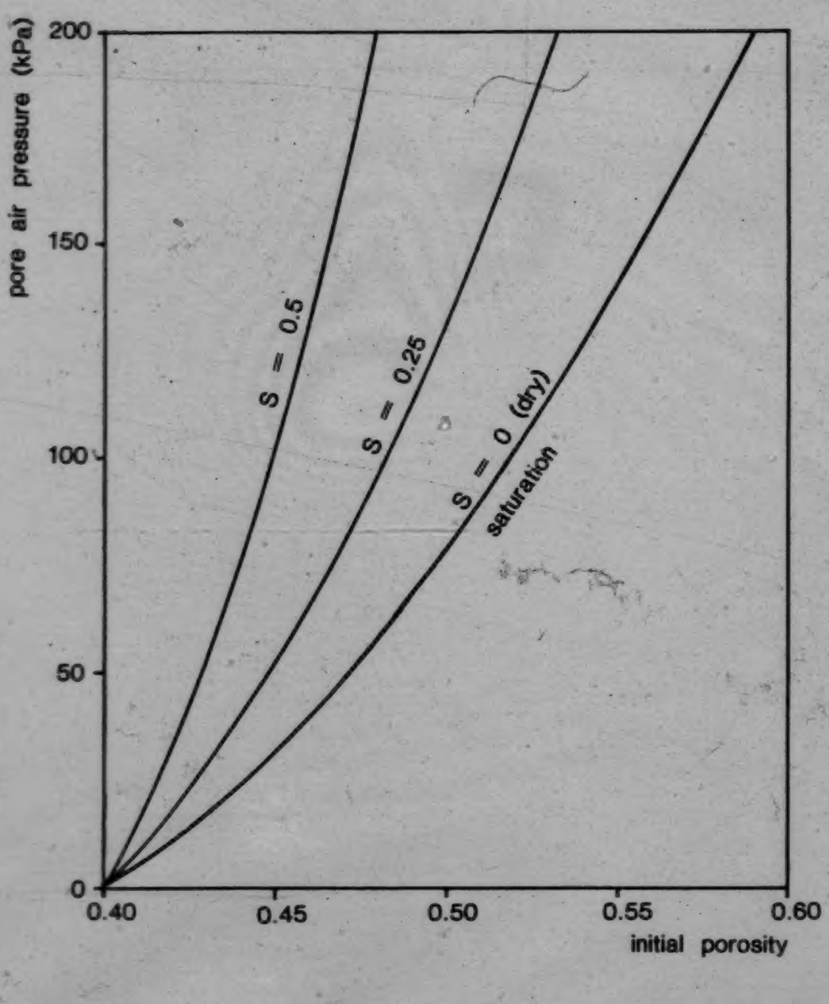

Figure 8.7 Pore air pressure generated by a soil structure collapse to a final porosity of 0.4 under undrained conditions.

mass. The viscosity of air at this pressure and 20 deg. temperature equals 0.0002 poise. Assuming a relative viscosity of the dispersion of 1000, a turbulent flow with a normal velocity of over 20 m/sec would be predicted.

Drainage of air from the flow sheet during its motion will be discussed in Section 11.2.

9. FLOWS OF MIXTURES OF SOLID GRAINS AND SLURRY

9.1 Debris Flows

Debris flow is a characteristic type of slope movement in mountainous and semi- arid regions, where it constitutes one of the major erosional processes (Rapp, 1960). Its definition and separation from debris avalanche, debris slide and rapid earth flow or mudflow is somewhat controversial (Blong, 1973). Nevertheless, debris flow is described here in a separate section, recognizing its importance and characteristic attributes which should become apparent from the following. Its analytical aspects, however, are dealt with together with those of other types of flows of mixtures of granular materials and clay slurry.

Strong rains or melting of snow in mountainous or steeply dissected semi- arid terrain release flows of loose weathering products including clay, sand, gravel and boulders, mixed with vegetation and timber remains and heavily saturated with water. The flows originate in steep upper slopes and in the heads of gullies often, although not exclusively, above the treeline. Various authors indicate that the source areas are usually as steep as 30 to 45 deg. Rapid weathering and other types of slope movements (especially sliding) supply the debris. Flows begin during periods of abnormally high runoff and quickly concentrate in existing drainage paths. They then flow through relatively long middle reaches, enlarging the existing channel to a U-shaped crossection ("gorge") and picking up further debris from side slumps and scouring. The middle reach generally slopes more than 10- 12 deg., since most flows would begin slowing down and depositing debris at flatter slopes (Campbell, 1975). The path followed is usually that of an intermittent stream where there is a large accumulation of erodible debris. Less commonly, the flows reach and follow a permanent water course. The debris flows issue out of the gorge onto a flatter slope, usually on an alluvial fan. Here the flow spreads out and thins, its velocity decreases and deposition occurs relatively quickly.

The processes which lead to the generation of debris flows in the source areas are numerous and varied. Perhaps the most important is the shallow earth slide in the steep upper reaches of mountain gullies and slopes. This may produce a debris flow spontaneously. For example, Williams and Guy (1971) quote eyewitnesses from the Appalachians observing sheets of soil and vegetation which started moving almost instantaneously over areas tens of metres wide. In this case, the shallow (1m) soil cover over impervious Precambrian bedrock was mobilized on slopes close to 40 deg. by a hurricane storm. The slides removed the soil cover entirely and exposed bedrock in narrow upward pointed scars. The soil sheets broke up almost instantaneously and flowed down the nearest drainage path scouring soil and forest along the way and leaving a strip of bare rock.

Similar spontaneous mobilization of a shallow block about 6 cu. m in volume has been filmed by A. Johnson near Wrightwood, California (Rodine, 1975). The block was a part of a mass of landslide debris in schist, lying at the head of Heath Canyon. It was observed to begin moving in a quick series of retrogressions starting from the toe and to change to a flowing mass resembling wet concrete within a few seconds.

Johnson and Rahn (1970) describe a related process by means of which debris flow masses may incorporate water from surface runoff. They observed debris flows initiating in a clayey landslide mass at Woodside, California. Masses of debris accumulated from individual block falls in the bed of a drainage channel. They began to move slowly after acquiring a certain volume, and incorporated water from a trickle flowing through the channel by means of internal shearing, tumbling and overriding. A similar effect appears to result from damming of the drainage channel by sluggish debris. The dam is overtopped and breached by water that accumulated behind it and the debris is remobilized, but at a higher water content.

A substantial part of the volume of some debris flows is contributed by material eroded from the bed of the channel. Indeed, all debris flows are highly erosive in their steeper upper reaches. Their erosive power derives from high viscosity, unit weight and presence of large particles. A typical longitudinal profile of a debris flow has a steep zone of erosion extending through the upper source region and through the intermediate gorge, bordering on an accumulation zone in the lower flatter reaches of the valley. A survey of six debris flow profiles from Japan (Daido, 1971, Suwa et al., 1973), one from New Zealand (Pierson, 1979) and one from the Alps (Breitfuss and Scheidegger, 1973) shows the slope at the transition between erosion and accumulation zones to average 10 degrees, ranging between 6 and 17. The accumulation zone often constitutes less than one- fifth of the total length of the profile, although this is not always the rule.

Daido (1971) suggests that in the case of some Japanese flows, bed erosion constituted the exclusive material supply mechanism. Similarly, Mears (1979) proposes that some debris flows may represent merely the limiting condition of bedload movement in large storm floods:

> "High velocity floods with a large sediment load may become so heavily laden with coarse- grained sediment, that parts of the bed load become decoupled from the flood wave and continue to advance even as the flood recedes".

The process of debris flow generation by flood has also been illustrated by the event of 1978 in the Kicking Horse Pass, B.C. (Jackson, 1979). Two surges of debris flow which transported about 175 000 cu. m of predominantly coarse material were apparently caused by a catastrophic outflow of meltwater from a glacier ("jokulhlaup"). The head of the drainage basin from which this flow originated bears evidence of extremely rapid erosion and slumping along the margins of a channel issuing from the ice front. It is interesting to note that the same basin gave rise to a debris flow in 1962, unaccompanied by flooding and apparently caused by a spontaneous liquefaction of material on the upper slopes.

Colluvium and residual soil are the primary source materials of debris flows. As a consequence, debris flows are typically well graded and contain a fair proportion of coarse sizes. A random selection of grain size distribution curves from different parts of the world is shown in Figure 9.1. These represent samples of the finer matrix material, not including larger clasts which are transported by some flows in significant quantities. Two of the examples illustrate changes in grading along the course of the flow. In both of these cases, the change occurred during flow over the gently sloping alluvial fan surface, i.e. in the accumulation zone. The grading curve, while remaining well distributed, shifts to the right possibly as a result of deposition of the coarser fractions onto the bed and side margins of the channel.

Bull (1964) observed vertical grading from coarse at the base to finer at the top of some deposits, accompanied by rough orientation of elongated clasts in the direction of movement. He postulated these deposits to be the result of

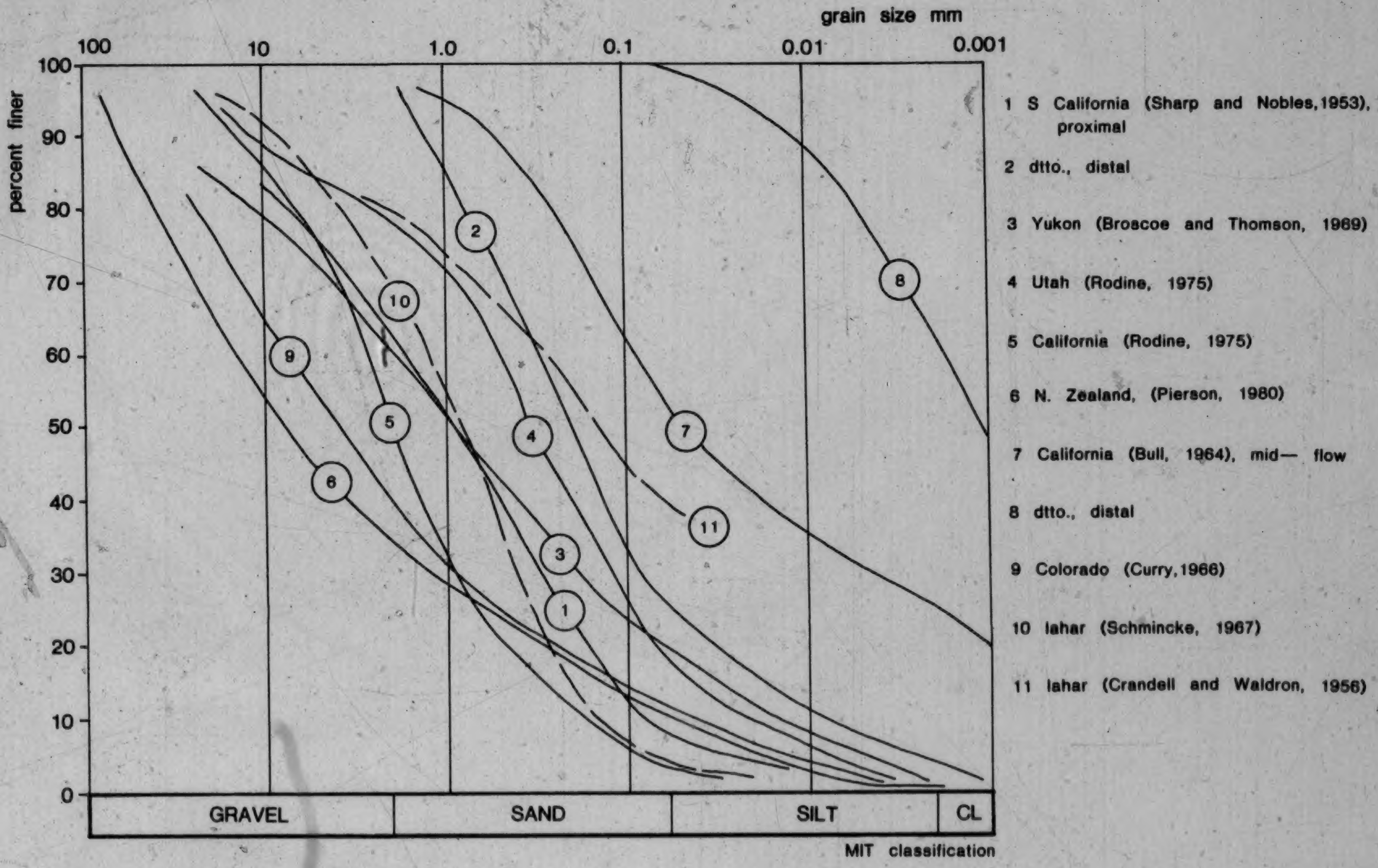

Figure 9.1 Grain size distributions of debris flow materials.

very fluid debris flows, bordering on flood transport processes. Similar grading has been reported by Crandell (1957) from lahar deposits in Washington.

Some investigators find debris flow deposits entirely unsorted and lacking in preferred grain orientation. Others noted inverse sorting, with coarse clasts concentrated near the surface and "floating" on the firmer matarial below. Mears (1979) found this in a very coarse grained frontal lobe of a debris flow in Colorado. Pierson (1980) observed cobbles and boulders being forced laterally out of the flow during the course of movement "by some internal sorting process".

Debris flows occur during periods of unusually high precipitation or snow melting, and often coincide with floods. Under such circumstances, the debris flow behaves as a cyclic phenomenon. Many accounts exist of periods during which one or several drainage basins discharged surges of debris for several days, at intervals ranging from a few minutes to several hours (e.g. Sharp and Nobles, 1953). The periodicity results from repeated cycles of accumulation of debris, damming of the channel, failure and flow. Generally, the surge magnitude and frequency reach a maximum during a "climax" period, when the erosional activity of the flows is extended to the farthest reaches of the channel (Morton and Campbell, 1974). During the immediately preceding and following periods, the surges are smaller in volume and less liquid, depositing material within a shorter range. The material accumulated by these lesser surges in the upper reaches of the channel is re- mobilized during the climax period, adding to the volume of flow at that time. Morton and Campbell (1974) observed climax surge volumes of approximately 200- 900 cu. m.

It must be stressed, however, that not all debris flows occur in this periodic manner. Some originate spontaneously, without prior warning, as a result of a large- scale rapid soil slip in the source area. Campbell (1965) described such a flow, which occured in 1965 in Newton Canyon, S. California. This flow had attributes quite similar to other debris flows described in this section, but it occurred as a single sudden surge with a volume of about 7 000 cu. m, unaccompanied by a flood. Most of the Appalachian debris flows occur in a similar way.

The writer has been able to observe the cycle of events accompanying a typical debris flow surge flowing in the middle reach, which was filmed in Japan (courtesy of Professor H. Suwa). The film shows a U- shaped channel, about 10 m wide and 6 m deep, with a rocky bottom through which a trickle of muddy water is flowing. The debris flow surge appears suddenly around the bend as a wall of boulders, approximately 2 m high. Boulders, distinct but covered with mud, form the entire steep front face and top surface for a distance of perhaps 15 m upstream. Some are at least 1 m in diameter. After a short while, the presence of boulders and cobbles on the surface gradually declines and the surface assumes the appearance of a smooth, laminar flow of mud. Gradually, the flow height is reduced and at the same time the mud appears to become more liquid and turbulent. The surge ends with a prolonged "tail" of muddy, turbulent flow resembling an ordinary flood. During the motion, the boulders at the front appear to be bound into a fairly coherent mass. Some internal rolling occurs and some boulders move down the front and are swallowed underneath the flow. The larger boulders, however, tend to resist this incorporation for some time and are being pushed ahead, rolling with some difficulty. The whole surge makes an impression of a dam of boulders, restraining a reservoir of mud behind it, while moving rapidly down the channel.

Suwa et al. (1973) observed the distribution of grain sizes in the boulder front of a debris flow. Ninety- five percent of the boulders had diameters between 20 and 60 cm, the remainder being larger (up to 130 cm).

Similar observations have been made by others. For example, Sharp and Nobles (1953) write about the 1941 debris flows at Wrightwood, California:

> "A bouldery embankment formed at the front of more viscous surges and the boulders therein rolled, twisted and shifted about but, for the most part, did not appear to be rolled under".

When the flow front reaches a section of shallower channel and milder slope (15- 20 deg.), it may begin to deposit levees of coarse material. Sharp (1942) describes good examples of these from debris flows in the St. Elias Range, Yukon. The levees appear as sharp longitudinal ridges of coarse material with steep flanks and narrow crests. They generally increase in size in the downstream direction and sometimes end on the alluvial fan in a bouldery lobe. They tend to be larger on the outside of bends. Sometimes the outside levee may locally be overtopped by liquid slurry, which then spreads out as a thin lobate sheet outside the channel (Bull, 1964).

Usually, a liquid clay slurry flow is well contained within the levees. This writer observed debris flow levees several days after the event near Kicking Horse Pass in the Canadian Rockies. The levees were composed entirely of coarse gravel, cobbles and boulders, cleanly washed by rain on the surface, but with a small amount of fine matrix in the interior. They were about 0.5 to 1. m high. Mud marks on trees remaining in the channel indicated that liquid slurry flowed at a maximum level equal to the crest elevation of the levees. But there was no overflowing; the forest floor immediately outside their toes was clean and undisturbed.

Pierson (1980) describes flow surges from New Zealand which differ somewhat in character. In this case, the frontal boulder accumulation was preceded by a surge of muddy water which thickened and rose gradually from a steady, turbulent base flow. At the crest of the surge, levees were deposited by lateral expulsion of boulders from the flow, as mentioned earlier. Perhaps, the viscous surge resulted from water and mud accumulated in the channel above the point of observation, which had been flushed out by the debris flow front and was being pushed ahead of it.

Some debris flows do not form the frontal boulder accumulations. This is especially true of the lesser surges and of some shorter and less rapid flows which perhaps lack the time to develop them. Or there may simply be a lack of large sizes in the debris. The debris flows of Port Alice, Vancouver Island (Nasmith and Mercer, 1979) were apparently relatively homogeneous in grading and water content. On the other hand, very liquid debris flows also do not exhibit frontal accumulations, if their material cannot support large clasts near the surface.

The accumulation region is characterized by a wide channel and low angle. Fluid debris flows without frontal boulder accumulations spread out into wide flat sheets which are typically only a few decimetres thick (Blackwelder, 1928). Those that are more viscous form relatively narrow lobate deposits (Nasmith and Mercer, 1979). Debris flows with boulder accumulations tend to remain inside their levees even on flatter ground and sometimes come to a stop in the form of bouldery lobes. More often, however, the fluid slurry breaks through the moving dam of coarse particles as the latter spreads and thins out. The slurry then spills out as a thin sheet of a remarkably flat and even surface. The accumulation zones of such flows contain a complex arrangement of two very distinct depositional features, i.e. ridges and lobate tongues of coarse materials and thin layers of fines (Broscoe and Thomson, 1969). In rare instances, the fine phase reconcentrates in a drainage channel at the toe of the alluvial fan and may continue flowing for a number of miles. This happened during the 1941 events at Wrightwood, California (Sharp and Nobles, 1953), where slurry flow continued for some 20 km past the toe of the alluvial fan.

In a summary of the above, it is possible to classify debris flows on the basis of their flow behaviour roughly into three classes, the physical attributes of which are illustrated in Table 9.1.

1. *Very fluid debris flows* are generally relatively shallow and turbulent. They transport coarse material only in the form of bedload and leave thin sheet- like deposits with vague sorting from fine at the top to coarse at the base. There are no accounts in the literature of those flows having been observed individually. Their character is known from deposits (Blackwelder, 1928, Bull, 1964) and from analogy with the interim fluid flows between debris surges (Pierson, 1980). This indicates water contents in excess of 50 percent and velocities of 1 to 2 m/sec. These debris flows often create deposits with large amounts of air bubble cavities (Bull, 1964, Crandell, 1957), attesting to a turbulent flow regime.
2. *Viscous homogeneous debris flows* have less water but do

location	type[1]	slope (deg.)	flow depth (m)	density (g/cm^3)	water content (%)	velocity (m/sec)	flood[2]	reference
Wrightwood, CA	B.A.	6	1.4-3	2.4	25-30	2.4-3.3	no	Sharp & Nobles (1953)
Colorado	B.A.	15-30	1.5	2.5	10	2.5-16	no	Curry (1966)
New Zealand	B.A.	6	1.0	2.1	28	2.5-5	yes	Pierson (1980)
New Zealand	F	6	0.2	1.7	67	0.8-2.4	yes	Pierson (1980)
Can. Rockies	B.A.	-	1.2	-	13-27	6	yes	Jackson (1979)
Vancouver Is.	V[2]	17	10	-	-	6-9	yes	Nasmith & Mercer (1979)
Vancouver Is.	V[3]	6	1-2	-	-	1.5	yes	Nasmith & Mercer (1979)
Wrightwood, CA	F	-	-	1.3	185	-	yes	Morton & Campbell (1974)

NOTES: [1] F = fluid flow, observed between surges
V = viscous unsorted flow
B.A. = flow with a frontal boulder accumulation

[2] in a narrow gorge
[3] on the alluvial fan

Table 9.1 Physical characteristics of some debris flows.

not exhibit longitudinal sorting. These occur by the process of spontaneous liquefaction in short basins and are therefore similar to debris avalanches which will be discussed in the following section. They do not develop frontal boulder accumulations because of their relatively short travel or possibly lack of coarse clasts in the source material. The Port Alice flows (Nasmith and Mercer, 1979) serve as an example.

3. Perhaps the most characteristic type of debris flow is that *with a frontal boulder accumulation*. It derives from a sufficiently high density and viscosity, which provide support for large clasts at the surface of the flow, where they tend to move under the influence of an internal sorting process. The water content of the clay slurry immediately behind the flow appears to be generally less than 0.30, although it gradually increases near the tail of the flow. Observed velocities of these flows vary between 0.5 and 10 m/sec but are typically about 1- 3 m/sec.

9.2 Debris Avalanches

The term "debris avalanche" is used here to cover flows of unsorted debris that are lacking some of the characteristic morphological attributes of the semi- arid and alpine debris flow. It describes flows that are too short or too far away from drainage features to develop significant chanelization. Also, it covers events triggered by unusual means- especially impact by rockfall or icefall. Finally, flows originating from man- made fills are considered under this heading.

Short, extremely rapid debris avalanches are among the most dangerous types of slope movement. They result by a spontaneous failure of a thin layer of saturated colluvium residual soil or fill on steep slopes. They do not channelize and become debris flows, because of a lack of a suitable sloping drainage feature or due to a lack of fluidity. There is a smooth transition between this type of debris avalanche and the rapid debris slide discussed in Section 3.1.

Lumb (1975) described the continuing hazard posed by debris avalanches in Hong Kong. The contributing factors to the frequency of occurrence of these slope movements there are steep developed slopes (over 30 deg.), high and seasonal precipitation and the presence of a continuous mantle of residual soil. The soil has a character of silt where it originates from volcanic rocks and silty sand from decomposed granite, with minor amounts of clay near the ground surface and with large core stones left as remnants of the parent rock. The soil is partially saturated in its original state and exhibits a drained cohesion of 2 to 110 kPa as a result of pore suction pressures. On wetting, the suction pressure is dissipated and the cohesion decreases to the point of failure. Lumb (1975) estimates that the wetting of a surficial layer several m thick can occur within a period of a few hours during heavy rain.

The most damaging debris avalanches in Hong Kong result from failures of poorly compacted mantle fills (Fig. 9.2a). Twelve cases of this type mentioned by Lumb had volumes of 370 to 54 000 cu. m, thicknesses generally less than 5 m and occurred on slopes of 25 to 43 deg. These failures are shallow in crossection, and contained within the fill. In plan, the avalanche scars narrow in the downhill direction. This narrowing is either gradual, on a straight slope, or abrupt if a pre- existing gully is available. Photographs shown by Lumb give an indication that the debris avalanches are predominantly erosive in their flow down the hillside. They reach velocities of up to 30 m/sec and have resulted in many deaths.

Investigation of some of the flow failures indicated that the fill material had been placed at low densities, so that it was able to contract during shearing (Morgenstern, 1978). Thus, the high mobility of these avalanches can be attributed to a collapsible state of the original material.

Another type of failure is the shallow slip of undisturbed residual soil from the surface of fresh cuts or from undercut natural slopes. These failures are somewhat less mobile than those in fill, perhaps due to a higher initial density, and should be classified as debris slides rather than avalanches. They usually stop when they reach the base of the cutting which helped to cause them. In an

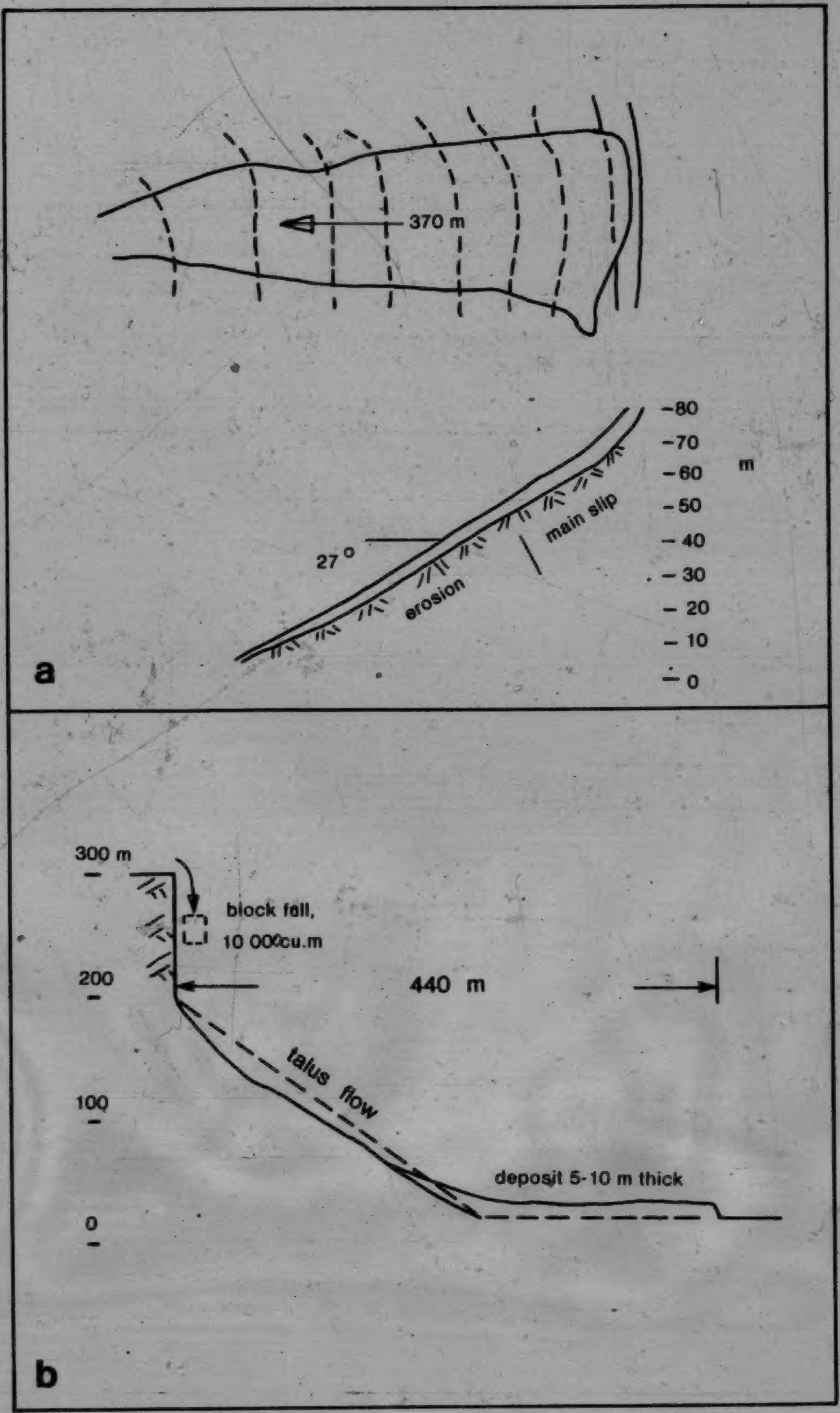
370 m
-80
-70
-60
m
-50
-40
-30
-20
-10
0
27 o
main slip
erosion
a
300 m
block fall,
10 000cu.m
200
440 m
100
talus flow
deposit 5-10 m thick
0
b

Figure 9.2 Debris avalanches. (a) Hong Kong flow of fill (Lumb, 1975) (b) Modalen flow slide (Bjerrum and Jorstad, 1968).

exceptional case, the soil from a large slip of this type impacted saturated deposits from another landslide and caused a catastrophic debris flow.

The debris avalanches in residual soil occur during or soon after periods of high precipitation. Although the material involved in flowage is often in a remoulded saturated condition, the soil beneath the slip surface at the base of the scar has been observed to be quite dry, indicating that the boundary of the movement coincided with the wetting front of water infiltration.

Debris avalanches and flows of a very similar character have been described in the Rio de Janeiro area of Brazil (Barata, 1969). In the same country, debris flows occurred on an incredibly intensive scale during a major tropical rainstorm. Costa- Nunes (1969) described this event, which resulted in the loss of 1 000 lives. He identified an initiation mechanism which involves both erosion and sliding. The intensive rains rapidly eroded gullies in the residual soil mantle. Slumping of the banks of the gullies supplied material to initiate debris flows of a conventional character, as described in the previous section. The last stage of the process, however, involved the avalanching of the forested residual soil mantle on steep slopes undermined by the sudden erosion and saturated by the rain.

Another series of destructive debris avalanches were reported by Campbell (1975) from S. California. The avalanches took place in colluvial soil derived from various sedimentary rocks. They were most common on slopes of 26 to 45 deg., but occurred sometimes on slopes as flat as 11 deg. Shallow seated sliding developed spontaneously as a result of building up of a perched water table above the bedrock. Avalanches as small as 200 cu. m moved at velocities exceeding 10 m/sec, destroyed houses and killed people. They developed lobate flow- like forms in the lower part of their paths, usually not much more than 100 m away from the source areas.

A special class of debris avalanches takes place in mining waste deposits. The most notable and tragic of these events was the flow slide of 1966 at Aberfan, N. Wales, where 144 lives were lost (Fig. 9.3). It is described by Bishop et al. (1969) and Bishop (1973) and mentioned in many other publications. The main facts appear to be as follows: A 67 m high pile of shaley waste from a coal mine had been placed on a 12 degree slope underlain by sandstone and a mantle of till. Slow moving rotational slumps existed in the toe area of the waste pile for several years. Following a rainy period, their movement accelerated during several hours, until it suddenly became rapid and assumed flow- like character. Remoulded waste material then flowed as a tongue shaped mass down the 12.5 deg. slope and reached a velocity of 5 to 10 m/sec, travelling for a distance of 500 m where it stopped among buildings.

Approximately 100 000 cu. m were removed from the scar and about 35 000 cu. m were carried to the frontal area, the

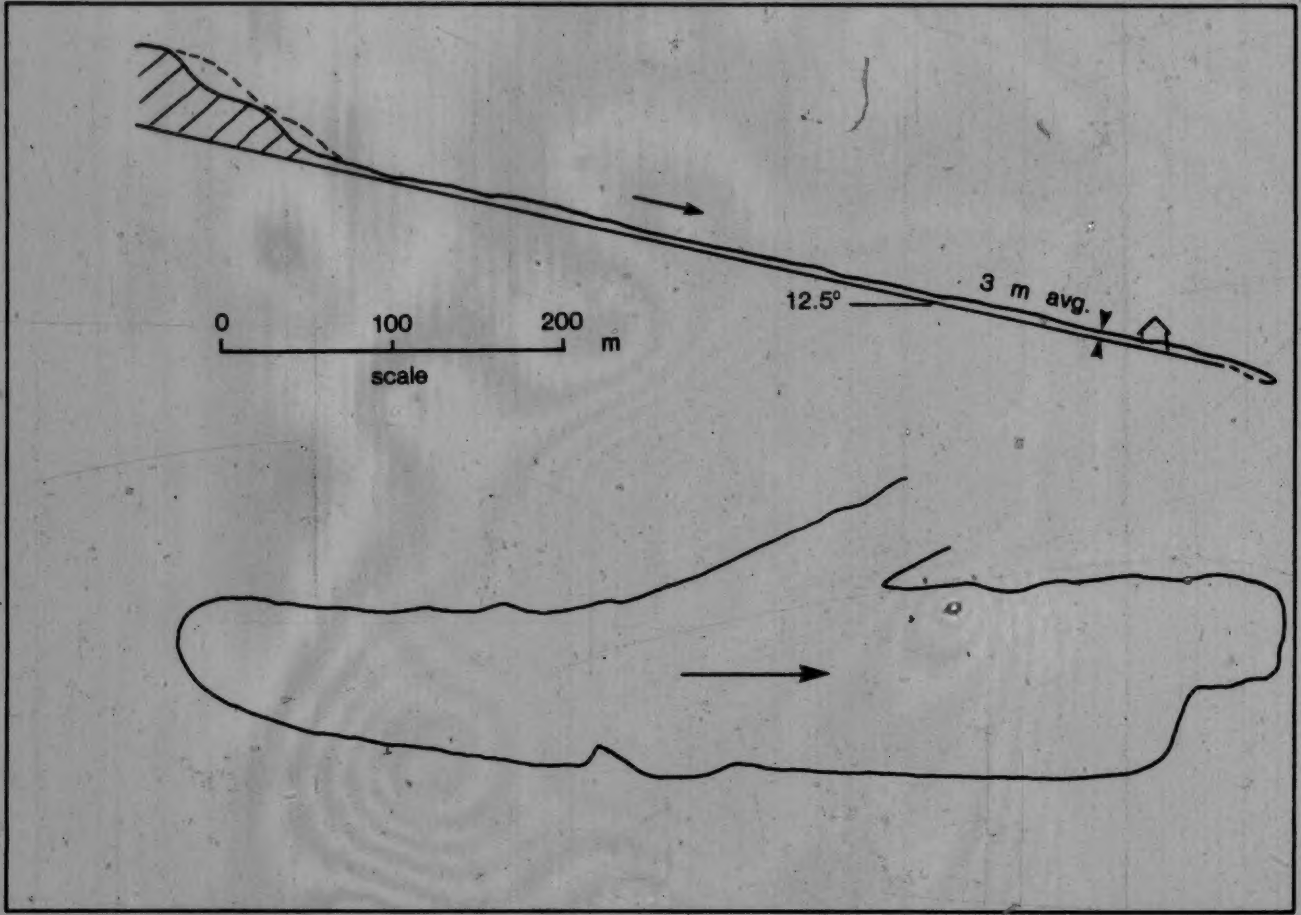
3 m avg.
12.5°
0
100
200
m
scale

Figure 9.3 Plan and section of the Aberfan flow slide of 1966 (after Bishop, 1973).

rest remaining deposited along the path of travel. Springs issued from the scar immediately after the failure, indicating artesian conditions in the foundation of the pile. The flow front was high and bulging and consisted of a relatively dry unsorted material. The tail of the flow had a higher water content.

The original waste material had less than 10 percent of fines and an internal friction angle of 39.5 deg. A thin distinct shear zone had been excavated and identified in the deposits, in which the material had degraded to a plastic state with a P. I. of 16 and a residual drained friction angle of 17.5- 18.5 deg (Bishop, 1973). This debris avalanche therefore also displayed attributes resulting from both sliding and flow.

There are several case histories in the literature of flow slides in mining waste that are difficult both to categorize and to explain. Bishop (1973) mentions a flow of a coarse limestone waste in Derbyshire. A relatively shallow slip occurred on the 40 deg. face of a 50 m high tip. About 10 000 cu. m of material flowed down the pile and slightly up a gently facing slope, was diverted at 90 deg. and continued down a 15 deg. slope to form a lobe with distinct flow- like features. The vertical angle between crest and toe of the flow was less than 15 deg., indicating a mobility greater than would be expected from a simple grain flow in coarse material. The waste did contain some amount of fines in the form of clay and "quick lime", but almost certainly was not saturated. The foundation of the tip was a well drained limestone.

Similar cases occur in Canada, as described by Campbell (1978). Failures took place on the faces of high waste dumps, developed on sloping ground in British Columbia coal mines. Some of them exhibited flow characteristics and reached a fahrboeschung of 17- 22 deg. The waste material was broken sedimentary rock, mainly siltstone, sandstone and shale. The dump foundations consist of glacial till overlying bedrock.

Campbell stresses that the waste piles are very well drained through a process of talus- like size sorting (see Chapter 2), which creates a layer of the coarsest sizes immediately above the original ground surface. The travel angle correlates roughly with the height of the waste pile. This author has examined a large failure of this type in south- eastern British Columbia. But this particular case obviously resulted from the flowage of native colluvial soils, due to sudden impact loading by waste which slid onto them over the toe of the dump. The deposit includes a large proportion of fines, and the trace of a fluid debris flow issues from its tip. Campbell (1978) suggests that some of the other flows may have occurred in a relatively dry condition. They should therefore be included in the discussion of grain flows (Chapter 7), although this would not be consistent with their great mobility. The question whether or not such phenomena exist cannot be answered at present. It should be pointed out that the supposition of good drainage of the waste dumps may be incorrect, as a result of internal migration of fines (I. Holubec, personal comm.)

The last important type of debris avalanches includes those cases where saturated debris is fluidized by the impact of a landslide or rock fall. Bjerrum and Jorstad (1968) reported a catastrophic flow of talus material in Norway, resulting from an impact by a large rock fall, that is diagrammatically described in Figure 9.2b. They state that the predominantly coarse talus "liquefied" by the impact, although it is not certain how much saturated clay matrix was contained among the coarse gravel and boulder sizes.

The Hope rock slide in B.C. released a debris flow which travelled more than three miles down the valley in a direction perpendicular to the motion of the main slide (Mathews and McTaggart, 1969). Visual evidence suggests that a part of the fine grained debris issued from underneath the sheet of rock deposited by the main slide, as if extruded under its weight. A similar flow has been mentioned by Terzaghi (1950). A tower of limestone, with a volume of 200 000 cu. m, overturned on its shale foundation and fell on saturated colluvium and weathered shale deposits, releasing a flow of approximately 7M cu. m of fluid material.

Avalanches of this kind are especially dangerous, since they are the result of phenomena distant and seemingly irrelevant to the location where the actual damage occurs. Unfortunately, they are among the least well documented case histories.

9.3 Lahars

Debris flows derived from recent volcanic materials are known as lahars. Active volcanoes create ideal conditions for generation of debris flows, by depositing granular and fine materials at rapid rates on steep slopes and by supplying powerful mechanisms for saturation of the loose masses and initiation of flows.

Five groups of lahar initiation mechanisms have been mentioned by Neall (1976). The first is the sudden draining of a crater lake either by an eruption through it or by the collapse of the crater wall. Some of the largest and most destructive events in Indonesia, New Zealand and Contral America had this type of origin. The second process leading to debris flows is the mixing of hot ash flows (nuee ardente) with surface water or water from concurrent rainstorms.

The third initiation mechanism is exactly analogous to the mechanism of conventional alpine debris flows, i.e. rapid erosion by rainstorm runoff and slumping or sliding of loose saturated volcanic material on steep upper mountain slopes (murgangs). They take place in areas of intensive rainfall and obviously do not need to coincide with an eruption. They occur more often shortly after the eruption, when the accumulation of volcanoclastics is at its maximum. A thick ash layer erupted from Irazu volcano in Costa Rica increased runoff dramatically by blocking infiltration over large areas on the slopes of the mountain. The resulting torrential streams eroded the partially cemented ash layer with such rapidity, that a catastrophic series of mud flows ensued.

Rapid melting of snow and ice during an eruption may likewise generate lahars. Cases of this type have occurred in the Americas and in Japan.

The last initiating process is steam explosion, which is accompanied by the ejection or upwelling of water or mud. Some of the postglacial lahars of the Pacific Northwest of the U.S.A. have been identified with this mechanism (Neall, 1976).

The statistics of lahars are incredible. Some have extremely large volumes, e.g. the prehistoric Osceola lahar from Mt Rainier comprised over 1 000 M cu. m (Crandell and Waldron, 1956). Others travelled as far as 240 km from their sources, attained velocities of nearly 200 km/h (55 m/sec) and took tens of thousands of lives (Neall, 1976). It is impossible to do justice to this phenomenon with regard to its variety of forms, materials, causes and scales of magnitude, except in a specialized monograph. Therefore, further discussion of it here will be limited towards pointing out some of the similarities with the conventional debris flow in the aspect of flow mechanism.

Like debris flows, lahars consist of clay- water slurry, silt, sand and coarse particles up to large boulder size. Their grading also tends to be well distributed as shown by two examples in Fig. 6.3, although it is conceivable that those derived from ash will have a large proportion of fines. They also move in the form of lobate masses, being more viscous and laminar in the frontal portion and increasingly fluid and turbulent in the distal part (Waldron, 1967). They erode on steep slopes and incorporate valley floor material (Schmincke, 1967) but spread out into thin digitate sheets in the lowland, filling depressions, overriding soil profiles and producing characteristically flat topography (Crandell, 1957 and Crandell and Waldron, 1956).

No mention has been found in the lahar literature of lateral ridges or lobes of selected coarse material, which are so characteristic of conventional debris flow deposits. This may be an indication of greater fluidity of volcanic debris, due to either greater water content or lower plasticity. Inverse grading has not been widely reported for lahar deposits. The predominant grading description is "unsorted". Some of the major lahar deposits of the Pacific Northwest are characterized by a faint normal grading, i.e. with large clasts concentrated near the base (Crandell, 1957). This would be indicative of a high water content and low bulk density. Schmincke (1967), on the other hand describes lahar sections from Washington State which exhibit a 20 cm base layer of vaguely stratified fine to coarse sand, grading upwards abruptly into several metres of unsorted coarse debris. The fines content of these lahars was less than ten percent.

One obvious distinction of lahars from ordinary debris flows is the potentially enormous size of the former. The previously cited Osceola lahar achived a thickness of over 100 m above a constriction in its channel. It flowed in a width of up to 1 km through the valleys for a distance of some 50 km and then spilled into a sheet almost 15 km in radius and up to 25 m thick. Ordinary alpine or semi- arid mudflows are several orders of magnitude smaller, with the exception of some catastrophes such as the Huascaran debris avalanche of 1970 (Chapter 10).

9.4 The Initial Conditions

Any analysis of a potential debris flow or avalanche must begin with a prediction of the initial conditions. More specifically, estimates must be made concerning the probable location of the source area, the volumes of debris likely to be released, the initial depth of debris accumulation within the flow channel, any initial velocity attained by the debris masses prior to flowage and, finally, the mechanical properties of the fluid debris material.

With regard to the first question, it is necessary to extablish which characteristics of a given site make it favourable for debris flow initiation by any of the several mechanisms listed previously. No exact quantitative criteria are available, although several authors suggested qualitative ones. They have been summarized by Rodine (1975) and by Azimi and Desvarreux (1974). The main attributes of a debris flow initiation site appear to be as follows:

Abundance of recent debris with high porosity, actively resupplied by fresh material. For spontaneous rapid flowage, it is necessary that the material should be porous enough to contract during shearing (Morgenstern, 1978) or to be brittle due to the existence of cementing (Waldron, 1967). The author feels that this requirement is necessary even in the case of initiation by flood erosion, since most accounts describe rapid bank slumping as being the most important element of debris supply in those cases.

The debris should be well graded and should contain at least a minor fraction of clay. On the basis of theoretical consideration of packing of spheres, Rodine (1975) showed that up to 95 percent of the debris could be well- graded clastic material, without significant particle interlocking taking place. The observed grain size distributions of debris flows shown in Figure 9.1 show several examples where the colloidal content was less than 2 percent, although there is nearly always at least 10 percent of fines (clay and silt). It is probable that some debris flows consist of liqufied granular material with the influence of colloids being minor. It is interesting that attempts to measure the viscosity of similarly graded mine waste tailings by Jeyapalan (1980) failed, since he was unable to prevent the material from settling.

The requirement of sufficiently steep slopes (30 to 45 deg.) in the source area has already been mentioned.

The last important aspect in debris flow generation is the availability of an abundant but irregular source of water. Bull (1974) noted that debris flows occur usually in drainage basins with sporadic or intermittent surface flows. Where there is a strong permanent water course, sufficient amounts of loose debris tend to be unable to accumulate. Similarly, sudden voluminous precipitation or melting occurring only once in several years is preferable to steady regular water supply.

The actual volume of debris which can be released and its initial depth in the flow channel can be estimated on the basis of a survey of volumes available and their stability, using conventional methods of soil mechanics and considering the probability of retrogressive failure. The question of initial velocity is relevant only in the case of short debris avalanches and can be investigated in those cases by the methods discussed in Chapter 3. Channelized debris flows with long paths are likely to develop velocity in mid- reach independent of any but unusually great initial impulses.

The mechanical properties of debris material of a given gradation are directly dependent on its water content, as illustrated for the case of a clay slurry in Figure 6.5. Such properties as strength, viscosity and unit weight can be determined by experiments. But first, it is necessary to estimate the relevant water content at which these experiments should be conducted.

Spontaneously released debris avalanches can be assumed to behave in an undrained manner, i.e. with a water content equal to the in situ water content at failure. The latter could be determined in the field, after a thorough soaking of the soil at the test site.[14]. The long, channelized debris flows, on the other hand, have mechanisms of mixing their flowing debris with surface runoff water, as described earlier. It is apparent from the discussion of Sections 7.1 and 7.3 that the water content of flowing debris is highly variable, not only in different materials and events but even in the course of a single event. For example, the tail of a typical debris flow surge represents a gradual transition from a relatively thick slurry to muddy water. No techniques exist for predictiong the water content. It can be expected to vary between 10 and 30 percent near the front of the surge, according to Table 6.1, but up to 70 percent during intersurge flow or in exceptionally liquid debris flow events.

---

[14] A large scale experiment of this kind was carried out in Japan (Engineering News- Record, 1971). A mass of loose silt fill had been soaked by sprinklers. A small debris avalanche was set off prematurely, killing 14 of the observers.

9.5 Flow Analysis

As shown in the previous sections, debris flows and avalanches comprise a variety of unsorted materials. They are characteristically well graded. The colloidal (clay) fraction varies from a trace to a substantial proportion of the flow mass. Boulders may predominate or be absent. The water content ranges from the point of saturation to the consistency of muddy water. The mode of travel varies from a rigid plug flow to turbulent flow. The constitutive models which could possibly be applied to these slope movements are therefore similarly varied. They include, for example, all of the models discussed in the previous three chapters, i.e. the Newtonian fluid of dilute slurries or dispersions, the pseudo- plastic or Bingham fluid of clays or the dilatant fluid of undrained concentrated dispersions. In addition, well graded materials might conceivably exhibit behaviour transitional to two of these models.

One unifying aspect of these flows is that they can safely be assumed to be either fully undrained or drained with a substantial delay relative to their high mobility. The slow drainage is caused by the good gradation and the presence of small sizes, which determine a low permeability. For example, Curry (1966), describing a relatively coarse-grained alpine debris flow (Fig. 9.1), noted that the material of the deposit remained plastic for several days. Weight of a person caused permanent deformation on the surface of an apparently coarse, stoney debris lobe. Water drainage out of the debris continued for 10 days, accompanied by shrinkage of the material. On the other hand, the toe of the Aberfan flow slide (Bishop, 1973) appeared relatively dry. But the sliding zone at the base of the flow must have had excess pore pressure, since the flow accelerated on a slope about 7 deg. flatter than the internal friction angle. Bishop (1973) points out particle degradation which lowers permeability locally by producing fines from soft rock fragments.

The variety of applicable flow models relating to debris flows and avalanches is reflected in the literature. At least five groups of models have been suggested by various authors. The following paragraphs discuss each in turn:

Some Russian authors suggested the use of Chezy stream flow formula for debris flow, with Manning equation expressing the resistance coefficient, as for the turbulent regime. But most references agree on the point that at least the more concentrated debris flows move in the laminar regime. The Chezy- Manning equation is probably applicable to the turbulent intersurge flow of low solids concentration. Other Soviet investigators developed empirical modifications of the Chezy formula (Goldin and Lubashevski, 1966, see also Scheidegger, 1975):

$$v = 3.15\, H^{1/6} d^{1/3}$$

Eqn. (9.1)

and

$$V = 5.15\, H^{2/3} S^{1/4}$$

Eqn. (9.2)

where v is the mean velocity, H flow depth, d the average grain diameter (all in m) and S slope. The equations are mutually incompatible, being each controlled by an entirely different and unrelated variable. The exclusion of slope from Eqn.(9.1) is unacceptable, cf. Table 9.1 Neither formula takes into an account the water content of the debris. They perhaps have some regional application, but seem hardly suitable for general use.

Several observers of debris flows (e.g. Sharp and Nobles, 1953), Curry, 1966), sought to express their mobility by calculating a Newtonian viscosity. They used the Poiseuille formula for wide uniform flow in open channels, substituting the observed values of velocity, flow depth, density and slope. The calculated values of 1 000 to 10 000 poise are several degrees of magnitude larger than the estimated viscosities of "quick" clay and sand flows mentioned in previous chapters. The laminar regime is indeed confirmed by most reports (e.g. Pierson, 1980). There is usually a striking difference between the turbulent behaviour of the liquid intersurge flow and the smooth laminar appearance of the surge itself. Frontal boulder accumulations must be the result of a vertical velocity profile.

As will be shown subsequently, the Newtonian model is inadequate for analysis of dense debris flows. Nevertheless, it provides a suitable means for rapid, single- parameter comparison of the mobility of these complex slope movements. Jeyapalan (1980) assembled a rough correlation of viscosity and water content. Viscosities were back- calculated from the few well documented field observations and measured in laboratory experiments. Although he meant the correlation to represent plastic (Bingham) viscosity, the bulk of the values in his plot are actually apparent viscosities, back-calculated by the Newtonian model. The correlation has been modified here by checking it using Eqn. (6.9) and data presented earlier, and reproduced in Fig. 9.4. It is of course very crude, failing to reflect differences in grain sizes and grading, channel roughness and crossection and the true rheology of debris. But it can be used, together with Eqn. (6.9) for an order of magnitude estimate of debris flow or avalanche velocity.

There is abundant evidence against the use of a constant Newtonian viscosity in predictions. The main point is the ability of the debris to support large clasts on the surface. This support derives only partly from the high density of the debris. Other possible factors include a limiting (Bingham) strength of the finer matrix and a substantial dispersive pressure (see Chapter 7). The existence of the latter would imply a frictional resistance. Other evidence of non- Newtonian flow, as collected by

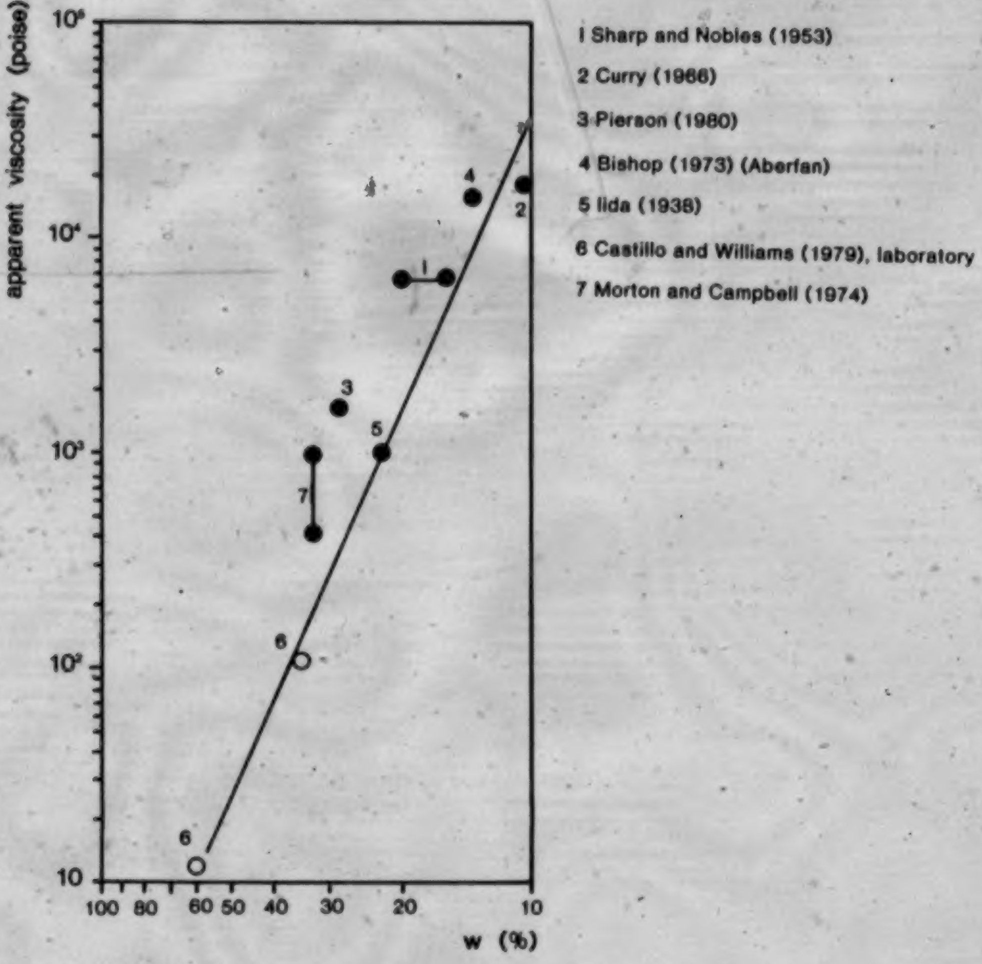

Figure 9.4 Correlation of the apparent viscosity of debris flows with water content. (Modified from Jeyapalan, 1980).

Johnson (1970) includes: steep rounded front[15], "dead" regions in the channel and the tendency to erode U- shaped channels. Johnson and several of his students (e.g. Hampton, 1972, Rodine, 1975), proposed the use of the Bingham model for analysis of debris flows:

$$\tau = \tau_o + \eta \dot{\gamma}$$

Eqn. (9.3)

is the shear stress, τ_o the Bingham yield limit, η plastic viscosity, and $\dot{\gamma}$ the velocity gradient.

A confirmation of Eqn. (9.3) derives from Johnson's experiments on the flow of slurries in laboratory flumes. These experiments, carried out with clay slurries and mixtures of clay and sand, in flumes of various crossections, showed characteristic velocity profiles with nondeforming central regions. Johnson (1970, p. 517) comments that a similarly good fit to the experimental velocity profiles could be obtained using a pseudo- plastic (power law) flow relationship:

$$\dot{\gamma} = \frac{\tau^n}{\eta}$$

Eqn. (9.4)

where η and n are constants. The two models result in surface velocity formulas for steady, uniform flow in wide channels:

$$V = \frac{1}{\eta} \left(\frac{H^2}{2} \gamma \sin\alpha - \tau_o H \right)$$

Eqn. (9.5)

---

[15] Although the roll wave theory (Chapter 6) shows that such fronts develop in laminar and turbulant Newtonian flows as well.

and

$$V = \frac{1}{\eta(n+1)} (\gamma \sin\alpha)^n H^{n+1}$$

Eqn. (9.6)

for the Bingham and pseudo- plastic relationships respectively. In these equations, H is the uniform flow depth and α the slope angle. In each case, two experimental results would be required to determine the pair of material constants. The Bingham model is widely used in slurry transport engineering (e.g. Bain and Bonnington, 1970) for calculating flow capacity of pipes.

But neither of these models can be accepted as having universal validity for the purposes of velocity predictions. Fig. 6.5 showed that even a clay slurry alone can have a flow curve consisting of a combination of pseudo- plastic and Bingham regions. The behaviour of a mixture of clay slurry and solids is likely to be more complex. The difficulty in analysis of slope movements is that parameters obtained in small scale experiments are to be applied to full scale flows. Therefore, if a flow model is assumed which is not valid over the large range of stresses represented by both the model and the prototype, a scale effect will be introduced. The flow parameters of a model may well be valid over the stress range of a single test configuration or field case. But their extrapolation to a different range will be incorrect in many cases. The problem is not of much significance in case of pipe flow design, where laboratory experiments can be carried out at a scale equal to that of the prototype.

Of course, the ideal solution would be to obtain a complete flow curve for a given material from viscosimeter measurements. But this has never yet been done for a heterogeneous mixture of fine and coarse grains such as natural slope debris. Standard viscosimeters cannot be used for such materials. Perhaps it might be possible to use a torsional vane viscosimeter in some cases, after removal of the larger clasts from the debris. Alternatively, the best results are likely to derive from pipe flow experiments. Johnson (1970) prefers semi- circular channel tests, in which the surface radial velocity distribution can be observed and for which simple axi- symmetric analysis is available. But the disadvantage of small scale open channel flow is that the range of applied shear stresses is very small and it is therefore impossible to eliminate the scale effect.

The situation in the related field of the rheology of mine tailings, as reviewed by Jeyapalan (1980) is little better. He describes two studies of saturated tailings. One, concerning fine grained phosphate tailing shows a yield strength of less than 0.1 psf (0.004 kPa) for porosities exceeding 0.5 to 0.8 and a viscosity- concentration relationship similar to that of Fig. 6.2. Both therefore concern basically Newtonian materials. Jeyapalan himself reports that his attempts at measuring the flow properties of tailings failed, as the essentially nonplastic materials tended to settle during the experiments.

Some Japanese investigators have also subscribed to the Bingham flow concept. Yano and Daido (1964) obtained flow curves for clay slurries by a viscosimeter and applid both the Bingham and pseudo- plastic analysis succesfully to laboratory flume experiments. They also formalized the open channel flow equations by deriving expressions for the mean flow velocity:

$$v = \frac{H\tau_0}{\eta}\,\frac{a^2\left(1-\frac{a}{3}\right)}{2(1-a)}$$

Eqn. (9.7)

for Bingham flow, where $a = 1-[\tau_0/(\gamma H \sin\alpha)]$ and:

$$v = \frac{\gamma H^2 \sin\alpha}{(n+2)\eta}$$

Eqn. (9.8)

for the visco- plastic flow. Then they derive resistance coefficients and modified Reynolds' numbers and present resistance charts for both laminar and smooth- turbulent flow. The charts relate to their pipe flow experiments only, unfortunately. The question of the separation between laminar and turbulent regimes in debris flow is addressed also by Enos (1977). He summarizes some amount of published data on pipe flow of Bingham materials and concludes that the transition is controlled mainly by the yield strenth, being insensitive to pipe diameter (for large pipes) and viscosity. A plot of yield strength versus velocity at the critical (transition) point indicates that the flow would be laminar at all velocities up to 10 m/sec if the yield strength was only 1 000 dynes/ sq. cm (0.1 KPa). Many other criteria exist in the literature of non- Newtonian flow. Hanks and Pratt (1967) express the critical Reynolds' number, calculated in terms of the apparent viscosity for a flow between parallel plates:

$$R_e = \frac{\gamma v H}{g \eta_a}$$

Eqn. (9.9)

where η_a is the apparent viscosity. The critical Reynolds' number depends on the value of the dimensionless Hedstrom number:

$$H_e = \frac{\tau_o \gamma H^2}{g \eta^2}$$

Eqn. (9.10)

The shear strength is taken into account both in the Hedstrom number and in the expression for the critical Re:

$$R_{e,crit} = \left(1/a' - 4/3 + 1/3\, a'^3\right) H_e$$

Eqn. (9.11)

where a' = 1- a and a is defined after Eqn. (9.7). Jeyapalan (1980) uses some estimated flow parameter values to show that by this criterion also, the typical debris flow would move in the laminar regime. This is in agreement with observations.

The Bingham model has been modified by the introduction of an apparent Coulomb friction (Morgenstern, 1967, Johnson, 1970 and others). The Bingham limit of Eqn. (9.3) is expressed as:

$$\tau_o = c + \sigma \tan \phi$$

Eqn. (9.12)

where c and ϕ are some dynamic undrained strength parameters and σ the total normal stress. The author is not aware of any experimental confirmation of the applicability of the Coulomb- viscous model. Rodine (1975) measured quasi-static total stress strength parameters of clay- sand mixtures using paired conical penetrometers. But volume changes taking place at the onset of a flow slide are likely to be undrained, under which conditions the $\phi = 0$ concept and constant τ_o should apply. When there is drainage, on the other hand, the material would be frictional as shown in Chapter 7.

A number of researchers proposed the application of the Bagnold dilatant model to debris flows. Bagnold himself suggested that it might be applicable (1968). Breitfuss and Scheidegger (1974) apply the theory of drained inertial grain flow (Eqns. 7.3 and 7.4), considering the fluid phase as being clay slurry and the solid phase as coarse material of a mean grain size of 10 cm. A special consideration needs to be given in such flows to the fact that the full weight of the dispersion, i.e. fluid and solids, generates the driving shear force, while the resisting stress arises only from the effective normal stress. Bagnold (1954) derived a condition for the maintenance of steady flow on slope :

$$\tan\phi = T/P = \frac{\rho + (\rho_g - \rho)C}{(\rho_g - \rho)C}\tan\alpha \qquad \text{Eqn. (9.13)}$$

where ϕ is the friction angle of the coarse fraction, ρ

and ρ_g are the densities of the slurry and grains respectively, and C is the concentration of the coarse sizes. Breitfuss and Scheidegger (1974) combined this with Eqns. 7.3 and 7.4 to obtain an estimate of a steady uniform flow velocity of a hypothetical debris flow. The conclusion is the same as discussed in Chapter 7: steady uniform flow is only possible at one slope angle, equal to α in Eqn. (9.13) and velocity is arbitrary, being strongly dependent on concentration. The authors find α to equal 7 deg. which is somewhat low, reflecting the use of T/P derived from Bagnold's wax beads experiments. They further use a value of ai that is too low according to Fig. 7.3, but compensate for it by using a very high λ of 53.4. Finally, the choice of representative grain size as well as of the cut off point between "fluid" and "solid" phases is exceedingly difficult for debris flows, as illustrated by Fig. 9.1.

In a summary, the use of Bagnold's model for analysis of debris flows, although interesting conceptually, appears of little practical utility. This is because the already considerable difficulties connected with the selection of parameters, as discussed in Chapter 8, are further compounded by the complex grading of these materials. These comments apply also to the work of Takahashi (1978). He develops the same concept of drained inertial flow, driven by the downslope component of the total weight of the material plus a surficial water overflow. The fluid phase is considered to be water. Again, the velocity expression is basically a combination of Eqns. 7.3, 7.4 and 9.13. Takahashi also presents a very thorough discussion of the process of bed erosion and the resulting growth of a debris flow surge. But the developments are based entirely on the assumption of drained loading of the bed by the approaching flow. Eqn. (9.13), with the density of water, then becomes an indicator of erosion potential. The flow would be erosive on slopes steeper than ϕ and depositing on flatter slopes. One should add that the angle ϕ , if used for erosion analysis, should be the peak angle of friction of the bed, not the Bagnold's dynamic friction angle. But the assumption of drained base loading by the front of the debris flow front is totaly unrealistic for any actual slope movements, except minor flows of coarse uniform material such as stream bedload surges. Takahashi's flume experiments, using uniform saturated gravel beds, are similar to such phenomena and confirm his theoretical results well. To analyse this aspect of natural debris flows or avalanches, however, one would need to use plasticity theory for undrained shearing.

In another paper, Takahashi (1980) elaborates on Bagnold's (1954) concept of the origin of inverse grading due to dispersive pressure. He calculates the difference between dispersive pressures at two levels in the flow, separated by a distance equal to the diameter of a large grain. This, reduced by the submerged weight of the grain and by a fluid drag, is a driving force which moves the large grain to the surface of the flow. A theoretical formula is derived for a two- size mixture, and compared succesfully with empirical observations form flume tests. Middleton (1970) proposed a different mechanism for the origin of inverse grading. According to this, small grains in a mixture of sizes fall into the "interstices" among large grains and displace the latter upwards. No theory is suggested. It is not clear how would such a process work in a well packed graded mixture, and especially under undrained conditions, where open interstices occur only on the scale of the smallest grains. The former theory therefore appears of greater merit.

Although the review of analytical aspects of debris flows is now already completed, the fundamental questions of how to predict the velocity or reach of such slope movements still has not been answered. The state of the art is at a stage where even the fundamental constitutive law has not yet been decided upon. The various laws that have been proposed are mutually very different. For example, the pseudo- plastic flow relationship proposed by some, is a diametrical opposite to the dilatant model favoured by others. It is, in fact, likely that all of the reviewed models are valid for certain types of debris flows and avalanches. For example, a saturated flow lacking fines would be dilatant and belong among the phenomena discussed in Chapter 8. If more coarse, it would be a frictional flow and if fine and dilute, a laminar liquefied flow. Flows with fines could be turbulent, laminar Newtonian or visco-plastic, depending on their water content. The greatest present deficiency is the lack of accepted procedures for laboratory measurement of flow properties.

Debris flows with large frontal boulder accumulations might even require an analysis combining two different models. While the fine grained mass of the main body of the flow is viscous or visco- plastic, the boulder accumulation is probably nearly ideally frictional, as it moves in the drained inertial regime. The dynamic friction angle of an accumulation of boulders is approximately 35 deg. (Carson. 1977). On slopes that are similar or steeper than this angle, the boulder accumulation would accelerate freely, keep ahead of the viscous mass and spread out along the channel as shown in Fig. 9.5a. On flatter slopes, the frictional material would decelerate and the viscous fluid would attempt to overtake the front. But this does not happen, probably because the surface of the viscous flow is charged with coarse particles for some distance behind the front and a rising of the flow level here would merely bring up some of these to build up the moving dam accordingly. The process creates the coarse levees and prevents lateral escape in the absence of a deep cut channel. Thus, the viscous debris is effectively confined behind a moving dam of boulders, as shown in Fig. 9.5b. One might also assume that the most liquid phase finds its way among the boulders in the rear of the accumulation, uplifting them partially. This situation is idealized by the diagram of Fig. 9.5c. The

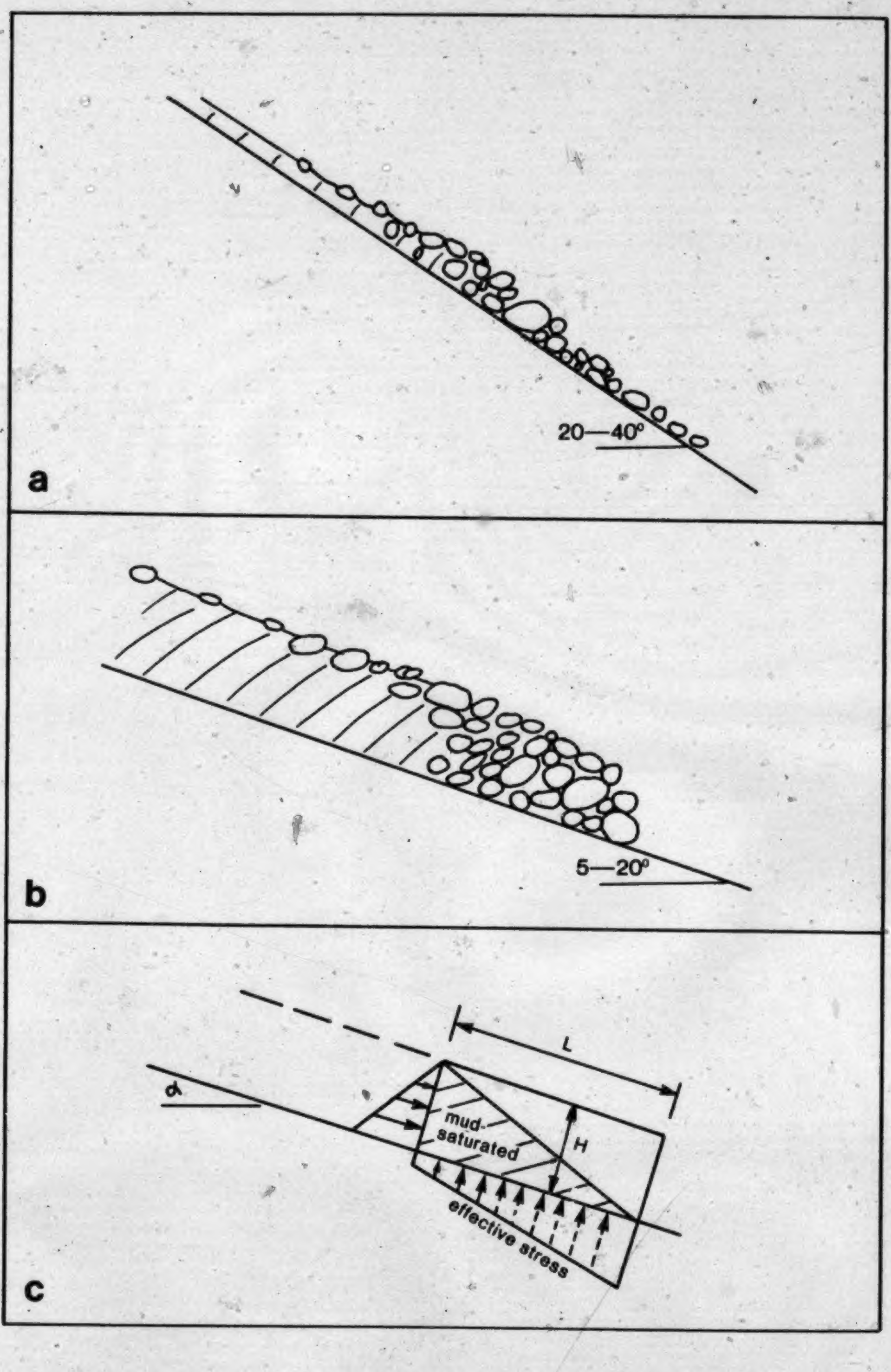
20—40°
a
5—20°
b
L
α
mud-saturated
H
effective stress
c

Figure 9.5 Frontal boulder accumulation in debris flow. (a) Steep slope, (b) flat slope, (c) schematic representation.

frontal accumulation is shown as a frictional block of a length L and thickness H. In its rear there acts a fluid pressure due to the retained debris. The normal effective pressure on its base could have a trapezoidal distribution, due to interstitial mud pressure as shown. The acceleration of such block would equal:

$$a = g(\sin\alpha - 0.6\cos\alpha\tan\phi + 0.4\,H/L) \qquad \text{Eqn. (9.14)}$$

which has been derived from an equation of motion based on the diagram of Fig. 9.5c, with the assumptions that the porosity of the boulder accumulation equals 0.4 and that its dry bulk unit weight is approximately equal to the saturated unit weight of the liquid debris. There will be some combinations of H/L and α, when the acceleration equals zero. These are plotted in Fig. 9.6a and delineate conditions of steady uniform flow. At slopes greater than about 22 deg., the accumulation would be spread out just in front of the slurry flow as in Point 1, Fig. 9.6b. At lower slopes, the elongated boulder mass would begin to decelerate, would be overtaken by the slurry and would contract in length to and beyond the normal depth of the viscous flow (Points 2 and 3). The velocity would still equal the normal velocity of the main body of the flow, but the front would be higher than the normal depth. At Point 4, the flow issues out of the confined channel and spreads out laterally. The height of the front is reduced, but the length remains the same. The front moves into the zone of

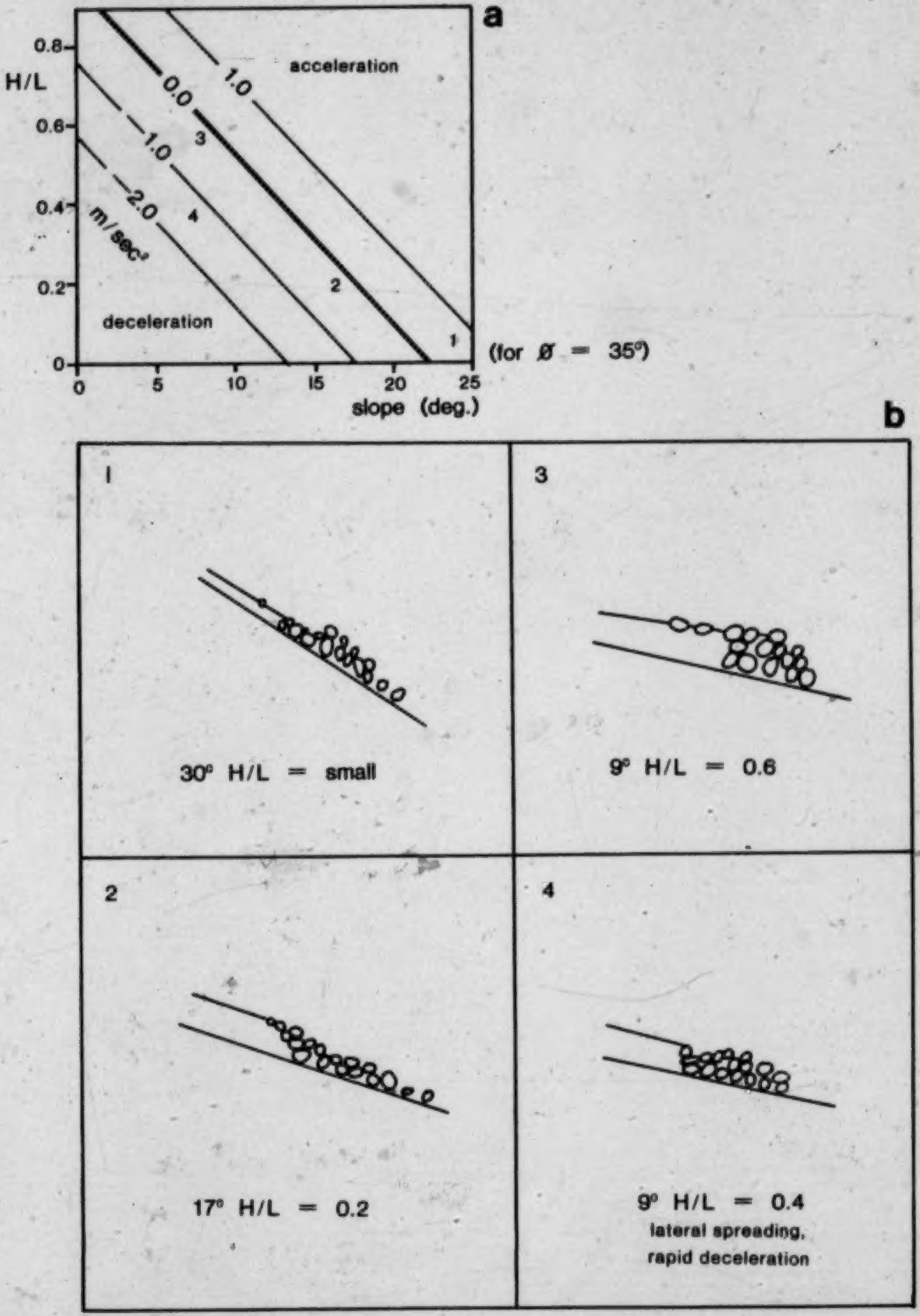

Figure 9.6 Dynamic equilibrium of a frontal boulder accumulation.

deceleration. It continues slowing down until it might be breached by the slurry, or until it freezes. This process could be followed quantitatively using Eqn. (9.14), if the volume of the boulder accumulation and the normal velocity could be known. The numerical values of acceleration shown in Fig. 9.6a are very great; for example a flow travelling at a velocity of 5 m/sec. on a slope of 10 deg. would stop within 10 seconds, if it became thinner by only 20 percent, due to lateral spreading. This would explain the sudden "freezing" of frontal accumulations on issuing from confined channels.

Debris flows are amenable to physical model analysis. Nasmith and Mercer (1979) describe the use of a physical model to design dykes for diversion of debris flows from a developed area of an alluvial fan. The flows were modelled by bentonite slurry, the consistency of which was calibrated to simulate the reach of observed events. This is an excellent practical approach but it relies on the model material having the same constitutive character at the debris. A clay slurry is a pseudo- plastic material and will model satisfactorily flows with sufficient fines content which obey the same law. It would not model undrained nonplastic debris, which is likely to be dilatant.

Analysis of debris avalanches meets with similar problems of selection of the constitutive relationship and determination of parameters. The author encountered only two attempts to predict the velocity and reach of a debris avalanche, both related to the Aberfan disaster (Fig. 9.3). Jeyapalan (1980) used his solution of the dam break problem in Bingham material. The strength and viscosity values were apparently arbitrarily chosen, with some guidance from a viscosity- water content relationship similar to Fig. 9.4. The initial analysis assumed a wide shallow channel, which would be in accord with the actual geometry, but predicted an excessive travel distance. A second analysis assuming a triangular channel yielded a better prediction.

Hutchinson and Bromhead (1981) based their solution on a combination of inviscid and frictional models, considering drainage of the flowing sheet by consolidation. They assumed the initial velocity to equal the frictionless dam break tip velocity 2.gH which, for Aberfan, gives 45 m/sec. They then took the flow sheet as being of constant (arbitrary) thickness and frictionless. Assuming a constant coefficient of consolidation and upper surface drainage, they estimated the time when the pore pressure isochrome of the layer, consolidating under its own weight, reaches the base. Then they calculated the gradual growth of effective stress and deceleration of the flow. The inviscid and frictionless model assumptions are too conservative, since even a fully fluidized material would develop viscous or turbulent resistance. Secondly, the use of consolidation theory for liquefied material is incorrect, as discussed in Chapter 8. The description of the Aberfan debris, as given by Bishop (1973) indicated that it was essentially nonplastic but relatively impervious and susceptible to liquefaction. The dilatant model would therefore be most likely applicable.

There is a possibility that the avalanche moved on a thin saturated layer. The bulk of the waste was relatively dry, as noted by Bishop (1973). The shear strains may have been concentrated in the lowermost region, where there was high saturation. Fig. 8.7 gives an indication of how strongly pore pressure due to a structural collapse depends on the initial degree of saturation. The situation is therefore envisaged as that of a rigid raft of unsaturated waste, floating on a thin liquefied layer. The variable thickness of this layer is an additional unknown to be considered in a realistic analysis of this case.

The empirical method of mobility analysis developed for snow avalanches (Section 10.4) would certainly be applicable to debris avalanches as well. Care will have to be taken to extrapolate data only between cases that are truly physically similar, with regard to the variety of possible models as described in this chapter.

10. ROCK AVALANCHES

10.1 Descriptive Introduction

Rock slides or falls of very large proportions take place occasionally in mountainous areas. Large slides may occur by slip on weak and plastic shear zones with low angles, in which case they have a character of slowly moving coherent blocks, as described in Chapter 3. At other times, large bodies of rock slide on brittle surfaces, topple or disintegrate spontaneously in a combination of sliding and toppling. High velocities are quickly reached, leading to fragmentation of the moving mass and its transformation into rapidly moving voluminous flows of granular material characterized by a well developed flow- like morphology and a large reach. Varnes (1978) called these *rock- debris flows* or *rock avalanches* . Hsu (1975) suggested the German term *sturzstroms* (rock fall streams). Again, there is a smooth transition between rock avalanches and other phenomena. Minor rock falls, although they may move with violence and disintegrate, do not generally form flows; their debris merely spreads over the surface of the talus slope, being no more mobile than a talus slip (Section 7.1). A somewhat indistinct dividing line between rock failures which do and do not form flows appears to lie near the volume of 0.5- 1 M cu.m, as is to be discussed below. Some large and very rapid rock slides, on the other hand, do not disintegrate. The leading example is Vajont, where disintegration was prevented probably by the presence of a smoothly curving, concave sliding surface.

Rock avalanches are classified as complex mass movements (Varnes, 1978), consisting of three more or less distinct stages: initial movement, disintegration and flow. Each stage will be discussed in turn.

The initial movement is most often simple sliding of large proportions. Some of these initial slides are amenable to conventional limit equilibrium analyses, for example the Frank Slide (Cruden and Krahn, 1978), or the Mayunmarca landslide (Kojan and Hutchinson, 1978). Many are dip slope slides, leaving characteristic bedding plane rupture surfaces (Fig. 10.1a). The slip surface angle normally varies between about 20 and 45 deg. The lower angle seems to represent slips along weak pelitic layers in sedimentary sequences, for example Vajont (Mueller, 1968), Gros Ventre [16] and Goldau. Higher angles apply in harder rocks, e.g. Hope, Mayunmarca and the seven landslides described by Cruden (1976) from the Canadian Rockies, whose sliding angles ranged from 26 to 48 deg.

There are cases of landslides whose source areas are limited by planar discontinuities in hard rock with very low inclinations. Eisbacher (1979), for example, describes about 50 cases of bedding slips from the MacKenzie Mountains, where the apparent "sliding plane" angle ranges as low as 13

---

[16] Where a case history is quoted without a reference, the reader should refer to the Key source listed in Table 10.1.

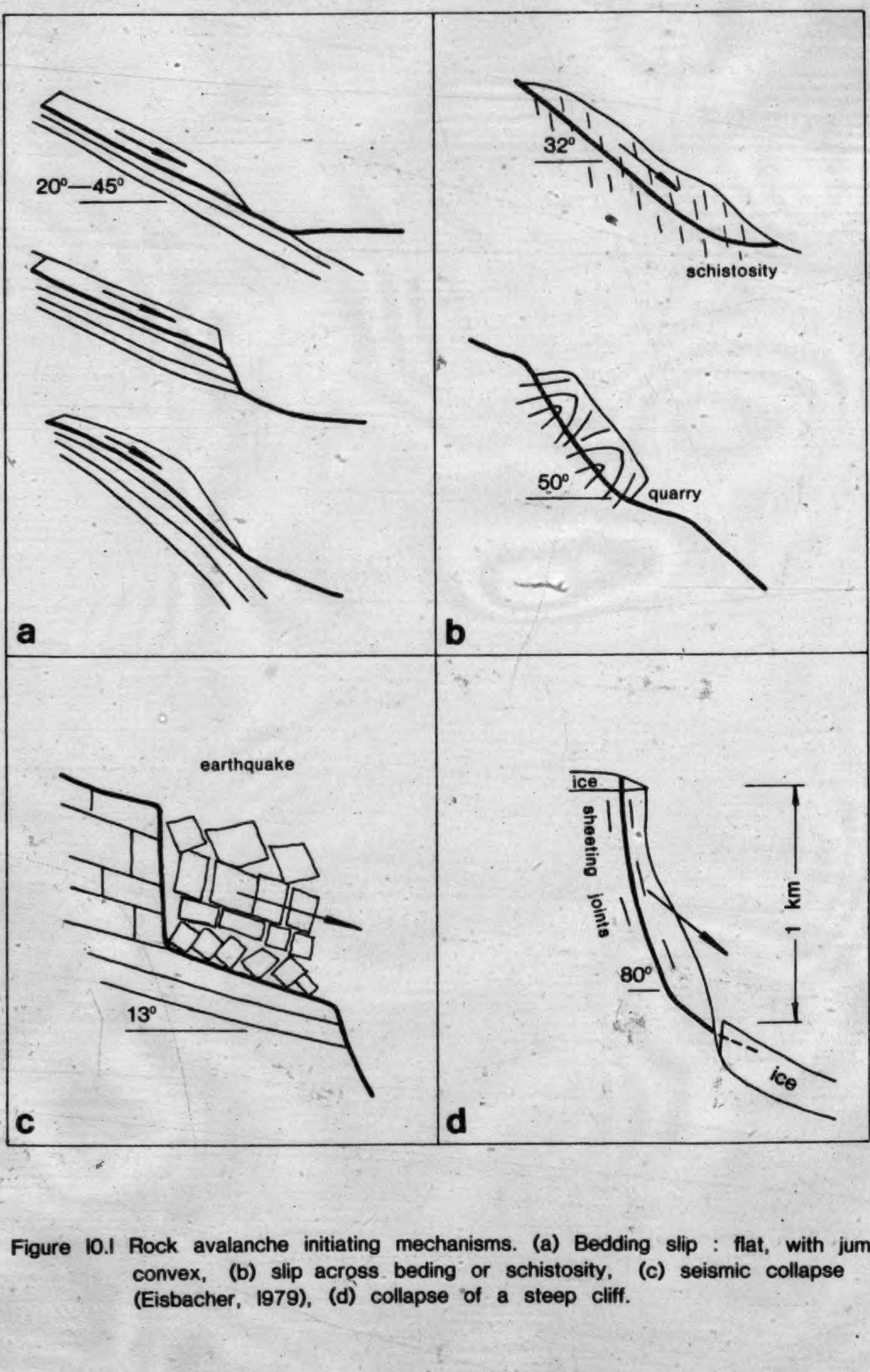
20°—45°
a
32°
schistosity
50°
quarry
b
earthquake
13°
c
ice
sheeting joints
80°
1 km
ice
d

Figure 10.1 Rock avalanche initiating mechanisms. (a) Bedding slip : flat, with jump, convex, (b) slip across beding or schistosity, (c) seismic collapse (Eisbacher, 1979), (d) collapse of a steep cliff.

deg. There is no evidence of either weak layers or exceptionally high joint water pressures, and it is therefore difficult to account for the onset of failure by an assumption of simple sliding. Eisbacher suggests an internal collapse mechanism, promoted by earthquake shaking and including elements of toppling as described in Chapter 2. (Fig. 10.1d). Solonenko (1977) ascribes a similar origin to a number of large "seismogenic" rock falls in the Pamirs, as well as to the Saidmarreh Landslide which evidently slid from a surface inclined at less than 20 deg.

Slips across bedding are less common (Fig. 10.1b). Until recently, the Frank Slide had been the prime example, but Cruden and Krahn (1978) found evidence that this also may be a bedding plane slip over a large part of the source area. The Madison case is an example of a cross schistosity slip in weak, weathered rock. The schistosity dips at about 60 deg., while the average sliding angle is approximately 32 deg. Other cross bedding slips occur on much steeper slopes, e.g. the Elm Slide where a block sheared off across flysch beds as a result of severe undercutting by a quarry operation. The range of slope angles for cross- bedding slips is about 30- 60 deg.

The fourth major type of initiation mechanism is the spontaneous collapse of a very steep, high slope under its own weight. An example is the Huascaran catastrophe sketched in Fig. 10.1e. An earthquake trigger was again provided in this case. But it probably was not the primary factor as in

Eisbacher's mechanism. Rather, the inherent instability of the uniaxially overstressed rock of the high face was the primary cause of the collapse. The Granier Landslide in France and the Rubble Creek case in British Columbia may have had similar origins.

An understanding of the initiating mechanism is important not only in the stability analysis, but also for determination of the initial velocity of the subsequent flow. In case of the sliding mechanisms, Figs. 10.1a and b, the dynamic analysis of sliding discussed in Chapter 4 can be applied until the point where disintegration occurs and granular flow begins.

Disintegration may not occur at all, if the sliding surface is smooth and concave so that moderate compression is maintained in the sliding mass, as happened at Vajont. Planar slides would probably disintegrate at the first major change of slope where excessive impact compression occurs (Hope Slide), or where the masses pass over a steep "jump" (Goldau). The initial velocity of the sturzstrom would then equal the slide velocity acquired at this point. Slides on convex surfaces (e.g. Maligne Lake, Cruden, 1976) would likely begin to disintegrate gradually at the very outset of motion, due to tensile stresses induced by the differences in slope.

Slides that move across bedding would also be expected to disintegrate early, due to failure of the weakness planes crossing the thickness of the sliding mass. This mechanism may produce a "block flow" failure (Coates, 1970), which does not include even an episode of coherent block movement but begins moving immediately in the form of a granular flow. Block toppling (Goodman and Bray, 1976) may play a dominant role in the cross- bedding failure of hard rocks, but this has not so far been sufficiently documented in cases of large scale rock avalanches.

The initiating mechanism of Fig. 10.1c is spontaneous disintegration, obviously with no significant initial velocity. That of the high cliff failure (Fig. 10.1d), on the other hand, is likely to impart very great initial velocities to a part of the rock mass, as has been observed at Huascaran. But not even rudimentary means of analysis of this process exist at present. The author offers a very simple toppling dynamics model in Chapter 2, that might serve for an order of magnitude estimate of the possible initial velocity. The model calculates the tangential (downslope) component of the velocity acquired by the topmost layers of a toppling block.after rotation, separation from the main block by centrifugal forces, and a free trajectory flight (Fig. 2.4). This velocity equals approximately 1.5- 1.6 $\sqrt{gh}$ where h is the total height of the cliff in cases of either full height or only partial (one- half) height toppling. Thus, some of the blocks resulting from the failure of the 1 km high cliff of the Huascaran could achive initial velocities of the order of 540 km/hour. Plafker and Ericsen (1978) estimate that some boulder missiles had been put into trajectory at velocities close to two times this value. Of course, this is a maximum estimate; the larger part of the rock mass is likely to benefit much less from the rotational mode of motion. Perhaps, a reasonable rule of thumb would be to estimate that the collapse of a steep cliff would accelerate fragments of the rock mass to velocities ranging from zero to the value of free fall velocity over the height of the cliff, which equals 1.4 $\sqrt{gh}$. The bulk of the mass would acquire perhaps one- quarter to one- half of this value.

The early part of the rock avalanche travel path also usually involves an air launch ("luftsprung" according to Heim, 1932). As the rapidly moving rock mass encounters a suitable ramp in the slope, it becomes momentarily airborne. Shreve (1968) suggests air launching as an essential feature of high mobility avalanches. Indeed, many observers do report significant episodes of free flight which is not surprising, considering the high velocities and rough terrain which characterize these slope movements. Notable examples include Elm, Goldau, Little Tahoma, Sherman, Blackhawk, Mayunmarca, and other landslides, in the descriptions of which air launching was specifically mentioned. In fact, the writer is not aware of a case history where the presence of a free flight episode could be conclusively disclaimed. But there are a few cases where there is no obvious evidence of it, for example Saidmarreh (Watson and Wright, 1967) or Gros Ventre (Voight, 1978). It would therefore appear premature to describe air launch or ramp as a recognizing feature of a rock avalanche, as was done for example by Mollard (1977).

After the initial acceleration and disintegration, the avalanche flows across the valley on flat slopes, even uphill, undergoing simultaneous displacement and longitudinal as well as lateral spreading. In most cases, the flow makes up the longest portion of the total travel and its dynamics is therefore most significant in determining the reach of rock avalanches. The following paragraphs summarize the main physical attributes of rock fall debris flows as inferred in the various case reports from examination of the deposits or from eyewitness observations.

Table 10.1 summarizes the key parameters of twenty one rock avalanches. The cases have been selected for being well documented, especially for having available detailed maps and crossections. They come from several parts of the world. has little regional bias.

Areal Spreading Flow of the avalanche distorts entirely the original geometry of the rock mass. Its area increases and thickness is reduced. In fourteen of the cases of Table 10.1 it was possible to estimate the area increase ratio from plans and crossections. Areas of both the source regions and the deposits parallel to the mean slope angle (i.e. not the horizontal projections) were expressed as ratios. The areas were either measured approximately, or the

Event	geology	init. mechanism*	source area incli- nation	volume of deris (10^{6}m^3)	avg. debris thickness (m)	avg. vertical drop (m)	area increase	avg. width increase	travel angle (fahrb.)	mean travel angle	main source
1. Elm	met.	cross.	50°	10	16	340	6.3x	1.5x	17.2°	19.7°	Heim (1932)
2. Goldau	sed.	bed.	20°	35	10	660	5.7x	3.5x	10.7°	12.8°	Heim (1932)
3. Flims	sed.	bed.	14°	12,000	230	1,200	5.0x	3.0x	7.4°	11.3°	Heim (1932)
4. Airolo	met.	cross.	45°	0.5	3	570	-	-		35 °	Heim (1932)
5. Granier	sed.			500	40	800	6.5x	2.4x	14 °	11.5°	Goguel & Pachoud (1972)
6. Koefels	met.										Erismann et al. (1977)
7. Diablerets	sed.	cross.	60°	50	31	1,400	6.0x	1.6x	19 °	28 °	Heim (1932)
8. Blackhawk	sed.	bed.	24°	350	25	600			7.4°	9.6°	Voight (1978)
9. Sherman	met.	bed.	40°	10	1.3	600	85 x	5.7x	11.8°	10.7°	Voight (1978)
10. Madison	met.	cross	35°	28	50	213	2.3x	2.0x	15.1	20.1	Voight (1978)
11. Gros Ventre	sed.	bed.	20°	40					9.6°		Voight (1978)
12. L. Tahoma	volc.	coll.		11					16.2°		Voight (1978)
13. Frank	sed.	bed.	40°	36	14	660	5.1x	2.1x	14 °	19.6°	this research
14. Hope	met.	bed.	30°	48	30	730	1.4x	2.0x	20.3°	22 °	Voight (1978)
15. Rubble Ck.	volc.	coll.	60°	35	12	845	9.7x	1.3x	7.5°	13 °	Patton et al. (1978)
16. Jonas Ck. N.	sed.	bed.	28°	10	5	800	6.7x	2.3x	24 °	24 °	Bruce (1978)
17. Jonas Ck. S.	sed.	bed.	30°	5	5	500	3.7x	1.4x	26.5°	27 °	Bruce (1978)
18. Saidmarreh	sed.	s. coll.	20°	20,000	100	900			4.6°		Harrison & Falcon (1938)
19. Huascaran	ign.	coll.	80°	75	5	3,200	13 x	5 x	16.7°	16 °	Voight (1978)
20. Mayunmarca	sed.	bed.	35°	1,000					11.5°		Voight (1978)
21. Barrier	volc.	coll.	80°	0.3	3	330	4.0x	1.3x	42 °	42°	Patton et al. (1978)

NOTE: Average value of reported ranges assumed. *bed = bedding slip, cross = slip across bedding, coll. = steep cliff collapse.

Table 10.1 Dimensional parameters of rock fall avalanches

original authors' estimates were accepted, where available. Only the main events were considered, not the secondary ones such as mud or debris flows. In 9 of the 14 cases, the average ratio is 5.4 with a range of 3.7- 6.7 and a Standard Deviation of only 20 percent. Two (Madison and Hope) had exceptionally low area increases. Both of these landslides fell across a confined valley and were thus limited in spreading. The remaining three had large area increases. The Sherman Landslide is certainly exceptional with its ratio of 85 : 1 and the corresponding dramatic reduction of thickness. It was deposited entirely on ice subgrade. The Huascaran avalanche also moved over glaciers in its higher reaches and had a high water content. The reasons for the large spread of the Rubble Creek event are not obvious.

Bulking factor Thickness reduction ratio could be obtained in each case as the reciprocal of the area increase ratio, divided by the "bulking" coefficient, or the factor of volume increase. Attempts have been made by the original authors to estimate the latter for several case histories. But it is not an easy task, since it combines the uncertainties of the source volume as well as deposit volume determination. For example, the Hope Slide is fully covered by both pre- and post- slide aerial photographs. Yet, detailed volume estimated by Mathews and McTaggart (1969) indicate a source volume greater than the deposit volume, which is physically impossible. There is a possibility of a vegetation correction error in the airphoto analysis (Bruce and Cruden, 1977). But it may also be due to a large scale displacement of unknown depth of alluvium and slide debris from the floor of the valley. The low area increase shown in Table 10.1 for this slide is based on the main "rockslide" deposit only. The area affected by a mud splash without a very significant elevation increase is at least as great, and a quantity of liquid fines was carried downstream in the form of a debris flow. Similar causes may account for the estimated bulking on only 7 percent at Devastation Glacier avalanche (Hardy et al, 1978). Madison had a bulking factor of 25 percent (Hadley, 1964). McConnell and Brock (1904) estimate that the Frank Slide deposit has a volume 17 percent greater than that of the source area. This author measured the loose porosity of a sample of fine Frank Slide debris as 26 percent. The actual bulking factor is therefore probably somewhat less than this value, due to the possible greater field density and the presence of boulders. The same technique yielded an estimate of 25 percent at Sherman (Marangunic, 1972).

Volumes of known rock avalanches range up to 20 000 M cu.m. Their incidence is likely to vary inversely with volume category, as noted in Chapter 2.

Thickness of the debris correlates roughly with volume, as shown in Fig. 10.2. Again, the glacier - based avalanches (Sherman and Huascaran) and those involving cross- valley movement (Madison and Hope) are different from others. The correlation suggests that volume is proportional to the

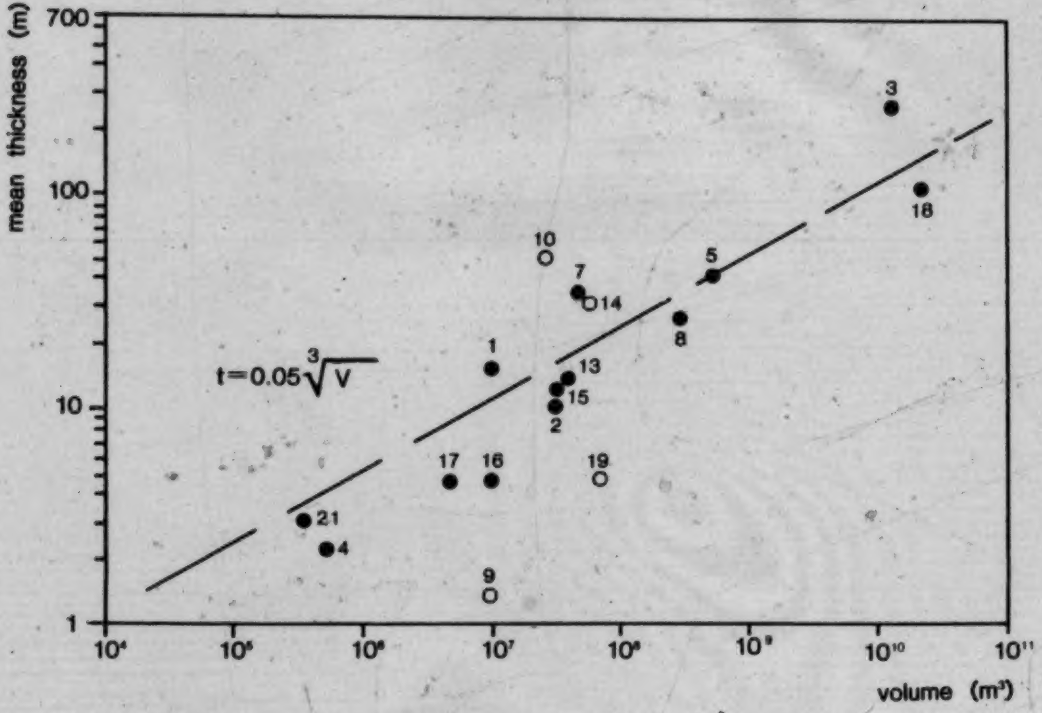

Figure 10.2 Correlation between debris volume and thickness.

third power of the thickness. Apparently, rock avalanche deposits tend to assume a preferred thickness/ avg. width ratio. From the equation of the line in Fig. 10.2, the mean thickness and area of a deposit can be estimated as:

$$h = 0.05\sqrt[3]{V}$$

Eqn. (10.1)

and

$$A = \frac{V}{h} = 20V^{2/3}$$

Eqn. (10.2)

where V is the volume of the debris.

Shapes of debris deposits are as variable as mountain topography. Three characteristic shapes can be often identified. An elongated deposit similar to an alpine debris flow (Section 9.1), but considerably larger in size, forms in narrow inclined valleys. The rock debris flows down the valley like liquid in a narrow channel, thickening upstream of constrictions, superelevating in bends and spreading into a fan- like lobe on reaching open terrain. The resulting deposit is spread in a long string along the length of the path beginning from the toe of the source area. A typical deposit of this type is at Rubble Creek. Eisbacher (1979) described several striking examples in the Mackenzie Mountains. He suggested that the deposit may in some cases be discontinuous, with parts of the channel being fully evacuated by the debris. The ratio of the mean widths of the source and the deposit, shown in Table 10.1 is generally less than 1.5 for these landslides. Some show remarkable sinuosity, e.g. the Diablerets debris stream which changed direction twice by 60 deg. (Heim, 1932).

The fan- like widely spread deposit (Fig. 10.5) is favoured by the rock avalanche, if it encounters wide flat terrain. It is a very common type of deposit, occurring where avalanches reach the base of a wide valley or a piedmont plain. The mean width of the fan is generally more than twice the width of the source area. Examples include Frank, Goldau and Blackhawk landslides.

A T- shaped short deposit with a wide lateral spread originates where the avalanche enters a narrow valley from its side wall. A high run up is usually reported on the opposite slopes, followed by a rebound of some material in reverse direction. Examples include Hope, Madison and several cases from the Mackenzie Mountains (Eisbacher, 1979).

Many rock avalanches exhibit complex geometries consisting of combinations of the three models. For example, the Mayunmarca landslide travelled down a relatively narrow side valley leaving a longitudinal deposit, then ended in a T- shaped termination on the floor of the main valley. Eisbacher (1979) described fascinating cases of avalanches changing directions and of "fingers" being catapulted from the main landslide mass by momentum transfer. These deposits have not yet been sufficiently thoroughly studied, however, to clarify the role of glacial ice transport in shaping them (Kaiser, 1980).

The *reach* of rock avalanches appears to oorrelate crudely with their volume. This was first noted by Heim (1932) p. 121, who defined several characteristic angles. The "fahrboeschung" (literally travel angle) is the inclination of a line connecting the highest point of the landslide crown with the most distant point of the toe. Scheidegger (1973) found the tangent of this angle to decrease in an inverse relationship with the volume, on a log- log scale (Fig. 10.3a).

"Schwerpunktsgefalle" is the dip of the line connecting the centers of gravity of the source block and the deposit, and could thus be termed "mean travel angle". The value of this angle was estimated for 16 landslides (Table 10.1). The center of gravity of the source block was estimated from the original authors' reconstruction of its shape, shown as a crossection or a contour plan. It was generally easy to do so in the frequent cases where the source block was approximately prismatic. Allowance was made visually for changes in thickness and/or width. The center of gravity of the deposit was estimated by balancing a paper cutout of its plan on the tip of a pin. This assumes uniform average longitudinal thickness, which in many cases appears not unrealistic as shown by crossections. Exceptions were made in the case of Elm Slide and Rubble Creek, where available crossections indicated gradual and systematic thinning of the deposits in parts of the longitudinal crossections. An allowance was made in each case by adjusting the width of

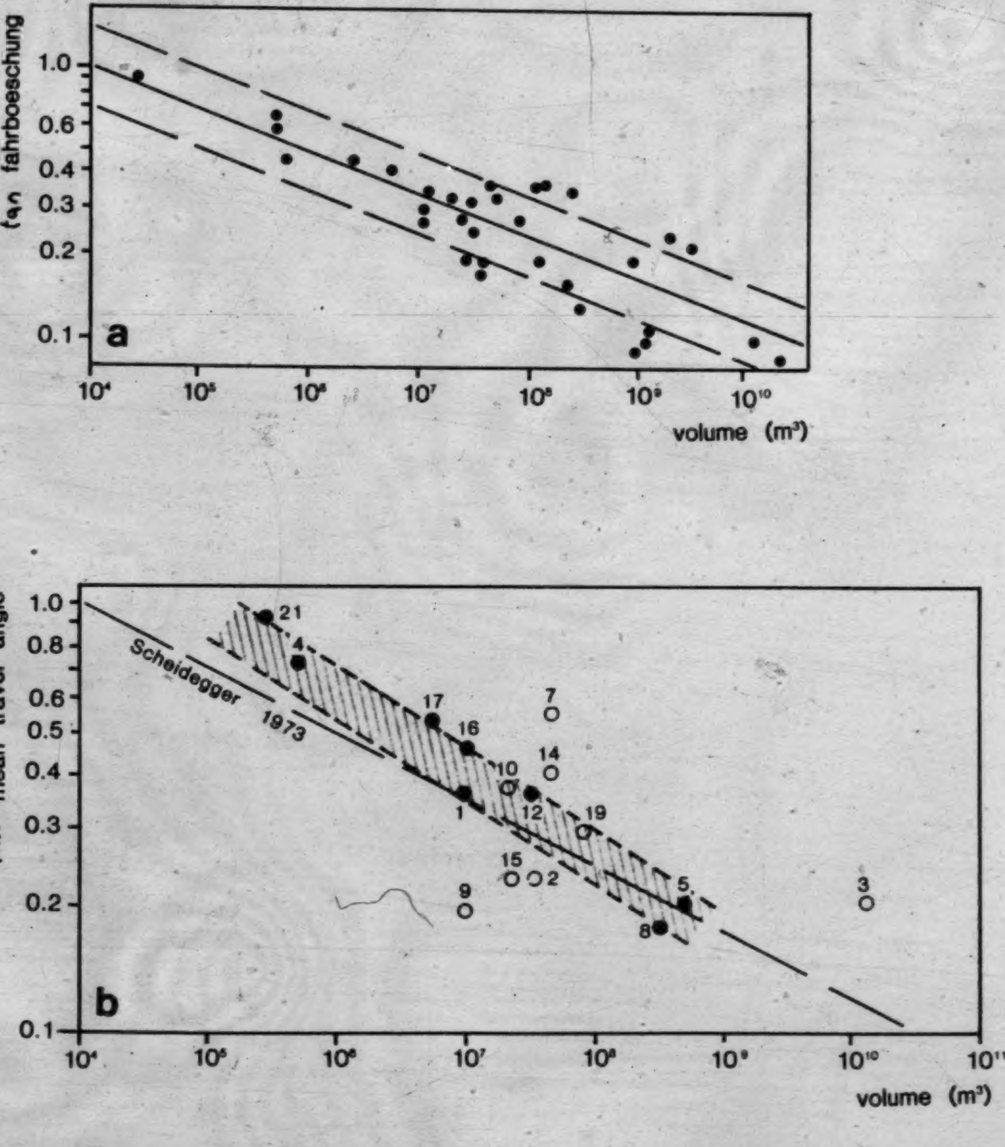

Figure 10.3 Correlations of (a) fahrboeschung (Scheidegger, 1973), and (b) mean travel angle with avalanche volume.

the cutout in proportion with the change in debris thickness. But it can be shown that, for a deposit of a uniform width, even an extreme amount of thickness variation could account at the most for an error of 3 deg. The measured angles are probably considerably more accurate.

The center of gravity of the Frank Slide was determined by a more elaborate procedure, dividing its plan into transverse strips and calculating a moment balance weighted for estimated thickness. The angles of Hope and the two Jonas Creek slides were determined by a similar detailed procedure by Bruce (1978) and Bruce and Cruden (1977). Those of the Blackhawk and Sherman events were estimated by unspecified means by McSaveney (1975).

The mean travel angle is usually not too different from the fahrboeschung, as was originally assumed by Heim. On average, for the 16 cases given in Table 10.1, the former angle is 2.2 deg. greater. But it may be as much as 9 deg. more as in the case of the Diablerets avalanche, which left much of its mass behind the sharp turns of its path and projected a narrow "finger" deposit to a considerable distance beyond. Sometimes the difference is negative, as in the case of the Granier rock fall, where the high crown of the scar stands to one side of the upper flow path [17].

Figure 10.3b shows a correlation of the tangent of the mean travel angle with volume, plotted in the same form as was done by Scheidegger. The trend of the new correlation is not much different and the scatter is even more significant. It should be noted that points which lie much outside the correlation represent landslides which appear untypical in some other major features as well. These are shown by open circles. They include cases with high water content or ice base (Sherman, Huascaran), large degree of spreading (Rubble Creek) low sliding angle of the source area (Goldau) and confined cross- valley motion (Madison, Hope, Flims, Diablerets). In view of these factors, the scatter is not surprising. But the general trend appears to be reasonably well demonstrated. For some reason, larger rock avalanches seem to be more mobile than smaller ones.

---

[17] This derives from an interpretation of the Granier avalanche geometry by Goguel and Pachoud (1972), which may not be entirely correct (D. M. Cruden, pers. comm.)

Due to their great inertia, rock avalanche debris sheets are capable of climbing onto or over sizeable topographical obstacles. This *"run up"* is often taken as evidence of velocity. Velocity estimates are made by equating the potential energy gained in the run up to the kinetic energy existing at the foot of the slope. Then:

$V=\sqrt{2g h_u}$, where hu is the vertical height of the run up. This neglects posible horizontal thrusts in the debris sheets, as well as flow resistance. Usually, only a small part of the debris manages to shoot up exceptionally steep slopes, and the amount of reach obviously depends on the topographic configuration. Nevertheless, some benefit may be derived from noting the magnitude of run up at different locations, normalized as a ratio to the total vertical drop in the center of gravity of the landslide mass (in metres):

Sherman ... 150/600 = 0.25(proximal)
Frank ... 123/660 = 0.19 (distal)
Blackhawk .... 60/600 = 0.10 (proximal)
Huascaran .. 230/3200 = 0.07 (Cerro de Aira)
Flims .. 500/1200 = 0.41 (distal)
Elm ... 120/340 = 0.35 (proximal)
Hope ... 150/730 = 0.20 (distal)
Saidmarreh .. 500/1000 = 0.50 (mid- course)

The run up potential thus appears related to volume, similarly as the travel angle.

Debris material consists, by definition, of rock in various stages of fragmentation. Heim (1932), p. 100 stresses the influence of the character of the source rock mass, height of fall and the state (smoothness) of the travel path on the resulting block size. Indeed, the gradation of the material seems to vary quite considerably among different sites. Unfortunately, little systematic analysis of the grain size distribution has been made. The grain size range is extreme, varying from rock flour to the largest boulders. An intact fragment of 36 000 cu.m has been transported by the relatively small Little Tahoma avalanche, for example. There is also some systematic sorting. Heim (1932) noted inverse grading in some deposits including Goldau, with large blocks floating on fully pulverized "molasses" underneath. A detailed analysis of a vertical column of the Frank Slide debris, as reported in the following section (Fig. 10.11) indicates an exponential increase of the median grain size from medium gravel near the base to large boulder at the surface. The analysis of a very large outcrop (Fig. 10.7) yielded an estimate that 60 percent by weight of the debris are boulders and cobbles [18] 36 gravel and 4 sand and fines.

The presence of inverse sorting often leads observers to overestimate the characteristic grain size, if they have no crossections available (e.g. McConnell and Brock, 1904). But the inverse grading does not seem to occur everywhere. It has not, for example, been found at three sites where particular attention was paid to the grain size distribution by the original investigators. Shreve (1968) did not report it from Blackhawk, where he made size- by- number[19] analysis of several debris scarps. He found a size range from powder to 25 cm with a mode of 2.5 cm. Johnson (1978) noted "an increased fines content" with depth in the Blackhawk deposit. Shreve also reports large zones of matching fragments ("three- dimensional jig saw puzzle") probably representing large boulders disintegrated in situ. These features have also been found by Shreve (1966) at Sherman. This author has found no suggestion of them in the extensive crossection of the Frank Slide.

Inverse grading was also absent at Sherman (Shreve, 1966, Marangunic, 1972, McSaveney, 1975), where the modal sizes of the deposit are reported variously as 25 to 50 cm or 5 to 10 cm, without a detailed analysis. It is not reported at Rubble Creek (Moore and Mathews, 1978, Hardy et al, 1978) and the author can confirm its absence on the basis of examination of an excellent crossection of the debris in the Cheakamus Dam borrow pit. The debris is reported to be very well graded, with a boulder content of 21 to 51 percent by weight (Hardy et al., 1978). But an examination of the borrow pit outcrop leaves an impression that the largest fraction (sizes of 1 m or more) is poorly represented in comparison with other deposits.

---

[18] Using M.I.T. classification.

[19] For a description of this and other methods of grain size analysis in outcrops see Kellerhals and Bray (1971).

Inverse grading has been specifically noted at Goldau, Saidmarreh (Watson and Wright, 1967), Frank and Madison (Hadley, 1964).

Longitudinal sorting is also sometimes mentioned. Heim (1932) states that the characteristic block size tends to increase vaguely in the down- valley direction. Shreve (1968) found no systematic change at Blackhawk. At Frank, the distal one- third of the deposit shows a relative lack of the largest boulders, as seen on an earial photograph, although the median size of the surface blocks appears approximately uniform. Perhaps, the longitudinal size changes simply reflect the original bed thickness, since the debris deposits typically preserve the stratigraphic sequence of the source block (Shreve, 1968).

The shapes of debris particles are angular with clean freshly broken faces and sharp corners. Several authors comment on the apparent lack of bruising on boulder surfaces. A number of accounts exist of moss or topsoil fragments on top of boulders having survived enormous displacements. But this clearly applies only to the surficial debris blocks. The fine material found in the interior of debris deposits has obviously been produced by a powerful grinding and crushing mechanism.

Material incorporation is a subject even more difficult to quantify than grain size. There is abundant evidence that rock debris flows are erosive. For example, the Elm Slide excavated buried water pipes. The surface of the Frank Slide debris at the foot of the proximal slope has an elevation some metres lower than the original bed of a river (McConnell and Brock, 1904). The slide also eroded a till terrace flanking the foot of the mountain. Traces of till material have been found in the base of and surrounding the debris deposit (Section 10.2). Large scale erosion and incorporation of valley glacial deposits has been reported from Huascaran. Hardy et al. (1978) estimated that approximately 6 to 9 percent of the Rubble Creek avalanche debris volume derived from material other than the original rock fall. Erosion is pervasive in the proximal regions of the deposits. Distal parts are probably not erosive as noted at Blackhawk (Shreve, 1968).

Rock debris flow deposits have several characteristic *morphologic features*. The distal parts of the deposits have lobate forms similar to lava flows (Hsu, 1978) or to the termini of boulder accumulations of debris flows (Section 9.1). On flat ground, the deposits tend to spread laterally and divide into longitudinal parallel trains (Sherman, Blackhawk, Elm, Mayunmarca) which show evidence of differential velocities. They are accompanied by a "digitate" outline of the distal margin. These features do not seem to occur in confined or channelled deposits (Hope, Madison, Rubble Creek). They are not apparent at Frank, where the "bays and promontories" of the margins occur mainly in response to the topographical lows or highs.

An extremely irregular, hummocky surface of the coarse debris is universal. Liquid saturated fines sometimes form "mud flats" in low- lying areas. Their incidence is a measure of saturated fines contents of the avalanche. At Frank they occur in an area outside the main deposit, representing up to 5 percent of the total area. At Mayunmarca they appear to have been equally rare. They often contain small cratered boils left by escaping water or air. Transverse (concentric) ridges and folds have been reported from the Hope, Madison and Sherman events and are visible in the distal part of the Frank deposit and of several of the deposits mapped by Heim(1932). They occur in areas where one would expect compression to occur, such as at concave changes of slope and near the distal margins. In fact, the distal margin itself appears usually to have the form of a raised pressure ridge called "distal rim" by Shreve and described at Elm, Blackhawk, Sherman and elsewhere. In some cases, the distal rims extend into lateral ridges bordering the edges of the deposit. They then probably witness transverse spreading motion of the debris (Heim, 1932). At Blackhawk, these lateral ridges are especially prominent and resemble somewhat the lateral levees of debris flows (Section 9.1). Elsewhere, they are but poorly defined (Sherman) or practically nonexistent (Frank).

Crevasses or transverse troughs (resembling chevron crevasses on glaciers) occur in areas apparently subjected to tension (Sherman, Mayunmarca).

Transverse lithologic bands (Hope, Madison) are found, reflecting the original stratigraphic sequence of the source. This, together with the apparent lack of comminution of the surface particles, led Shreve (1968) to describe rock debris avalanche motion as that of a flexible sheet moving on a relatively thin shear zone. There is no information which would enable one to estimate the actual thickness of this shear zone. Johnson (1978) suggests that the Blackhawk deposit lobe is underlain by a possibly continuous contorted layer of sandstone debris, derived from a rock unit originally located beneath the toe of the landslide scarp. He mentions the hypothesis that this material might have been "smeared" underneath the overlying marble debris in a highly mobile condition. The sandstone seems to have a thickness of about 1 m. Vertical contorted clastic dykes extend upward through the marble debris, which may have originated as intrusions of the fluid sandstone material.

Johnson believes that this basal layer may have been saturated. A description of the basal debris of the Frank Slide is given in the following section. It yields no precise information about the probable thickness of the shear zone, except that it probably was not a discrete plane.

Another characteristic feature of avalanche debris morphology consists of conical mounds of unsorted material (debris cones). They have been noted on the Frank deposit by McConnell and Brock (1904) and observed there by the author. They are conspicuous by being superimposed abruptly onto the general hummocky topography, usually in low spots. Their sides stand at the angle of repose. They contain debris that tends to be considerably finer than the surrounding surficial material, although it is also poorly sorted. Occasionally, large fragments are located on top or sides of the cones. Shreve (1966) described similar cones at Sherman and noted them as characteristic of these deposits. He described some that rested on top of large boulders, as if they represented fine material lifted up by large fragments rising to the surface. This is definitely not the typical mechanism of formation of these features, since if it was, one would observe numerous cones with boulders at their core in various stages of formation. But this has never been described. The usual descriptions do not mention any systematic role of large particles in cone formation. This author would describe the conical features as locations of upwelling of finer debris from the interior of the deposit. A liquefied material extruded upwards through vertical channels would leave similar features. But they do not contain marks of escape of any fluidizing agent, such as water or gas. This was noted by Griggs (1920) who described excellent examples of debris cones from the 100 M cu.m Mageik landslide in Alaska. He compared them to the sand boils observed in zones of earthquake liquefaction, but found the comparison untenable (p 342):

> ...in the mounds under discussion there is absolutely no suggestion of a radial structure or of an axial throat terminating in a crater at the apex. On the contrary, these cones are made up of materials of all sizes mixed together in the most hit or miss fashion.

The cones occur in locations where the debris sheet is relatively thin. They are not found in the regions of pressure ridges or piling up. At Frank Slide, they occur mostly near the eastern margin of the deposit, where the valley is wide and the debris sheet flat and thin.

Shreve and Griggs proposed that the cones originated from large fragments transported intact to the location and shattered there by a final impact. This may be a feasible hypothesis in case of extremely weak rocks that do not require much energy for disintegration. But it is not a realistic one in case of hard, elastic rocks such as limestone, sandstone or basalt which were involved at Frank and Mageik. A fragment of this type of rock cannot disintegrate at the place of an impact and remain there. It must necessarily be shattered or gradually ground up, either of which processes would leave its fragments spread over a wide area. Therefore, the extrusion or "upwelling" hypothesis appears more reasonable, but it implies the existence of liquefied debris in the interior of the debris sheet.

The border of the main debris lobe, as described in most accounts, forms a clean steep scarp of coarse material similar to that of the debris surface. In many cases, a thin cover of debris ranging from mud to boulders has been found projecting outside this main debris edge. It is variously referred to as "spray", "splash" or "splatter". Frank Slide contains good examples of it around most of its periphery, as described in the following section. It consists mainly of fine crushed debris with some boulders but partly of a mixture of debris and valley deposits.It represents a fraction of about 15 percent of the total area of the deposit and is on average probably less than 1 m thick. Heim (1932) describes the splash ("spritzzonen") phenomenon as a general characteristic of deposits. He mentions first of all the "solidarity" of the main debris mass resulting in its sharp, steep outline. This main mass "ploughs" through valley floor soils and talus and ends up surrounded by a ring of such debris resembling a terminal moraine of a glacier (p 100). Obviously, the amount of splash depends on the quantity and character of the valley deposits. It has been described at Madison, Mayunmarca, and especially at Huascaran and Hope. The Huascaran avalanche (Plafker and Ericksen, 1978, Browning, 1973), apparently eroded a large volume of moraine from its upper course and spread much of this into a huge splatter and mud blast zone in the middle part of its path. Furthermore, it initiated a large debris flow at its toe.

The masses of Hope Slide (Mathews and McTaggart, 1969) apparently crashed into a deposit of saturated alluvium and old landslide debris, ejecting this both forward against the steep opposite side of the valley and to both sides. The splash material flowed away from steep slopes and spilled into a thin wide and flat sheet to the east (upvalley). On the downvalley side, it channelled into an existing stream course and followed it in the form of a debris flow for several miles. Thus, the area affected by the mud splash is nearly as large as the area covered by the rock debris deposits. This is, however, not typical.

Velocities of motion of rock debris avalanches have been often estimated. A selection of published estimates is shown in Table 10.2, including mean, maximum and random spot velocities.; Perhaps the most reliable method is based on timing the events by eyewitnesses, although such data are only rarely available. The range of velocities estimated this way is 20- 80 m/sec. Another method utilizes equations

Event	velocity (m/sec)		method*	source
	average	local		
Elm	50	-	1	Heim (1932)
	30	80 (max)	3	Heim (1932)
Goldau	40-70	-	1	Heim (1932)
Frank	28	-	1	McConnell & Brock (1904)
Blackhawk	-	33	4	Shreve (1968)
Sherman	-	52	4	Shreve (1968)
	-	12	2	McSavenney (1978)
Rubble Creek	-	30-40	2	Moore (1979)
	25	60-90	3	Kaiser (1978)
Huascaran (1970)	80	-	1	Plafker & Ericsen (1978)
	50	116 (max)	3	Koerner (1976)
Huascaran (1962)	47	-	1	Koerner (1976)
	25	58 (max)	3	Koerner (1976)

* 1. eyewitness estimate of slide duration
2. superelevation in bends
3. polynomial fitting (one term by Heim, two by the others)
4. frictionless run up analysis (Eqn. 10.1)

Table 10.2 Some estimates of rock fall avalanche velocities

of hydraulics to calculate the superelevation of the fluid flow in bends. The estimate of Sherman velocity made by a variant of this method by McSaveney (1978) is probably incorrect. The calulation is based on the curvature of "flow lines" in the debris sheet. But surficial lineaments reflect only the internal distortion of the debris sheet; they need not be parallel with the velocity direction of the basal shear zone. The third method derives a velocity profile along the travel path by integrating an equation of motion, using an estimate of the resisting forces based on an empirical polynomial equation. In its simplest form, pioneered by Heim (1932) and his advisor Mueller, it assumes the resisting force to be caused by a constant friction, equal to the tangent of the fahrboeschung or of the mean travel angle. Koerner (1976) used a two term polynomial including a constant and a square velocity term (Section 10.4) This is likely to be a relatively reliable approach. The last method is based on Eqn. (10.1)(run up analysis). It has been used by many investigators, but is probably not very reliable. According to it, the largest landslides could have velocities exceeding 100 m/sec (360 km/hour).

Detailed eyewitness reports concerning the *mode of motion* are available only from Elm (Hsu, 1978), Frank (McConnell and Brock, 1904) and Huascaran (Plafker and Ericsen, 1978). The main descriptions include smooth flowing wave- like motion, a rounded bulging front, particles generally keeping together in a coherent mass but rolling rapidly as if boiling. Boulder missiles and mudblasts seem to be launched only at jump points where the debris is forced to leave the ground. On even ground, the stream is quite coherent. People at Elm stood within one m of the moving debris without being injured, except by small flying stones. Air blasts occur frequently, but only in some locations on the debris periphery. They have been observed on the right hand side of the Frank Slide but not on the left, near Youngay at Huascaran but not at Ranrahirca, and not at all to any large extent at Elm. Very strong air blasts occurred at Madison (Hadley, 1964). Dust clouds are nearly always mentioned, but not to the extent that the entire flow would be totally enveloped by them. Eyewitnesses have in all cases been able to see the surface of the moving debris. This is not the case, for example, with powder snow avalanches.

Local ground shaking, as of an earthquake origin, was felt by survivors in the vicinity of the flowing debris at Huascaran and at Frank. The Mayunmarca event is said to have generated seismic shocks recorded as far as Brasilia. The calculated energy release was 6 x 10^{19} ergs (Radbruch- Hall and Varnes, 1976). On the other hand, the Hope Slide failed to generate any measurable shock, even though there are measuring stations a relatively short distance from this location (Mathews and McTaggart, 1969).

Extraterrestrial landslides are often included in the dicussion of aspects of rock avalanches (e.g. Howard, 1973, Hsu, 1978). Features resembling large terrestrial landslides, consisting of slip scars on mountain or crater rim flanks and fan- like deposit lobes on the flat land beneath, have been observed on the Moon and on Mars. Some of these debris deposits contain volumes that are greater than those of the largest landslides on earth. Howard (1973) and Lucchita (1978) showed that Scheidegger's correlation between travel angle and volume, shown in Fig. 10.3a, remains valid for the large extraterrestrial events. This would considerably expand the data base of the correlation, both in terms of volume (up to 1 200 000 M cu.m) and in terms of environmental conditions, especially as regards the presence of water and air. But they are known only from photogrammetric records and there is little detailed information about them. Howard (1973) mentions the possibility of some of the larger lunar events being associated with some aspects of cratering processes.

Exceptionally well described is the avalanche in Taurus- Littrow Valley, site of the Appollo 17 lunar mission (Howard, 1973, Schmitt, 1973). The deposit, known as the "Light Mantle", is a fan- like sheet of a digitate outline covering an area of valley floor of 21 sq. km at the base of a 2 300 m high massif. It has a volume of 200 M cu.m, average thickness of 10 m, and a maximum thickness at the proximal end of 20 m. Complete vertical sections have been examined on site in minor craters by the Appollo 17 crew. The material consists of fine debris corresponding with the regolith mantle of the source massif, but conspicuously lacking fragments greater than several cm in diameter. There is an indication of vertical sorting, with larger fragments concentrated at greater depth as in a fluidized deposit. The surface of the debris mantles larger features of the valley floor in a uniform thickness. There is no indication on the massif slope of a scar or a rock ledge from which the avalanche originated.

10.2 Frank Slide, Alberta, Field Observations

It appeared from the survey of literature that quantitative information is lacking on the actual character and variation of debris material. The field work carried out in the course of this research was therefore focused towards answering this question. Most of it took place at Frank Slide, Alberta, although Hope, Rubble Creek and several minor sites in the Canadian Rockies were also visited.

If there is a "type description" of a rock avalanche, containing most of the more general attributes listed in the previous section, the Frank Slide of 1903 (Fig. 10.4a and Figs. 10.5 and 10.6) must resemble it closely. It is of a moderately large size (Table 10.1). Its overall geometry is relatively uncomplicated, the deposit being of a spread out fan- like shape. Its degree of spreading and travel angles (Figs. 10.2 and 10.3) are close to the average trends. It originates from a strong, relatively undisturbed limestone

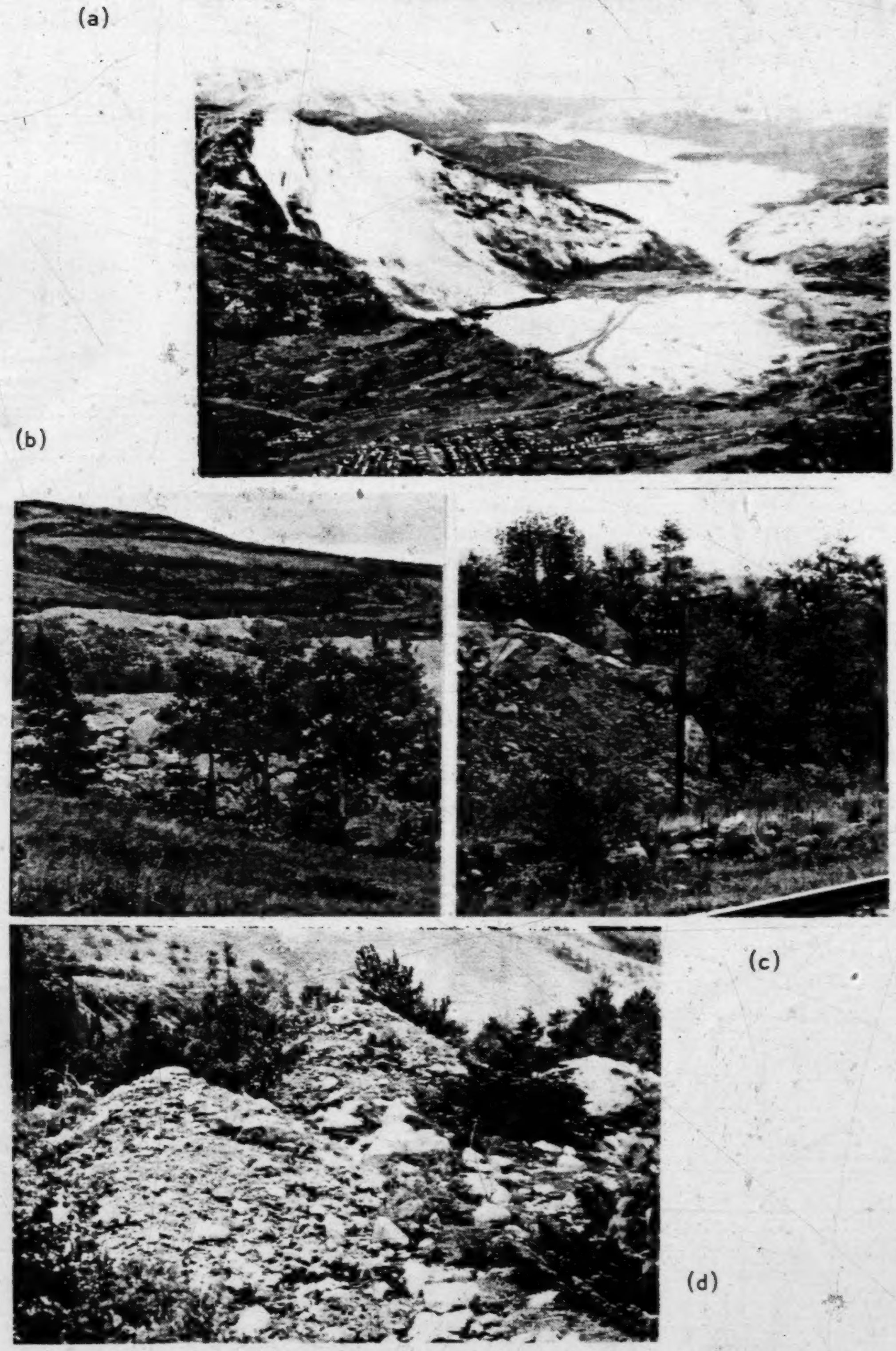

Figure 10.4 Frank Slide, Alberta. (a) Overview, (b) clean edge, (c) edge with "splash", (d) debris cones.

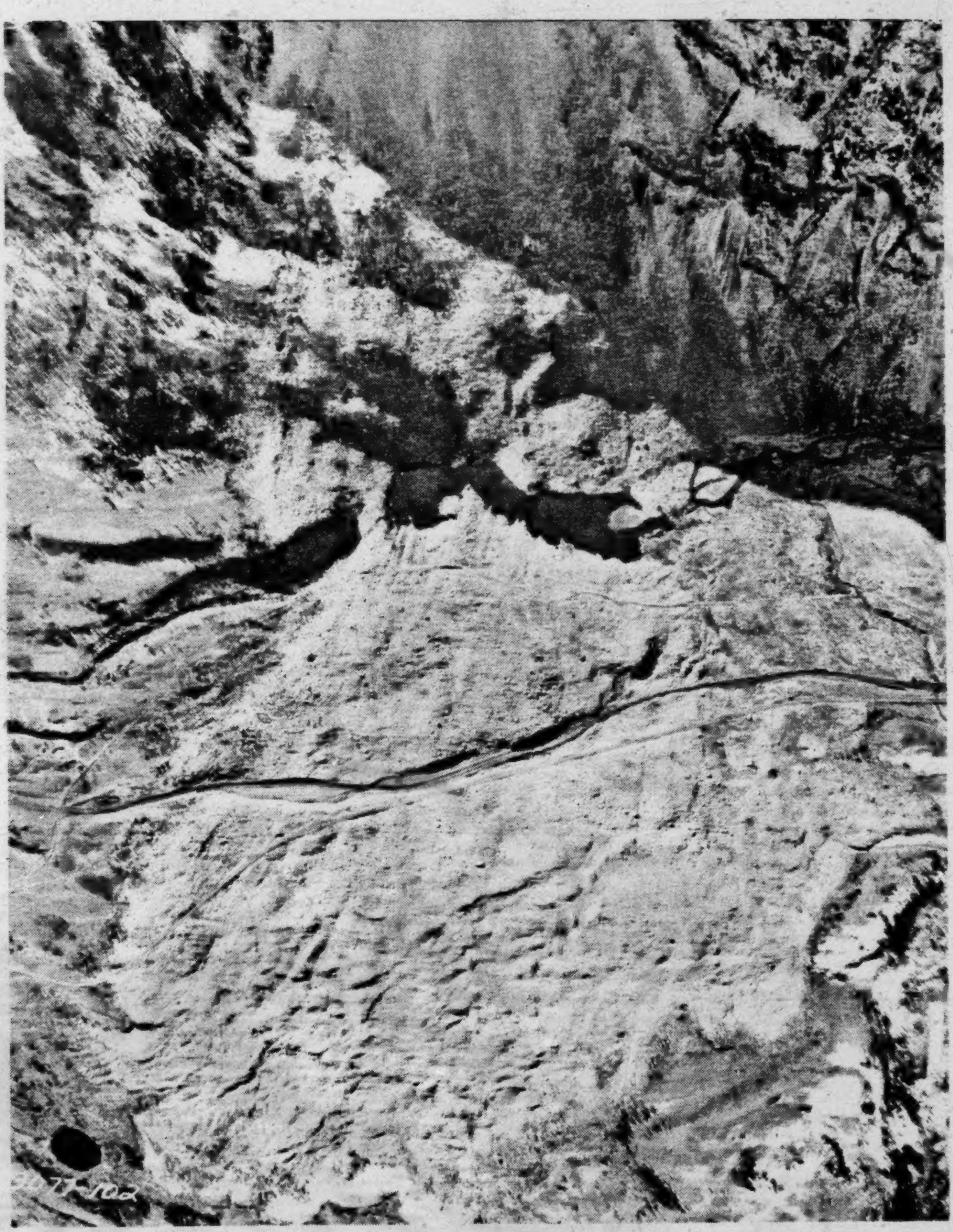

Figure 10.5 Frank Slide debris deposit.
(Gov't of Canada Airphoto A13077-102)

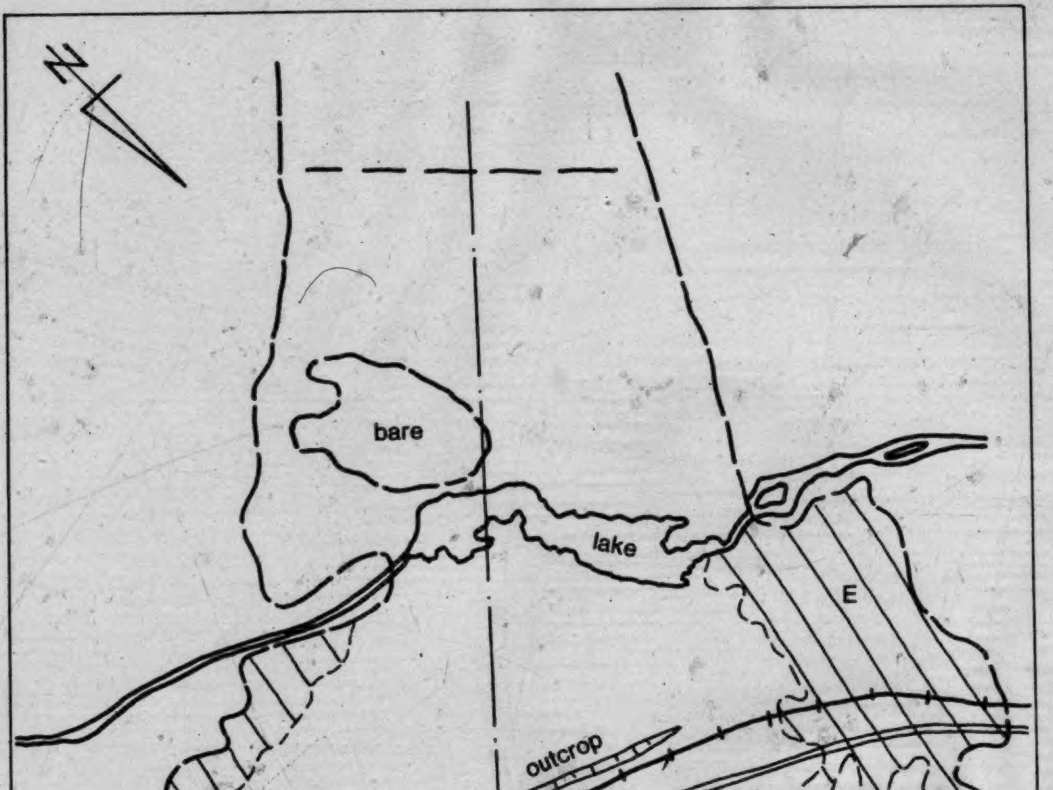
bare
lake
E
outcrop
CPR
B
highway
COARSER
FINER
D
A
C
SECTION LINE
A
A
A
C
0
500 (m)
splash areas

Figure 10.5a Plan of the Frank Slide deposit. Overlay for Fig. 10.5.

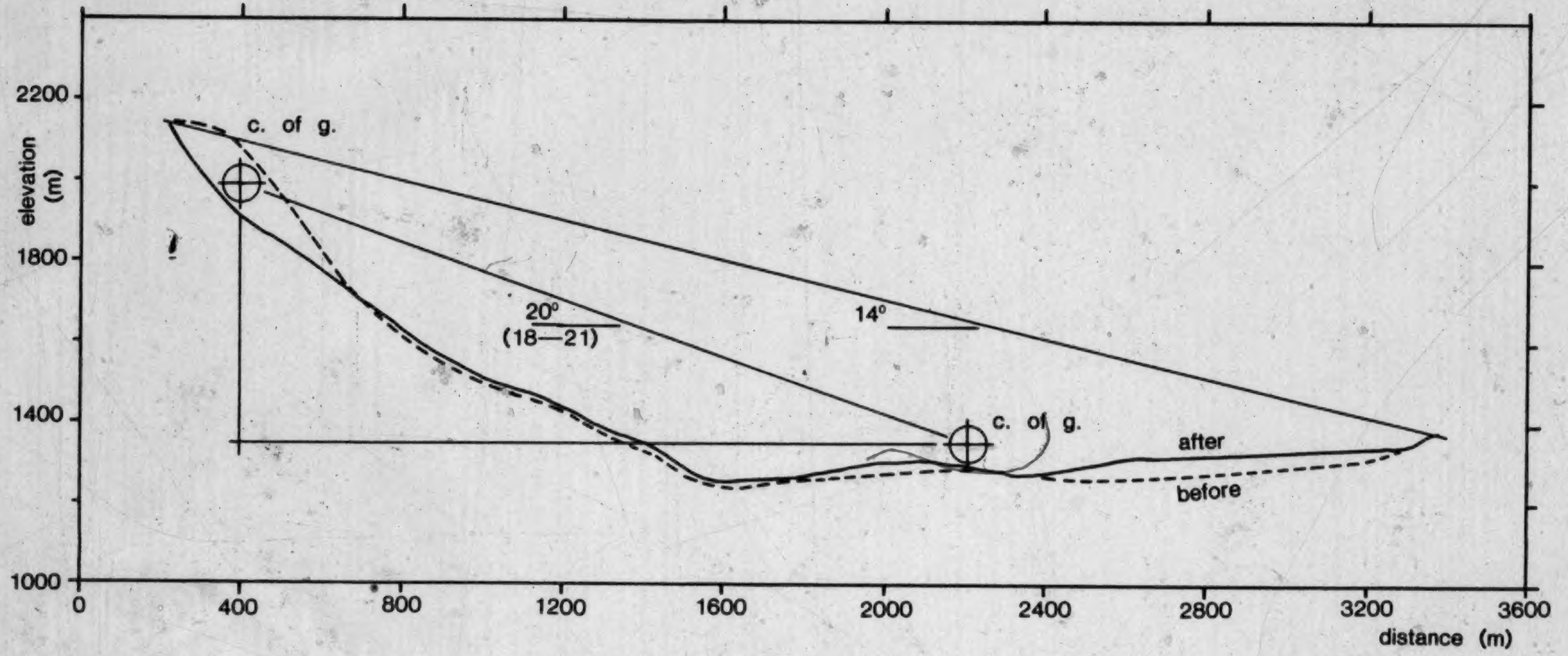

Figure 10.6 Profile of the Frank Slide. (From contours by Daly et al., 1912).

and shale rock mass. As elsewhere, moderate quantities of valley sediments participated in the motion.

The only detailed description of the debris deposit is that of the original report by McConnell and Brock (1904). Later investigations, including those by the Daly Comission (1912), by Krahn (1974) and Cruden and Krahn (1978) focused on the stability aspects of the catastrophe rather than its mode of motion. The Daly Comission produced a detailed map of the event on which the profile (Fig. 10.5) is based.

McConnell and Brock's description of the deposit refers to most of the general features listed earlier, including hummocky surface covered by large boulders, pressure ridges, depressions, steep terminal and lateral scarps (although no ridges), debris cones and "splash". Debris trains and lithologic bands were not noted, probably due to the lithologic uniformity of the source rocks. Some additonal facts were obtained during the present field investigation:

The main surficial features of the debris are unoriented hummocks with a relief of 2- 10 m. Near the foot of adverse slopes, these become gradually elongated in the transverse direction, until they can be described as ridges (A in Fig. 10.5). The crests of the ridges usually have the coarsest sizes. Zones of fine (gravel) material are sometimes found on their upstream flanks. Finer material can otherwise only be seen in low spots and in the debris cones. Elsewhere, the surface of the deposit is covered with boulders of a modal size of about 1- 3 m.

The debris cones occur in areas of lower relief, and not far from the edges (Fig. 10.4d). Particularly numerous examples were observed in the vicinity of B. They contain relatively fine, although unsorted material, which appears to have been extruded from the interior of the debris. The cones are generally about 2 m high and vary from some 30 cm to 5 m.

The edges of the landslide fall into two categories. A clean, sharply defined edge of boulders occurs only locally in three of the highest spots of the deposit, at the crest of steep slopes which the debris had run up (C in Fig. 10.5 and Fig. 10.4b). Wherever the relief is flatter, the deposit has two edges. Walking out from the center of the sheet one first comes to the border of the coarse debris, appearing as an irregular, sometimes digitate scarp some 2 to 8 m high. (Fig. 13.4c shows this boundary in crossection). At the foot of the scarp begins a low area characterized by small but very frequent hummocks (about 1 m high), scattered boulders and dense vegetation of brush and trees, indicating a substantial proportion of fines. This is the "splash" area, which may be a few m and up to a 100 m wide. Its outer scarp is again steep and irregular, but very low, suggesting a thickness of the splash sheet of not much over 1 m. The general impression from this geometrical configuration is that the splash was extruded from underneath the main debris layer and/or pushed ahead, and that its greater fluidity enabled it to spread out thinner and wider than the coarse debris.

At the distal margins, beneath adverse slopes, the splash areas contain a greater frequency of boulders and the boundary between it and the main debris deposit is less distinct. There is an indication that some of these splash areas formed when the coarse surficial layers slid back from the slopes which thay had climbed, spread out at their foot and left behind a veneer of basal fines. Such a fall back process had actually been observed by eyewitnesses[20]. An area where it almost certainly must have taken place was found at letter D. The character of the splash is again different at the former location of the Frank townsite (letter E), where a width of almost 300 m had been covered by a relatively flat deposit of mud with occassional boulders. The fine fluid material was both more abundant and fluid here than elsewhere. The mud blast apparently caused much of the damage suffered by the town and had been well described by the eyewitnesses.

The splash area, as outlined in Fig. 10.5 amounts to approximately 0.4 M sq.m or 15 percent of the area of the main deposit. Of this, perhaps one- third is the apparently extruded material of the eastern margin, one third the coarser "fall back" residue of the distal edge and another third the mud splash of the townsite location

The reconstruction of the CPR rail line formed a deep crossection through the full width of the slide deposit, providing a unique opportunity for a study of the internal composition of the debris sheet (Fig. 10.7). Dimensions of the central part of the excavated scarp [21] are shown in the upper half of Fig. 10.7 and a crossection appears in Fig. 10.8. The present track bed is near the original level, and it is assumed that the base of the debris is less than 2 m beneath the toe of the scarp. This would make the average debris thickness at this location equal about 18 m, or 4 m more than the estimated average for the slide. Even a cursory examination of the photograph reveals distinct vertical sorting of the debris. Close- up photographs (Fig. 10.9) indicate it even more clearly. The four shots are located on a vertical line near the highest point of the scarp, as shown by the squares in Fig. 10.7. The dimensions of the reference frame are 4 m x 4 m. Location (sample) 5 is about 2 m above the base of the cut, in a material consisting predominantly of sand and gravel sizes and practically devoid of boulders. This was called "base" material. Immediately above it, (Sample 6) the material becomes gradually coarser, with boulder sizes more frequent. This transition is refered to as "middle material". The "coarse" material higher up (Sample 7) is dominated by boulder sizes. Fines are filling the interstices among the boulders. Only at the very top of the scarp occurs the accumulation of large boulders which characterizes the

---

[20] McConnell and Brock (1904), p.6.

---

[21] Surveyed approximately by triangulation using a pocket transit and pacing.

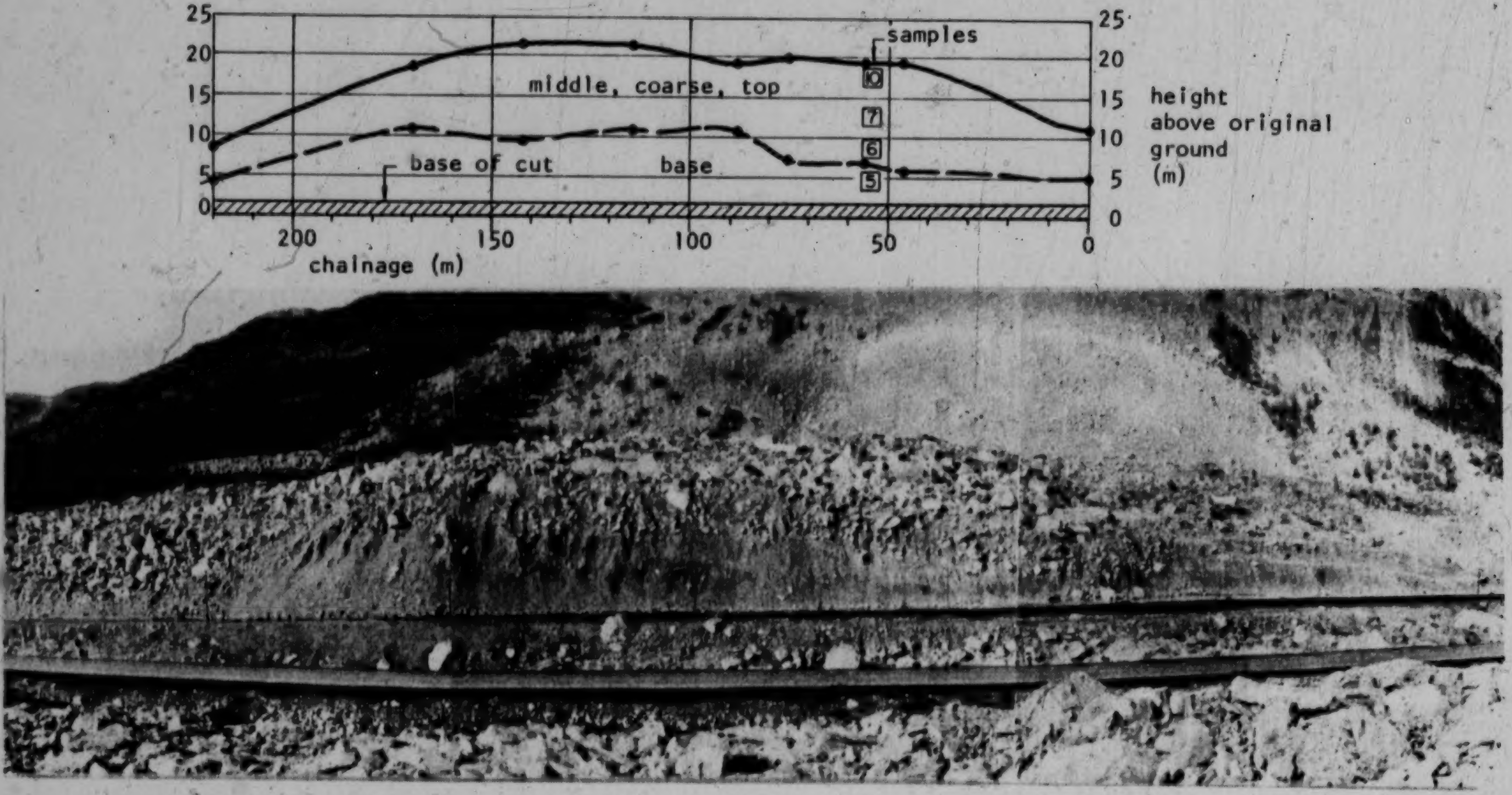

Figure 10.7 The central portion of the CPR railroad cut through the Frank Slide debris. The elevation of the base of the deposit is estimated.

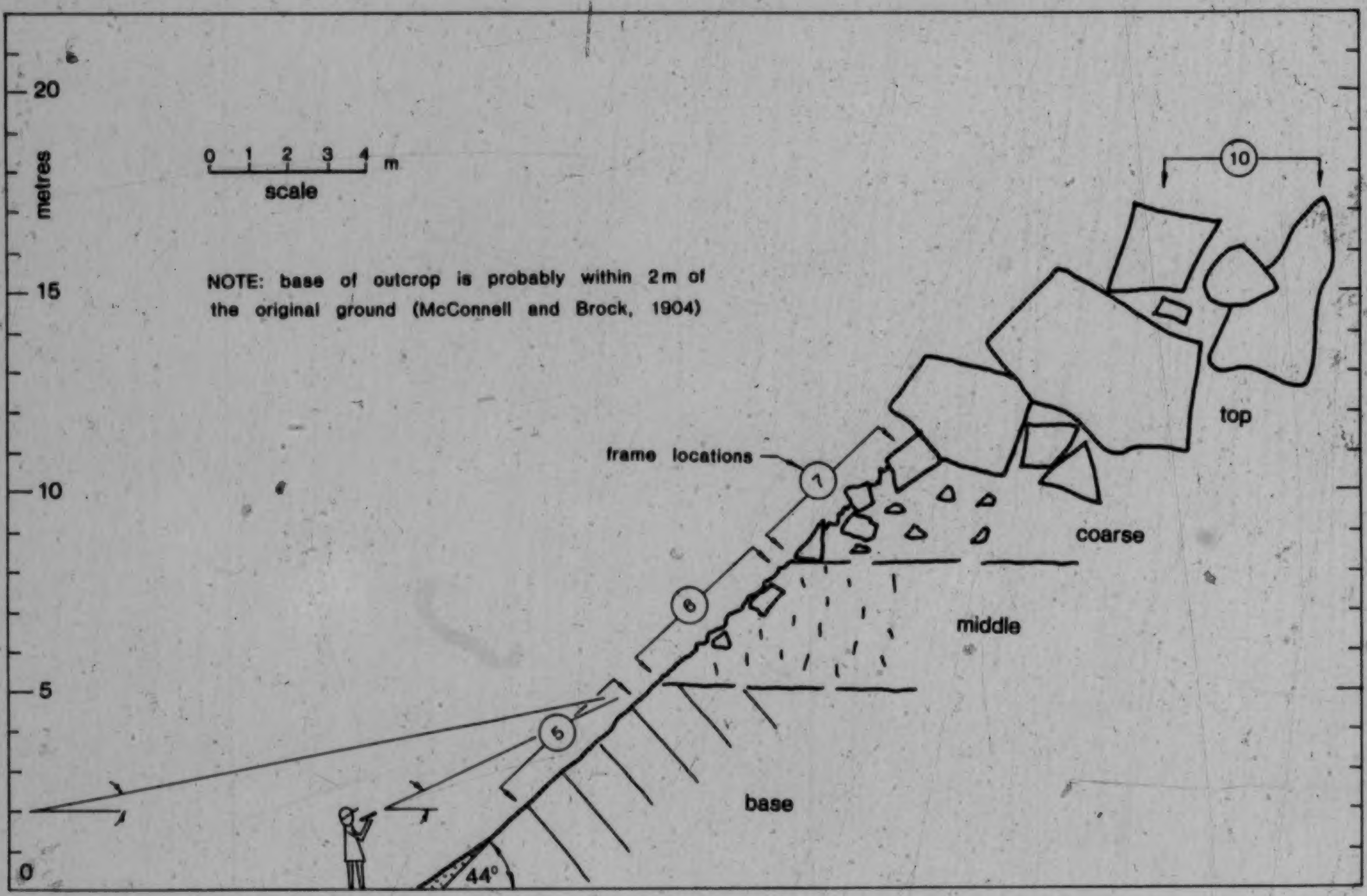
20
metres
15
10
5
0
0 1 2 3 4 m
scale
frame locations
5
6
7
10
top
coarse
middle
base
44°

NOTE: base of outcrop is probably within 2 m of the original ground (McConnell and Brock, 1904)

Figure 10.8 Crossection of the examined outcrop, showing vertical sorting.

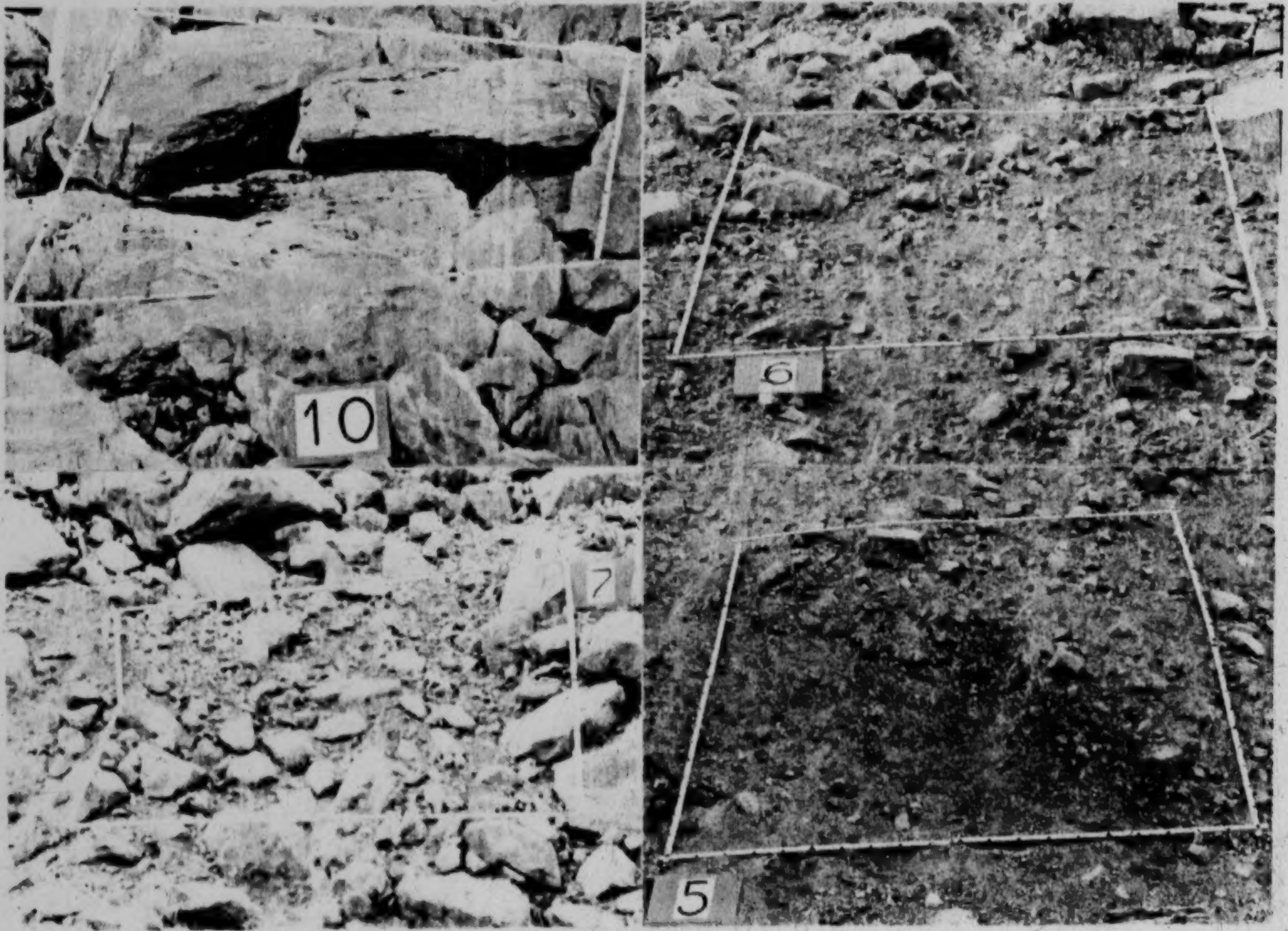

Figure 10.9 Vertical sorting of the Frank Slide deposit. Frame dimensions 4 x 4 m.

landslide surface. Sample location 10 is the horizontal upper surface of the debris, rather than the scarp, since the upper edge of the scarp was difficult to access.

At each location, a bag sample of about 3- 5 kg of the fine material (less than 5 cm), was taken. A grain size analysis was conducted for each location, combining laboratory sieve method and a frequency- by- area optical technique as described in Appendix A. The combined grain size curves appear in Fig. 10.10. All four samples are evenly graded, except for "tails" of fine material; the main difference among them is an overall shift of the curves. The base material indeed has only a little over 10 percent of boulders , the middle has 30, coarse 50 and top 100. The presence of boulders in the three coarser materials enables them to be separated from the base on the large outcrop photograph. The dividing line is sketched in Fig. 10.7. Calculating the relative proportions above and below the dividing line and using the curves of Fig. 10.10, one can estimate the mean fractions of boulders, gravel and fines (sand and rock flour) as 60, 36 and 4 percent respectively. The remarkably smooth increase of three characteristic grain sizes with height above the base of the cut is plotted in Fig. 10.11.

The bulk of the material, from fines to boulders, consists of the characteristically angular fresh crushed limestone. Traces of other materials have been found near the base of the outcrop, including rounded pebbles from till or alluvium and black organic sand. But it must be stressed that these materials exist only in trace quantities in the center of the landslide. It takes a relatively long search before a few rounded pebbles can be found in the outcrop. Thus, incorporated material appears to be unimportant to the mechanics of motion of the landslide centre.

The situation seems different near the edges of the slide. A major part of the "splash" material near the western margin (where the mud blast occurred) consists of rounded particles and must have been derived from the glacial and alluvial valley deposits. Rounded pebbles are also found in the splash material along the eastern margin, but only in a minor proportion in relation to the predominant crushed limestone. An inclined clastic dyke of dark till or alluvium could be observed in a new road cut near the eastern margin, resembling an overthrust of two blocks of relatively fine debris. Similar imbricated structures have been observed by Shreve (1968) at Blackhawk. The distal splash deposits apparently consist exclusively of crushed landslide rock, although no outcrops or sections exist to prove this. Sieve grain size analyses of the fine (gravel and sand) fractions revealed no systematic difference between splash, clean base material or base material with till traces. All show the same even grading indicated on Fig. 10.8.

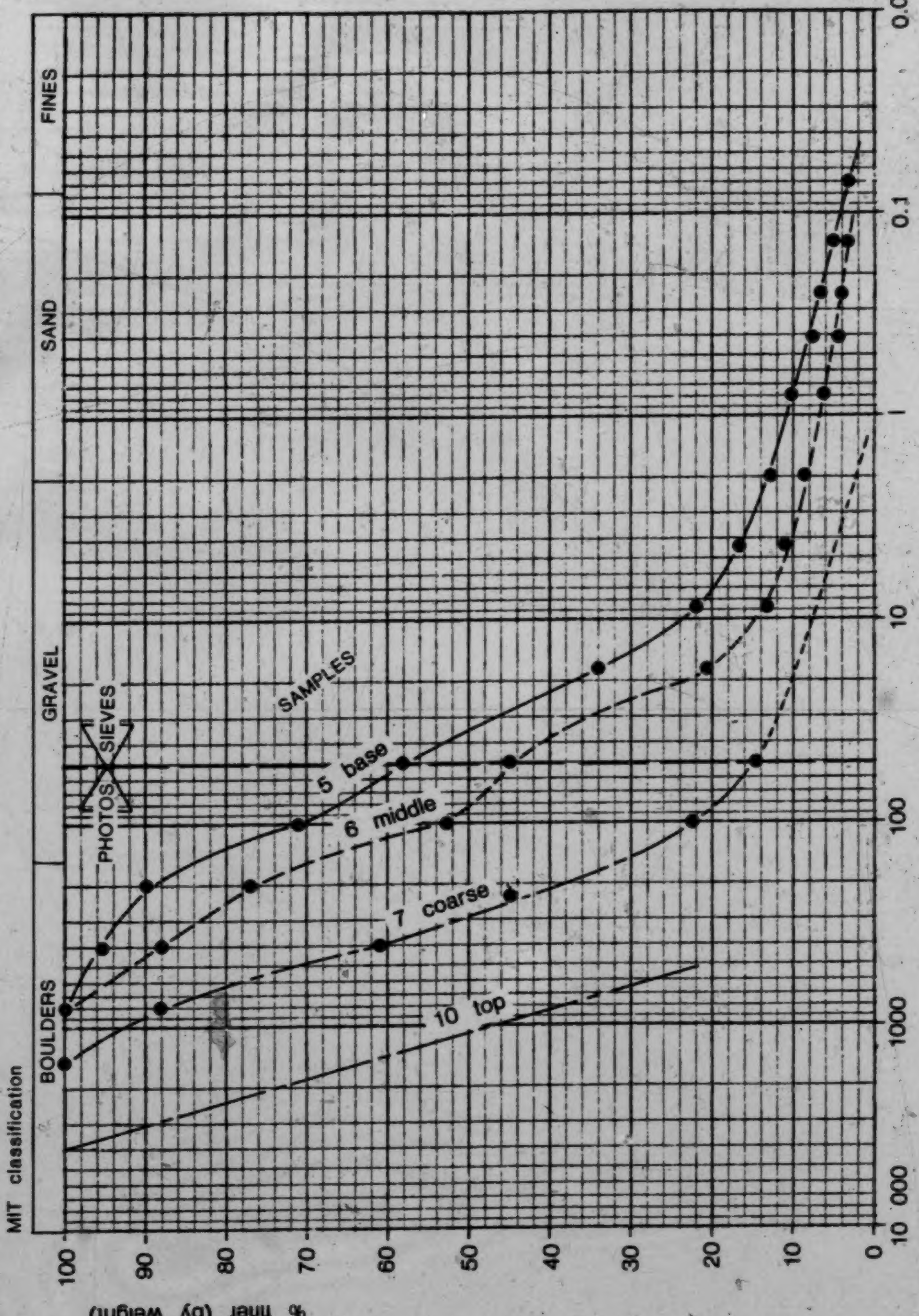

Figure 10.10 Grain size curves in a vertical crossection of the debris. Sample numbers correspond to those in Figs. 10.8 and 10.9.

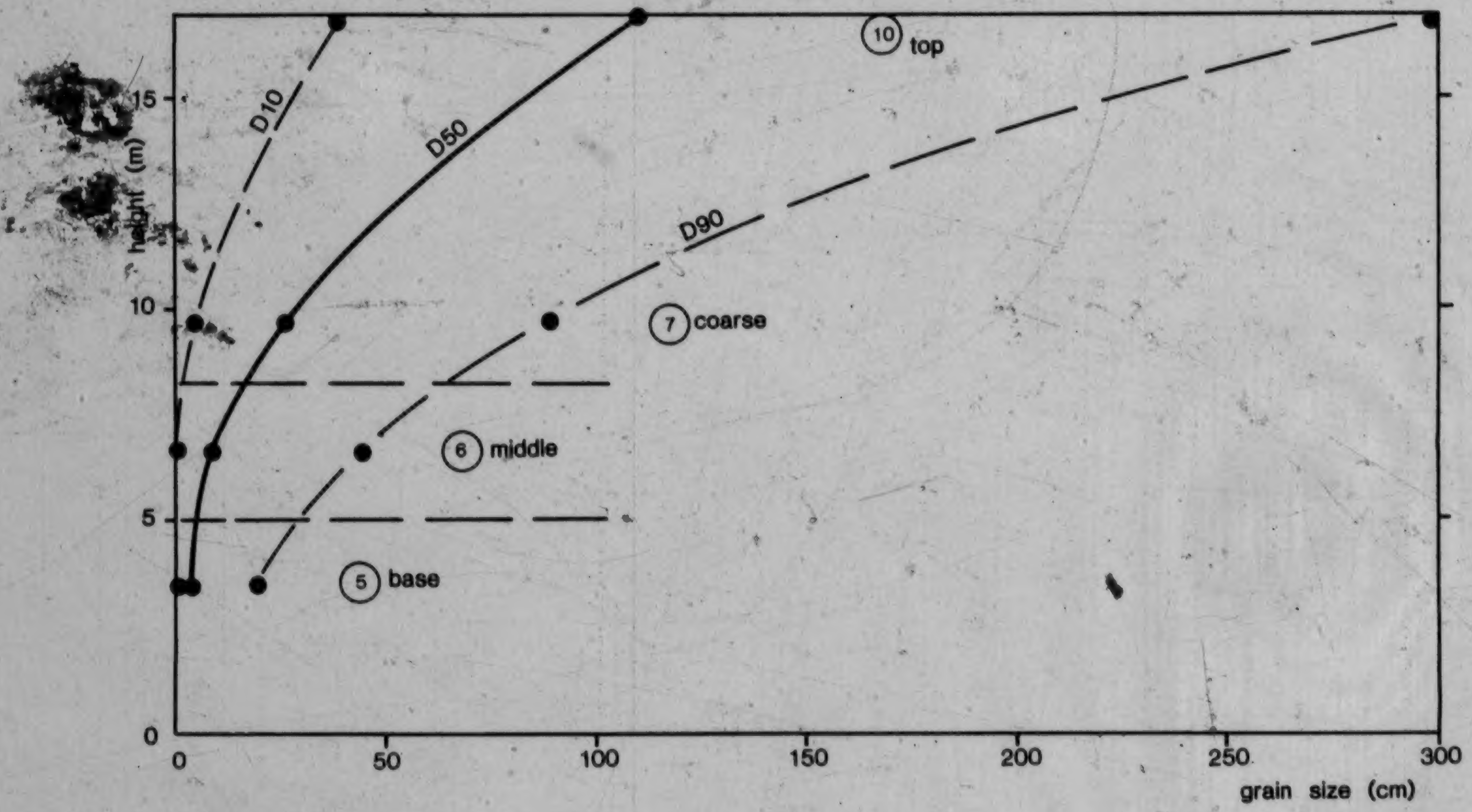

Figure 10.11 Change of characteristic grain sizes above the base of the railway cut (based on Fig. 10.9).

10.3 Analysis- Energy and Friction

The earliest attempt at developing a method of analysis for rock avalanches, by Mueller and Heim (1932), assumes their motion to be analogous to that of a rigid frictional block. Consider a block of a weight W, sliding down a vertically curved path to develop a total elevation loss H. The lost potential energy will equal:

$$E_p = WH$$

Eqn. (10.3)

During motion of the block, work is being done against the resisting frictional force T. The amount of this work performed on a path with a total curvilinear displacement S is:

$$E_e = \int_0^S T\,ds = \int_0^L \frac{W\cos\alpha\tan\phi\,dl}{\cos\alpha}, = WL\tan\phi$$

Eqn. (10.4)

where α is the local inclination of the path, l the horizontal coordinate and L the total horizontal displacement of the block. This equation assumes zero pore pressures and a constant ϕ . The subscript e added to the work symobol denotes that the work is being done against *external* frictional forces, acting across the boundary between the block and its path. Equating the energy lost with the work done:

$$f = \tan\phi = H/L$$

Eqn. (10.5)

In other words, the *effective friction coefficient* of the sliding movement, f, should equal the ratio between the vertical and horizontal displacements of the center of gravity. Heim (1932) recognized that ϕ is the "Schwerpunktsgefalle", but settled on equating it with the "fahrboeschung", recognizing that the earlier angle is more difficult to obtain (p. 113). His main reason for estimating the friction coefficient seems to have been to estimate slide velocities using the equation of motion; hence perhaps the lack of concern over precision.

Scheidegger (1973) took up Heim's notion that the effective friction angle appears to be less in events of larger volume. He assembled a list of 33 landslides and plotted the tangent of the travel angle against volume on a logarithmic scale (Fig. 10.2). A linear trend of decreasing f with increasing volume became apparent, although there was a considerable amount of scatter in the data. Cruden (1976) pointed out that there is sometimes considerable difference between the fahrboeschung and the mean travel angle. A repetition of the plot in terms of the latter angle was produced in Fig. 10.2 and shows relatively little change in the trend. The likely imprecision of the angle determination can acount neither for the scatter, nor for the trend itself.

It was noted by Shreve (1968), Scheidegger (1973), and others, that only the small landslides produce travel angles corresponding to the expected magnitude of the effective friction angle. Considering that the major part of a rock avalanche involves the flow of disintegrated rock fragments over a rough base, the applicable friction angle should be that of sand or talus, i.e. 30 to 40 deg. The corresponding f is 0.57- 0.83. Only the cases with volumes less than about 500 000 cu.m have travel angles approaching these values. Larger avalanches appear progressively more mobile. For more than ten years, various investigators have attempted to find the reason for this increased mobility, but so far the problem remains unsolved. The various hypotheses that exist will be reviewed in the following section.

The presence of pore pressure, applied by air or gas would of course explain the apparent decrease in f. A simple approximate way of accounting for pore pressure would express it as a fraction of the normal component of the total weight of the sliding block:

$$u = r \gamma H \cos\alpha \qquad \text{Eqn. (10.6)}$$

where γ is the unit weight, H the average height of the debris and r is a pore pressure factor. The f in Eqn. (10.4) would then simply be replaced by f (1- r). Reasons for having pore pressure in an apparently dry rock mass will be discussed in the following section.

Hsu (1975), McSaveney (1978) and others suggested that the reduction of apparent friction arises because the large avalanches do not slide, but flow. Caution must be excercised here to express what kind of flow is meant. If viscous or turbulent flow occurs, then Equation (10.4) becomes meaningless. The resisting stresses are in such flows dependent on velocity or its square, the basic assumption of Eqn. 10.3 is invalidated, and an entirely different approach must be taken. McSaveney (1978) apparently did not recognize this in his analysis of the Sherman avalanche, which concluded by describing the motion as that of a complex non- Newtonian fluid. In the first step of the calculation he estimated strain rates in the moving and deforming debris sheet geometrically, considering its gradual spreading and thinning. Then he associated these rates with shear stresses obtained from a version of the frictional relationship of Eqn. (10.4). The basis of the second step was an assumption that the stress- strain rate relationship thus determined is a material characteristic or flow curve, which can be described in terms of viscosity and strength. This is fallacious, as it negates the assumption of the first step, i.e. that of a constant friction.

The assumption of frictional flow, which means the co-existence of boundary sliding and internal shear, with Coulomb's Law applicable throughout, would not modify Eqn. (10.4) too much. This is shown by a review of the "equivalent friction coefficient" concept given in Appendix B. Unlike the previous equations, the new development recognizes that energy is spent doing work not only against external forces, but also internally in the form of shearing and vibration. It is indicated that vibration losses are insignificant. Internal shearing losses do not modify the conclusion of Eqn. 10.4, as long as the shearing direction coincides with the direction of movement. In other words, the travel angle of the centre of gravity of a longitudinally spreading block will be equal to that of a rigid block. Lateral spreading perpendicular to the direction of movement, on the other hand, will result in an "unproductive" expenditure of energy, modifying Eqn. 10.4 as follows:

$$f = \frac{H}{L + 0.5(l - b)}$$

Eqn. (10.7)

where H and L are the displacements of the center of gravity, and b and l are the original and final average width of the debris mass respectively. At Frank Slide, the width of the scar is about 600 m, while the deposit is on average 1270 m wide. Using Eqn. (10.6), f is found to be 0.30, corresponding to an equivalent friction angle of 16.8 deg. This is a reduction of 14 percent from the mean travel angle determined from the centers of gravity. At Sherman, the lateral spreading was from 400 to 2 300 m. The equivalent friction angle is 7.6 deg. and the lateral spreading reduction equals 29 percent. Thus, for the same value of the equivalent friction coefficient, a wide, spread out avalanche would be expected to appear somewhat less mobile than a narrow channelled one. For highly spread deposits with an approximately square plan, the fahrboeschung would be a better estimate of the effective friction angle than the mean travel angle.

Since 1973 other correlations have appeared, attempting to improve Scheidegger's result. Howard (1973) plotted the total potential energy of landslides against the tangent of the fahrboeschung, obtaining a similarly scattered correlation. Several large lunar events were shown to follow the trend of the terrestrial ones.

Hsu (1975) attempted to bypass the notion of an equivalent friction coefficient by defining an "excessive travel distance" as the horizontal travel of the avalanche toe beyond a line sloping at 30 deg. down from the crown in the direction of motion. A plot of this distance against the logarithm of the volume of the event is shown in Fig. 10.12. As pointed out by McSaveney (1975), the concept of excessive travel distance has no theoretical basis. Nor does it perform very well in the correlation.

But the correlation that is there can perhaps be explained by a very simple consideration. Most rock avalanches have an approximately bi- linear profile, as shown in Fig. 10.6. One could assume that the large events exhibit for some reason a very low shear strength, and that therefore most of their debris deposits beyond the break of the slope. A further approximate assumption is that the break of the slope occurs at a point lying on a 30 deg. dip line from the source of the avalanche. This is a reasonable average; although some mountain slopes would of course be somewhat steeper or flatter. The excessive travel distance is now simply equal to the horizontal length of the deposit.

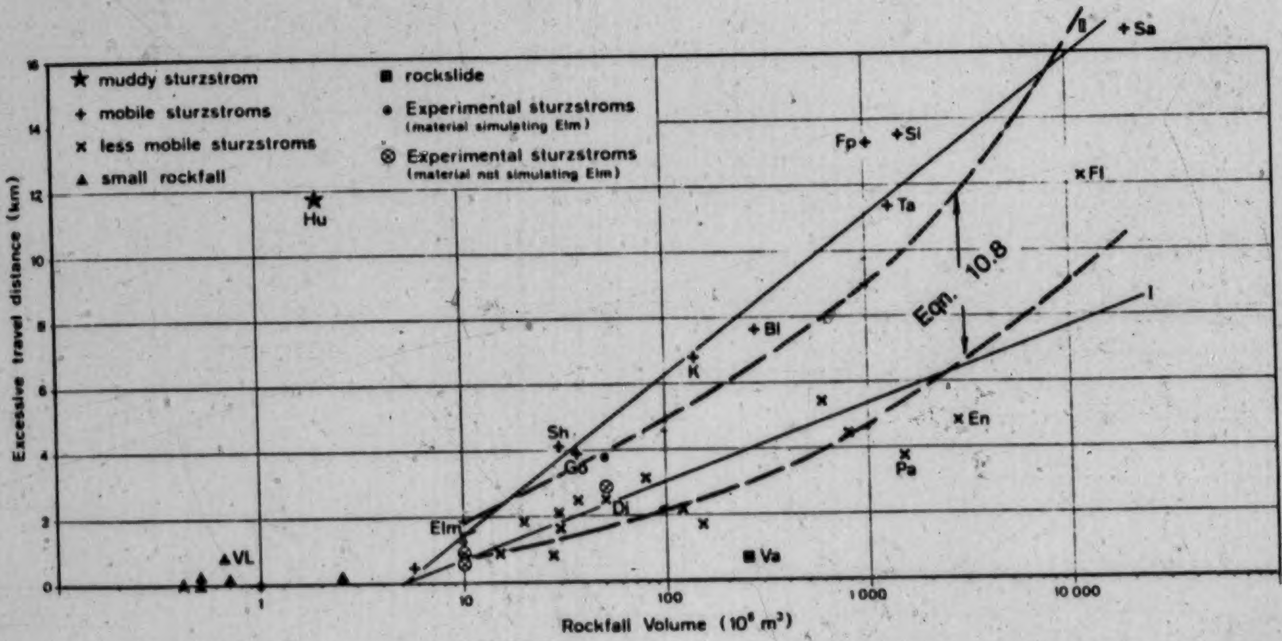

Figure 10.12 Correlation of the excessive travel distance and volume of large rock avalanches (Hsu, 1975).

The area of the deposit, from Equation 10.2, equals on average 20 $V^{2/3}$, where V is the volume. Taking a length to width ratio between one and two, one obtains an estimate of the excessive travel distance:

$$L \simeq 4.4 \text{ to } 8.8 \sqrt[3]{V}$$

Eqn. (10.8)

This is plotted by the two curved dashed lines in Fig. 10.12 and shows a good correspondence with the empirical data. The Huascaran event falls far outside the estimate, perhaps not so much due to an exceptional mobility, but because of an extremely long continuous slope which was available. Thus, the correlation appears to be a reflection of the characteristic geometrical setting of most rock avalanches and the low strength fluid character of their motion. It is possible that the other correlations derive from the same source although, as noted earlier, their theoretical basis is invalidated by the assumption of fluid behaviour.

The same phenomenon has been noted for snow avalanches. Bovis and Mears (1976) found that of all the possible path variables, starting zone area had the highest correlation with the runout distance. Thus, the frictional model has a strong competitor in an approach assuming that rock avalanches flow as low strength fluids.

McSaveney (1975) plotted the potential energy loss against the total travel distance on a logarithmic scale. This has the same theoretical background as Scheidegger's correlation, i.e. the energy balance, and shows a similar trend and scatter. Francis and Baker (1977) correlated volume directly with distance of travel for landslides as well as pyroclastic flows inferred from large ignimbrite sheets. This approach is equivalent to that by Hsu, but the "initial slope" of 30 deg. is left out of consideration. It is probably insignificant in the case of ignimbrite sheets. The correlation is relatively good.

10.4 Analysis- Empirical Approach

The evidence collected so far leaves the impression of a dilemma: do rock avalanches behave as flows of frictional materials with a reduction of the effective angle of friction by some agent? Or is frictional resistance secondary to some velocity dependent stress which permits the masses to travel to positions of low slope angles, i.e. to conform to topography as fluids of negligible strength? A very similar dilemma had been faced by the investigators of snow avalanches, who responded by developing an empirical approach. If the resisting shear stress could be either constant or velocity dependent, it may be evaluated by a polynomial consisting of a combination of both relationships. In analogy with Newtonian and Bingham fluid mechanics, one would expect the polynomial to have a constant (frictional), linear (viscous) and square (turbulent) term:

$$\tau = \sigma f + \frac{\eta v}{H} + \frac{\gamma v^2}{c^2}$$

Eqn. (10.9)

where τ and σ are the shear and normal stresses at the base of the flow, f the effective friction coefficient, the unit weight of the flow, c turbulent resistance coefficient,H flow thickness and v the mean flow velocity. Voellmy (1955) first introduced this relationship, without the viscous term. Salm (1966) confirmed Voellmy's assumption by showing that the viscous term is unimportant in snow avalanches. The resisting shear stress is thus dependent on two constants, which must be evaluated empirically. The effective friction coefficient is considered to be a material constant. The turbulent resistance coefficient may depend on the Reynold's number, and on the flow surface roughness, as it does in water flow. Numerical values for snow avalanches have been determined by Schaerer (1975) and others.

The application of this constitutive relationship to actual flow problems is usually realized using the Bernoulli equation for steady flow in open channels, which has already been introduced in the connection with frictional flow of dry sand (Eqn. 7.14). The form in which it has been used for calculation of avalanche velocity can be written (Heimgartner, 1977):

$$\frac{\Delta (v^2)}{2g} = \Delta Z - \Delta \left(\frac{k\sigma}{\gamma} \cos \alpha \right) - \Delta Z_e$$

Eqn. (10.10)

where the symbol Δ signifies the change between two subsequent positions on the flow path, Δx distance, v is the mean velocity, z the base elevation, σ the normal stress on the base, k a stress ratio (lateral pressure coefficient), γ unit weight and α slope angle. The elevation difference of the energy head is given from (10.9), with H being the flow depth.

$$\Delta Z_e = \frac{\Delta x}{H}\left(\frac{f\sigma}{\gamma} + \frac{v^2}{C^2}\right) \qquad \text{Eqn. (10.11)}$$

Knowing the velocity and flow depth at a reference crossection (upstream, if the flow is supercritical on steep angles), a step- by- step procedure can be used to determine one of these variables at subsequent crossections. But the variation of the other must be determined by other means. Salm (1968) makes the assumption of a steady flow, using the equation of continuity (Eqn. 7.15). But this is only realistic in the middle portion of the travel path, where the unsteady flow changes are less significant. Such an assumption cannot be used in the runout zone, where deceleration occurs without an increase in thickness. Various artifices are used to approximate to the unsteady flow solution, although a discussion of their significance is rare. Salm (1966) derived a solution for the runout of a constant volume avalanche in passing from a steep track onto a flat runout. Force equilibrium between the two sections of the avalanche above and below the slope break is used, instead of the continuity equation. Heimgartner (1977) uses a one step solution of Eqn. (10.10) for the same geometry, making an empirical assumption (due to Voellmy, 1955) that the square of the velocity in the runout zone equals one-half the square of the velocity on the track. Koerner (1976) assumes simply that the flow thickness is constant throughout the movement and, in addition, neglects the pressure head. The same approach is taken by Cheng and Perla (1979). With this simplification, Eqns. (10.10) and (10.11) reduce to:

$$\frac{\Delta\ (v^2)}{2g} = \Delta Z - \Delta x \left(f \cos\alpha + \frac{v^2}{HC^2} \right) \qquad \text{Eqn. (10.12)}$$

This modification of Heim's sliding block model can easily be solved by trial and error, or rewritten in a differential form and solved for an explicit step- by- step formula as was done by Koerner.

These simplified solutions are sufficiently accurate when: (a) the length of the avalanche is considerably less than the length of the path. Therefore, the additional velocity and reach of the front due to the spreading of the avalanche sheet are insignificant compared to the velocity and reach of the center. (b) The path is relatively smooth and free of sharp vertical curves, so that the depth of the flowing sheet does not in fact change too much.

Where these criteria are not met, one could make use of existing computer programs for flood routing in stream flow. These are written on the basis of the Chezy formula which consists of only the third term of Eqn. (10.9). To eliminate the frictional term, one would simply subtract the frictional slope from the geometrical slope or:

$$\tan\alpha' = \tan\alpha - f$$

Eqn. (10.13)

where α' is the slope angle to be input into the stream flow program. The program would further require an initial hydrograph, which could be estimated from some collapse model. This procedure would easily provide a very precise solution of avalanche travel, but has not yet been attempted to the author's knowledge.

Refinements of flow solutions sometimes consider energy losses in abrupt breaks of vertical angle, due both to internal shearing and centrifugal forces. But these are not too significant (Salm, 1966). Also, an allowance for side friction should be made in very confined gullies.

Koerner (1976) pointed out similarities in the behaviour of snow and rock avalanches and applied Eqn. (10.12) to the latter. He analysed the Huascaran, Elm and Goldau avalanches many times, using various combinations of constant f, c and H. The mean flow depth H could be roughly estimated from eyewitness reports and the dimensions of the deposits. But in each case there was only one combination of f and c that would match both the total length of travel [22] and the reported travel duration. These combinations are plotted in Fig. 10.13. It was necessary to use relatively low or negligible friction factors for all of the rock avalanches otherwise, too great velocities and excessively short duration times would be predicted. Kaiser (1978) repeated the same procedure for the Rubble Creek case. He was able to make use of a record of flow depths left by the slide on the walls of the Rubble Creek valley (Moore and Mathews, 1977). Travel duration is not known, but the calculation could be made to match four spot velocities estimated by Moore and Mathews from superelevation in bends. The resulting flow parameters are also plotted in Fig. 10.13 for three approximations, the first two of which assume constant depth.

---

[22] Estimated from the fahrboeschung

These results are a further indication that the resisting forces in rock avalanches are not frictional but velocity dependent, as those in fluids, in saturated granular materials under undrained conditions (Chapter 8), or in colloidal slurries (Chapter 6). Despite its approximate nature, this approach is at present the best existing method of analysis for these phenomena.

Another approximate method of estimating rock avalanche reach is suggested by the apparent consistency of the area increase ratio, as shown in Table 10.1. It is equal to approximately 5.4 in all of the listed events that did not possess any obvious unusual attributes. If one was able to estimate the area of the source region, this ratio gives an estimate of the area of the debris deposit. This could then be fitted into the topography using the run up ratios collected in Section 10.1 to estimate the likely vertical climbing potential. Also, it should be assumed that little

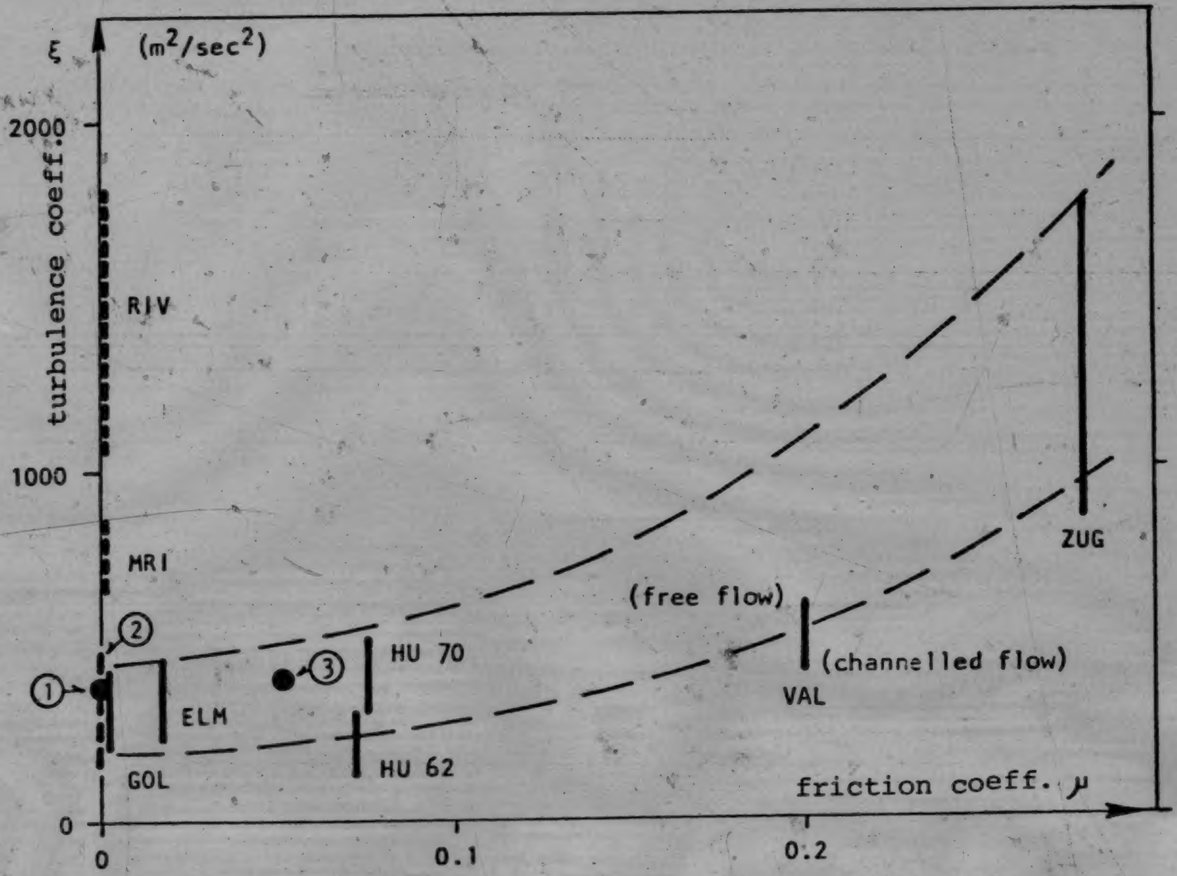

HU 62 - Huascaran (rock & ice) 1962
HU 70 - Huascaran (rock & ice) 1970
ELM - Elm (rock)
GOL - Goldau (rock)
ZUG - Zugspitze (avalanche)
1, 2, 3 - Rubble Creek (assumptions)
RIV - River in smooth bed
MRI - Mountain river (rough bed)
VAL - Val Buera (Avalanche)(Salm, 1968)

Fig. 10.13 Coefficients of friction and turbulence for rock avalanches (Hardy et al.,1978 and Koerner,1976)

material will remain above the toe of the source slope. These rules would allow one to map the deposit approximately.

The last alternative would make use of physical models. Hsu (1975) used a bentonite slurry to model the displacement of the Elm case. He was able to adjust the thickness of the slurry so as to simulate the event completely in its geometrical aspects. At the same time, perhaps fortuitously, the time of travel was also matched to the appropriate scale. This method would be very valuable in cases of complex geometry.

10.5 Analysis- Physical Hypotheses

The empirical methods of analysis of rock avalanches rely on assumptions of material behaviour which are practically arbitrary, being based on analogies with different processes such as sliding of frictional blocks and water flow. A valid constitutive relationship for these phenomena has not yet been conclusively established, although attempts to do this have been numerous. They are described on the following pages. The reader who is interested simply in learning how to analyse rock avalanches will find little enlightenment in this section; none of the proposed hypotheses has so far left the domain of speculation.

The theories can be divided into three conceptual groups. The first assumes that rock debris is carried on a discrete lubricating layer of another material, namely mud or compressed air. The second group adopts the frictional model of Mueller- Bernet and Heim, but assumes the existence of gas pore pressures which reduce the effective friction angle. Within this group are theories which envision a full fluidization of the debris, i.e. with effective stresses equal to zero. Finally, a group of researchers, including the present author, favour a notion that rapidly shearing granular masses assume spontaneously liquid properties characterized by a low strenth and a stress or velocity dependent viscosity.

Lubrication by mud. The lubrication layer hypotheses originate with Heim (Buss and Heim, 1881). He suggested, in his first- hand description of the Elm catastrophe, that the base of the debris was lubricated by a layer of mud. It is certainly true that rock avalanches, excluding the extraterrestrial events, override saturated unconsolidated deposits on large parts of their paths. In some cases such as Huascaran, there is no question of the dominant role played by saturated fines. But elsewhere it is a question of quantities and availability, concerning which there is very little information. The Frank Slide for example, travelled over four types of base: bare limestone, sandstone and shale rock, talus of similar origin, alluvium of a minor stream, and glacial deposits overlying bedrock in various thicknesses. Considering the motion of the center of gravity, the proportion and sequence of these materials was approximately 20 percent rock, 25 talus, 15 a till terrace, up to 20 alluvium, and another 20 valley till over irregular bedrock. Thus, the lubricating layer could not form in the first 45 percent of travel, where the materials were coarsely granular and probably well drained. It is unknown how much liquid slurry could have been derived from the alluvium belt. Much of it was displaced by the avalanche front, as evidenced by thy large volume of mud blast thrown to one side of the foot of the slope. This is also indicated by the scarcity of rounded particles in the basal part of the debris, which evidently participated in the shearing process judging by its high degree of comminution. Finally, the left hand side of the avalanche, where there was evidently much more alluvium available, does not show a greater mobility than the right hand side. The mud lubrication hypothesis was reportedly abandoned by Heim by the time of his 1932 publication (Hsu, 1978), and has been only rarely referred to by other authors, although it is unquestionably applicable to some events such as Huascaran.

Air layer lubrication has been suggested by Shreve (1968). The rock avalanche is presumed to gain a great speed by an initial fall and sliding, be launched by a suitable ramp, and in its descent compress a volume of air which has too little time to escape through the debris sheet by upward seepage. A discrete cushion of air exists, on which the debris layer travels friction- free. Shreve estimated the launch velocity at Blackhawk to be 270 km/hour, followed by uniform acceleration in frictionless flow to 432 km/hour before the dissipation of the air cushion and sudden freezing of the avalanche. The air cushion thickness was about 0.6 m (Shreve, 1968a). Lateral escape of air is assumed to be restrained by the weight of the lateral marginal ridges. The possibility of upward escape by seepage was analysed by Shreve (1968a) by considering steady Darcian flow of air through a granular material under adiabatic conditions. The volume rate of leakage at the base of the debris layer was calculated as:

$$Q_B = \frac{k\,p_B}{1.57\,\eta_B H}\left[1 - \left(\frac{p_o}{p_B}\right)^{1.57}\right] \qquad \text{Eqn. (10.14)}$$

where k is the debris permeability, pB and po the base and athmospheric absolute pressures, η_B viscosity of air at base pressure and H thickness of the debris. Shreve estimated that the air layer supporting the Blackhawk avalanche would not dissipate in the estimated 80 sec duration of the event, if the mean permeability of the debris was less than 1 Darcy (0.001 cm/sec).

The theory gained wide acceptance, but has also been frequently criticized. Hsu (1975) raised three main objections, one concerning the flow- like structure of debris deposits, another based on the lack of observed air escape at Elm and third pointing to the presence of "sturzstroms" on the airless moon. The first objection is weak; Shreve considered the existence of many of the structures as supportive of his theory. The second is controversial as it is apparently difficult to distinguish between air movements caused simply by air displacement in front of the avalanche, and those caused by escape from the debris interior. The third objection has been countered by Shreve (Schmitt, 1973, p. 690) by stating that the lunar events were probably fluidized by "solar wind gases absorbed within the original talus materials". Bishop (1973) expressed disbelief in the continuity of the air layer beneath the avalanche. Considering the highly variable thickness of debris sheets, a continuous gas support is inconceivable. If the pressure of the cushion was sufficient to support the points of maximum thickness, the gas would necessarily break through in points where the sheet is much thinner, draining the cushon and forming escape structures. Voight (1978) and Erismann (1979) further questioned the mechanism of trapping of air. The volume of air enclosed under a sheet of air- launched debris is not compressed, unless the debris slows down, changing its trajectory. Minor compression results from the "aerofoil" effect of the leading edge, which appears insufficient (Erismann, 1979). The air cushion mechanism should be less effective in the case of thick avalanches such as Koeffels, yet they are among the most mobile.

Air fluidization has been postulated by Kent (1966) in analogy with industrial fluidization processes. But the typical attributes of fluidization are missing in the descriptions of rock avalanches. Fluidized beds are characterized by dilation, high degree of turbulence, channeling and upward flow structures, elutriation of fines to the surface and fall of large particles to the base (e.g. Brown and Richards, 1970). Powder snow avalanches do fluidize, in which case they become covered by turbulent dust clouds (e.g. Mellor, 1978) so prominent that the main body of the avalanche can never be seen. If a similar phenomenon took place on the scale of Frank Slide, then wide surroundings would be covered by vast quantities of dust. This has neither been reported from Frank, nor from elsewhere. Inverse grading, which appears relatively ubiquitous in rock avalanches, is the opposite of what occurs in fluidized granular beds, although it is typical of vibrated beds (Brown and Richards, 1970). Marangunic (1972) proposed fluidization by a mixture of air and snow as the transport mechanism of Sherman avalanche. Evidence for it was the high mobility of the debris and its ability to travel over an undisturbed layer of snow, as observed in test pits. Fluidization would explain the unusual degree of lateral spreading which took place in this event. But no other evidence supporting this hypothesis has been presented.

Pore pressure. It is of course not necessary to fluidize a debris mass to increase its mobility. Provided that the resisting stresses are frictional, the presence of any pore pressure will reduce the effective friction coefficient. But pore pressures in moving rock avalanche debris cannot be derived from water, because of the bulking which occurs during the initial disintegration of the rock mass. There can never be enough water available to saturate the newly created void space. The pressure must therefore derive from some gas. Air is again an obvious possibility although again, the trapping mechanism by which it should by collected and pressurized is unclear. It should be noted that initial negative pressures must exist as the breaking mass expands. Only when these are dissipated can positive pressures develop.

A group of authors (Habib, 1975, Pautre et al., 1974, Romero and Molina, 1974, Goguel, 1978) suggested that the pore pressures result from vapour generated by the boiling of interstitial water on the sliding surface. All presented approximate equations showing that (a) there is sufficient amount of energy available to vaporize pore water, provided that the sliding zone is sufficiently thin; (b) heat loss by convection away from the sliding zone is insignificant. The analyses have been applied to the Vajont and Huascaran events.

There is no question that this is a feasible mechanism. It is impressive to consider that the 1970 Huascaran avalanche had sufficient energy to melt and vaporize a layer of ice 3.9m thick in its travel down the glacier (Pautre et al., 1974). One might express doubt concerning the availability of a sufficient quantity of water, which has not been considered in the given references. It could of course be taken for granted in the two cases mentioned; at Huascaran due to the presence of the glacier and at Vajont due to the fact that the rock mass remained relatively coherent and so there could only be little mass flow away from the sliding surface. But, in the general case, only the joint water of a dense rock mass is available, while a sufficient quantity of steam is required to fill the new void space generated in the vicinity of the sliding plane by fragmentation. The equation of state for water vapour is:

$$pV = \frac{m}{18} RT \qquad \text{Eqn. (10.15)}$$

where V is the volume of a mass m (grams) of vapour, R the universal gas constant and where the absolute pressure p and temperature T are connected by the vapour pressure relationship of water. The equation can be used to estimate the volume of steam with a given pressure, derived from a unit volume of water. Assuming only negligible movement of fluids within the mass, the ratio of the vapour and water volumes approximates to the required ratio of porosities necessary for this development of pressure to be feasible. To obtain a pressure of 400 kPa, capable of fully supporting an 18 m column of broken rock, the steam volume is 386 cc per gram of water. If the porosity of the fragmented material is equal to 25 percent, the required initial saturated porosity of the source rock would be 25/386 = 0.06

percent. This is certainly feasible, even in a tight rock mass. Water escape has been neglected, but Shreve's analysis (1968a, see Eqn. 10.14) indicates that it would be relatively insignificant.

Erismann (1979) proposed another source of pore pressure, derived from the thermal dissociation of carbonate rock into lime and carbon dioxide under the heat of friction. His analysis assumes that all of the work done by the frictional resisting forces is used in the process of dissociation, irrespective of the stress level and the thickness of the sliding zone. This may be a reasonable assumption in cases where the rock mass is very thick and the sliding zone thin. Where it is not, various other forms of heat consumption would need to be taken into an account if one were to avoid overestimation of this mechanism's efficiency.

The mechanism would of course not be available in other rocks than carbonates. Erismann therefore suggested a related hypothesis of frictional melting lubrication. This has some substantiation in finds of melted rock pumice ("frictionite") in the debris of the Koefels landslide. Also, the frictional melting lubrication has benn reproduced in laboratory experiments (Erismann et al., 1977) as described in Section 3.4. Both the experimental results and theoretical estimates indicate that the mechanism would only be effective at a debris thickness in excess of 100 m, combined with a very small thickness of the sliding zone.

The Koefels slide is exceptionally thick, over 400 m over a large part of its area (Erismann, 1979).

Three general comments to the above mechanisms should be raised: Firstly, with so much vaporization and melting taking place, it is surprising that the existence of hot mud or of steam clouds has never been reported. Rock heating in a minor fall has been mentioned by Romero and Molina (1974). Secondly, there appears to be a lack of evidence for large scale compressed gas escape. As an example, assuming that the average dry friction angle of the Frank Slide material is 30 deg., the pore pressure ratio (Eqn. 10.6) would need to be about 0.5 to achive an effective friction angle of 16.7 deg. (Eqn. 10.7). Taking the average debris thickness as 14 m, one finds that the mean pore pressure at the base of the slide would need to be sufficient to uplift and fluidize portions thinner than 7 m, causing the origin of escape structures, elutriation, normal sorting etc., none of which has been observed. Thirdly, increased pore pressure cannot account for the evidence presented in the preceding two sections, which indicates that velocity- dependent resisting forces are more important in rock avalanches than frictional forces.

Rock dust liquefaction. After a criticism of Shreve's hypothesis with an emphasis on the lunar avalanches, Hsu (1975) proposed a mechanism of flotation of coarse debris particles in a liquid dispersion of dust, quoting Bagnold's (1954) results as a basis for his hypothesis. To be able to exist in a vacuum, the dust dispersion would have to be inertial and "drained" as defined in Section 8.4. There is no indication in Bagnold's work that such a dispersion would have other character than frictional. A fluid dispersion could only form in air, in an undrained condition, and in the macro- viscous regime. This could presumably occur,, although not on the moon. High velocity ring shear experiments conducted on mixtures of sand and rock powder (Section 12.3) failed to indicate an increased mobility, although they were run at representative levels of stress and strain rate.

Mechanical fluidization. When a dry granular material is slowly sheared, its grains slide over each other being in a constant contact. The shearing resistance derives from interparticle friction, modified by the kinematics of the process (Rowe, 1962). Rolling friction is apparently irrelevant, since the particles are confined on all their sides. When the shearing is rapid, continuous particle contact can no longer take place as the mass dilates. This was illustrated by the flume experiments (Chapter 11), in which the mean density of uniform sand at high velocities was about 7 percent lower than the loosest static piling density. Under such conditions, particle contacts are brief impacts, the momentum of which transfers both the shear and normal stresses within the dispersion. Assuming that the impacts are elastic, the only dissipative mechanism is again interparticle friction. But the kinematic freedom of particles in the intervals between collisions would suggest that some rolling might occur, increasing the apparent mobility of the whole. Frictional forces only participate in angular momentum transfer [23] and the efficiency of the mobilizing process could therefore presumably be connected with the relative importance of linear and angular particle momentum. Kinetic theory of ideal gases, for example, which neglects angular momentum of the molecules, can be used to deduce viscous (frictionless) behaviour.

The possibility of a fundamental change in the shearing process at the high velocities found in "stuerzstroms" has been suggested and vividly described byl Heim (1932, see also translation byl Hsu, 1975 or 1978). It was also considered by Bagnold (1954), who carried out a semi-empirical analysis of shearing of dispersions. As discussed in Sections 7.3 and 8.3, his inertial model would be applicable to the shearing of dry debris. Bagnold concluded in 1966 that even rapidly shearing concentrated dispersions remain rheologically equivalent to ordinary frictional materials with their "angles of repose". This view is somewhat vaguely supported by his test results, as indicated by the right hand side of the curve in Fig. 8.1. But other authors took up the hypothesis, quoting Bagnold (e.g. Howard, 1973, Scheidegger, 1974, Hsu, 1975, Koerner, 1977, McSaveney, 1975). McSaveney (1978) coined the phrase "mechanical fluidization", refering to the change from simple frictional to complex velocity- dependent flow behaviour at high shearing rates, and proposed a phase diagram for dry debris dependent on normal stress and "internal kinetic energy" levels.

---

[23] Assuming spherical particles.

The experimental program conducted as a part of this research had the objective of demonstrating this expected change in rheology at high rates of shearing of granular material. At first, sand flow experiments in an inclined flume were conducted (Chapter 11), attempting to achieve high velocities. The test velocities were as high as 6 m/sec. Extremely high shear strain rates developed near the base of the faster flows, which had almost constant velocity profiles. Some degree of volumetric dilation was observed but the sand remained frictional, as demonstrated both by direct stress measurements and by observations of accelerations. The normal stresses effective in these tests were very low; only less than 2 kPa. It was then considered that the mobilizing phenomenon might be restricted to the condition of high normal stresses. Four pieces of evidence appeared to support this:

a. The "scale effect" of rock avalanches as discussed in Section 10.1, by which larger (and therefore thicker, cf. Fig. 10.2) events are the more mobile.

b. A theoretical analysis of the process of momentum transfer in a dispersion of equal spheres was carried out by Dr. G. Parker and the author. Following partly Bagnold's reasoning (1954), only linear momentum transfer was considered. The normal and shear stresses were equated to the vertical and horizontal momentum transfer rates of cyclically moving grains. The analysis yielded the following expression for the shear stress/ normal stress ratio:

$$\frac{\tau}{\sigma} = \Omega \frac{dV}{dz} \frac{1}{\sqrt{\sigma}} d \qquad \text{Eqn. (10.16)}$$

where Ω is a constant, dV/dz the shear strain rate and d particle diameter. This is a viscous relationship, the viscosity being dependent on inverse square root of normal stress. It was assumed that the neglecting of angular momentum would be valid only when the material is highly dispersed, and that there would be a gradual transition from the frictional state to the viscous one. For the same degree of dispersion, the viscosity would decrease with greater normal stress.

c. The experiments of Bridgwater (1972), discussed in Section 3.4 with results shown in Table 3.4 and Fig. 3.4, indicated that there is a drop of friction with increasing velocity, but only at relatively high normal stress levels (exceeding 25 kPa).

d. Dimensional analysis (Section 11.2) showed that the flume tests were lacking primarily in their low normal stress levels as compared to full scale rock avalanches.

To prove this point, high velocity and stress ring shear experiments were conducted on several materials, including dry sand, wet sand, polystyrene beads and mixtures of sand and rock flour. The maximum shearing velocity was about 1 m/sec, the dimensionless shear strain rate 50/sec and the normal stress 200 kPa. These key parameters are close to what would be expected at the base of a moderately large rock avalanche. The results, reported in Chapter 12, are simple and consistent: there is no change in the material behaviour over the entire range of variables studied. It therefore appears that the mechanical fluidization hypothesis, although intuitively attractive, is not correct. Probably, neglecting of the angular momentum transfer and associated frictional energy losses is inadmissible at these high concentrations.

Acoustic fluidization. It has recently been proposed (Melosh, 1979) that granular debris involved in a rock avalanche may be fluidized by acoustic (pressure) waves generated by the movement of the landslide itself. It has long been known that dry granular materials loose strength when vibrated. Mogami and Kubo (1953) described "heaving" of (presumably) dry sand observed during an earthquake. They also conducted direct shear tests on dry sand samples subjected to harmonic vibrations, obtaining frictional strenth reduction by as much as 85 percent. Barkan (1962) described similar experiments, in which various degrees of reduction of frictional strength were achieved. The reduction increased with both the amplitude and frequency of vibration. Fig. 10.14a shows its dependence on the acceleration of the vibrations, determined as the product of amplitude and square of frequency. The effect is stronger, the smaller the grain size. According to Barkan, a true fluidization can be achived in some sands so that they behave as liquids. Falling sphere viscosity measurements have been conducted in a vertically vibrated sand reservoir, deriving a Newtonian viscosity ("vibroviscosity") versus acceleration of vibrations relationship shown in Fig. 10.14b.

Melosh (1979) derived theoretically a relationship between vibroviscosity, frequency and amplitude of acoustic waves which is not dissimilar from that of Barkan (Fig. 10.14c). He derived his analysis assuming a field of random normal pressure waves, acting on a granular mass of a constant frictional strength subjected to a sustained mean shear stress. A further assumption was that a large part of shear strain is permanently (plastically) relieved, each time the normal stress within the debris falls temporarily to zero as a result of the vibrations. Energy considerations are introduced to show that, under certain conditions, the fall energy of the landslide might be sufficient to supply both the vibration mechanism and losses.

This hypothesis appears very attractive in having experimental and theoretical support and being in agreement with most of the field evidence. Release of vibration by

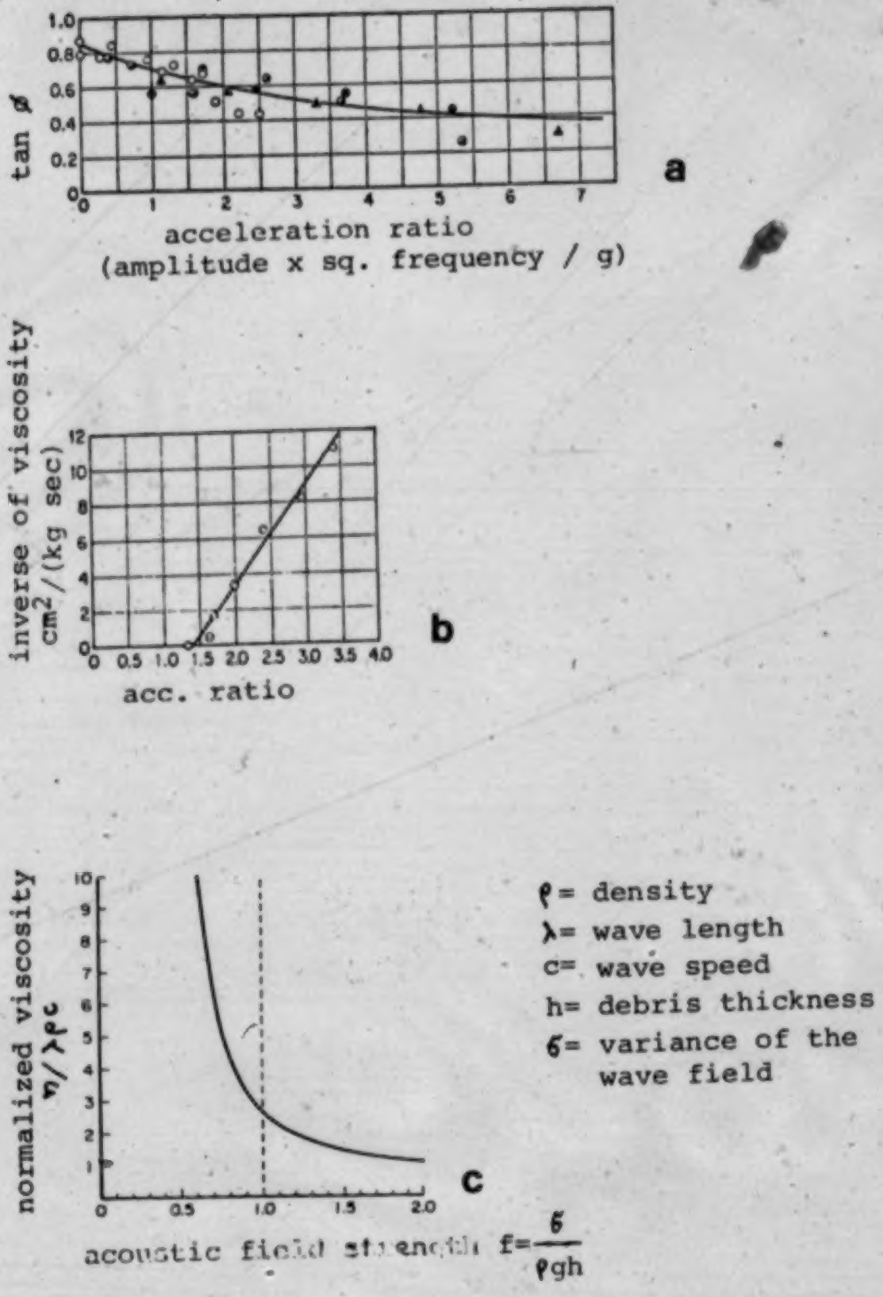

Fig. 10.14 Acoustic fluidization: a) strength reduction b) vibro-viscosity vs. acceleration ratio (Barkan, 1962); c) vibro-viscosity vs. stress amplitude (theoretical, Melosh, 1979)

rock avalanches has been reported several times. It must result both from unevenness of the flow path and from turbulence within the flowing sheet. The amplitude of stress waves is probably greatest near the base of the sheet. The existence of inverse grading may be explained by both greater comminution near the base of the debris, and by natural sorting caused by Bagnold's dispersive pressure (Section 9.5). It could thus be imagined that only the fine basal material is fully fluidized, both because of the stronger wave field and because of its smaller grain size. The coarser upper layers ride on this mobile layer without much distortion. Debris cones and some of the splash may represent extrusions of the vibro- fluidized material under the pressure of its surcharge.

The theoretical development of the hypothesis presently provides only an approximate indication of its feasibility. Quantitative treatment capable of making velocity and reach prediction has not yet been developed and will be extremely difficult to achive, due to the complexity of the process of random wave generation, transmission and dissipation in the flowing debris sheet. The point is that the vibration intensity is determined by the *boundary conditions* of the particular flow. One therefore does not have a unique predetermined constitutive relationship, since the material behaviour is controlled by the conditions of the flow.

Acoustic fluidization is also likely to occur in debris sheets flowing during earthquake shaking, as suggested by

Solonenko (1977).

10.6 Conclusion

Eight different hypotheses have been described in the preceding section, with claims to being able to explain the rheology of rock avalanches. All are well reasoned and most appear supported by a fair amount of circumstantial evidence. Nevertheless, none has so far been proven as the sole means of explaining all of the observed facts. The author thinks it likely that all of the proposed mechanisms play certain roles in the process described as rock avalanche. Some events, for example, are unquestionably lubricated by a large amount of liquefied saturated debris. The airfoil effect certainly provides a brief discrete air layer support for the frontal edge of an air- launched sheet. Pore water and snow or ice water vaporization probably occurs under certain conditions. So does mineral dissociation and melting in very thick landslides. Dust suspensions exist. The "mechanical fluidization" concept should be abandoned in favour of "acoustic fluidization", as it appears impossible to change the shearing behaviour of a granular mass without an externally generated acoustic field.

The questions are: (a) is one of these mechanisms always dominant; or (b) is every particular event controlled by a different mechanism? The author finds the acoustic fluidization hypothesis as having the strongest supporting evidence and being free of serious objections. It is therefore considered as the dominant mechanism of rock avalanche motion. But other proposals appear relevant in certain unique cases. For example, it appears likely that avalanches travelling over glacial snow and ice may be fluidized by water vapour, resulting in the observed unusually high degree of spreading (e.g. Sherman). Others, which move along valleys with large quantities of unconsolidated deposits, may gather sufficient amount of saturated fines to assume a character of large debris flows (e.g. Huascaran).

A deterministic quantitative method of rock avalanche analysis may yet be long in coming. In the meantime, the empirical methods of Sections 10.3 and 10.4 must serve our needs. In extrapolating empirical information from one case to another, one should make allowance for possible differences in physics. Specifically, one should identify the possibility of the landslide travelling over glacial snow and ice, eroding too great a quantity of saturated fine material, or becoming saturated by some other means. Specific geometrical aspects should also be considered, as discussed in Section 10.1.

11. LABORATORY FLUME EXPERIMENTS

11.1 Introduction and a Statement of Objectives

Gravity flow of granular materials is an important geological process, playing a dominant role in several types of slope movements. These include small scale sand and talus flows, subaqueous quick sand flows, and debris flows and avalanches. Besides its geological significance, this process is also of direct practical interest in the industrial field of bulk material handling. Nevertheless, it is still poorly understood even in its simplest form, the dry inertial flow of cohesionless grains (Chapter 7). It is felt that little progress can be made in the understanding of the more complex two phase flows (grains in slurry or water), until the behaviour of the granular phase alone can be satisfactorily explained.

The present state- of- the- art, as outlined in Chapter 7, is poorly developed. Empirical data are scarce and theoretical developments lack substantiation. Much research work has, of course, been done concerning the statics of granular materials as plastic media, but consideration of their dynamics is rare. The situation can be placed in perspective by comparing it to the state of affairs in fluid dynamics. Theories of open channel fluid flow began with Chezy in 1775. The still widely used empirical equations formulated in the second half of the last century were based on substantial empirical data which were already then in existence (Chow, 1959). Open channel grain flow, on the other hand, has even until today been studied only by a handful of workers. Most of the significant studies have been described in Section 7.2.

Experimental study of grain flow is considerably more difficult than that of a fluid. There is a geometrical scale effect determined by the grain size and distribution. The minimum experimental grain size is limited to fine sand, as finer sizes would be affected by electrostatic forces. Density is nonuniform, presenting an additonal variable, and cannot be measured by sampling. The material is thixotropic, changing its bulk properties on passing from a state of rest to motion. The finite size of grains and the existence of static friction makes it impossible to use standpipes or submerged velocity measuring devices. Finally, the opacity of the material eliminates some conventional possibilities for optical measurements.

The basic objective of this study is to examine the validity of the hypothesis of mechanical fluidization (Section 10.5) The specific task is to determine whether the Coulomb's law of friction, applicable to any granular material under quasi- static conditions, remains valid at very high rates of shearing. For this reason, the main consideration in the design of the experiment was to achieve as great velocities as possible under laboratory conditions. The maximum flow speed was nearly five times that tried by earlier researchers. The geometrical size effect was minimized within reasonable limits by making the least characteristic dimension of the flow two orders of magitude greater than the grain size. (One order of magnitude was barely exceeded in any of the previously published studies). The dynamic similitude condition was addressed by testing two materials of different grain stiffness. Rounded and angular grains were tried, as well as mixtures of grains and rock flour. Velocity, flow thickness and path angle were varied.

Besides of the primary task stated in the previous paragraph, the study has a secondary aim to provide a contribution to the body of data concerning the parameters of granular solids flow. Power input per unit of length [24] has been increased about 200 times over those of the previous tests.

In the organization of this chapter it was decided to defer consideration of a number of details of the measuring technique and data processing to the last two sections, in order to make the presentation of the basic results briefer and more understandable.

11.2 Considerations of Similitude

These flume experiments were not intended as exact scale models of rock debris avalanches, as it would hardly be feasible to produce such models. It was simply attempted to generate laboratory flows of granular material over rough surfaces, that would be rapid enough to bring the anticipated process of mechanical fluidization into effect. It was recognized, nevertheless, that the chances of reproducing a phenomenon believed to be acting in full size events would be improved, if the various dimensional similitude requirements were satisfied to the greatest possible degree.

---

[24] (proportional to the product of the crossectional area of the flow times the maximum velocity)

The postulated phenomenon (Section 40.5) is a purely mechanical one, being based solely on the concept of elastic- frictional contacts between grains. Consequently, only the mechanical and geometrical properties of the granular materials, and the parameters of the flow itself, shoud be considered. These include the mean grain size (taken as the grain size of the 50 percent weight fraction), uniformity coefficient (Terzaghi and Peck, 1968), grain density and modulus of deformation, and the intergrain friction coefficient. Strength of the grains was not considered. This is because very little or no breakage was observed in the tests. Breakage does, of course, occur in the prototype (Section 10.1) and consumes additonal energy there. Therefore, its neglect in the dimensional analysis is a conservative assumption , which should lead to a slight overestimate of prototype mobility. Variables connected with the flow itself include flow thickness, surface velocity, mean volume concentration of grains in the flow mass, and slope.

The variables are summarized in Table 11.1 together with three dimensionless parameters obtained by an application of Buckingham's theorem. Numerical quantities are given both for the model flows and for a prototype landslide. Values for the three model materials used, i.e. uniform quartz (Ottawa) sand, plastic beads and mixture of sand and rock flour, are given (Table 11.2). The prototype values were chosen to correspond to the estimated average parameters of the Frank Slide. Mean flow thickness and velocity agree with estimates by McConnel and Brock (1904). The mean grain size and uniformity values are derived from the average of grain size curves determined for the "fine matrix" samples collected at the base of the railroad cut in the centre of the Frank Slide debris deposit (Fig. 10.10). Other quantities were chosen as typical from various published sources.

The ratio between dimensionless parameters of the test and prototype, found in the last column of Part B of the table, is a measure of mechanical similarity between the two systems. It equals 1.5 for the Froude number, indicating that velocities achieved were large enough from a dimensional point of view. Volume concentration, intergranular friction and slope, all show satisfactory agreement. Perhaps the most serious violation of the similitude requirements is connected with the elasticity ratio, which is different by one order of magnitude in the case of the quartz sand. Grain size ratio is also

A. DIMENSIONAL VARIABLES

Variable	dimensions	test	prototype
D = mean grain size	mm	0.7 (quartz) 1.2 (plast.)	10
ρ = grain density	Mg/cu.m	2.7 (quartz) 1.1 (plast.)	2.7
E = grain deformation modulus	GPa	60 (quartz) 2 (plast.)	40
H = flow thickness	m	0.1	15
V = surface velocity	m/sec	5	50
g = gravity	m/sec^2	9.81	9.81

B. DIMENSIONLESS PARAMETERS

Parameter	test	prototype	ratio
$V^2/(gH)$ = Froude No.	25	17	1.5
$E/(\rho gH)$ = elasticity ratio	250×10^5 (quartz) 19×10^5 (plast.)	2×10^5	10-125
D/H = grain size ratio	0.01	0.0006	17
C = volume concentration	0.5	0.5-0.9	1.0
U = uniformity coeff.	1.0 (uniform) 50 (mixed)	75	0.01-0.7
f = intergranular friction	0.5 (quartz) 0.25 (plast.)	0.5	0.5-1.0
S = slope	0.45-0.75	0.0-1.0	1.0

Table 11.1 Dimensional analysis of the flume experiments

material	median grain size D_{50}(mm)	uniformity coeff. D_{60}/D_{10}	grain shape	grain specific gravity	loosest bulk density (g/cm^3)	angle of repose* (degrees)	
						high	low
Ottawa sand (ASTM (190)	0.7	1.1	rounded	2.65	1.57	35	31.6
polystyrene beads	1.5	1.2	smooth spherical	1.04	0.63	29.9	27.4
angular sand (coarse)	1.4	1.6	elongated angular	2.67	1.30	39.5	37.8
angular sand (fine)	0.3	4.0	angular	2.67	1.53	40	37
10-14 sand (ring shear, Chapter 12)	1.5	1.2	sub-rounded	2.65	1.60	38	35.1

*Measured using the rotating drum method of Carrigy (1970)

Table 11.2 Properties of test materials

significantly different. The uniformity coefficient of the natural slide debris is very high and contrasts with that of the Ottawa sand almost by two orders of magnitude. It is, however, not much different in the case of the bi- modal mixture of sand and rock flour used in several of the experiments.

One other variable that has not yet been mentioned is particle shape, which has not been expressed quantitatively. Both the slide debris and the experimental materials have predominantly equidimensional particles. The slide debris is of course angular, whereas the Ottawa sand is well rounded and the plastic beads are perfectly spherical. For this reason, several tests were run with crushed angular sand.

In a summary, it may be stated that most of the similitude requirements have been met satisfactorily. The two exceptions ,which are particle stiffness and size, will be addressed by the second type of test conducted in this study, as reported in the following chapter.

11.3 The Test and the System of Mesurements

These experiments observed the high velocity flow of granular material on an inclined flume. The base of the flume was lined with the experimental material glued onto a flat plate. The characteristic roughness dimension was therefore approximately equal to the grain size in each case. The sides of the flume were made of Perspex.

Sand flow from a conical hopper was accelerated by free fall down a vertical chute of rectangular crossection. It was then introduced onto the inclined measuring flume by a Teflon- lined cycloidal knee (see schematic diagram and photographs, Figs. 11.1, 11.2 and 11.3). After leaving the flume, the sand was collected in a cubical pan.

Dimensions of the apparatus were selected as follows: The maximum flow depth of 13 cm was chosen to exceed 100 times the particle diameter. The width of 20 cm makes the minimum width to flow ratio equal nearly 2 : 1. The length of the test section of 150 cm was decided as a result of space limitations. With this length, the maximum height of the apparatus is 7 m. The maximum velocity of 6 m/sec was achieved by a free fall of 400 cm. The maximum corresponding flow rate is 0.1 cu. m/sec. With a hopper and pan capacity limited to 0.3 cu.m, the largest flows could only be maintained for 3 seconds. The average test duration, however, was over 10 seconds. Inclination of the test path was arbitrary. In order to investigate the possibility of uniform flow, it was found necessary to vary the angle only between the limits of 25 to 35 deg.

Simultaneous and continuous measurements were conducted during the experiments of the mass flow rate, the thickness of the flow sheet at several locations, the weight of the flowing material on the flume, the surface velocity, and the shear stress on the base of the flow path. By combining these variables together at the data processing stage, it

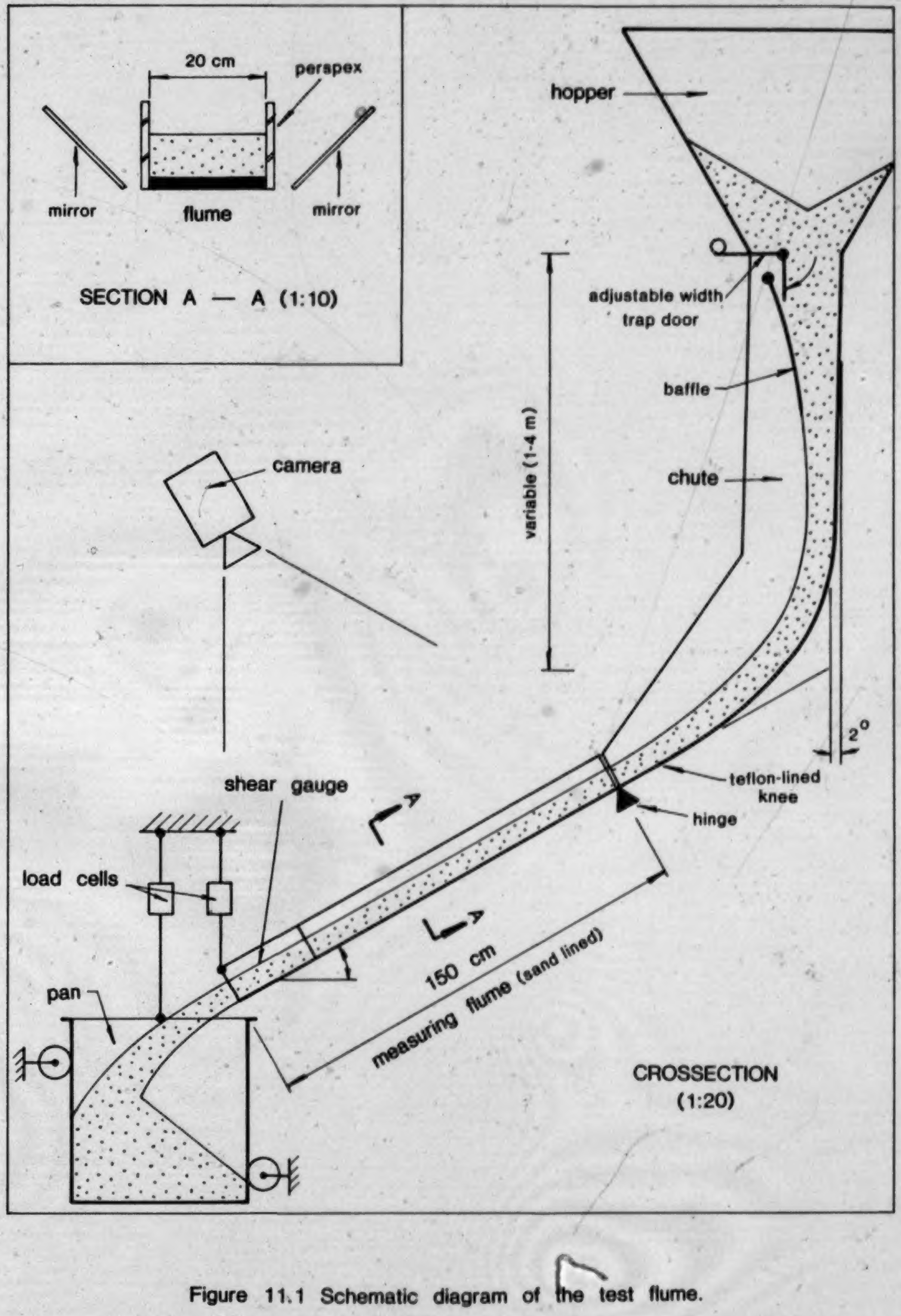
20 cm
perspex
mirror
flume
mirror
SECTION A — A (1:10)
hopper
adjustable width
trap door
baffle
chute
variable (1-4 m)
camera
2°
teflon-lined
knee
hinge
shear gauge
A
load cells
A
150 cm
measuring flume (sand lined)
pan
CROSSECTION
(1:20)

Figure 11.1 Schematic diagram of the test flume.

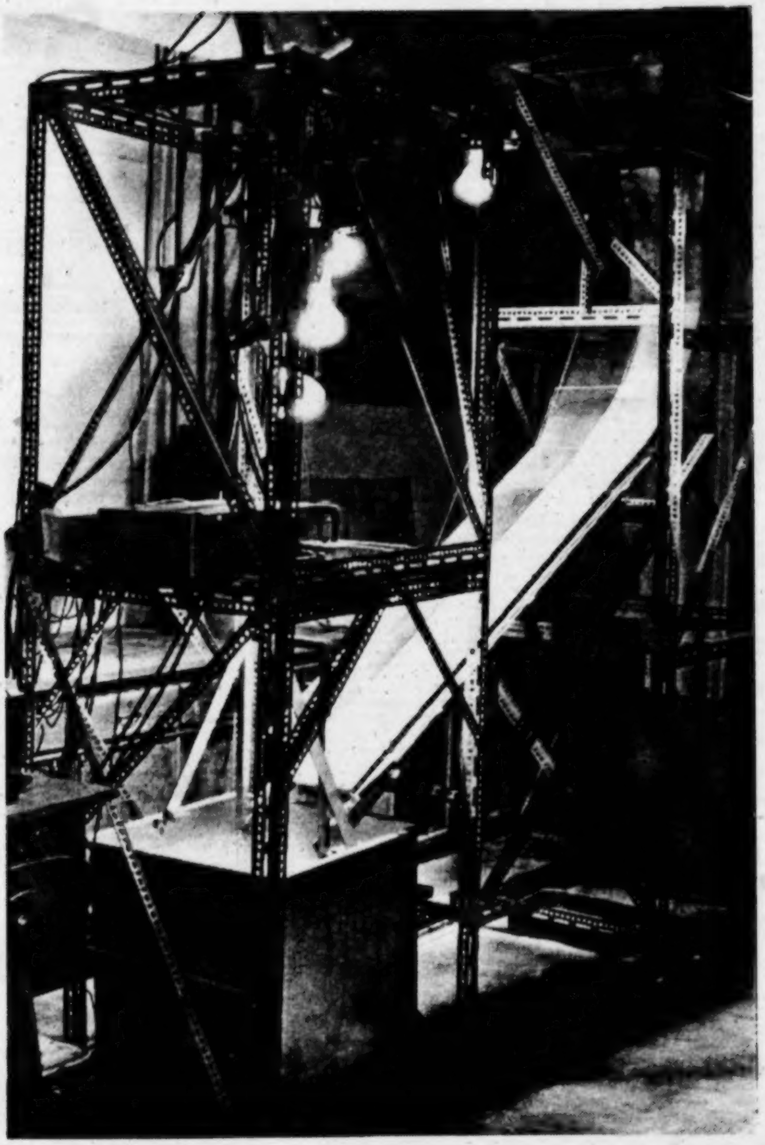

Figure 11.2 An overall view of the flume apparatus.

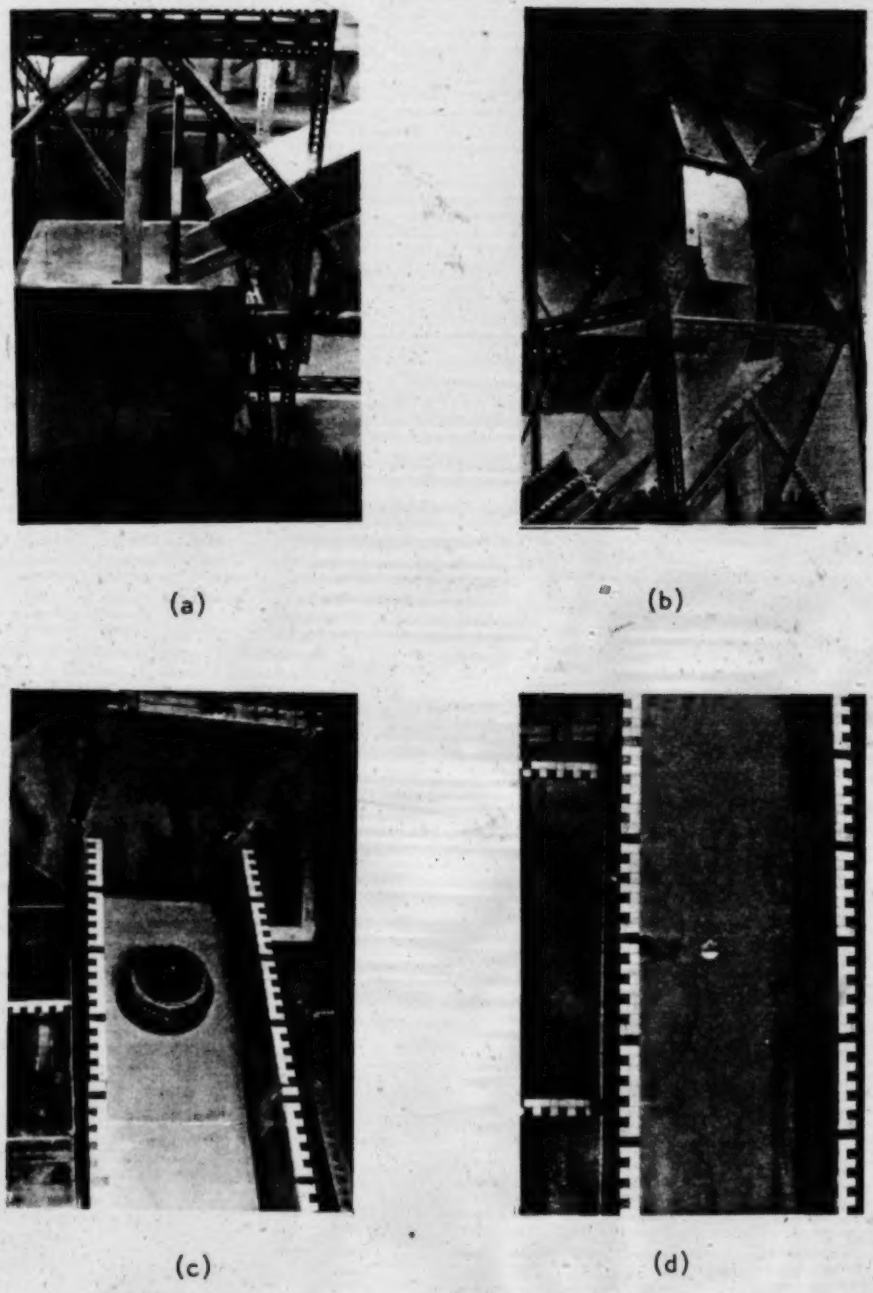

Figure 11.3 (a) End of the flume and the receiving pan, (b) hopper and knee, (c) calibration of the shear table using weights, (d) flume bed with observation windows and scale strips.

was possible to derive the basic parameters of the flows as functions of time. A flow chart in Figure 11.4 explains how these principal variables (shown in bold frames) derive from the primary measurement parameters.

The measurements were conducted by the following means (Fig. 11.1):

a. The receiving pan was suspended on a load cell, which continuously monitored its increase in weight (Fig. 11.3a). The mass flow rate out of the measuring flume in kg/sec was obtained by differentiating this record. The pan was kept from rocking by a set of vertically mounted balancing wheels.

b. The upper end of the flume was mounted on a hinge, while the lower end was suspended by a stiff load cell. this provided a continuous record of the weight of one end of the flume, while sand was flowing over it. Combining this with flow thicknesses along the flume length, it was possible to calculate the mean density of the flowing material. Since the calculation was based on moment equilibrium with respect to the hinged end, the density values are biased towards the lower end of the flume. This is convenient, as other measurements were being conducted near this end as well.

c. A high speed camera (used at 200 and 400 frames per sec) with wide angle lens was placed above the flume

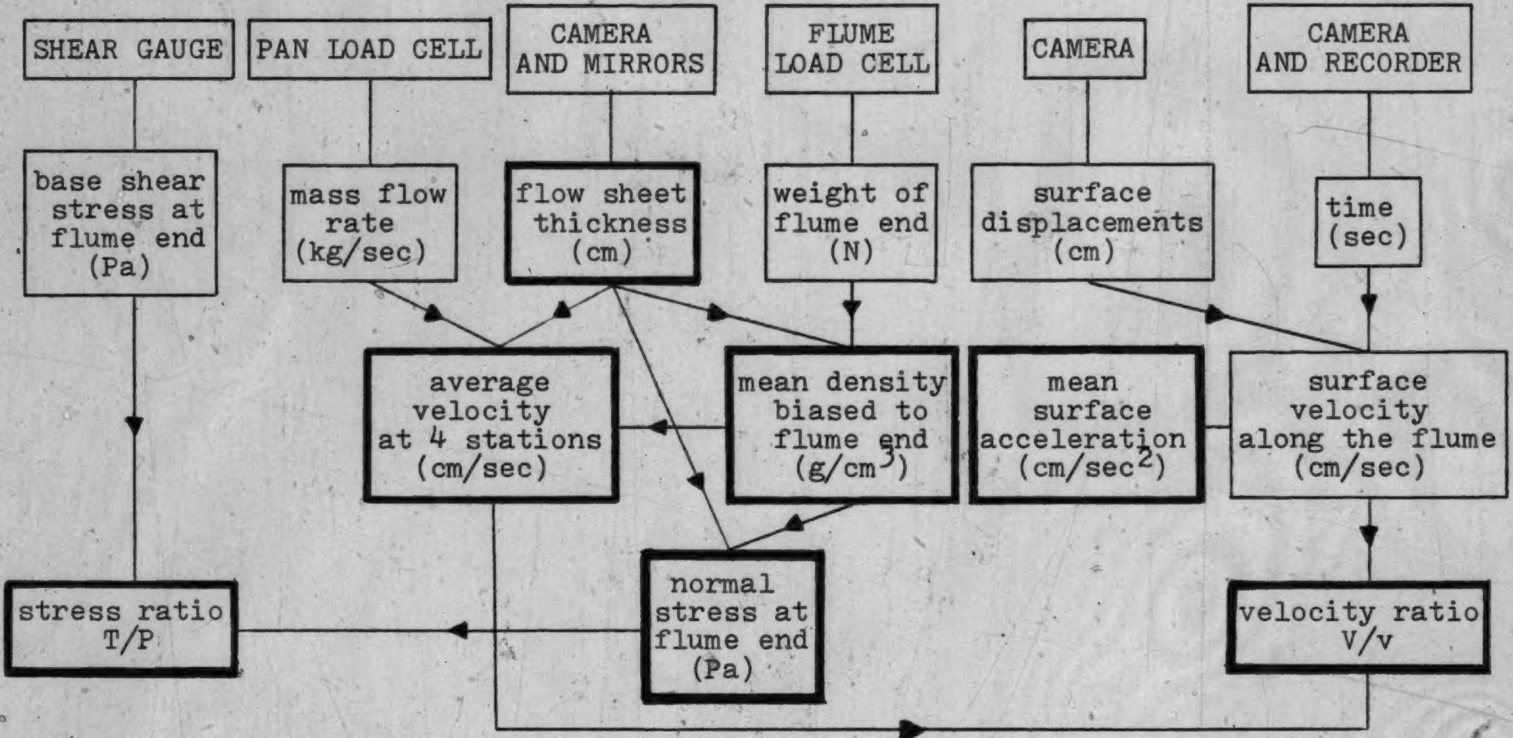
SHEAR GAUGE
PAN LOAD CELL
CAMERA AND MIRRORS
FLUME LOAD CELL
CAMERA
CAMERA AND RECORDER
base shear stress at flume end (Pa)
mass flow rate (kg/sec)
flow sheet thickness (cm)
weight of flume end (N)
surface displacements (cm)
time (sec)
average velocity at 4 stations (cm/sec)
mean density biased to flume end (g/cm³)
mean surface acceleration (cm/sec²)
surface velocity along the flume (cm/sec)
normal stress at flume end (Pa)
stress ratio T/P
velocity ratio V/v

Fig. 11.4 Flow chart of the system of measurements

Bold frames designate primary output variables so as to be able to observe almost its entire length. A long mirror was placed alongside the flume and tilted 45 deg. with respect to the flume wall (see inset of Fig. 11.1). A side view of the flow was thus obtained on the same film where the surface could also be observed (see Fig. 11.6). Vertical scale strips were glued on the Perspex wall of the flume at four measuring stations, located at 10, 50, 90 and 130 cm down from the upper end. The flow thickness could thus be read off the film at these four locations without the need for any geometrical adjustments. During the course of the experiments, a second mirror was added on the other side, as it was recognized that greater precision could be obtained by averaging the flow thickness on the two sides of the flow. The difference between the two sides was negligible in all but the fastest experiments.

d. Coloured plastic beads were mixed with the test material in small quantities, and could be observed on the picture of the flow surface (Fig. 11.6) Their progress down the flume could be measured in successive frames with the help of scale strips mounted on top of the flume walls, which can also be observed in the figure. A slight geometrical adjustment to the displacement values, dependent on flow thickness, was necessary near both ends of the flume, where the angle of observation was relatively

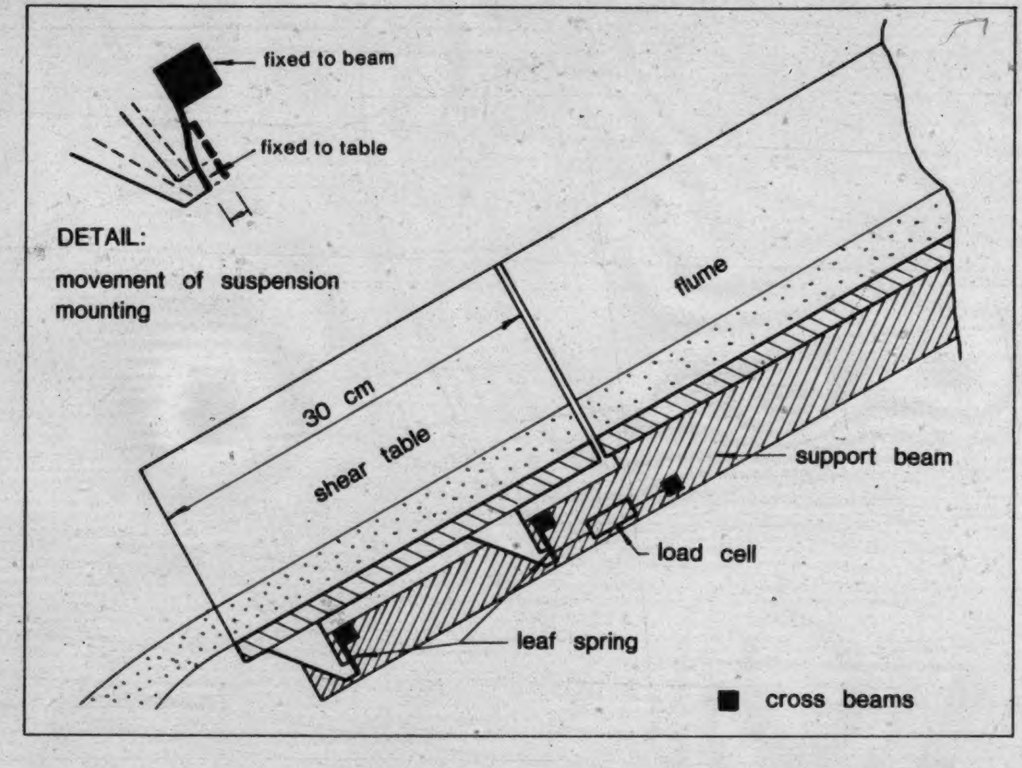
fixed to beam
fixed to table
DETAIL:
movement of suspension mounting
flume
30 cm
shear table
support beam
load cell
leaf spring
■ cross beams

Figure 11.5 Principle of the bed shear measuring device.

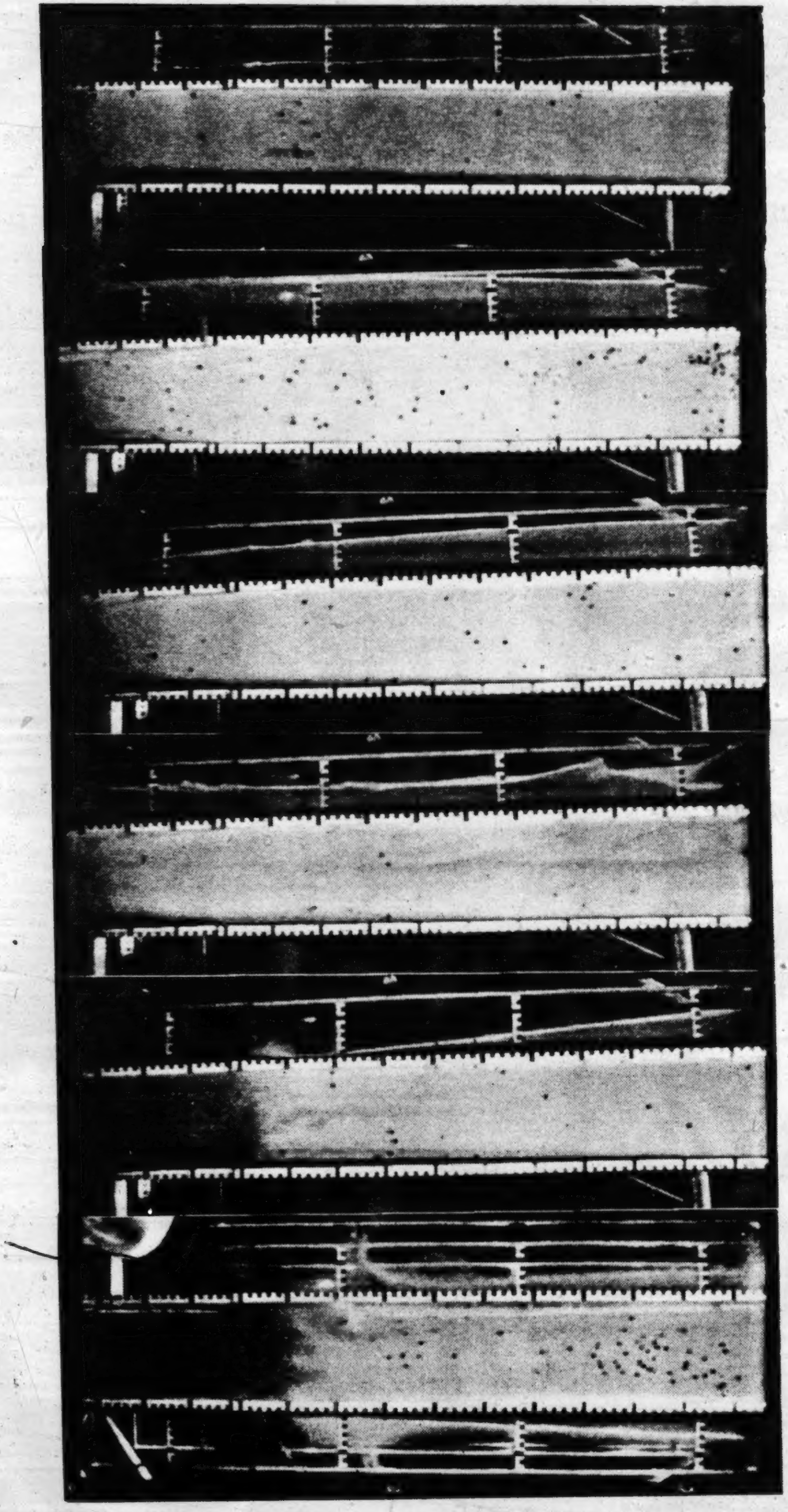

α = 28.4°

v = 25 cm/sec

stagnant wedge

α = 33.6°

v = 170 cm/sec

α = 33.6°

v = 350 cm/sec

α = 33.6°

v = 520 cm/sec

cloud of saltating particles

α = 33.6°

v = 260 cm/sec

front

α = 33.6°

v = 500 cm/sec

front

Flow is from left to right

Figure 11.6 Examples from the camera records.

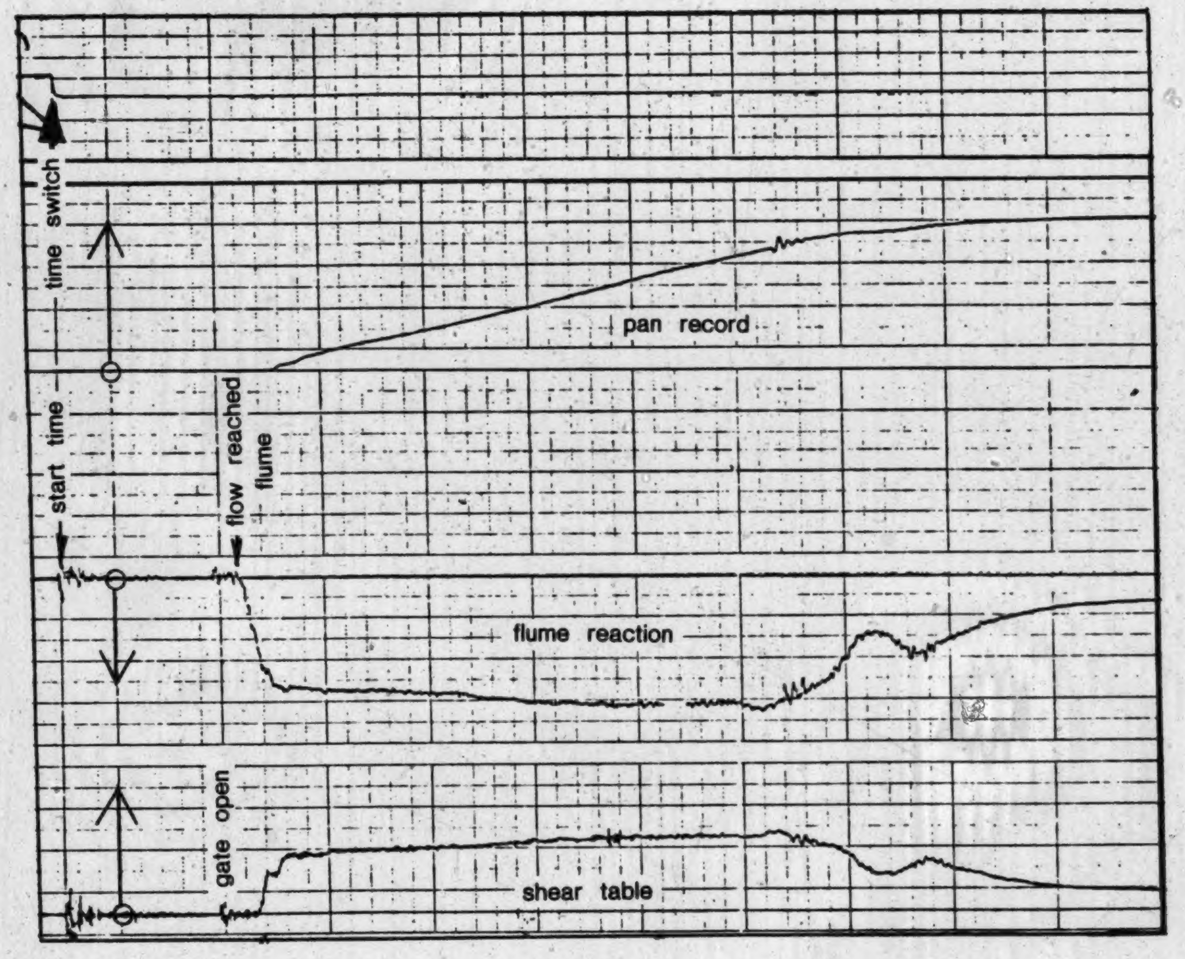

Figure 11.7 An example of the chart record.

sharp. Surface velocities were determined by a numerical differentiation of the successive displacements for groups of four particles at a time, in order to reduce measurement error.

e. The last 30 cm of the measuring flume were detached from the remainder and hung on suspension mountings allowing free longitudinal desplacements (Figs. 11.3c and 11.5). A stiff tension load cell was used to measure the total shear force applied by the sand to this section (both base and walls). The shear stress on the bed was calculated by correcting for the estimated value of the side friction. The value of the correction was found to be rather small, especially for the thinner flows. Details are given in Section 11.6.

f. Time was recorded separately for the camera and the gauge readings. The camera was equipped with a timer strobe which produced tic marks with a 0.01 sec period on the edge of the film. The gauges were timed by the movement of a six channel simultaneous chart recorder with a time marker. The two timing devices were synchronized using a visible switch similar to that used in sound cinematography.

The complete record thus consisted of a film of the experiment consisting, typically, of 2000 to 3000 frames and a chart record containing the traces of the three load cell channels. The load cells were calibrated to establish their linearity, stability and lack of hysteresis, all of which proved satisfactory. A two point calibration was, in addition, carried out and recorded on the chart prior to each individual experiment. A typical example of the chart record is shown in Figure 11.7.

Processing of the data began by a manual collection of flow thickness values and beads displacements from the films. Thicknesses at the four measuring stations were collected at sampling points spaced at 0.2 and 1.0 sec intervals, depending on the speed of the test. The values of mass flow rate, flume weight and bed shear were obtained at the same intervals by measuring with a precise ruler, under magnification, from the amplitudes of the chart record. [25] The required differentiation of the pan weight record, to obtain mass flow rate, was done graphically, by constructing tangents to the recorded line. This method was found to be considerably more precise than numerical differentiation which was attempted earlier. A computer program was used to combine the flow thicknesses and gauge records and to produce the following output variables (for details of the numerical procedures implemented by the program, cf. Section 11.6):

Flow sheet thickness at stations located 10, 50, 90 and 130 cm past the start of the measuiring flume.

---

[25] A four channel tape recorder was used initially to transfer load cell data directly into the computer. This machine was found to be unreliable and the data processing from it too complex. Therefore, it was decided to rely on the simpler process using the chart recorder.

Mean density of the flow sheet, linearly biased to the flume end.

Mean velocity at the four measuring stations.

Normal stress, P, on the base of the flume at the fourth station, 20 cm before the end.

Tangential stress, T, on the base of the flume at the same point, and the stress ratio T/P.

Displacements of the flow surface were measured near two time points, selected so as to lie in the interval of steady flow near the middle of the experiment. At each of these points, a group of four coloured particles was chosen and ~~its~~ displacements measured at 5 to 8 successive time intervals as it progressed down the flume. Average surface velocities were then calculated for each of these time intervals and a mean acceleration value was obtained as the slope of a line, fit to the velocity- time record of each of the two particle groups. The use of four particles at a time was found necessary, in order to reduce measurement error by averaging. Also, any systematic difference between the velocities of individual particles (which were also calculated) would indicate the existence of a lateral velocity profile caused by wall friction. No such systematic velocity variation was found, however, as shown in Fig. 11.8. A sample of an output table produced by the test data processing programs from a single run is shown as Table 11.3.

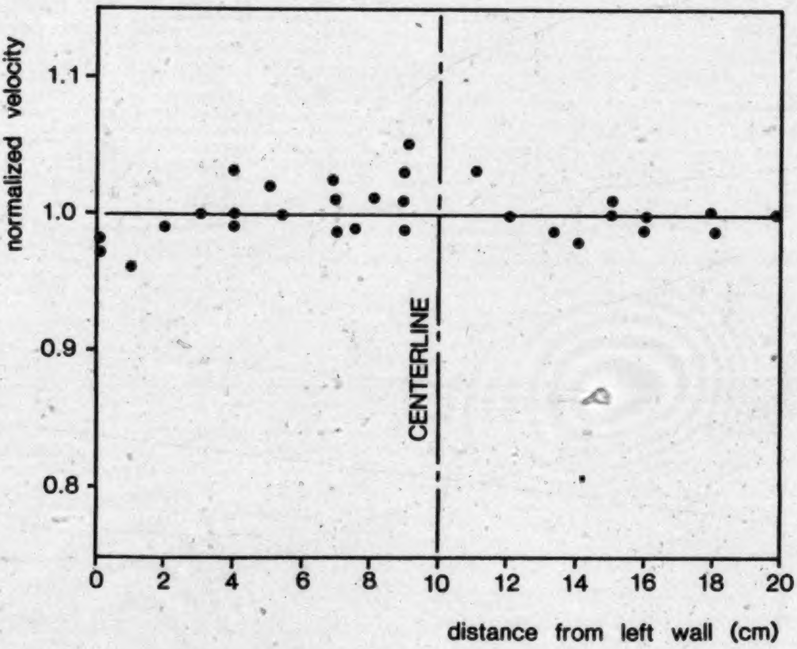

Figure 11.8 Velocities of individual particles normalized with respect to the velocity of the group.

```
GRAIN FLOW TEST NO.   26
ANGLE =25.22 DEG.

TIME  MASS FLOW   H50     H90       H130    V50       V90      V130      A AVG      GAM        N       SIG        TAU       A EQ.       FI
(SEC)  (KG/SEC)   (CM)    (CM)      (CM) (CM/SEC) (CM/SEC)(CM/SEC)  (CM/SEC2)  (G/CM3)           (GF/CM2)   (GF/CM2) (CM/SEC2)  (DEG)

 2.0    12.2      3.9     3.6       2.2     204.      183.     257.     141.8     1.602    0.396     3.19       1.77    -88.99     28.99
 3.0    31.9      4.2     4.9       4.8     277.      237.     241.    -107.5     1.382    0.478     6.00       3.18    -85.80     27.92
 4.0    32.4      4.3     5.2       5.2     258.      216.     219.    -106.5     1.381    0.479     6.50       3.20    -55.40     26.23
 5.0    30.3      4.6     5.6       5.6     229.      192.     195.     -80.8     1.327    0.499     6.73       3.31    -58.01     26.22
 6.0    27.6      4.6     5.6       5.8     224.      184.     178.    -104.5     1.334    0.497     7.00       3.35    -46.76     25.56
 7.0    27.6      4.4     5.1       5.7     124.      133.     142.      30.5     1.356    0.488     6.99       3.21    -29.50     24.68
 8.0    15.1      2.5     2.8       3.5      88.      108.     122.      48.0     1.254    0.527     3.97       2.12    -80.95     28.13

SURFACE VELOCITIES, TEST NO.  26  ANGLE=  25.22 DEG.


DISPL.(CM)    TIME(SEC)  VEL.(CM/SEC)

     16.1     3.1889     313.9
     33.2     3.2444     304.4
     50.1     3.3000     303.9
     66.9     3.3556     298.7
     83.3     3.4111     291.5
     99.4     3.4667     291.0
    115.4     3.5222     281.5
    131.0     3.5778     280.6
AVERAGE TIME=     3.3833 SEC.
AVG. ACCELERATION=      -84.17CM/SEC2
INDIVIDUAL PARTICLE VEL. (CM/SEC):       294.0       294.3       292.3       301.7

DISPL.(CM)    TIME(SEC)  VEL.(CM/SEC)

     15.5     6.4833     317.2
     32.8     6.5389     307.2
     50.0     6.5944     312.0
     67.2     6.6500     304.4
     84.0     6.7056     300.6
    100.4     6.7611     289.6
    116.4     6.8167     286.3
    132.2     6.8722     282.5
AVERAGE TIME=     6.6778 SEC.
AVG. ACCELERATION=      -89.68CM/SEC2
INDIVIDUAL PARTICLE VEL. (CM/SEC):       301.1       309.9       294.9       296.7
```

Table 11.3 An example of the processed test data.

In all, 25 succesful tests were run with Ottawa sand, 8 with polystyrene beads, 5 with angular sand and 6 with mixtures of angular sand and rock powder. Approximately 20 preliminary runs preceded and served to indicate necessary changes and improvements in the testing technique. Some 10 tests were aborted due to various malfunctions.

11.4 Results

The major finding of this testing program is, that the internal friction angle of the various materials shows absolutely no systematic dependence on the shear strain rate. In other words, even during the most rapid flows, at mean velocities of over 5 m/sec, the materials continued to behave as Coulomb frictional solids, with friction angles only slightly lower than the quasi- static constant volume angle. This conclusion derives both from direct measurement of stresses at the base of the flow and from the fact that nonaccelerating flows could only be established on slopes near this particular angle.

There was a slight reduction in bulk density with increasing flow speed, amounting to some 10 to 20 per cent over the spectrum of velocities achieved. At any given velocity, the density was not affected by flow thickness, but only as long as the latter was not less than 3 cm.

The fully developed flows tended to assume nearly linear vertical velocity profiles. Slower flows tended to deposit stagnant layers, particularly in the corners of the flume. Faster, probably not fully developed flows exhibited substantial base slips, approaching the condition of a plug flow. These general findings are further expanded on in the following paragraphs.

A summary of the friction measurement data is given in Figs. 11.9, 11.10 and 11.11. The large diagram in each figure shows the distribution of the friction coefficient, calculated as the ratio of the measured shear to normal stresses at the base of the flow, with the mean velocity. Each of the points plotted represents a sampling point during the course of a test; approximately 2 to 12 points derive from each test. The data is sorted with respect to the thickness of the flow, represented in the form of the normal stress P at the base. The symbols appropriate to each category of P are given in the legend. A large triangle shows the friction coefficient corresponding to the lower value of the angle of repose for each material. The data shows a considerable amount of scatter, especially in the case of the angular sand, but less so in the case of polystyrene beads. The scatter is due mainly to the imprecision in measuring flow thickness from the films, as explained in Section 11.7. This was especially serious for angular sand, due to the presence of dust.

The trends of change in friction coefficient with increasing velocity are negligible in all three materials, as shown by the best fit lines drawn across the diagrams.

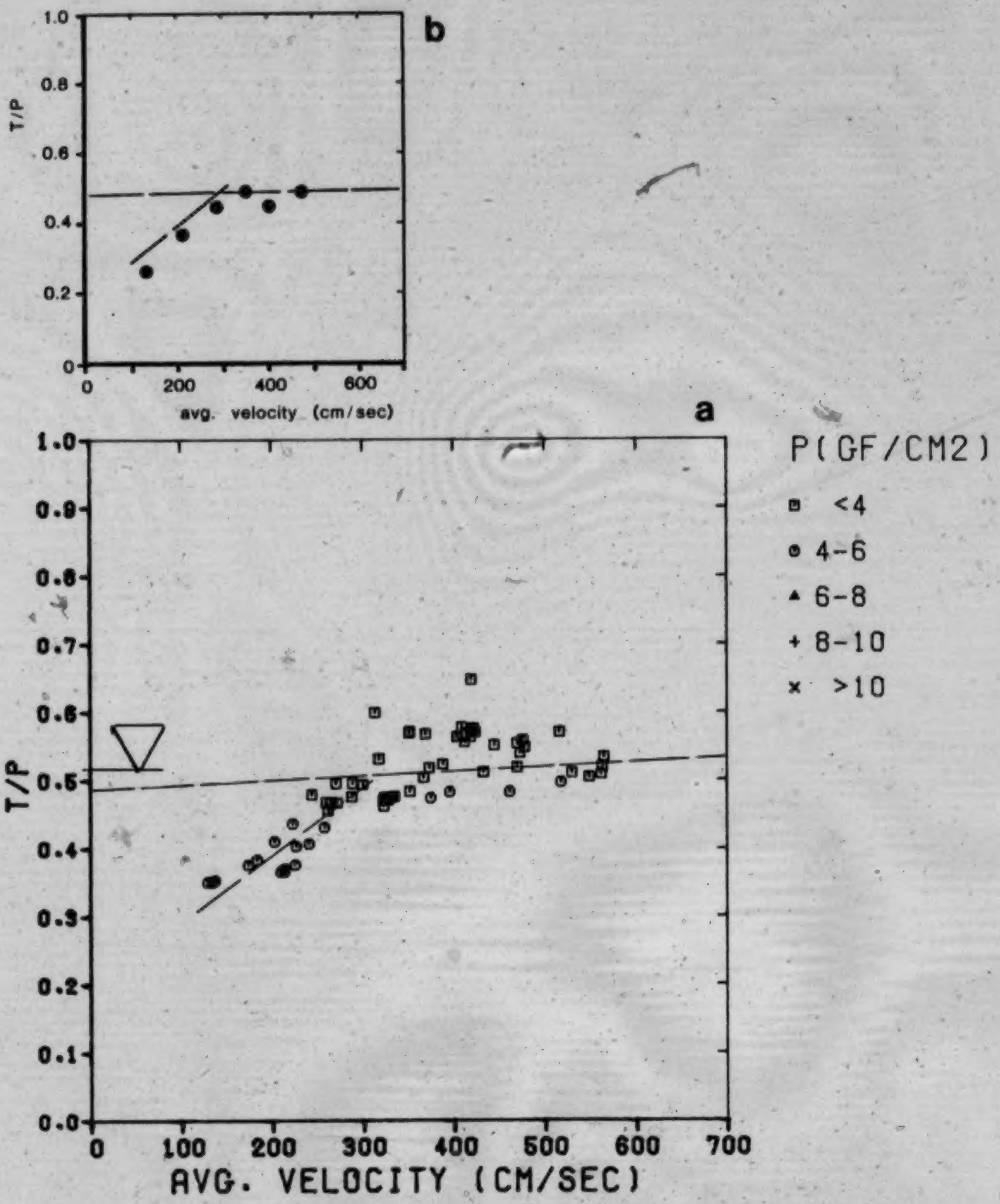

Figure 11.10 Bed friction coefficient, Polystyrene beads. (a) From direct measurement, (b) from accelerations.

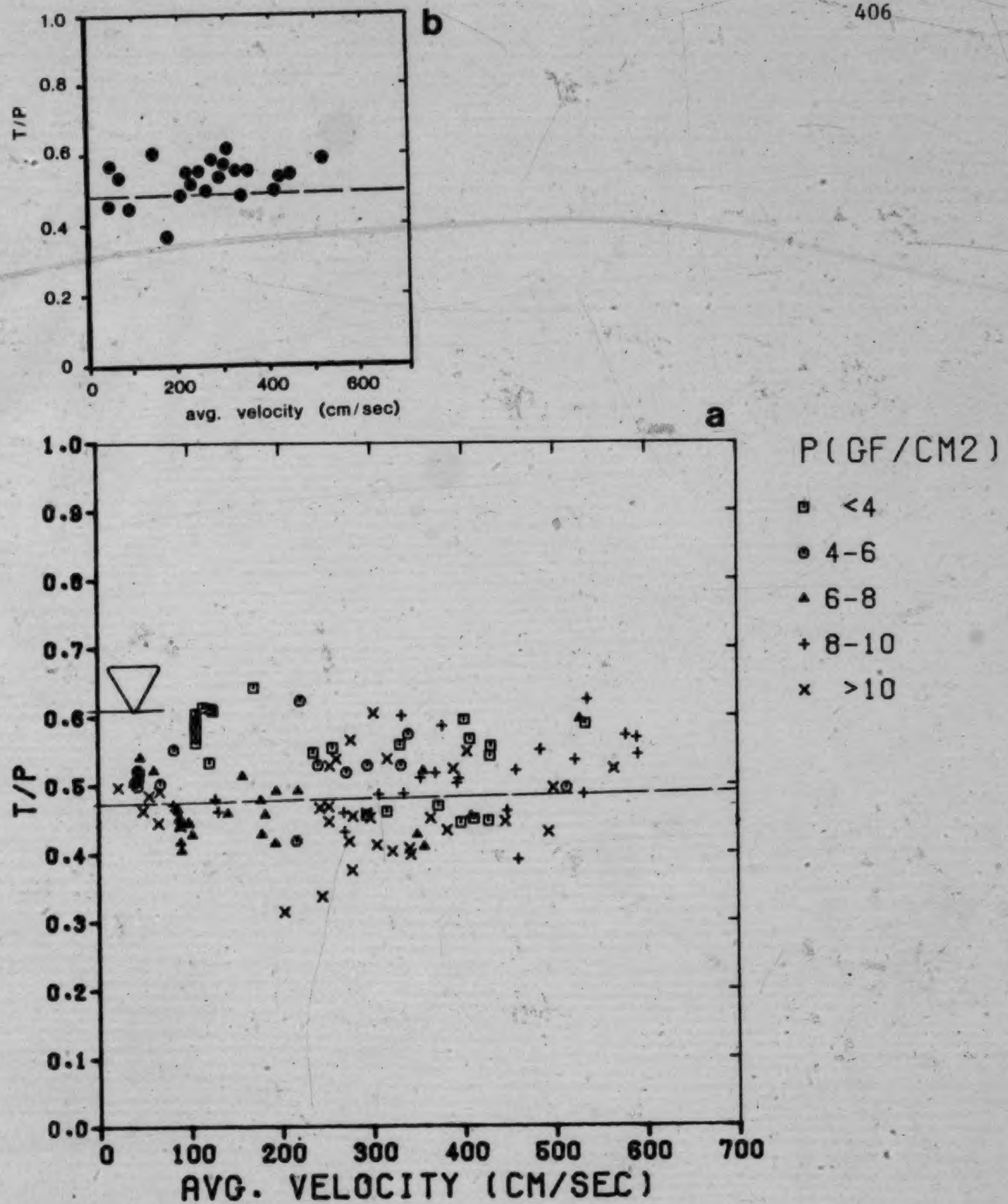

Figure 11.9 Bed friction coefficient, Ottawa sand. (a) From direct measurement, (b) from accelerations.

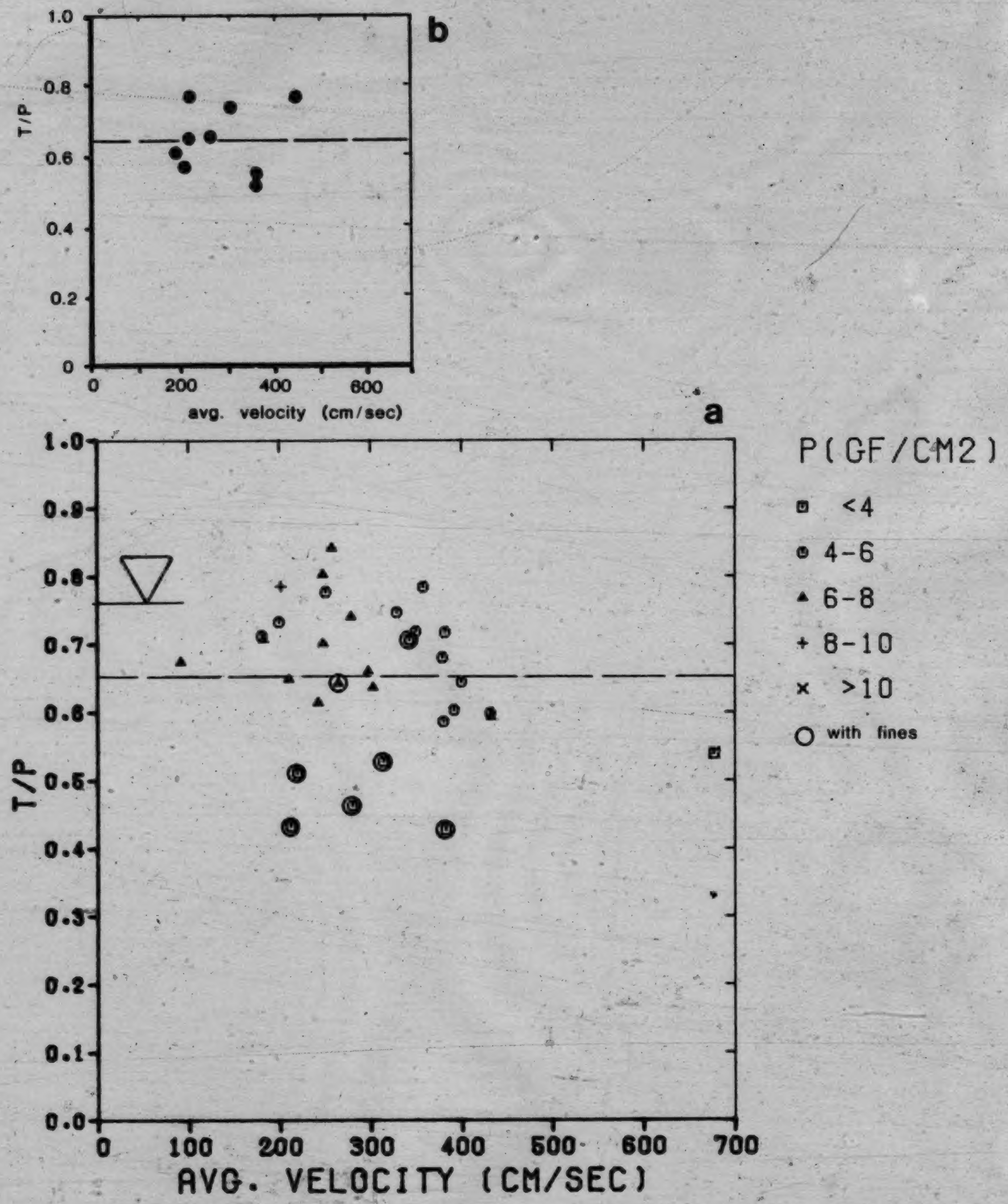

Figure 11.11 Bed friction coefficient, angular sand. (a) From direct measurement, (b) from accelerations.

The Ottawa sand exhibits an essentially constant internal friction coefficient of about 0.49, corresponding to an angle of 25.5 deg., or about six degrees below the lower value of the angle of repose. Similar result was found for the angular sand, the average angle being equal to 33 deg. Tests using mixtures of angular sand with more than 50 percent by weight of rock flour are accentuated in Fig. 11.11 by large circles. These show somewhat reduced friction angles, as might be expected even under quasi- static conditions. But no strong trend towards reduction with increasing velocity is apparent. The friction angle of the polystyrene beads (Fig. 11.10) increases with velocity. The main group of the experimental points lies near a line intercepting the ordinate near the quasi- static friction coefficient of 0.52 (corresponding to an angle of 27 deg) and rising by about 1.5 percent for each 100 cm/sec of mean velocity. A smaller group of points indicates a downturn of the trend at lower velocities, with a minimum of 0.37 (20 deg.) near 120 cm/sec.

These results were checked also by deriving the stress ratio T/P from surface acceleration records, and plotting the results in the small diagrams shown at the top of the three figures. The general equation of motion of unsteady, nonuniform flow in open channels was used for this purpose:

$$\beta v \frac{\delta v}{\delta x} + \frac{\delta v}{\delta t} - g \sin\alpha + g \cos\alpha \frac{\delta H}{\delta x} = \frac{-\tau}{\rho H} \qquad \text{Eqn. (11.1)}$$

where v is the mean velocity, x the distance along the flume, t time, α flume inclination, ρ bulk density, H flow thickness and τ shear stress at the base. The term is the velocity distribution coefficient (Chow, 1959).

The acceleration term can be simplified using:

$$\beta v \frac{\delta v}{\delta x} + \frac{\delta v}{\delta t} = a$$

Eqn. (11.2)

which is valid, because of the method used to derive surface acceleration by following the motion of a given group of particles. The pressure term was re- defined to account for the behaviour of granular material, assuming that the normal stress parallel with the base of the flow equals k times the perpendicular normal stress, where k is a lateral pressure coefficient assumed equal to 0.75. The equation of motion could then be simplified approximately as:

$$\frac{\beta}{\cos\alpha}\,\frac{a}{g} - \tan\alpha + 0.75\frac{\delta H}{\delta x} = -\frac{\tau}{\cos\alpha\,\rho g H} = -\frac{T}{P} + S$$

Eqn. (11.3)

(The correction factor S was added to account for the side friction.) This was used to derive the points shown in the small diagrams. Although the pairs of plots shown in each of the three figures are derived from entirely different measurements (shear table and surface accelerations), they show very similar results, especially where trends are concerned. This comparison therefore proves the absence of a systematic error in the measurements.

An alternative use of the acceleration data is shown in figure 11.12, which summarizes surface velocities and slope angles at one point of each of the experiments with Ottawa sand, indicating at the same time whether the flows were accelerating or decelerating. Only two flows had accelerations whose absolute values were small enough (less than 15 cm/sec^2) so that they could be classified as nonaccelerating flows. These occurred at an angle of approximately 28 deg. or 2.5 degrees above the measured average base shear stress from Fig. 11.9. This difference probably represents the influence of the side friction, for which the data in Fig. 11.9 have been corrected.

The terms "uniform flow" and "nonaccelerating flow" are not synonymous in the case of granular materials, due to density changes. This is illustrated by Figures 11.13 through 11.16, which show the complete surface velocity and flow thickness fields for four typical tests run on Ottawa sand. Surface velocity variations in space and time are shown on the left in a form of bar diagrams and velocity contours. Flow thicknesses are shown on the right as bar diagrams only. Fig. 11.13 shows an accelerating test, with velocities exceeding 250 cm/sec. Despite the increasing speeds, the flow thickness remains relatively uniform due to changes in mean density and in vertical velocity distribution as will be discussed later. The flow in Fig. 11.14 is nonaccelerating and relatively slow. In a pattern that was found typical of flows slower than about 150

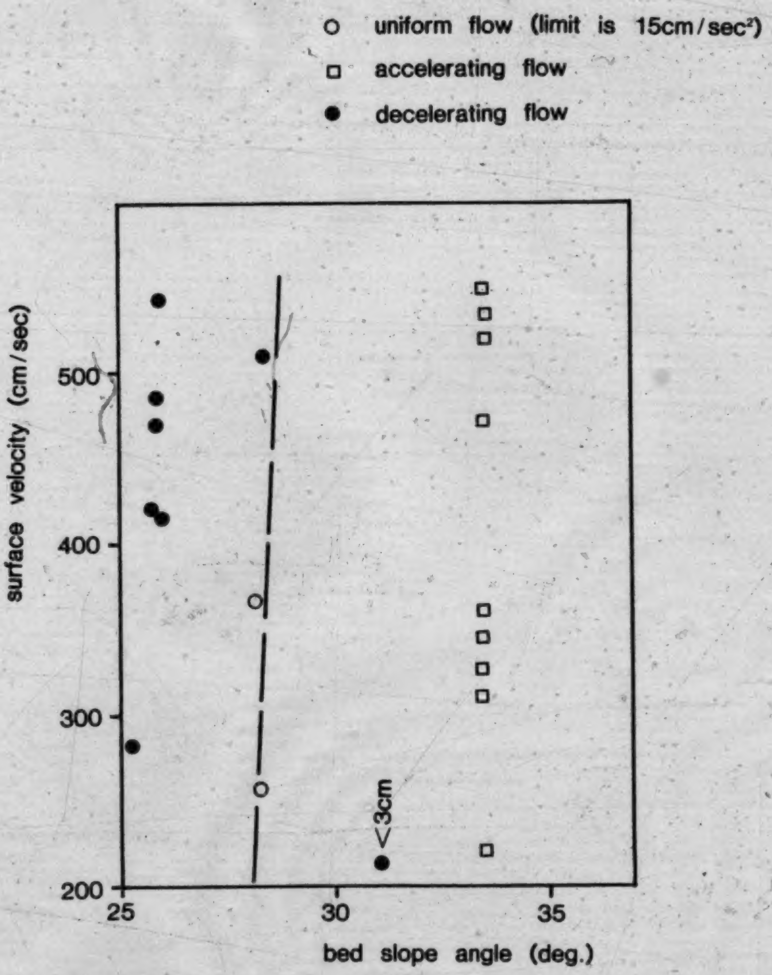

Figure 11.12 Flow classification versus bed slope angle and surface (maximum) velocity.

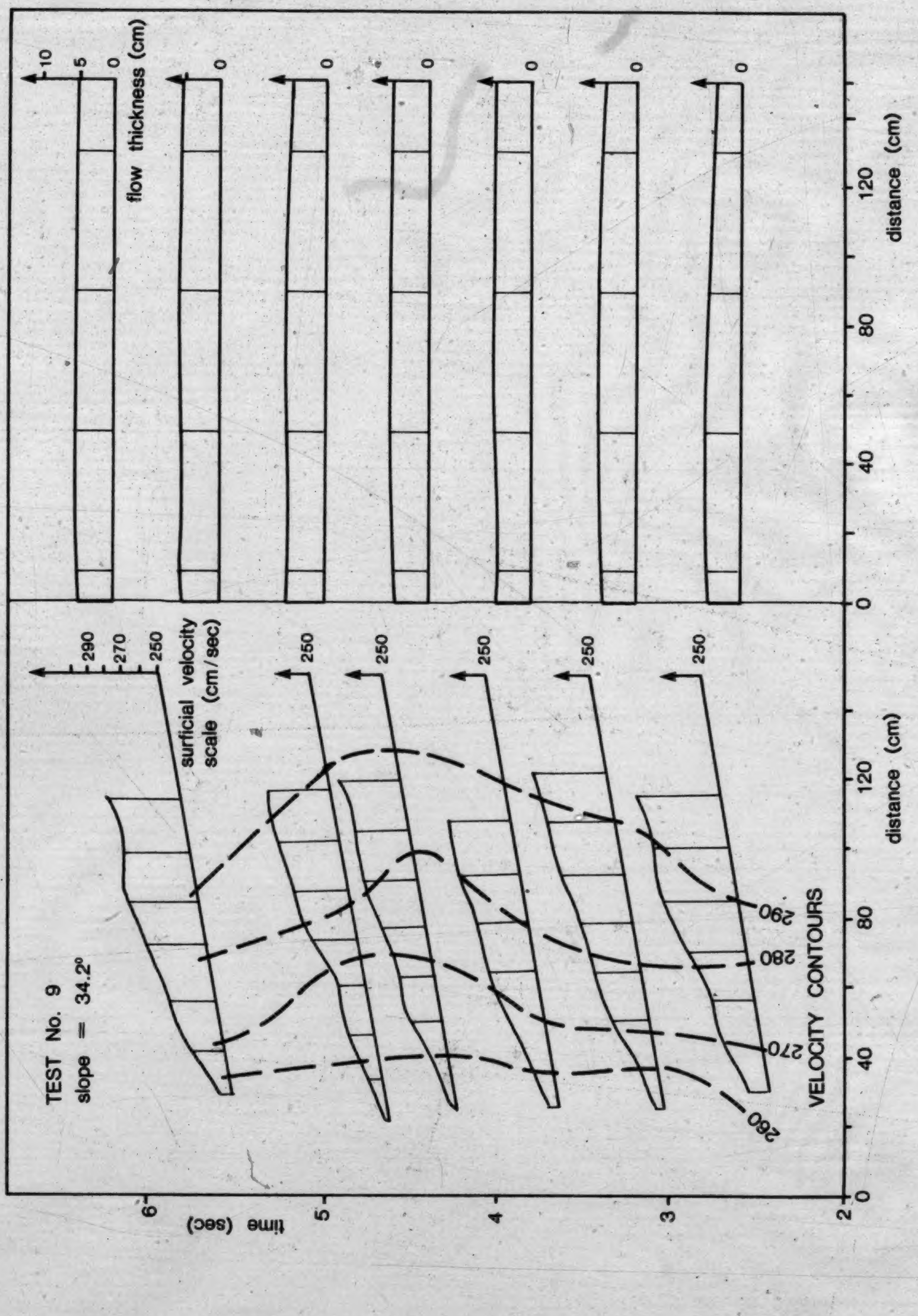

Figure 11.13 Velocity and flow thickness vs. time and position on the flume, Test No.9.

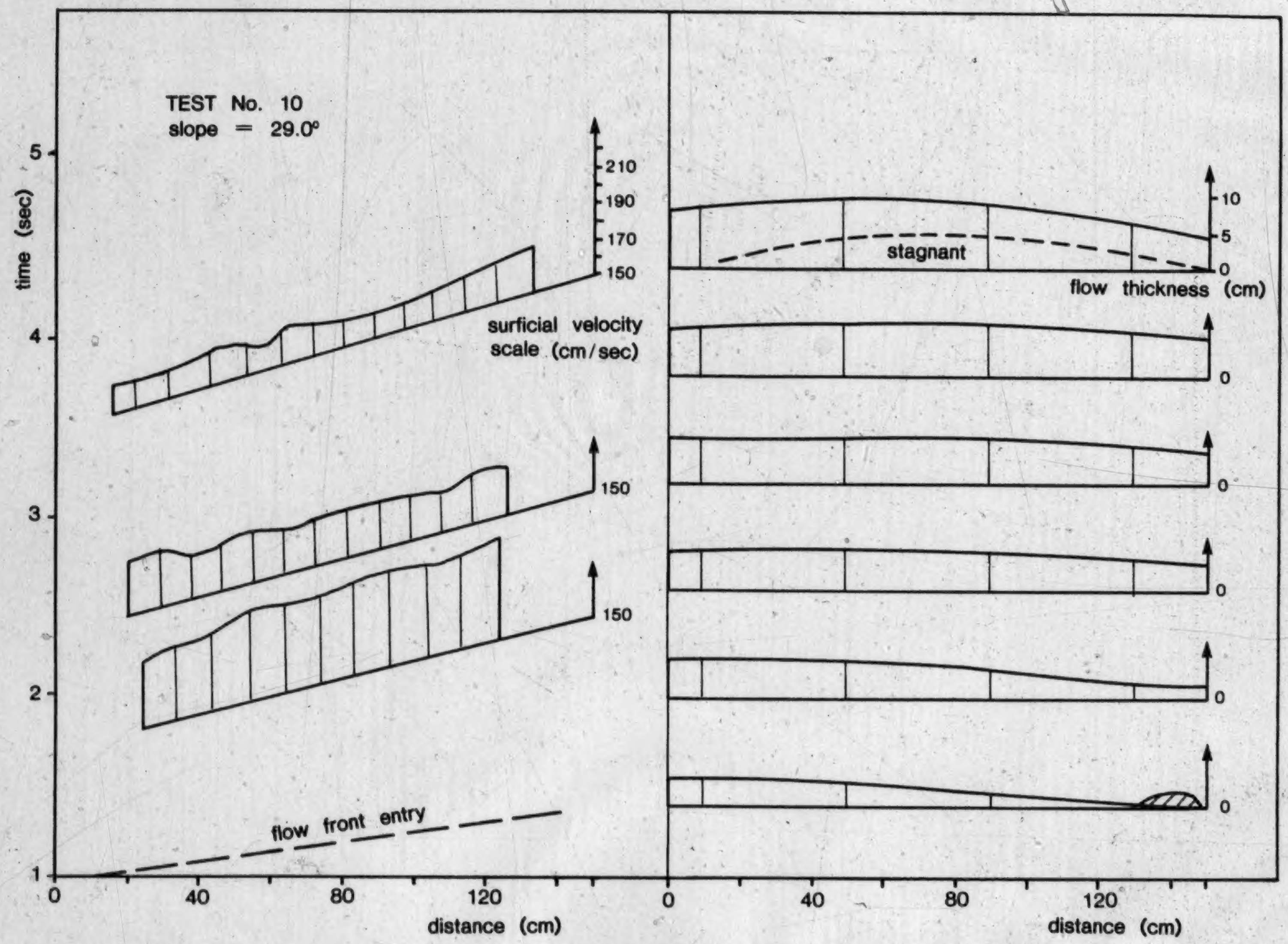

Figure 11.14 Velocity and flow thickness vs. time and position on the flume, Test No. 10.

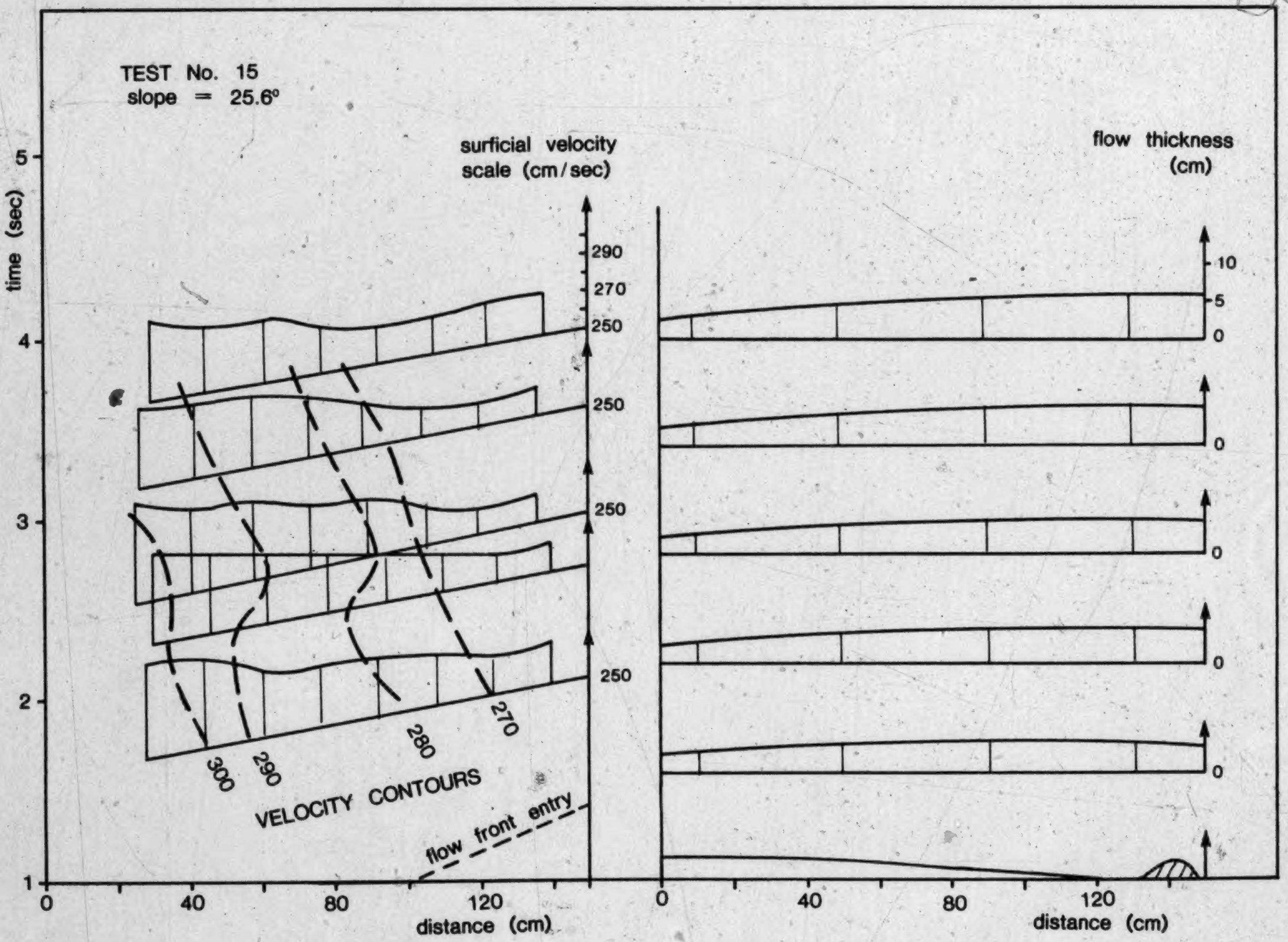

Figure 11.15 Velocity and flow thickness vs. time and position on the flume, Test No.15.

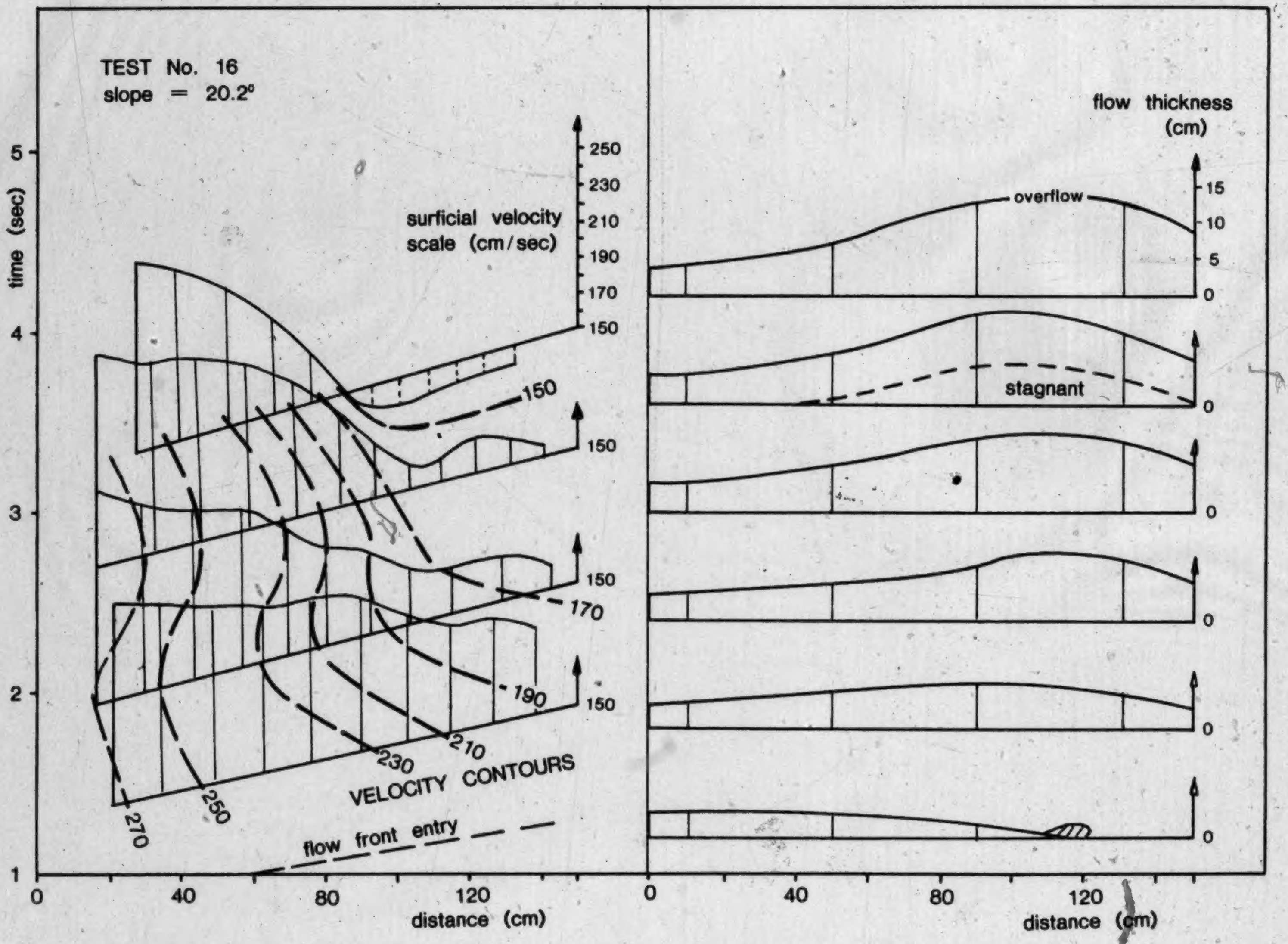

Figure 11.16 Velocity and flow thickness vs. time and position on the flume, Test No.16.

cm/sec, a wedge- shaped stagnant layer developed near the upstream end of the flume, leading to a gradual thickening of the sand sheet in that area and thinning towards the end. Two decelerating flows are represented by Figures 11.15 and 11.16. The first is fast enough to maintain full- thickness of the flow for the length of the flume, with only a gradual thickening to account for the slight decrease in velocity and change in the vertical velocity distribution. The last test is seen to decelerate very sharply below 150 cm/sec due to the very flat slope. Again, a build up of a stagnant mass is observed at the lower velocities, somewhat as indicated by the dashed line drawn in the second thickness profile from the top. The thickening eventually led to an overflow during this experiment. It does not, however, represent a hydraulic jump as all of the flows observed in these experiments were supercritical with Froude numbers considerably above 1.0.

Plots of average bulk density values versus mean velocity appear in Figs. 11.17, 11.18 and 11.19. Again, a similar scatter is observed as in the case of T/P, in fact the random error probably has its origin in the bulk density determination. The trends are again readily apparent, though. All three materials decrease in density, starting from an intercept equal to the loosest static piling and with an average rate of drop of about 0.02 g/cu.cm per 100 cm/sec. The density also varies with thickness of the flow which is a measure of the normal stress acting on the base.

This was investigated by obtaining least squares best fit lines for each of the normal stress categories shown in the legend of Fig. 11.17. The intercepts of these lines with the ordinate at velocities of 100 and 500 cm/sec are plotted against the normal stress in Fig. 11.20. It is found that, at normal stresses exceeding about 5 gf/sq.cm (corresponding to a flow thickness of 3.5 cm), the density remains relatively constant, being close to the static density at the lower speed and somewhat less at the highest. At lower normal stresses, on the other hand, an abnormal degree of dispersion is seen to occur. The plots of T/P presented previously did show some rather unsystematic trend towards an increase of this parameter with thinner flows. This suggests that thin flows may be controlled by a somewhat different mechanism and that one should be careful in extrapolating information obtained from them.

The last aspect studied in detail is the flow velocity profile. This was firstly characterized by the velocity ratio, defined as the ratio of maximum (surface) to mean flow velocity. A plot of the velocity ratio versus mean velocity is shown in Fig. 11.21, as determined from the Ottawa sand tests at both the 50 cm and 90 cm measuring stations (i.e. near the middle of the flume.) It is seen to decrease strongly for faster flows. On average, the velocity ratio is greater than 2 at velocities of less than 150 cm/sec, indicating the existence of a stagnant layer at the base. This was actually observed during the experiments. Two

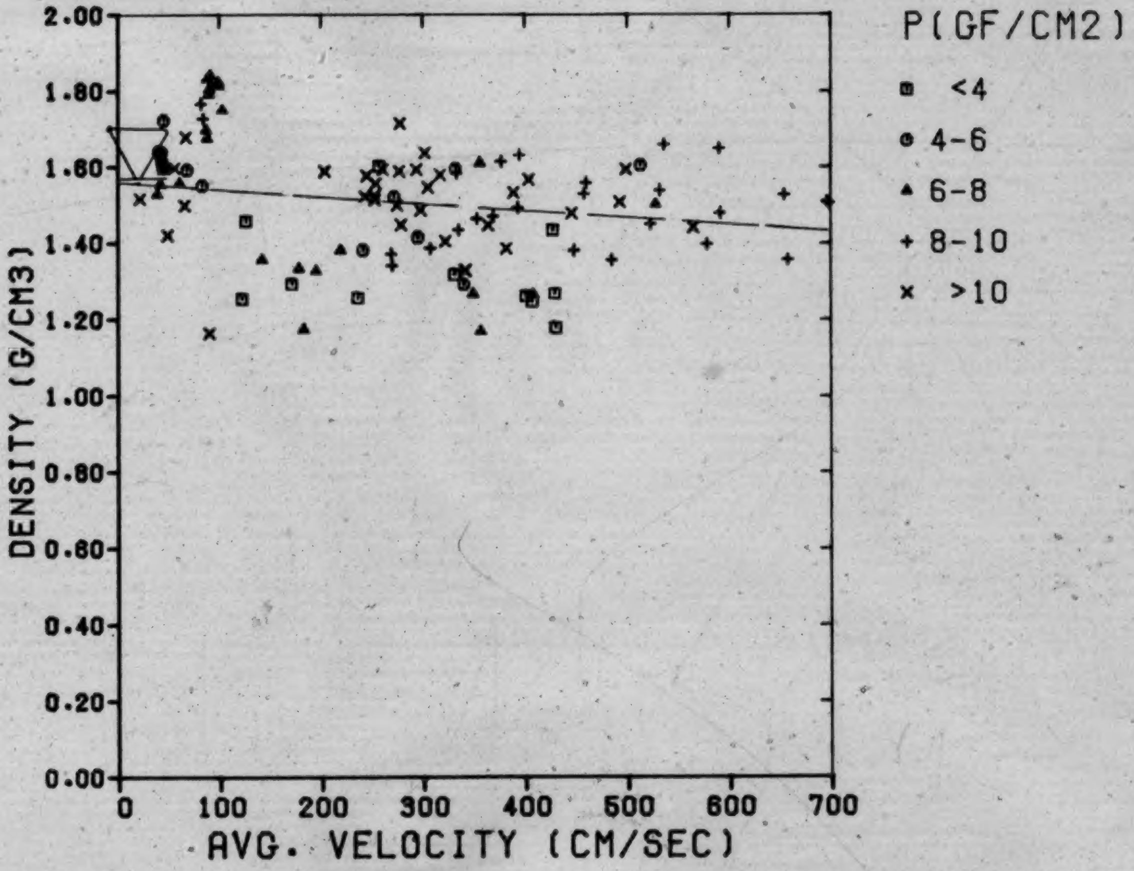

Figure 11.17 Density of Ottawa sand during flow.

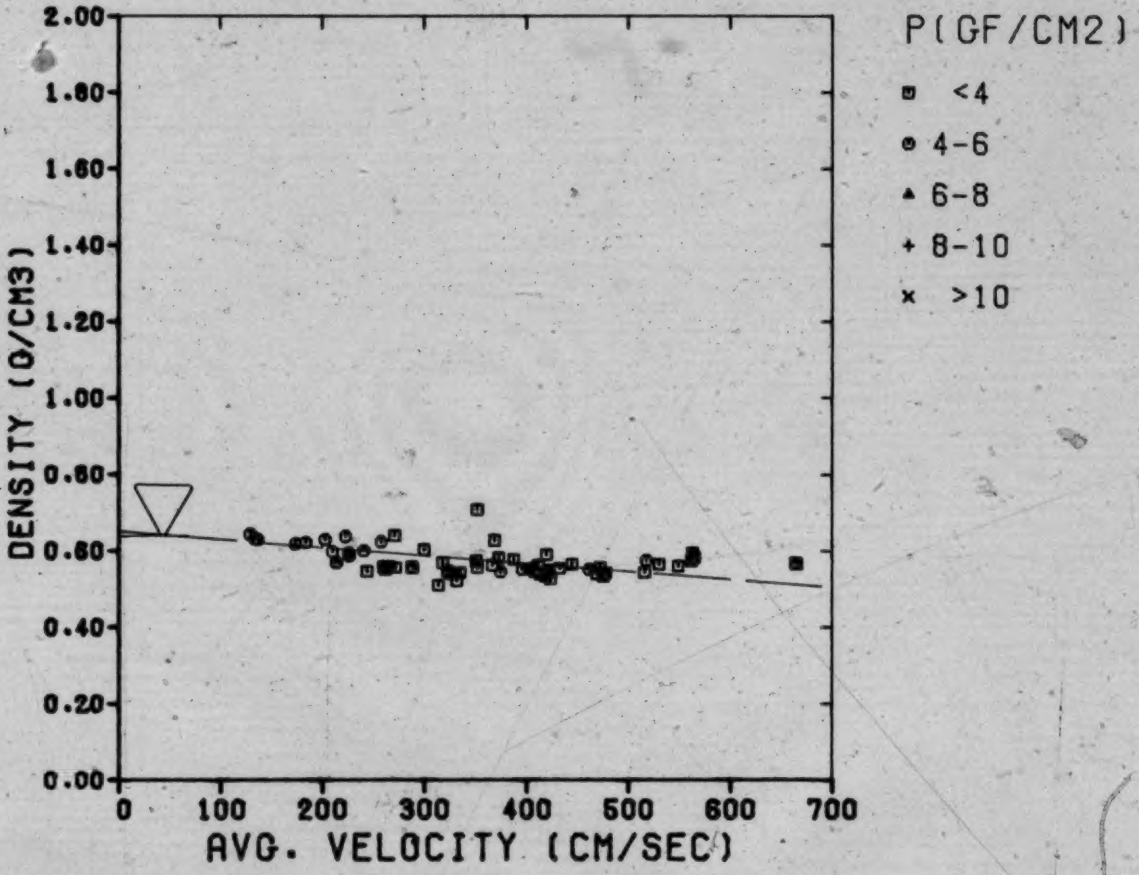

Figure 11.18 Density of Polystyrene beads during flow.

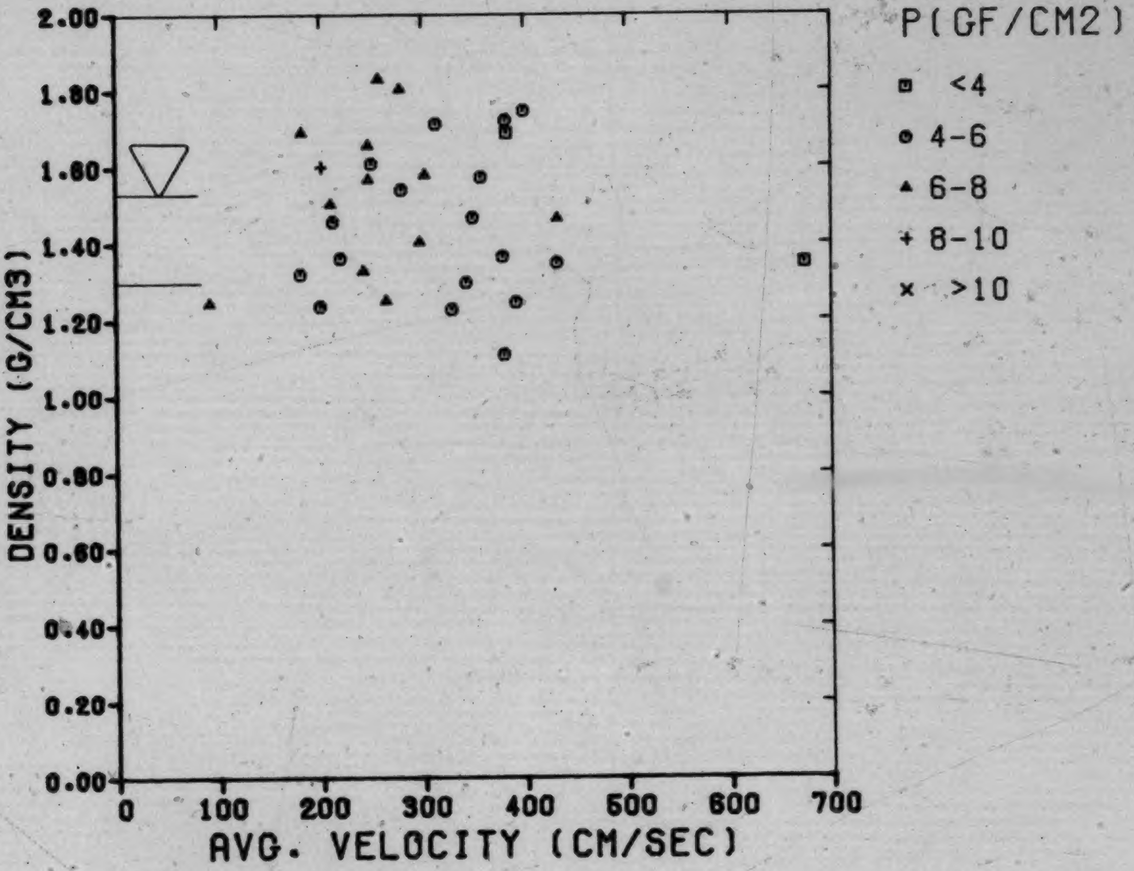

Figure 11.19 Density of angular sand during flow.

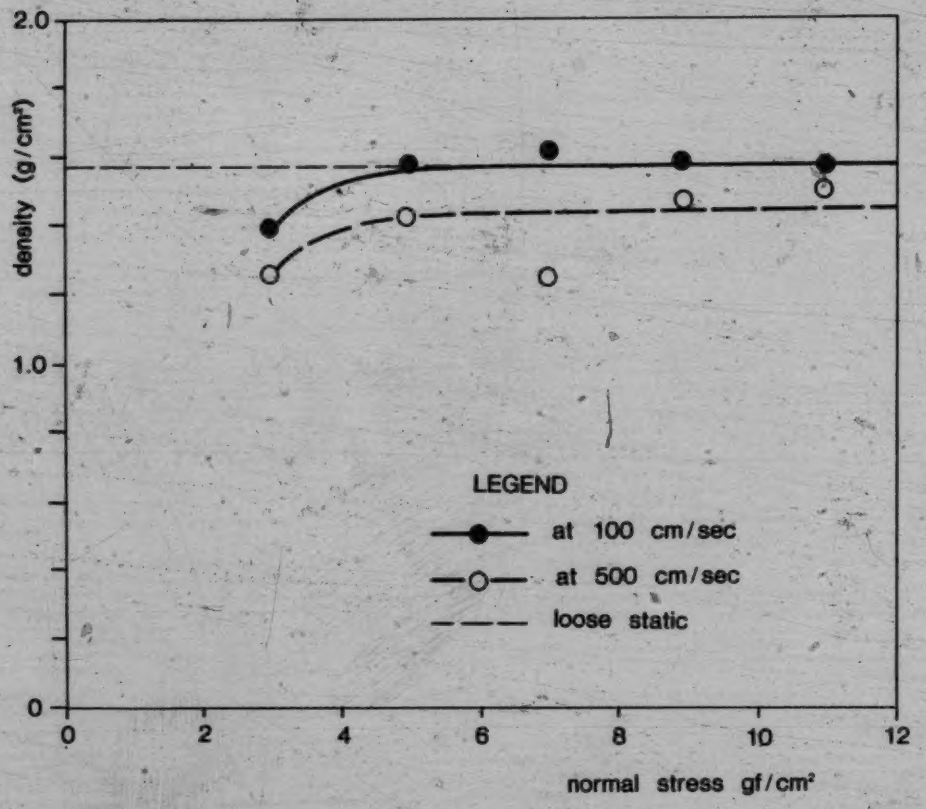

Figure 11.20 Mean density vs. normal stress at two velocities, Ottawa sand.

circular windows, 2 cm in diameter, were cut through the bed of the flume near the mid- length (Fig. 11.3d). One was placed on the longitudinal axis of the flume and the other immediately next to the side. Both were closed with glass plates aligned with the average plane of the surrounding rough bed. During most of the experiments, the existence (or the contrary) of a finite base shear velocity was observed through the windows using a mirror. The observations were only qualitative. Nevertheless, a pattern emerged according to which flows faster than 150 cm/sec (in terms of mean velocity) generally developed base shear, while the slower flows (for example during Test No. 10 shown in Fig. 11.14) built up a stagnant layer at the base, if they took place on slopes less than about 30 deg. The stagnant layer always developed first in the corners of the flume, next to the walls. Thin stagnant corners were observed even in the fastest flows. Even where base velocity occurred, it was commonly perceptibly slower in the window placed near the side. In the slower flows, however, stagnant mass developed in both windows, covering the entire bed. One is tempted to draw a parallel with the behaviour of debris flows, which are known to erode at steep slopes (i.e. at high velocities) and deposit during the final slower stages of movement. The stagnant corners and base layer never developed immediately behind the front of the flow, rather after a period of about half a second when they began to build up gradually.

Returning to Fig. 11.21, the velocity ratio falls to unity at velocities approaching 500 cm/sec, indicating a plug flow. Ratios smaller than 1.0, exhibited by some of the points, are due to an error in the measurement of the mean velocity, as explained in Section 11.7. The variation of the velocity ratio shown in Fig. 11.21 has been confirmed by independent measurements of the vertical velocity profiles. These were conducted by a second camera stationed during two of the tests close beside the end of the measuring flume, and observing the side of the flow through the Perspex wall. Velocity vectors were later collected by observing the displacements of individual particles in the films, and are shown for three time points of two tests in Fig. 11.22. In each case, the velocity distribution was approximately linear, except for a distortion near the base by the stagnant corner effect mentioned previously. The data represented by Fig. 11.21 could be summarized by stating that the velocity ratio is a set function of the mean velocity for these tests. The function has been expressed as a parabola drawn in the figure. If one further assumes, that the vertical velocity distribution is linear, it is possible to plot a series of idealized velocity profiles for various velocities as shown in Fig. 11.23. At least for the three profiles which were directly measured, the idealization is confirmed, as shown by the straight lines derived from Fig. 11.23 and plotted in Fig. 11.22. Further, the idealization is in agreement with the observation of base shear appearing

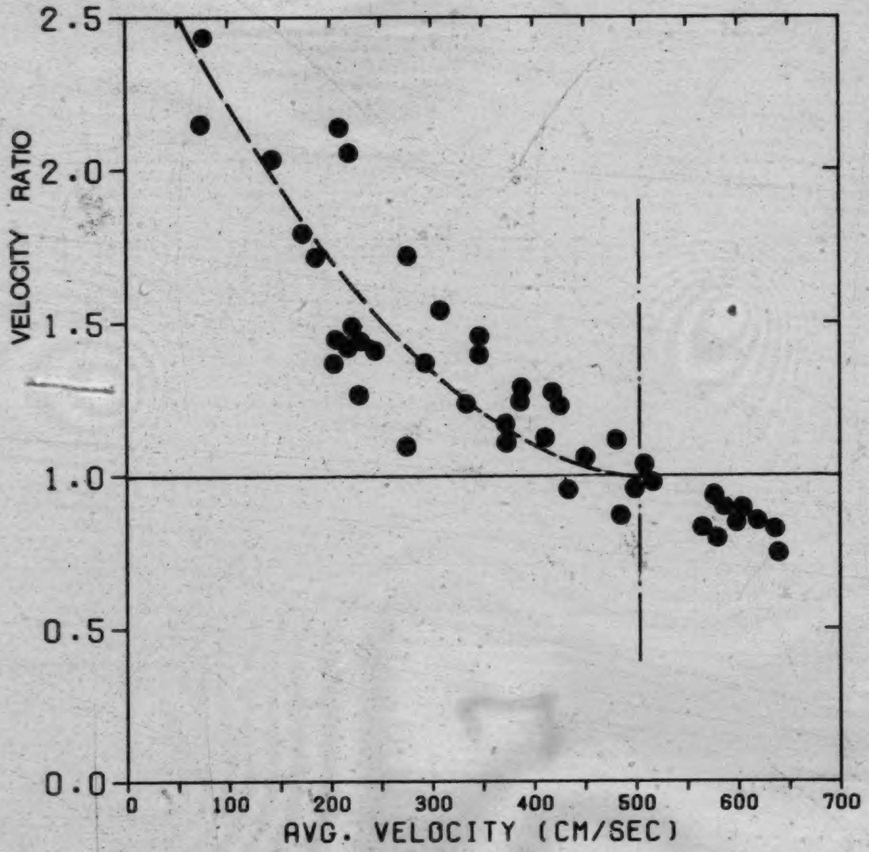

Figure 11.21 Velocity ratio vs. mean velocity, Ottawa sand.

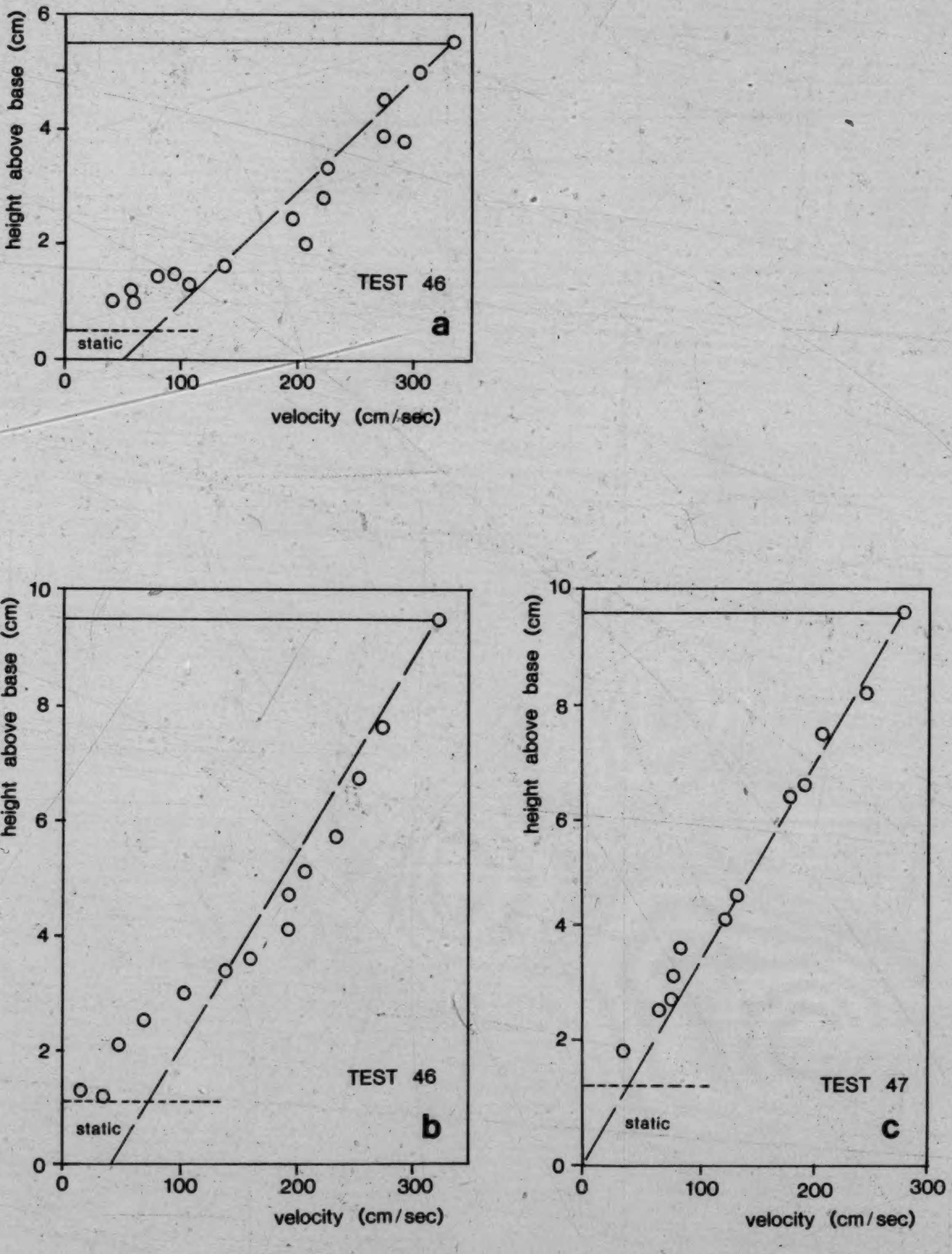

Figure 11.22 Velocity profiles measured through the side of the flume.

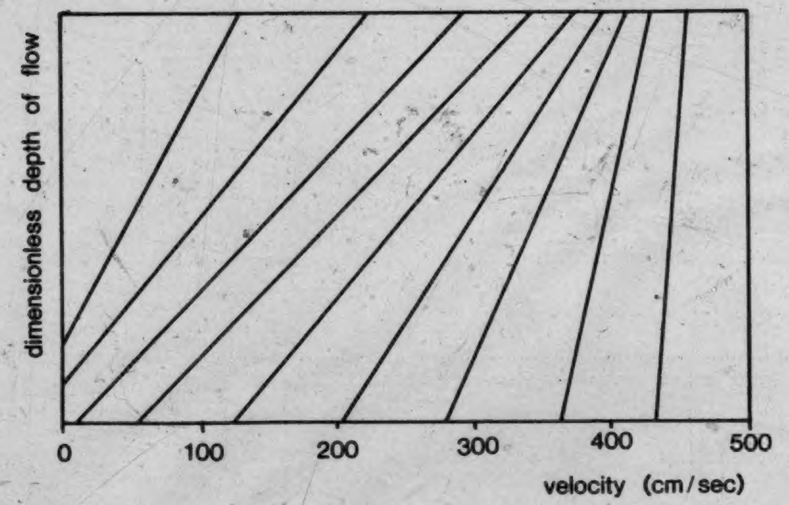

Figure 11.23 Idealized velocity profiles, derived from the relationship of Fig. 12.21, assuming linear velocity distribution.

at mean velocities in excess of 150 cm/sec, and stagnant layers existing in slower flows. The trend of Fig. 11.21 was reproduced nearly exactly by the data resulting from both polystyrene and angular sand tests.

Finally, the fact that no significant horizontal velocity distribution existed at the surface of the flows, is proven by Fig. 11.8. Surface patterns of particles were usually observed to travel down the flume without any distortion, even though they included particles travelling in an immediate contact with the wall. Individual particle velocities rarely varied by more than 5 percent with respect to the velocity of the group.

Two typical flow fronts are shown in the lower part of Fig. 11.6. Except in the fastest flows, the fronts had a smooth appearance of a straight taper, with a small cloud of saltating particles being pushed ahead. The inclinations of the flow fronts were steeper on greater slopes in correspondence with the roll wave theory of Section 5.2. Many of the flow front inclinations approximated to the difference between the bed and frictional slopes, as predicted by the theory; some were slightly different.

The fastest flows (exceeding 5 m/sec) had turbulent clouds of saltating particles above their surfaces.

11.5 Conclusions

Four of the main conclusions deriving from the above results present a strong contrast between the respective behaviour of flowing sand and continuous fluids. These are:

a. The shear resistance of the granular material is practically independent of velocity.

b. The material may move either as a plug flow or with an approximately linear velocity distribution.

c. The material has a tendency to create stagnant (dead) zones at the base of the flow.

d. Density changes accompany changes in velocity.

It should be noted that conclusion b) makes a) more important in terms of shear strain rate. The faster plug flows must have developed almost infinitely high shear strain rates near the flow base; yet, this did not bring about any significant increase in shear stress. A viscous fluid would have exhibited a stress increase proportional to the increase of strain rate, while a turbulent fluid would have a resistance controlled by the square of velocity.

On the other hand, it is interesting to note that the slower flows tended to assume a unique (i.e. linear) vertical velocity profile. In fluids, a velocity profile such as the Poiseuille parabola is a manifestation of stress- strain rate dependence. It is true that the velocity profile did not develop easily in the experiments. The existence of base shear velocity and plug flow in the faster flows must probably be attributed to the fact that these flows did not fully develop within the relatively short length of the flume. If this assumption is taken as valid, one could propose that flows at any velocity or slope angle would eventually converge to the linear velocity profile. If this were the case, then Equation (11.3), with β =1.33 for a linear velocity distribution, could be used to analyze steady- state fully developed flows of granular materials. Step- by- step flow profile calculations could then be carried out using this equation in the form:

$$\Delta H = 1.33\,\Delta x\left(\tan\alpha - T/p - s - \frac{1.33}{\cos\alpha}\,\frac{a}{g}\right)$$

Eqn. (11.4)

where a could be extimated from velocities between successive stations 1 and 2 as:

$$a = \frac{V_2^2 - V_1^2}{2\Delta x}$$

Eqn. (11.5)

And the result would have to match the equation of continuity:

$$\frac{\rho_2 H_2}{\rho_1 H_1} = \frac{V_1}{V_2}$$

Eqn. (11.6)

The density ratio could also be related to velocity ratio by means of Fig. 11.21.

The correspondence between friction coefficients obtained from direct measurement and those calculated from accelerations using Eqn. 12.3 shows that this theory is valid. A difficulty in its application, which arises in case of the slower flows, is the presence and unknown thickness of the stagnant zones. Although these have only been studied qualitatively, the apparent conclusion is that permanent stagnant base layers will only develop in low velocity flows at angles flatter than the angle of friction. Such flows would quickly develop the linear velocity profile with zero velocity at the base and then decelerate further, aggrading at the base. If there is a free outlet at the end of the flume, the stagnant layer would grow in the form of a wedge as observed in Test 16, Fig. 11.16 The sand flow managed in this example, with a delay in time and space, to build up its path to the preferred slope equal to the dynamic angle of repose. A similar occurrence is observed on a minor scale in Test No. 10, Fig. 11.14, which is also aggrading, although its slope must be close to the dynamic angle (including side friction correction).

Flows at steeper angles, on the other hand, always appear to accelerate. They disperse with a reduction in density and decrease in thickness, probably until the normal stress at the base drops to below 5 gf/sq.cm, at which point the flow begins to develop a different physical character, transitional towards saltation of grains. These accelerated flows do not deposit particles, although they may exhibit stagnant corners of decreasing size. From the above, it would appear that "normal depth" and associated velocity, which in fluid mechanics are a manifestation of the stress-strain rate constitutive relationship, do not exist in granular flow. The exception, perhaps, is the terminal velocity of thin accelerating flows, where the above-mentioned change of mechanism probably produces an increased flow resistance.

11.6 Detailed Description of the Data Processing Techniques

The following paragraphs contain the explanation of several analytical and experimental techniques which were used to derive the results presented earlier, but the description of which would have detracted from the clarity of presentation of the previous sections.

Density calculation was carried out by combining the thickness values at four measuring stations with the weight of the end of the flume as monitored by the load cell. The moment equilibrium equation was written with respect to the hinged end of the flume, assuming a constant bulk density ρ:

$$M = \rho g \int_0^{\ell} x\,H(x)\,dx = W\ell_1 \qquad \text{Eqn. (11.7)}$$

where x is the distance from the hinge, H(x) is the observed flow thickness, W the measured reaction, l the length of the flume and l the distance from the hinge to the load cell (Fig. 11.24a). As H(x) was only known as four discrete values, the equation was integrated using the Simpson's rule and then solved for the average bulk density.

Average velocity calculation involved combining the values of mass flow M, material unit weight w, and flow thickness h at any given station. The calculation is trivial

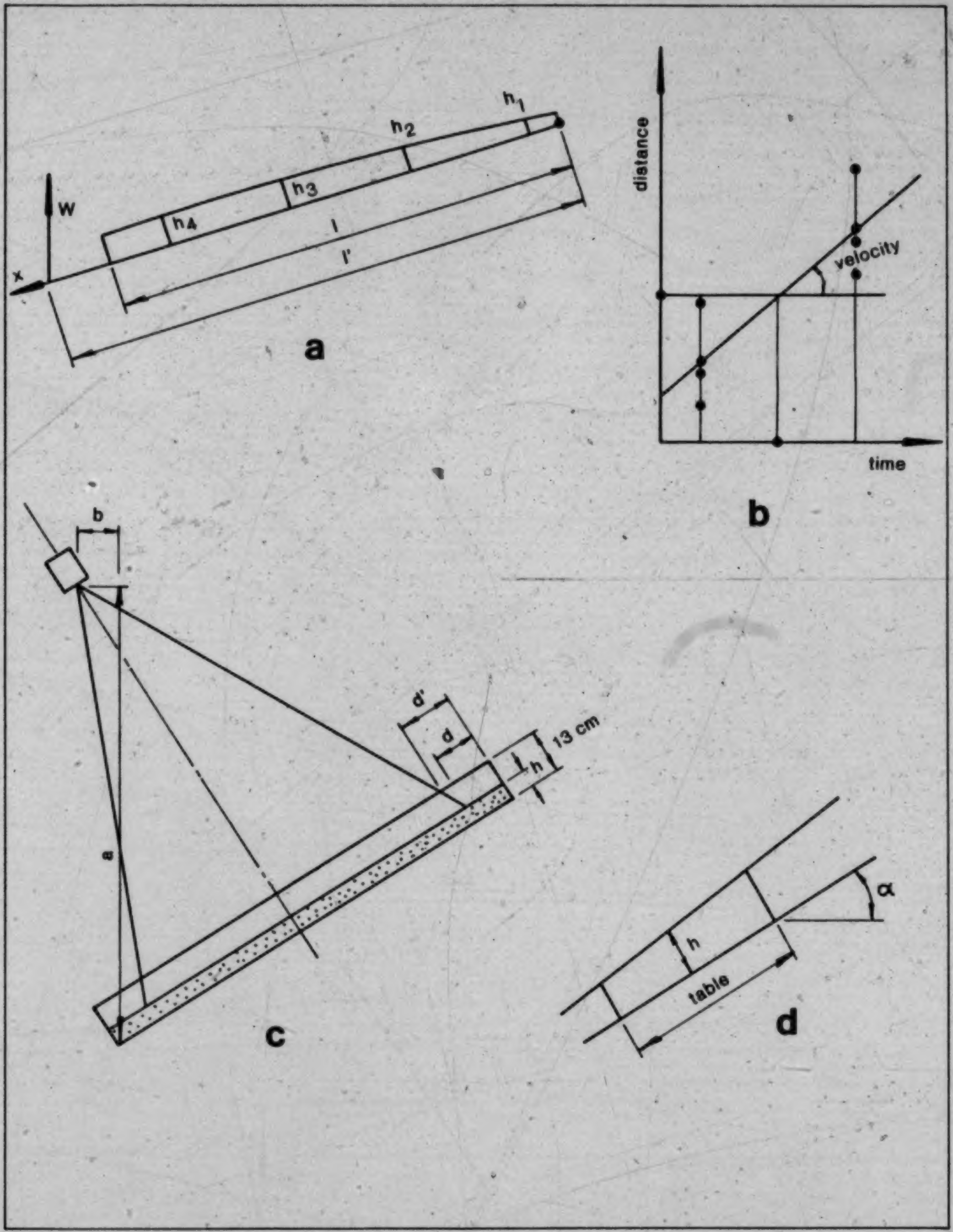
h1
h2
h3
h4
W
x
l
l'
a
distance
velocity
time
b
b
d'
d
13 cm
h
a
c
h
table
α
d

Figure 11.24 Diagrams for flume test data processing.

while the flow is steady, the velocity being equal to Mg/(wbh) where b is the width of the flume. The experiments were of relatively short duration, however, and many of the measurements were conducted close enough to the start or end of the flow to make an assumption of steady flow incorrect. In such cases, the mass flow measured at the bottom of the receiving pan was different from that passing through the measuring stations on the flume at any given maoment. Therefore, an interpolation procedure was used to synchronize the mass flow record with that of the other measuring points. A first estimate of the velocity was obtained by the above formula. Using this velocity, the time of travel of particles from the station under consideration to the bottom of the pan was calculated. The distance considered in the calculation included the remaining length of the flume and the estimated chord length of the trajectory after leaving the flume, reduced by the height to which the pan was already filled. The time of travel was then used to interpolate ahead in the table of mass flow values, with a linear Lagrangian interpolation formula. A new estimate of velocity was obtained from this new mass flow value and the interpolation procedure was repeated once more before accepting the final estimate of mass flow and velocity. This procedure was carried out successively at all four measuring stations.

Derivation of surface velocity from displacements. Determination of velocity and acceleration from displacementns of particles is a procedure involving single and double numerical differentiation respectively. It is exceedingly difficult to control the magnitude of the error in such procedures (e.g. Hildebrand, 1974). The method of data collection in some of the earlier tests involved displacements of single particles (coloured beads) and attempts to obtain velocity record continuous in time. Various frequencies of displacement reading were tried. Experiments were then conducted with fitting different degrees of polynomials to the data by the least squares technique. None of these laborious attempts was successful, however, leading to the conclusion that more data must be collected for each velocity value in order to reduce the random measurement error. The procedure finally adopted was to observe the displacementns of groups of four particles at distance intervals of 20- 30 cm. The particles were chosen so as to be as close together in the direction along the flume as possible, while being preferably widely spaced in the crosswise direction. From every two successive positions of the group, eight values of displacements were obtained, associated with a known time interval. A line was fitted to the eight points by the least squares method and its slope designated as velocity related to time and location marks calculated as algebraic averages of the eight points (Fig. 11.24b). Consistent and relatively smooth velocity- time- distance records were thus obtained, indicating that the random error has been satisfactorily smoothed out.

Acceleration was then calculated for each particle group, again by fitting a straight line to about 5 to 9 velocity-time points.

Perspective correction for displacements. The displacements of particles were read on the scale strips mounted at the top of the side walls. Perspective distortion resulted near the ends of the measuring flume, if the flow thickness was less than the height of the walls which was of course always the case. Perspective correction was derived form the geometry of Fig. 11.24c, to obtain true displacement d from the apparent displacement d'. The other variables used in the correction formula were the camera position coordinates a and b and the average flow thickness h.

Calculation of stress ratio. The average shear stress on the shear table was derived directly from the measured tangential force, S, and divided by the area of the shear table A. The normal stress was calculated by dividing the normal component of the weight of the volume of sand on the shear table byl the area (Fig. 11.24d):

$$P = (AH\rho g \cos\alpha)/A = \rho g H \cos\alpha$$

Eqn. (11.8)

Correction for the side friction. The total lateral thrust of the sand on both sides of the flume above the shear table was estimated as:

$$P_H = 2\cdot 0.5 k \rho g H^2 \ell$$

Eqn. (11.9)

where H is the depth of flow, l the length of the shear table and the coefficient of earth presure, K, is estimated as equal to 1.0. The side friction force, S, was then calculated as

$$S = P_H \tan \phi_w$$

Eqn. (11.10)

The friction angle ϕ_w between the test material and the Perspex wall was measured by tilting tests and found equal to about 8 deg. for both kinds of sand and 13 deg. for polystyrene.

All of the above calculations were implemented by two computer programs, one processing the surface motion data and the other combining all the remaining measurements. Input into these programs comprised records of flow thickness, load cell data and surface particle displacements versus time. The output was in the form of tables, samples of which are given in Table 11.3.

11.7 Error analysis

As stated in Section 11.4, the results were checked against systematic error through the application of the equation of motion. There remains, on the other hand, a considerable amount of random error in the various measurements, which must be analysed. The primary source of the random error is in the precision of the primary data. This is assessed in the following paragraphs, while the influence of these errors on the precision of the final output variables is discussed afterwards. The flow chart in Fig. 11.4 explains the purpose of each measurement within the sytem.

The precision of the shear gauge and flume load cell records is controlled by calibration and by readout precision. Calibration of all the three load cells was carried out in the same physical setting and environment as that of the tests. All three calibration curves were highly linear and free of hysteresis, with a least squares correlation coefficient exceeding 0.999 in every case, for a load- unload cycle of 15 to 20 points. Readout from the chart recorder was done manually using a precise scale under magnification. The resolution of the scale was at the most equal to 5 percent but more commonly only 2- 3 percent of the reading value. The repeatability of the readings was bounded by less than one- half of the resolution. Thus, the random error arising from the load cell data did not exceed about 2 percent. Vibration of the load cell record occurred occasionally, probably as a result of shaking of the apparatus. In general, however, the records were quite smooth, as shown in Fig. 11.7. Vibrations that did occur, usually after opening of the trap door and the initial impact of the sand into the knee, always quickly decayed.

Somewhat lesser precision must be expected from the measurements of mass flow rate, which were obtained by graphical differentiation of the pan load cell record. The differentiation was done using a protractor with a resolution of, at the most, 10 percent. The repeatability of the rate readings was only a fraction of the resolution in straight parts of the record. But it was not much less than the resolution in curved parts of the record, expecially near the start and end of the test, where a tangent had to be constructed to the local curvature. Thus, errors of up to 10 percent could occur at such points. Another source of error in the flow rate measurements arose from the interpolation procedure used to synchronize them with the other data. The interpolation was based on the assumption of a uniform velocity after the material left the measuring flume. This of course may not be true, most likely there would be some degree of acceleration. In highly curved parts of the record, such as near the end of the flow, even minor imprecision in the estimate of the time lag might lead to a relatively large error in flow rate. In summary, while most of the mass flow data collected is correct at least to within 5 percent, a few of the points may conceivably be in error by as much as 20 percent. This error would be reflected in the mean velocity output data only.

Reading of flow thicknesses was conducted on a still projection, scaled down approximately three times from the actual size. An LW Athena analysing projector was used, capable of viewing the film at a variety of speeds or frame-by- frame, with full light intensity. The flow thickness readings were taken using a piece of glass with a hairline, placed so as to smooth out local irregularities of the flow surface, for a true distance of about 30 cm. In most cases, however, the flow surface was quite smooth and this would not really be necessary. In a few instances, especially during the faster flows, local turbulences developed at the surface due to gaps in the side wall at the start of the flume and above the shear table. It was then sometimes necessary to project the flow surface from the nearest undisturbed point using the hairline. During most of the sand tests (except two), only one mirror was used, so that thickness observations were only done on one side. Another mirror was then added, and the thickness values were checked on two sides, both being recorded only if they were different.

Although the scale strips were graduated only to the nearest cm, the readings could be estimated with a considerably higher resolution. Some readings were made in the laboratory on a stagnant layer of sand 0 to 2 cm thick. These were reproduced later by reading from the film, in a conventional manner, to within 1 mm of the correct values. Repeatability of the readings taken from moving sand sheet was determined by analysing one of the tests twice, on different dates. Approximately one hundred readings were repeated, with the following results:

30 were exactly the same
25 were diffent by one mm
14 by two mm

9 by three mm
6 by four mm
5 by five mm and
2 by 6 mm.

This corresponds approximately to the normal distribution. Consequently, about 80 percent of the readings were repeatable to within 2 mm (plus or minus) and 98 percent to within 5 mm. The error arising from reading in a single side mirror only was unmeasurable in case of most of the flows slower than about 3 m/sec on the surface. Some of the fastest flows, however, produced differences as great as 1 cm between the two sides, which amounts to a possible error of 5 mm in term of the average flow thickness.

In a summary, the thickness observations are estimated to be correct to within plus or minus 2 mm for about three-quarters of the data and to about plus or minus 5 mm for the rest. In terms of the average flow thickness of approximately 6 cm, this amounts to a 3 percent and 8 percent error respectively, while in terms of the thinnest flows (about 3 cm thick) it is 6 and 16 percent.

The errors of the individual primary variables may conceivably compound in the data analysis. This possibility was studied using an especially written computer program. This program utilized the same procedure as used in standard data analysis to calculate bulk density and the friction coefficient T/P, but conducted the calculations repeatedly, perturbing each of the six input variables[26] by a set percentage. In every calculation, each of the input variables was in turn either perturbed downward, left intact or increased in all the possible combinations. If all of the primary error was in the same direction and of the same magnitude, the resultant variables were exactly correct. Certain combinations, however, could compound the error up to two times in the case of density and more than three times in the case of friction coefficient. If, for example, all of the thickness measurements but the last one plus the shear table reading were overestimated by 5 percent, while the last thickness and the flume weight were underestimated by the same margin, the resulting friction angle would be more than 17 percent too high.

The results of this program could also be used to estimate the contribution of error in each individual primary variable to the variance of the output. Table 11.4 summarizes these results. The first column of the table lists the primary variables; the second and third columns give their most likely and maximum error limits respectively, as determined above. The remaining columns give first the percentage error of the output variable resulting from a 5 percent upward perturbation of each primary variable (error contribution) and then the appropriate magnificatioon factor calculated by dividing the error contribution by five. The relative importance of the

---

[26] The four flow thicknesses, flume load cell and shear gauge record.

OUTPUT VARIABLE →			DENSITY		T/p	
PRIMARY VARIABLE	probable error (%)	max. error (%)	error contr. per 5%	magnif. factor	error contr. per 5%	magnif. factor
H10*	3-6	8-16	0	0	0	0
H50			-1.0%	-0.2	1.2%	0.2
H90			-1.2%	-0.2	1.3%	0.3
H130			-2.6%	-0.5	-3.3%	-0.7
flume cell	2	2	5%	1.0	-5.5%	-1.1
shear gauge	2	2	-	-	5.7%	1.1
total			9.8%	2.0	17 %	3.4
thicknesses only			-4.8%	-0.9	5.9%	1.2
probable error limit			5-8%		7.5-11%	
max. error limit			10-18%		13.5-23%	

*The number refers to the measuring station to which the flow thickness is related (in cm from the start of the flume).

Table 11.4 Error analysis of the density and apparent friction coefficient determination

various primary measurements can now be seen. In general, the flow thickness measurements are more influential towards the free end of the flume. Their combined effect, shown in the third line from the bottom, amounts to a magnification factor of about 1, or approximately the same as that of each of the two load cell measurements. The total magnification factors which would obtain by the most unfavourable combination of the same error margins are also shown. The last two lines of the table show the final error limits, estimated by increasing the primary errors of Columns 2 and 3 by their appropriate magnification factors in their absolute value, i.e. at their most unfavourable combination. It is estimated that more than 75 percent of the output data should have a random error limited by the most probable limit, while the other limit estimates the maximum possible deviation. The range of the limits applies to average thickness and very thin flows respectively.

It will be noted that only the polystyrene data (Figs. 11.10 and 11.18) agrees with the error limits determined in Table 11.4. The Ottawa sand and angular sand data (Figs. 11.9 and 11.17, 11.11 and 11.19) often show scatter of up to 20 percent from average value, approaching the maximum estimated. The most likely explanation for this is in the local heterogeneity of the density of the material which, in the case of the polystyrene beads, may have been reduced due to the regular shape of the grains and possibly the presence of a slight electrostatic adhesion.

The precision of the surface velocity measurements was relatively high. The displacements were measured by laying the hairline across the image of the flume so as to intersect the centre of the coloured particle and to obtain equal readings on both of the scale strips. A graphical presentation of the percentage random eror involved in the velocity determination for individual particles is given by the scatter of the points in Fig. 11.8. It is always less than plus or minus 5 percent, and generally less than 2 percent.

12. HIGH VELOCITY RING SHEAR EXPERIMENTS

12.1 Introduction

The results of flume experiments reported in Chapter 11 showed that granular material retains its frictional character under very high rates of shearing. But a question remains whether this would also be the case when normal stress is high. The apparent coefficient of friction of rock fall avalanches, as reflected by their travel angle, decreases with the volume of the event (e.g. Scheidegger, 1973 and Section 10.1). Theoretical considerations described in Chapter 10 indicate that decrease of the friction angle with increasing normal stress might be possible at high rates. Finally, the high velocity ring shear experiments by Bridgwater (1972) seem to indicate the beginnings of a rate effect in tests of glass beads at velocities of approximately 50 cm/sec and normal stresses exceeding 25 kPa. In order to decide conclusively whether or not such a phenomenon actually exists, it was necessary to conduct tests that would subject a sample of granular material to a combination of both high shear rate and relatively high normal stress.

Obviously, the most practical test arrangement to fulfil these requirements is the ring shear test. This test has been used extensively with cohesive soils, where it is favoured mainly for its ability to achieve long uninterrupted displacements. A limited number of attempts have been made to adapt the technique to granular materials, as shown in Table 12.1. Bishop et al. (1971) offer an excellent review of the history of the test and the general considerations of design and interpretation of results.

A high velocity ring shear apparatus was designed and constructed in the course of this research and experiments were carried out on a range of materials. Besides uniform sands, mixtures of sand and fine rock flour were also tested, in order to examine the hypothesis of Hsu (1975) concerning liquefaction of rock debris avalanches by dust dispersions. Tests were also carried out in a water bath.

The experimental apparatus was designed to increase substantially the power input per unit volume [27] into the material achieved by previous investigators. At the same time, a relatively large sample was used in order to minimize possible boundary effects.

A summary of the key parameters of previous ring shear tests on granular materials is given in Table 12.1. It may be seen that all of the previous tests had power input at least an order of magnitude less than the present ones. Also, the range of materials is increased and the sample volume is relatively large.

The tests address the similitude requirements not met by the flume experiments. The elasticity ratio (Table 11.1), defined as the ratio between material Young's modulus and

---

[27] Defined as the maximum shear strain rate times the maximum normal stress.

Author	materials tested	sample volume (cm^3)	max. velocity (m/sec)	max. stress (kPa)	sample height (cm)	power per cm^2 (kW/cm^3)	rate effect
Healy (1963)	Ottawa sand	20	0.03	63	0.28	6.8	slight
Novosad (1964)	glass beads	254	0.5	2	3.0	0.3	none
Scarlett & Todd (1969)	sand	1,200	0.03	6	4.0	0.5	none
Bridgwater (1972)	glass beads and plastics	940	2.0	25	4.0	12.5	yes
this research	coarse sand, sand and rock flour, sand and water	660	1.0	200	2.0	100	none

Table 12.1 Parameters of previous ring shear tests on granular materials

the applied normal stress, equals 3 x 10^5 , or only approximately 1.5 times that estimated for the average thickness of the Frank Slide rock fall avalanche. The maximum velocity gradient is also not much different than in the prototype. The prototype velocity is estimated as 50 m/sec, which would produce a shear strain rate of 50 sec on a 1 m thick shear zone. The strain rate corresponding to the maximum circumferential velocity obtainable in the test was also equal to 50 sec. The uniformity coefficient similitude was fulfilled by using a two component material whose two grain sizes had a ratio of 1.7 mm to 0.044 mm, i.e. 39 to 1. This compares to the average uniformity coefficient of 75 for the prototype.

To minimize possible boundary effects on the expected dynamic behavior, the sample was made relatively large. The sample thickness of approximately 2 cm is more than ten times the grain diameter of the coarse sand tested. The sample width of 4 cm should minimize the relative effects of side friction as much as feasible. The average radius of the sample is 14 cm, maintaining the circumferential velocity constant to within plus or minus 15 percent across the sample width.

Nevertheless, as will be seen in the following sections, all of the tested materials retained their frictional behaviour with practically unchanged parameters over the entire range of test conditions. It therefore appears unlikely that the scale of the shearing process taking place at the base of a large rock debris flow affects the validity of Coulomb's Law as it applies to that situation.

12.2 Apparatus Design.

The main dimensions and capacities of the apparatus were determined by the considerations described in the previous section. Next, it was decided to adopt the test configuration of Hvorslev (1939) (Fig. 12.1a). This forces the sample to begin shearing at mid- height, where the upper and lower annular boxes are separated by a set gap. Volume changes are acommodated by a free vertical movement of the upper loading platten, independent of the sides of the box. The volume changes of course generate side friction, which adds to the normal load transmitted by the loading platten. Bishop et al. (1971), made a provision in their design to measure this side friction separately, so that the actual normal load transmitted by the sample between the upper and lower boxes could be determined as the sum of the platten load and the side friction load. This is an ideal solution of the problem of side friction, but it requires two superimposed independent vertical constraint systems, which complicates the mechanical design.

In the new apparatus, the platten pressure is generated by an annular ("doughnut" shaped) inflated rubber membrane, which bears against the back wall of the upper box (Fig.

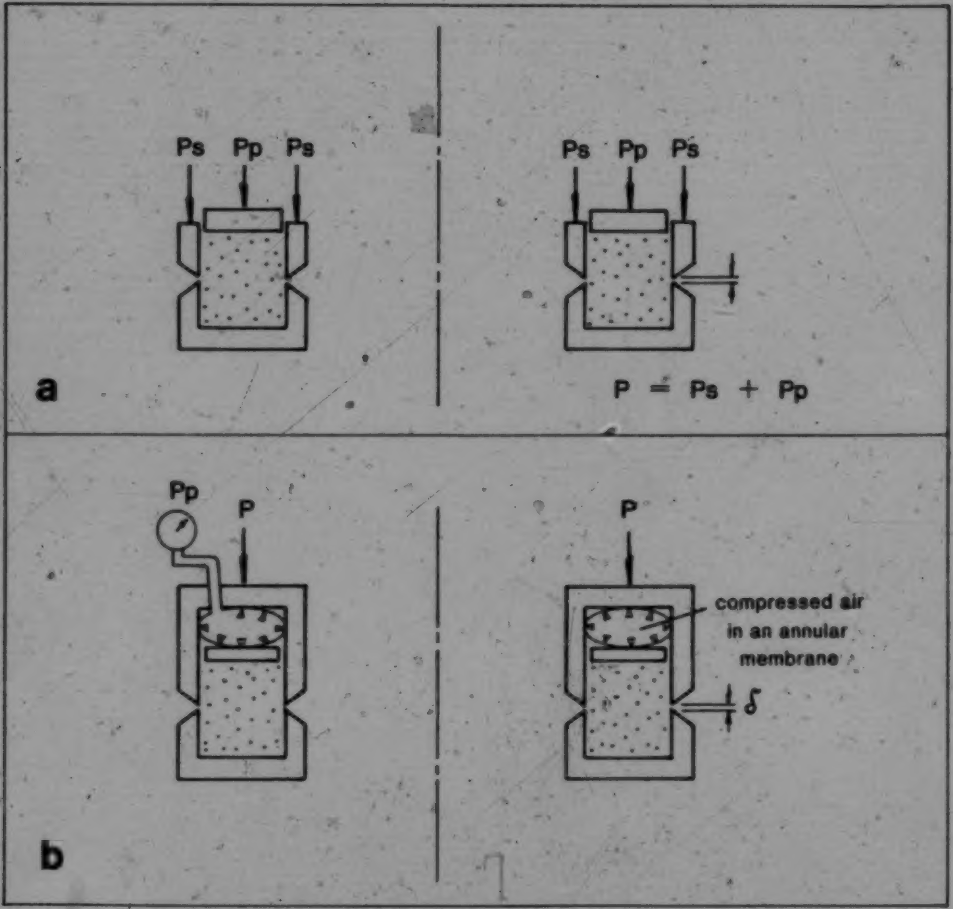
Ps
Pp
Ps
a
Ps
Pp
Ps
P = Ps + Pp
Pp
P
b
P
compressed air in an annular membrane
δ

Figure 12.1 Comparison of the design principles of the Imperial College — N.G.I. ring shear apparatus (Bishop et al., 1971) (a), and the present design (b).

12.1b). The upper box can then be rigidly enclosed and kept a fixed distance from the lower one; the volume changes of the material being acommodated by the flexibility of the membrane. The vertical retention of the upper box is achieved through a stiff load cell which then measures precisely the *total normal load*, i. e. both the platten load and the side friction. This arrangement achives a comparably reliable control of the total normal load as exists in the Imperial College design, but with a substantial mechanical simplification.

A disadvantage of the present version of the design is that it does not allow volume change measurements. This was acceptable for the purpose of the present program, since all that was required was to measure the variation of the shear strength with normal load and velocity. It should not be difficult to add a volume change measurement facility in the course of future development.

The remaining aspects of the design are relatively simple. A schematic crossection is shown in Fig. 12.2 and photographs of the apparatus appear in Figs. 12.3 and 12.4. The lower box (shown empty in Fig. 12.4a) rotates on a fixed hardened steel vertical shaft. The upper box is mounted on the same shaft by means of two Thomson linear ball bushings, which allow free vertical motion as well as rotation. The box can be disassembled by lifting the back wall with the membrane and pressure platten, to gain access to the interior of the space occupied by the sample. During the test, the box is bolted together.

A strain gauge instrumented double arm, attached to the hub of the upper box by strong set screws, restrains rotation of this box and measures the torque. Its ends bear against adjustable bearing platforms through rollers (Fig. 12.3b). The vertical motion of the box is restrained by a large compression load cell, connected to a loading yoke. This connection is adjustable, to allow setting of the gap between the boxes to a specified opening.

The compressed air membrane is made from 1/16 inch thick vulcanized rubber, reinforced by unidirectional fibre strands. The strands are laid so that in any side view of the membrane they would always appear dipping at 45 deg. in the direction of shearing. This orientation of the reinforcement enables the membrane to sustain the shear load which it must transmit from the back wall of the box to the loading platten. At the same time, the flexibility of the rubber in the direction perpendicular to the strands permits membrane expansion. The membrane is permanently glued both to the box cover and to the platten. It has four air inlets, to ensure fast response and uniform pressure distribution. Rough surfaces of glued down coarse sand cover both the bottom of the lower box and the pressure platten, to prevent slip at the horizontal boundaries of the sample.

The gap between the boxes has a fitting conical surface (Fig. 12.2). This is a result of attempts to restrain fine grained material from escaping through the gap by closing it

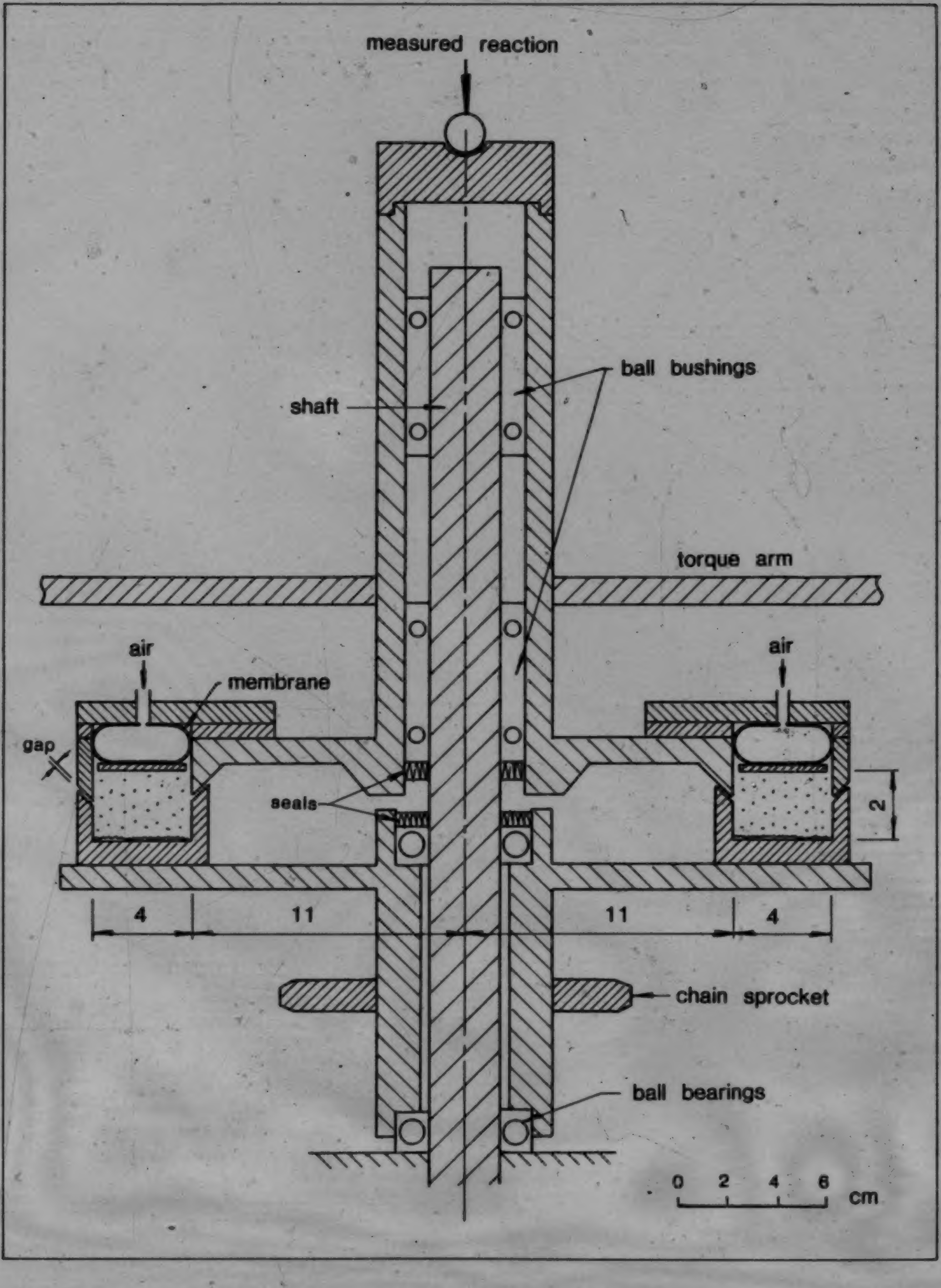
measured reaction
ball bushings
shaft
torque arm
air
membrane
air
gap
seals
2
4
11
11
4
chain sprocket
ball bearings
0 2 4 6
cm

Figure 12.2 Vertical section of the ring shear boxes. Dimensions in cm. Lower box rotating, upper fixed.

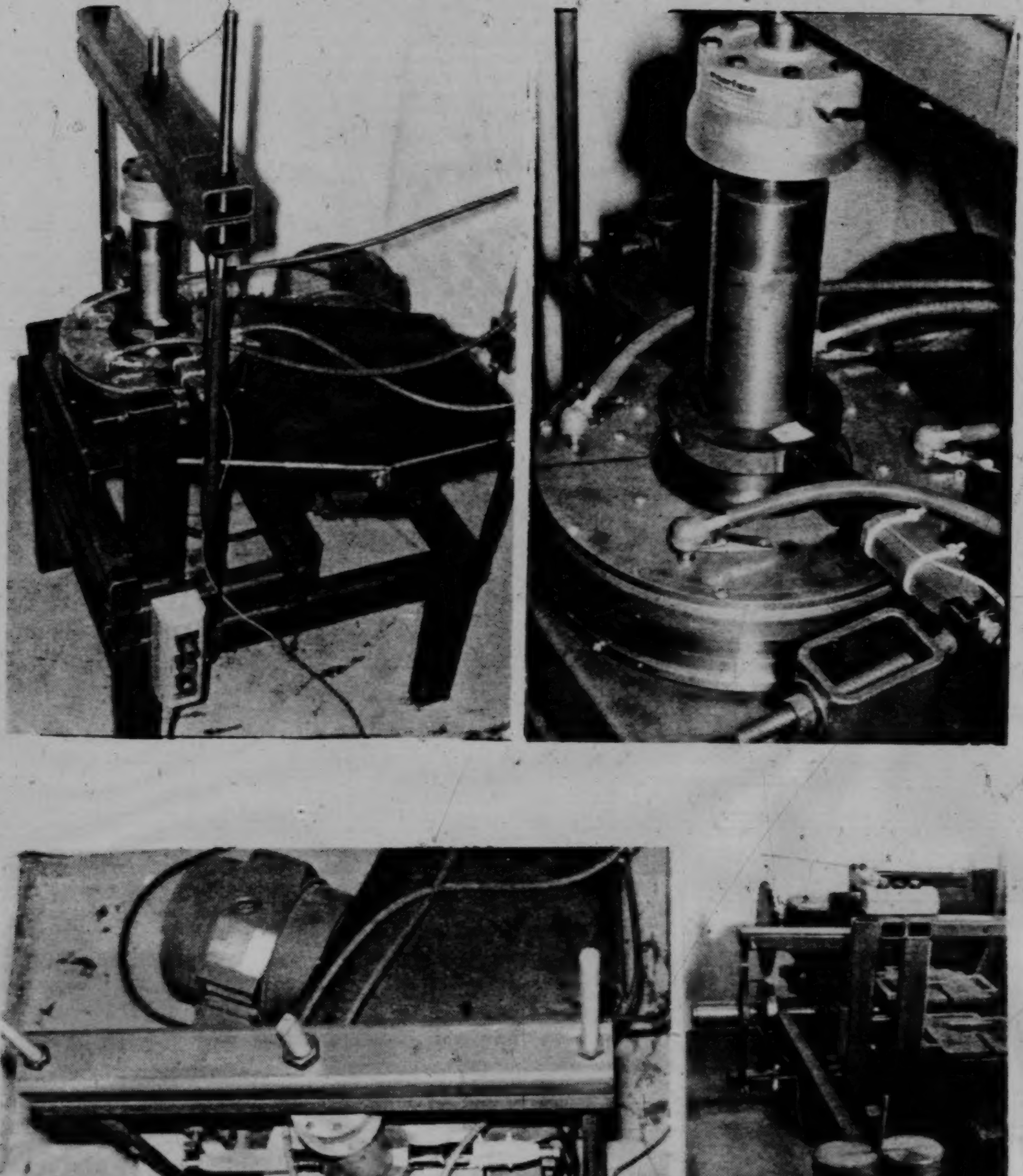

Figure 12.3 Ring shear apparatus. (a) overall view, (b) detail of upper box with torque arm, load cell and air inlets, (c) top view, (d) torque arm calibration.

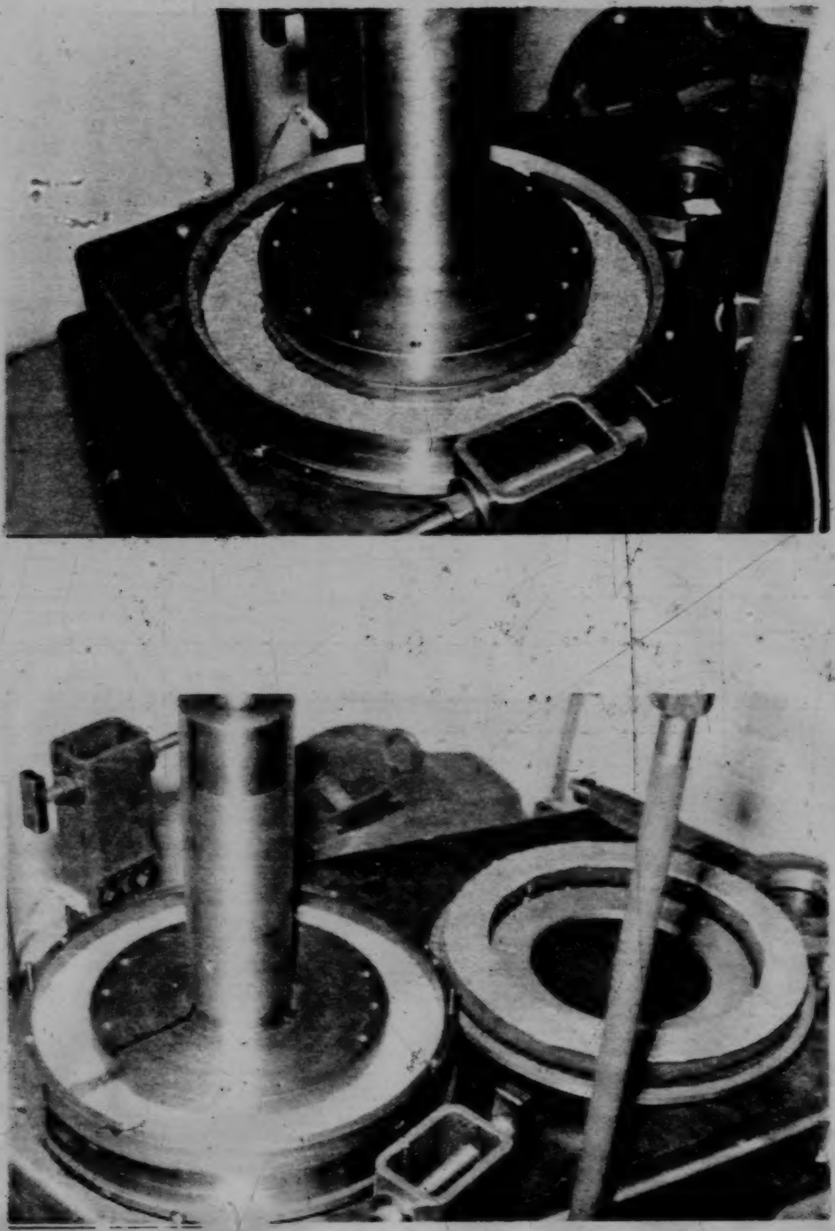

Figure 12.4 (a) Empty lower box, (b) sample in place, loading platten and membrane (right).

with nominal pressure and filling with silicone grease. These attempts were so far unsuccessful; fine particles would always find their way into the gap and generate friction. This arrangement of the gap is therefore probably inferior to the conventional double knife edge (Fig. 12.1), but it is of no consequence in case of the present tests, since no grains were allowed to enter the gap.

One of the principal difficulties of this design was to obtain a sufficiently high torque and power from the driving train. The tests were driven by a 7 HP three phase electric motor, connected to the lower box by a worm gear and a two speed heavy duty chain drive. The speeds of rotation were 11.8 and 72.2 RPM, corresponding to mean circumferrential velocities of 16.0 and 98.2 cm/sec at the mean radius of the sample. For testing in water, the boxes were surrounded by a transparent plastic barrier and could thus be submerged to a level approximately 1 cm above the top cover. The bearings and bushings were provided with rubber seals to prevent water and dust from entering.

The total normal force, torque and displacement were all monitored continuously during each test. The normal force was measured as the reaction between the hub of the upper box and the restraining yoke, using a standard compression load cell. The weight of the upper box was added. The torque was registered in the form of bending strain in the torque arm which was restrained against stiff columns projecting from the main frame. To calibrate the torque arm, the machine was tilted and laid on its side, with the main shaft horizontal. A long beam was then attached to the upper box and loaded with weights to apply suitable calibration torque (Fig. 12.3d). Thus, the calibration of the arm took place under conditions equivalent to those of the test. A highly linear and stable response was found. Circumferential displacement was monitored by a trip switch, contacting the lower box 6 times per revolution in the slower tests or 1 times in the faster ones. All three measurements were registered simultaneously by a Honeywell six channel chart recorder, whose chart velocity also served to monitor the time.

Test execution consisted of the following steps: The cover of the upper box with membrane was removed (Fig. 12.4a). The vertical side rings of the box were put in place and secured by temporary restraining screws. Sample was loosely piled into the boxes and leveled to the proper height using a template. A 1 cm wide vertical strip of coloured sand was placed to indicate possible nonshearing zones (Fig. 12.4b). The top cover was put in place carefully, without bolting it down. Normal load was applied to the upper box hub by the gap adjusting screw, in order to keep the gap between the boxes firmly closed during the placement of the bolts. The cover plate was then bolted closed, the torque arm was set and the four air hoses attached. Some air was then applied and the gap opened up a small amount. Increasing air pressure tended to open the gap further, as a result of the elastic stretch of the restraining yoke. Therefore, the pressure had to be raised in several steps, always checking the gap opening using a feeler gauge and adjusting as necessary. This was to ensure that the gap did not open wider than the specified amount, which could have caused sand grains to enter it.

The gap was maintained in general at 0.5 mm or approximately one- third of the minimum grain size of the coarse sand tested. No grains were observed to enter the gap. An exception was the rock flour which in tests of flour- coarse sand mixtures escaped through the gap in small amounts. The grain size of this material was, however, so much smaller than the gap opening, that it could not cause any significant friction there. The absence of friction in the gap was checked by conducting several tests with greater and smaller gap openings (0.3- 1.0 mm), without a change in results. Also, two tests were run with continuous changes of air pressure in the membrane up and down for several cycles, without intermediate readjustments of the gap. The normal and vertical stresses registered throughout these tests remained always on the linear strength envelope (Fig. 12.6). If there had been a gap friction, this could not be the case, but the apparent strength curve would necessarily have to show curvature. This is because, unlike the sample frictional strength, the gap friction would not be affected by the membrane pressure.

All of the tests were run as multi- stage tests, obtaining results in series of up to three levels of normal pressure from each sample. The staging direction was periodically reversed in order to be able to identify possible effects of sample degradation. In one series of tests the normal pressure was progressively increased and in the next series decreased. But this was found to have no measurable effect on the results. Since the main purpose of the tests was to study rate effects, a new sample of fresh sand was placed at every change of speed.

Tests were carried out at the two speeds of the apparatus and also at a low rate, when the drive train was rotated slowly by hand. The circumferential velocity of this last testing method varied between 0.025 and 0.1 cm/sec and was of course semewhat variable. Better selection of speeds could be obtained with the use of a variable speed motor, but this would substantially increase the cost of the apparatus.

The normal load applied before the start of each test usually changed within the first second, usually dropping by 0 to 30 percent but sometimes increasing. This was the result of side friction. Bishop et al. (1971) commented that it is both difficult and unnecessary to keep the normal load constant, as long as its magnitude is reliably monitored. This is even more strongly true of the present experiments, in which rapid gains of velocity probably resulted in very significant volume changes in the granular material.

Attempts were made to obtain quantitative measure of grain deterioration in the fast tests at the highest normal pressure. But even after a series of 3 tests, there was no noticeable increase in the content of material passing the finer limiting sieve. The degree of deterioration of the rounded quartz sand particles was therefore negligible.

A simple analysis of the results was used, assuming that both the normal and tangential stresses are uniformly distributed over the sample area. This would be exactly correct if the residual friction coefficient of the material could be assumed to be constant with both displacement and velocity, which indeed turned out to be the case. If there was a rate dependence, it might then have been necessary to consider the variation of circumferential velocity across the width of the sample, which amounted to plus or minus 15 percent, as already stated.

12.3 Results

Tests have been carried on several kinds of materials including two sizes of relatively coarse sand, mixtures of sand and rock flour, polystyrene beads and sand in water. All of these materials have been tested under varied velocities and normal stresses. All exhibited straight linear residual strength envelopes with zero cohesion and unique angles of residual friction, practically unaffected by the speed of the test.

The main test material was a medium uniform quartz sand with rounded grains, obtained as the fraction between U.S. Standard sieve sizes 10 and 14 (grain diameter 1.5 to 2.0 mm, cf. Table 11.2, Sectoon 11.2). This was selected over Ottawa sand, since this coarser material could be more easily kept from entering the gap between the boxes. The resulting strength envelope for this material in the air dry state is shown in Fig. 12.5 and that for the sand submerged in water in Fig 12.6. The last figure also shows an example of the continuous test previously described, in which the membrane air pressure was varied cyclically up and down. No velocity or normal stress effect can be observed within the range of test conditions in either of the two materials. The residual friction angle of 29 deg. is about 4 deg. less than the lower angle of repose measured by the rotating drum experiment. This is not unusual, since the latter test represents conditions of extremely low shear rate and normal stress. The friction angle in water is 26 deg.

Figures 12.7 and 12.8 show the results of tests on coarse rounded sand (fraction between sieves 8 and 10, or particle diameter of 2- 3 mm) and smooth spherical polystyrene beads similar to those used in some of the flume experiments. Only one series of tests was carried out on each of these materials, comprising very slow and slow velocities. No rate effects can again be observed. In case of the polystyrene beads, very strong stick- slip vibration was observed at normal stresses exceeding 70 kPa and with

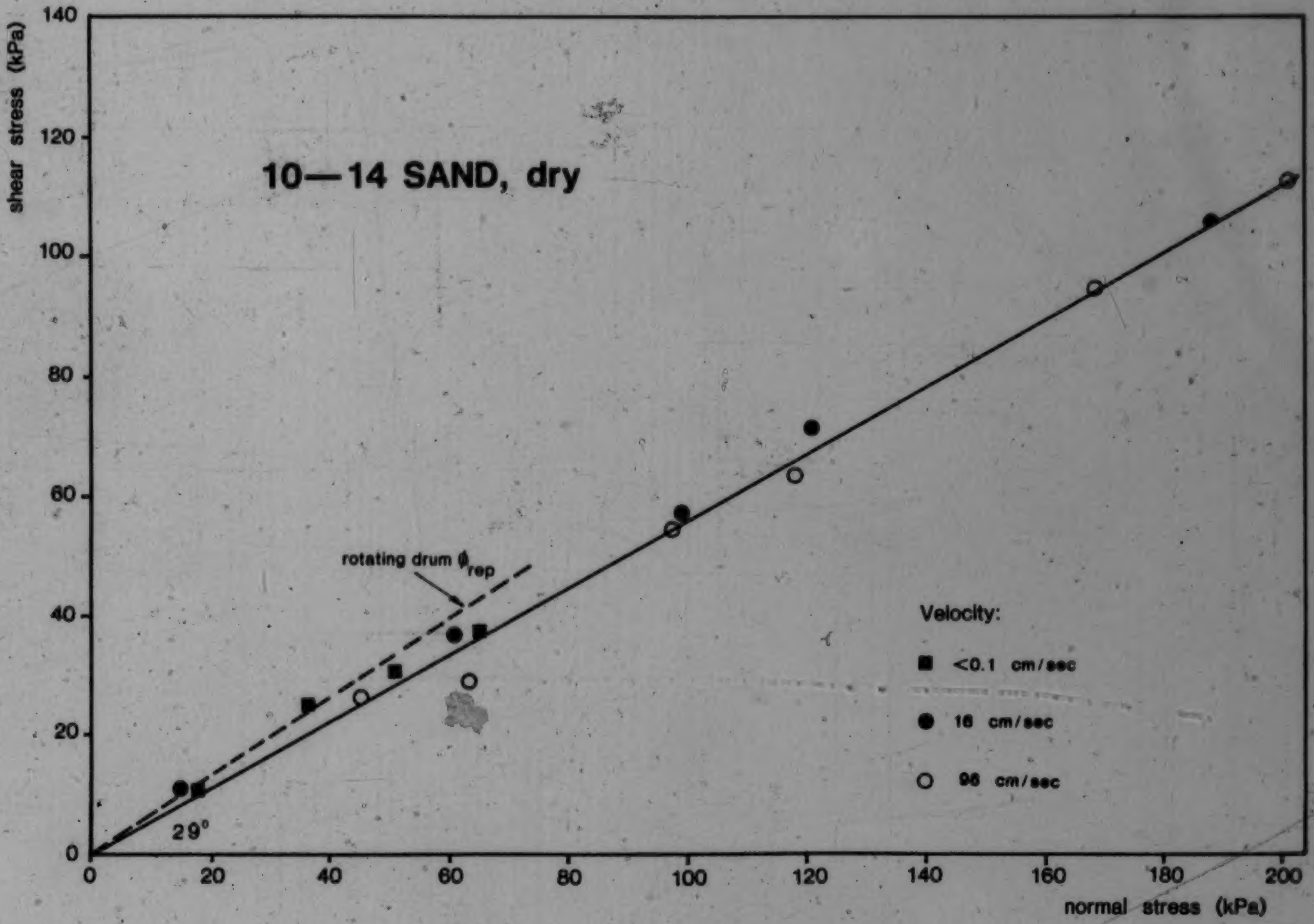

Figure 12.5 Strength envelopes of the dry 10—14 sand.

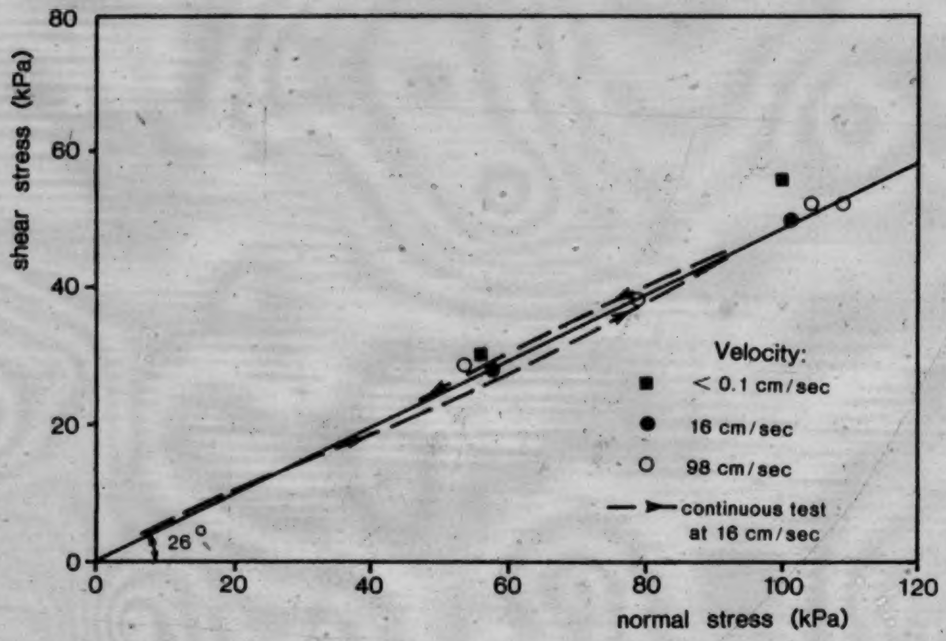

Figure 12.6 Strength envelopes of the 10—14 sand submerged in water.

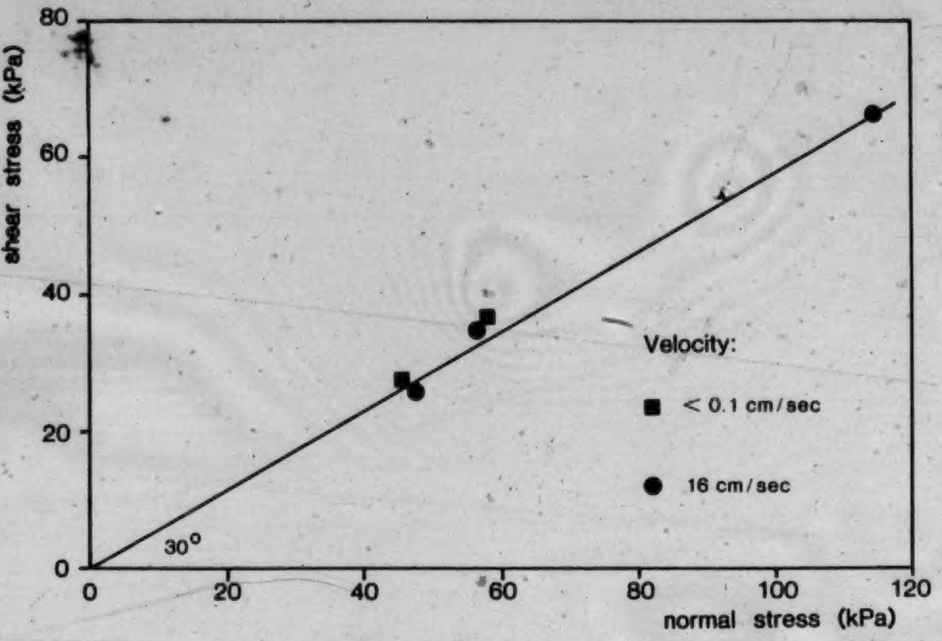

Figure 12.7 Strength envelopes of the dry 8—10 sand (coarse).

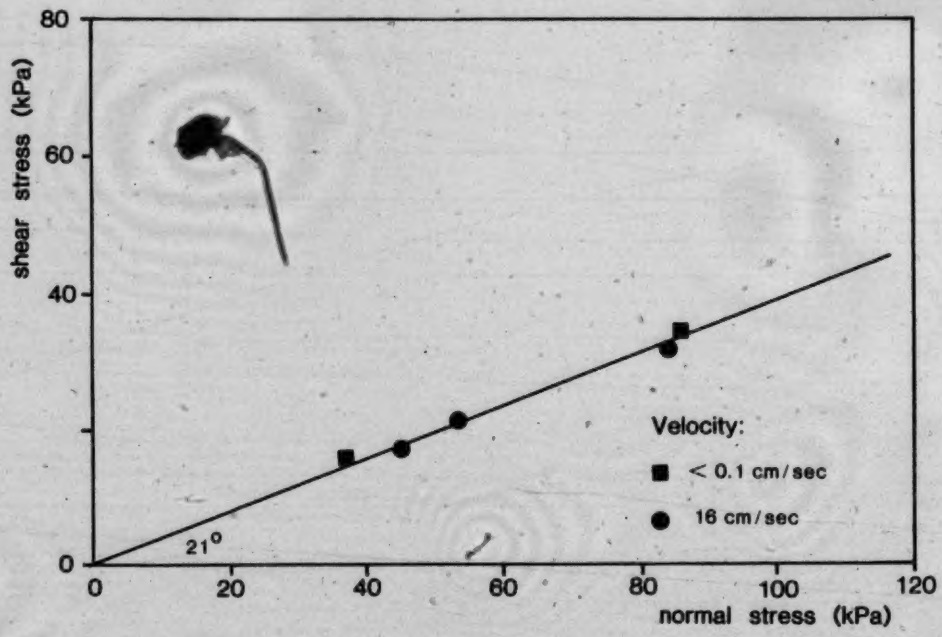

Figure 12.8 Strength envelopes of the polystyrene beads.

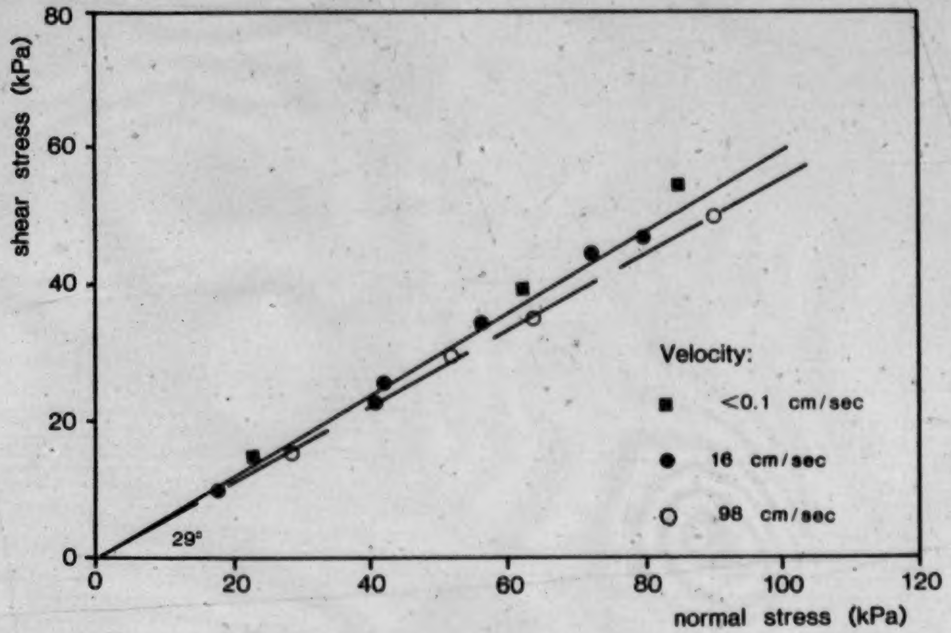

Figure 12.9 Strength envelopes of the 4:l sand and rock flour mixture.

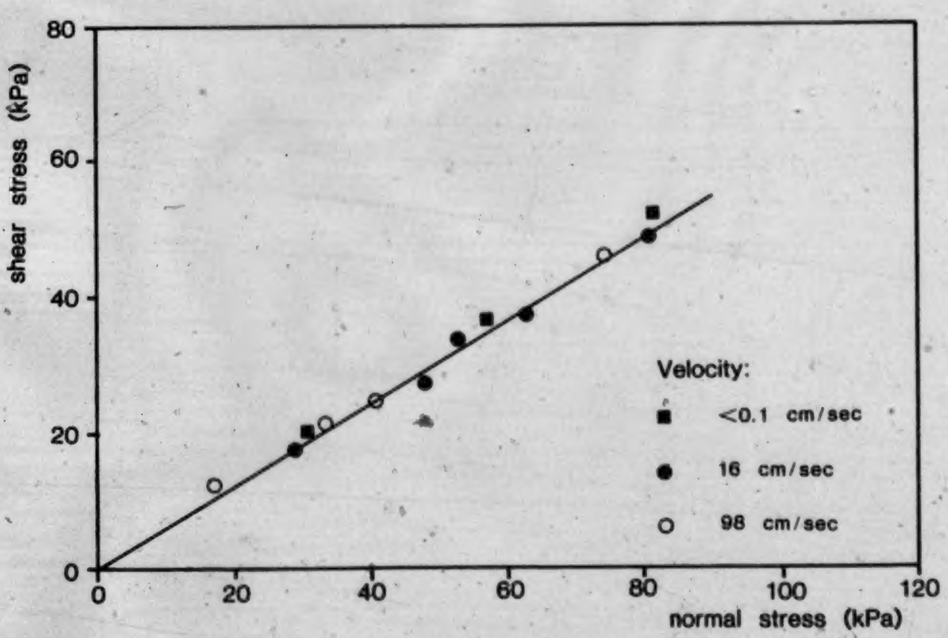

Figure 12.10 Strength envelopes of the 4:2 sand and rock flour mixture.

the "slow" velocity. This is probably a phenomenon connected with the fundamental frictional properties of this material. Consequently, no fast tests have been conducted, for fear of damaging the apparatus.

Two mixtures of rock flour and the 10- 14 sand have been prepared. The rock flour was crushed pure quartz with a mean grain diameter of 0.044 mm. At first, 25 percent by weight of this was added, so that the flour would just fill the void space of the sand in loose static piling. This is the only case (Fig. 12.9) where a slight rate effect could be discovered. The slow and very slow tests yielded a friction angle similar to that obtained in the tests with greater proportion of rock flour. The fast tests, on the other hand, were comparable to those of the sand alone. One might interpret this so that the more angular rock flour controls the friction angle at low rates, while the more rounded large particles dominate at high velocity, perhaps by virtue of their greater dispersive pressure (cf. Chapter 7).

Another mixture was formed by adding 50 percent of rock flour to a unit of sand, that is twice as much as was needed to loosely fill the void space. The sand grains would thus be expected to "float" in the powder in this mixture. No velocity or normal stress effects were found.

Table 12.2 contains a summary of all the measured residual friction angles, together with a few other results for comparison. It will be seen that the observed angles of friction agree well with typical values and show little scatter. The polystyrene beads result agrees remarkably well with that obtained in the flume tests at comparable velocities. The comparison of the flume test and ring shear test results for sand reflects the greater degree of roundness of the Ottawa sand used in the former. It can be concluded, that a proof has been given of the absence of a rate and normal stress effect over a range of conditions and material characteristics that do not leave much room for exceptions.

Observations of the thickness of the shearing zone, carried out by means of the vertical strip of dyed sand, indicated full depth shearing in both the "slow" and "fast" tests. Only in the "very slow" tests was the shearing zone limited to the middle one- third, approximately, of the sample thickness.

The significance of these results is simple and it is felt that they do not require further discussion. Their application to the problem of rock avalanche mobility is covered in Section 12.5. It may be argued that a behaviour change might obtain at still higher shearing velocities. The author feels that this is improbable, considering the high value of shear strain rate produced by shearing a thin sample at the maximum velocity achieved.

Material	residual friction angle (deg.)		
	v. slow 0.1 cm/sec	slow 16 cm/sec	fast 98 cm/sec
10-14 sand, dry	29	29	29
10-14 sand in water	26	26	26
4:1 sand-flour mixture	31	31	29
4:2 sand-flour mixture	31	31	31
8-10 sand, dry	30	30	-
polystyrene beads	21	21	stick slip
Ottawa sand in flume tests		25.5	
polystyrene beads in flume tests		21.8 25	(2m/sec) (2m/sec)
nonplastic silt*		26-30	
uniform fine-medium* sand		26-30	

*Typical range of low velocity constant volume friction angles (Lambe and Whitman, 1979).

Table 12.2 Summary of residual friction angles measured in the ring shear tests

13. SUMMARY AND RECOMMENDATIONS FOR FURTHER RESEARCH

The text of the first ten chapters hes been arranged following the logic of the subject matter, without regard to separation of original contributions from review. This is to serve the convenience of a reader who might read this thesis for the sake of its subject alone. However, such a format is not usually adopted in theses. It is therefore necessary to present a recapitulation of the material and to point out those aspects in which an original research contribution has been made. At the same time, it will also be useful to list the main areas in which this work indicated the need for further research.

The main objective of the review part of the thesis was to identify the method of analysis applicable to each type of slope movement. This resulted in a list of categories, each of which would yield to a certain analytical method combined with a certain type of constitutive relationship. Each category has been given separate discussion in the review. In some cases it has been possible simply to reference methods found in the literature. More often, it was necessary to review such methods critically. Special emphasis was placed in relating various proposals to each other. In some cases it was found possible to supplement the state- of- the- art by new models based on simple physical laws or observations.

Usable methods of analysis emerged for some types of slope movements. None did for others, but qualitative concepts were discussed and directions were indicated for further work. The main of these concluding arguments are presented in the following paragraphs, in an arrangement corresponding to that of Chapters 1 to 10.

(a) An analysis has been presented of the impact conditions for *rock fall*, showing that the rebound angle of rock fragments is likely to be considerably flatter than the incident angle. This was compared with empirical findings. Observations by several authors have been brought together. Further research in rock fall analysis must concentrate on the statistical aspects .

(b) A simple model of *toppling* dynamics has been presented. Evidence was reviewed that toppling possibly adds a brittle aspect in spontaneous disintegration failures of steep cliffs. This mechanism requires further study.

(c) Laboratory data on residual strength of rock discontinuities , and the evidence of *rock slides* of limited volume indicate the validity of the frictional approach in the analysis of these movements. The approach is not valid for large slides, however, whether they form rock avalanches (sturzstroms) or not. The frictional heating hypothesis was recommended as applicable in the latter case. The frictional approach is probably very conservative in the case of slides and slumps in massive shale, due to macroscopic dilatancy which reduces pore- pressure. Velocity of such events appears invariably low.

(d) *Slides and slumps in overconsolidated clays* again appear to be slower than one would expect considering the brittle character of the material. An increase of undrained strength with velocity is suggested, which may be measurable in laboratory tests, unless it is due to macroscopic dilatancy caused by unevenness of shear surfaces.

Slides in insensitive normally consolidated clays also cannot be fully rationally analysed at present, because of a lack of knowledge of shear zone thickness and the dependence of undrained residual shear strength on velocity. Some approximate approaches have been suggested.

(f) To analyse *sliding in highly contractant saturated soils* such as loose fills or sensitive clays, one would require a reliable knowledge of the critical state line of the material.

(g) Field evidence indicates that only decelerating *deepseated creep* exists in soils. This could be analysed using existing laboratory- derived relationships.

(h) *Bedrock creep* rates do not seem to have been measured as yet in nature. Reported cases of such measurements can be identified with previous landsliding.

(i) *Slow earthflows* are complex phenomena, involving interaction of zones of different mobility. A method of analysis has been proposed based on a drained strength-shearing velocity relationship determined from laboratory tests. But it is difficult to establish boundary conditions (especially the groundwater pressures) which vary in time and space.

(j) *Rapid earthflows* have been shown to be amenable to analysis as flows of a viscous (Newtonian) slurry. A model has been proposed which accounts for the presence of solid rafted blocks of desiccated soil. The roll wave solution has been suggested as applicable to subcritical channeled flows of earth materials.

(k) A thorough analysis of *grain flows* (flows of dry granular materials) has been presented, based mainly on the results of Bagnold (1954) and of laboratory flume experiments reported in Chapter 11. It was shown that a Coulomb- type frictional law persists over a wide range of strain rate levels. The preferred velocity distribution with depth has been shown to be close to linear.

(l) *Grain flows in water* have also been discussed in the light of Bagnold's results. A connection was established between the frictional sliding model, Bagnold's transitional state and a macro- viscous region explored by a number of researchers in the field of chemical engineering. The viscous analysis was shown to be applicable to subaqueous flows of "quick sand". An analysis was proposed for the drainage of such flows. Adiabatic generation of pore air pressure in flows of collapsive silts has been analysed. The theory and phenomenology of turbidity currents was briefly reviewed for completeness.

(m) Conflicting theories for the analysis of *debris flows* have been critically reviewed. The difficulty of

7

determining realistic constants for two- parameter (Bingham and Power Law) models from laboratory tests was pointed out. A thorough phenomenological description of debris flows has been compiled and a model suggested for the analysis of flows with frontal boulder accumulations.

(n) The analysis of *debris avalanches* appears similarly problematic. Their initiating mechanisms have been discussed. The importance of vertically uneven degree of saturation has been pointed out. A suggestion has been made to apply an empirical analysis approach similar to that used for snow avalanches.

(o) *Lahars* have been discussed descriptively, for completeness.

(p) An extensive phenomenological review of *rock avalanches* has been presented, based on reported case histories and on the author's field work at the Frank Slide. Several typical attributes of rock avalanches have been pointed out and correlations were established. It was shown that there is field evidence that these landslides move as fluids rather than frictional bodies. This corresponds with the findings of Hsu (1975) and Koerner (1976). Strong inverse grading and the existence of a peripheral "splash" zone has been demonstrated for the Frank Slide debris deposit.

A critical review of eight existing hypotheses intended to explain rock avalanche motion has been presented. The hypothesis of mechanical fluidization was rejected on the basis of high velocity ring shear experiment results, reported in Chapter 12. These experiments have been conducted at velocities of up to 1 m per sec, the sample thickness being equal to about 2 cm. The strain rates achieved must therefore have been comparable or greater than those occurring in full size rock avalanches.

The group of existing hypotheses which rely on high pore pressures has been criticized on the basis of circumstantial evidence. A case has been made for acoustic fluidization caused by vibration within the debris sheet travelling over an uneven path. Empirical approach towards practical analysis of rock avalanches is recommended.

The main value of this thesis should be seen in its attempt to bring together a collection of material truly relevant to the complex and poorly explored problem of landslide mobility.

14. REFERENCES

Afrouz, A. and Harvey, J.M., 1974. Rheology of rocks within the soft to medium strength range. *Int. Journ. Rock Mech. and Geomech. Abstr.* Vol. 11,pp 281-290.

Allen, J. R. L., 1970. The avalanching of granular solids on dune and similar slopes. *Journ. of Geology*, Vol. 78, pp326-351.

Allen, J. R. L., 1971. Mixing at turbidity current heads, and its geological implications. *Journ. Sed. Petrol.*, pp 99-113.

Andresen, A. and Bjerrum, L., 1968. Slides in subaqueous slopes in loose sands and silts. *NGI Publication* No. 81, Oslo.

Anon., 1979. Southern California Landslides. An editorial review in *California Geology*, Jan. 1979.

Augenstein, D. A. and Hogg, R., 1978. An experimental study of the flow of dry powders over inclined surfaces. *Powder Technology*, Vol. 19, pp 205-215.

Azimi, C. and Desvarreux, P., 1974. A study of one special type of mudflow in the French Alps. *Quart. Journ. Eng. Geol.*, Vol. 7, pp 329-338.

Bagnold, R. A., 1941. *The Physics of Blown Sand and Desert Dunes.* Chapman and Hall, London, 265 pp.

Bagnold, R. A., 1954. Experiments on a gravity-free dispersion of large solid spheres in a Newton fluid under shear. *Royal Soc. London Proc.*, Ser. A, Vol. 225, pp 49-63.

Bagnold, R. A., 1961. Auto-suspension of transported sediment; turbidity currents. *Royal Soc. of London Proc.*,Ser. A, Vol. 265, pp 315-319.

Bagnold, R. A., 1968. Deposition in the process of hydraulic transport. *Sedimentology*. Vol. 10, pp 45-56.

Baltzer, A., 1875. Uber die Bergsturze in den Alpen. *Scheweizer. Alpenclub, Bern, Jahrb. 10*, pp 409-456.

Banks, D. C. and Strohm, W. E., 1974. Calculations of rock-slide velocities. *Proc., 3rd Congress ISRM*, Denver, Vol. II-B, pp 839-847.

Barata, F. E., 1969. Landslides in the tropical region of Rio de Janeiro. *Proc., Int. Conf. Soil Mech. Found. Eng.*, Mexico, Vol. 2, pp 507-516.

Barkan, D. D., 1962. *Dynamics of Bases and Foundations*. Mc Graw Hill, New York.

Bentley, S. P., 1979. Viscosimetric assesment of remoulded sensitive clays. *Canadian Geotech. Journ.*, Vol. 16, pp 414-419.

Biarez, J. and Boucek, B, 1973. Viscoplasticite de l'argile in-situ et au laboratoire. *Proc., Int. Conf. Soil Mech. Found. Eng.*, Moscow, Vol. 1.1, pp 51-56.

Bishop, A. W., 1967. Progressive failure with special reference to the mechanism causing it. *Proc., Geotech. Conf. Oslo*, Vol. 2, pp 142-150.

Bishop, A. W. 1973. Stability of tips and spoil heaps. *Quart. Journ. Eng. Geol.*, Vol. 6, pp 335-376.

Bishop, A. W., Green, G. E., Garga, V. K., Andresen, A. and Brown, J. D., 1971. A new ring shear apparatus. *Geotechnique*, Vol. 21, pp 273-328.

Bishop, A. W., Hutchinson, J. N., Penman, A. D. and Evans, H. E., 1969. Geotechnical investigations into the causes and circumstances of the disaster of 21st October 1966 at Aberfan. In *A selection of technical reports submitted ot the Aberfan Tribunal*, Welsh Office, H. M. S. O., London.

Bjerrum, L. and Jorstad, F. A. 1968. Stability of rock slopes in Norway. *NGI Publication*, 79.

Bjerrum, L., Simons, N. and Torblaa, I., 1958. The effect of time on the shear strength of a soft marine clay. *Proc., Conf. on Earth Pressure Problems* , Brussels, Vol 1, pp 148-160.

Bjerrum, L., 1971. Effect of rate of strain on undrained shear strength of soft clays. *NGI Publication*, No. 85, pp 41-42, Oslo.

Bjerrum, L., |971a. Subaqueous slope failures in the Norwegian fjords. *NGI Publication* No. 88, Oslo.

Blackwelder, E. 1928. Mudflow as a geological agent in semi-arid mountains. *Bull., Geol. Soc. of Am.*, Vol. 39, pp 465-484.

Blong, R. J. 1973. A numerical classification of selected landslides of the debris slide- avalanche- flow type. *Engineering Geology*, Vol. 7, pp 99-114.

Bovis, M. J. and Mears, A.,I., 1976. Statistical prediction of snow avalanche runout from terrain variables in

Colorado. *Arctic and Alpine Research*, Vol. 8, pp 115-120.

Breitfuss, G and Scheidegger, A. E., 1974. On a possible mechanism of Alpine debris flows. *Annali di Geofisica*, Vol. 27, pp 47-57.

Bridgwater, J., 1972. Stress-velocity relationships for particulate solids. A. S. M. E. Paper No. 72-MH-21.

Broadbent, C. D. and Ko, K. C., 1972. Rheological aspects of rock slope failures. *Proc., 13th Symp. on Rock Merchanics*, Urbana, Ill. pp 579-593.

Broscoe, A. J. and Thomson, S., 1969. Observations on an alpine mudflow, Steele Creek, Yukon. *Can. Journ. Earth Sci.*, Vol. 6, pp 219-229.

Brown R. L., and Richards, J. C., 1970. *Principles of powder mechanics*. Pergamon Press, Oxford, 223 pp.

Browning, J. M., 1973. Catastrophic Rock Slide, Mount Huascaran, North- Central Peru. *Am. Assoc. Petroleum Geologists Bull*. Vol. 57, pp 1335-1345.

Bruce, I., 1978. Field estimation of shear strength in rock. Ph. D. Thesis, U. of Alberta.

Bruce, I. and Cruden, D., 1977. The dynamics of the Hope Slide. *Bull., Int. Assoc. Eng. Geol.*, No. 16, pp 94-98.

Brunsden, D., 1979. Mass movements. In *Processes in Geomorphology*, Embleton, C. and Thornes, J., Eds., Edward Arnold, London, pp 130-186.

Bull, W. B., 1964. Alluvial fans and near- surface subsidence in Western Fresno County, California. *U. S. Geol. Survey Prof. Paper*, 437-A.

Buss, E and Heim, A., 1881. *Der Bergsturz von Elm*. Worster, Zurich, 133 pp.

Calembert, L. and Dantinne, R., 1964. The avalanche of ash at Jupille (Liege) on February 3rd, 1961. in *The Commemorative Volume Dedicated to Professeur F. Campus*, Liege, Belgium, pp 41-57.

Campbell, D. B., 1978. Performance of a waste rock dump on moderate to steeply sloping foundations. *Proc., Symposium on the Stability in Coal Mining*, Vancouver.

Campbell, R. H., 1975. Soil slips, debris flows and rainstorms in the Santa Monica Mountains and vicinity, S. California. *U. S. Geol. Survey Prof. Paper*, No. 851.

Camponuovo, G. F., 1977. ISMES experience on the model of f.San Martino. in *Rockfall Dynamics and Protective Works Effectiveness*, ISMES Publication No. 90, pp 25-38, Bergamo, Italy.

Carriggy, M. A. 1970. Experiments on the angles of repose of granular materials. *Sedimentology*. Vol. 14, pp 147-158.

Carson, M. A., 1977. Angles of repose, angles of shearing resistance and angles of talus slopes. *Earth Surface Processes*, pp 363-380.

Carter, R. M., 1975. A discussion and classification of subaquaeous mass transport with particular application to grain flows, debris flows and fluxoturbidites. *Earth Science Review*, Vol. 11, pp 145-177.

Casagrande, A., 1936. Characteristics of cohesionless soils affecting the stability of slopes and earth fills. *Contributions ot Soil Mechanics, 1925-1940*. Boston Soc. of Civil Engineers.

Casagrande, A., 1965. The rôle of calculated risk in earthwork and foundation engineering. *Journ. ASCE, Soil Mech. and Found. Eng. Div.*, Vol. 91, No. SM 4, pp 1-40.

Casagrande, A., 1976. Liquefaction and cyclic deformation of sands: a critical review. *Harvard Soil Mechanics Series* No. 88, Cambridge, Massachusetts. 26 pp.

Castro, G., 1969. Liquefaction of Sands. *Harvard Soil Mechanics Series*, No. 81, Cambridge Massachusetts. 112 pp.

Cheng, T. T. and Perla, R., 1979. Numerical computation of avalanche motion. Nat. Hydrology Res. Inst. Paper No. 5, Environment Canada.

Chow, Ven Te, 1959. *Open Channel Hydraulics*. Mc Graw Hill, New York, 680 pp.

Chowdhury, R., 1978. Analysis of the Vajont Slide - a new approach. *Rock Mechanics*, Vol. 11, pp 29-38.

Coates, D. F., 1970. *Rock Mechanics Principles*, Mines Branch Monograph 874, Govt. of Canada.

Coates, D. R., 1977. Landslide Perspectives. In *Landslides*, ed. by author, Reviews in Eng. Geology III, Geol. Soc. of America, pp 3-28.

Conlon, R. J., 1966. Landslide on the Toulnustonc River, Quebec. *Canadian Geotech. Journ.*, Vol. 3, pp 113-144.

Costa Nunes, A. J. da, 1969. Landslides in soils of decomposed rock due to intense rainstorms. *Proc., Int. Conf. Soil Mech. Found. Eng.*, Mexico, Vol. 2, pp 547-563.

Crandell, D. R., 1957. Some features of mudflow deposits (Abstract). *Bull., Geol. Soc. of Am.*, Vol. 68, p 1821.

Crandell, D. R. and Waldron, H. H., 1956. A recent volcanic mudflow of exceptional dimensions from Mt. Rainier. *Am. Journ. of Science*, Vol. 254, pp 349-362.

Crandell, D. R. and Varnes, D. J., 1961. Movement of the Slumgullion earth flow. *U. S. Geol. Survey Prof. Paper*, 424-B, pp 136-139.

Crawford, C. B., 1959. The influence of rate of strain on stress. *ASTM Special Tech. Publication* . No. 254, pp 36-48.

Crawford, C. B., 1968. Quick clays of Eastern Canada. *Engineering Geology*. Vol. 2, pp 239-265.

Cruden, D. M., 1976. Major rockslides in the Rockies. *Canadian Geotech. Journ.*, Vol. 13, pp 8-20.

Cruden, D. M. and Krahn, J., 1978. Frank Rockslide, Alberta, Canada. *Rockslides and Avalanches*, Voight, B., Ed., Elsevier,, Vol. 1, pp 97-112.

Cundall, P. A., 1971. A computer model for simulating progressive large- scale movements in blocky rock systems. *Proc., International Symp. on Rock Fracture*, Nancy, Paper II-8.

Cundall, P. 1976. Computer interactive graphics and the Distinct Element Method. In *Rock Engineering for Foundations and Slopes*, ASCE Conf, Boulder, Colo. Vol. II, pp 193-199.

Curry, R. R., 1966. Observation of alpine mudflows in the Tenmile Range, Central Colorado. *Bull., Geol. Soc. of Am.*, Vol. 77, pp 771-776.

Daly, R. A., Miller, W. G. and Rice, G. S., 1912. Report of the comission appointed to investigate Turtle Mountain, Frank, Alberta. *Can. Geol. Survey Mem.* pp 27-34.

Daido, A., 1971. On the occurrence of mud- debris flow. *Bull, Disaster Prevention Research Institute*, Kyoto Univ., Vol. 21, part 2, pp 109-135.

Dascal, O., Tournier, J. P., Tavenas, F. and la Rochelle, P., 1972. Failure of a test embankment on sensitive clay. In *Performance of Earth and Earth-Supported Structures*, ASCE, Vol, 1, Part 1, pp 129-158,

da Silva, J. M. J., 1979. Itaipoo Lagoon, instrumented failure. M. Sc. Thesis, P. U. C. R. J., Rio de Janeiro, Brazil.

De Beer, E., 1967. Shear strength characteristics of the Boom clay. *Proc., Geotech. Conf. Oslo*, Vol.1, pp 83-88.

De Freitas, M. H. and Watters, R. J., 1973. Some field examples of toppling failure. *Geotechnique*, Vol, 23, pp 495-514.

Dill, R. F., 1964. Sedimentation and erosion in Scripps submarine canyon head. In *Papers in Marine Geology*, Miller, R. L. Ed., Macmillan, New York.

Dodds, R. K., 1966. Rock movement along fractures during failure. *Proc., 1st Congress ISRM*, Lisbon, Vol. 2, pp 133-137.

Dredge, L. A. and Thom, B. G., 1976. Development of a gully flow near Sept-Isles, Quebec. *Can. Journ. Earth Sci.*, Vol. 13 pp 1145-1151.

Eden, W. J., Fletcher E. B. and Mitchell, R. J., 1971. South Nation River Landslide, 16 may 1971. *Canadian Geotech. Journ.*, Vol, 8, pp 446-451.

Eisbacher, G. H., 1979. Cliff collapse and rock avalanches (sturzstroms) in the Mackenzie Mountains, north-western Canada. *Canadian Geotech. Journ.*, Vol. 16, pp 309-334.

Emery, J. J., 1978. Creep of slopes. In *Rockslides and Avalanches*, Voight, B., Ed., Elsevier,, Vol 1.

Engineering News Record, 1971. Contrived landslide kills 15 in Japan. Vol. 187, p 18.

Enos, P., 1977. Flow regimes in debris flow. *Sedimentology*, Vol. 24 pp 133-142.

Erismann, T. Heuberger, H. and Preuss, E., 1977. Der Bimsstein von Kofels (Tirol), ein Bergsturz- Friktionit. *Tschermaks Mineralogische und Petrologische Mitteilungen*, Vol. 24, No. 1, pp 67-119.

Erismann, T. H., 1979. Mechanism of large landslides. *Rock Mechanics*, Vol. 12, pp 15-46.

Evans, S. G. 1979. Unpublished research on angles of repose of granular materials.

Fahnestock, R. K. 1978. Little Tahoma Peak rockfalls and avalanches, Mount Rainier. In *Rockslides and Avalanches*, Voight, B., Ed., Elsevier,, Vol. 1, pp 181-197.

Farris, R. J., 1968. Prediction of the viscosity of multimodal suspensions from unimodal viscosity data. *Trans., Soc. Rheology*, Vol. 12, pp 281-301.

Fisher, R. V., 1971. Features of coarse grained, high-concentration fluids and their deposits. *Journ. Sed. Petrol.*, Vol. 41, pp 916-927.

Fookes, P. G. and Sweeney, M., 1976. Stabilization and control of local rock falls and degrading rock slopes. *Quart. Journ. Eng. Geol.*, vol. 9, pp 37-55.

Ford, T. F., 1960. Viscosity- concentration and fluidity concentration relationships for suspensions of spherical particles in Newtonian liquids. *Journ. Phys. Chem*, Vol. 64, pp 1168-1174.

Francis, P. W. and Baker, M. W., 1977. Mobility of pyroclastic flows. *Nature*, Vol. 270, pp 164-165.

Gardner, J., 1972. Rockfall as a morphologic agent in high mountains. *Albertan Geographer*, Vol. 6, pp 15-20.

Gol'din, B. M. and Lubashevski, L. S., 1966. Computation of the velocity of mudflows in Crimean rivers. *Soviet Hydrology*

Goguel, J. and Pachoud, A., 1972. Geology and dynamics of the rockfall of the Granier Range wich occurred in November 1248. *Bull., Bur. Rech. Geol. Min. Hydrogeologie* No 1, pp 29-38.

Goldsmith, W., 1960. *Impact, the Theory and Practice of Colliding Solids*, Edward Arnold, London, pp 379.

Goodman, M. A. and Cowin, S. C., 1971. Two problems in the flow of granular solids. *Journ. of Fluid Mech.*, Vol. 45, pp 321-339.

Goodman, R. E., 1969. The deformability of joints. *ASTM Spec. Tech. Publ.* 477.

Goodman, R. E. and Bray, J. W., 1976. Toppling of rock slopes, in *Rock Engineering for Foundations and Slopes*, ASCE Conf., Boulder, Colo., Vol. II, pp 201-234.

Gould, J. P., 1960. A study of shear failure in certain tertiary marine sediments. In *Shear Strength of Cohesive Soils*, ASCE Conf., Boulder, Colo., pp 614-641.

Govi, M., 1977. Photo-interpretation and mapping of the landslides triggered by the Friuli earthquake (1976). *Bull., Int. Assoc. Eng. Geol.*, No. 15, pp 67-72.

Griggs, E., 1920. Great Mageik Slide, Alaska. *Ohio Journal of Science*, Vol. 20, pp 325-354.

Habib, P., 1975. Production of gaseous pore pressure during rock slides. *Rock Mechanics*, Vol. 7, pp 193-197.

Hacar Benitez, M. A., Bollo Mi. F. and Hacar Rodrigues, M. P., 1977. Bodies falling down on different slopes- a dynamic study. *Proc., Int. Conf. Soil Mech. Found. Eng.*, Tokyo, Vol. 2, pp 91-94.

Hadley, J. B., 1964. Landslides and related phenomena accompanying the Hebgen Lake earthquake of August 17, 1959. *U. S. Geol. Survey Prof. Paper* 435-K, pp 107-138.

Haefeli, R., 1965. Creep and progressive failure in snow, soil, rock and ice. *Proc., Int. Conf. Soil Mech. Found. Eng.*, Montreal, Vol. III, pp 134-148.

Hampton, M. A., 1972. The role of subaqueous debris flow in generating turbidity currents. *Journ. Sed. Petrol.*, Vol. 42, pp 775-793.

Hampton, M., 1975. Competence of fine-grained debris flows. *Journ. Sed. Petrol.*, Vol 45, pp 834-844.

Hamel, J. V., 1972. The slide at Brilliant Cut. *Proc, 13th Symposium on Rock Mecanics*, A. S. C. E., pp 487-510.

Hamel, J. V., 1976. Libby Dam left abutment rock wedge stability. *Rock Engineering for Foundations and Slopes* ASCE Conf., Boulder, Colo., pp 361-385.

Hammett, R. D., 1974. A study of the deformation of a discontinuous rock mass. Ph. D. thesis, James Cook University of North Queensland, Australia.

Hanks, R. V. and Pratt, D. R., 1967. On the flow of Bingham plastic slurries in pipes and between parallel plates. *Journ. Soc. of Petr. Engs.*, pp 342-346.

Hardy, R. M., Morgenstern, N. R. and Patton, F. D., 1978. The Garibaldi Advisory Panel Report. Dept. of Highways, Prov. Govt. of British Columbia, Vols. 1, 2 and 3.

Harrison, J. V. and Falcon, N. L., 1938. An ancient landslip at Saidmarreh in South- western Iran. *Journ. of Geology*, Vol. 46, pp 296-309.

Hayley, D. W., 1968. Progressive failure of a clay slope in

Northern Alberta. M. Sc. thesis, U. of Alberta.

Healy, K. A., 1963. The dependence of dilation in sand on rate of shear strain. Ph. D. thesis, Mass. Inst. of Technology.

Heezen, B. C. and Ewing, M., 1952. Turbidity currents and submarine slumps and the Grand Banks earthquake. *Am. Journal of Science*, Vol. 250, pp 849-873.

Heim, A., 1932. *Bergsturz und Menchenleben*. Zurich, Vierteljahrsschrift 77, No. 20, Beiblatt. pp 218.

Heimgartner, M., 1977. On the flow of avalanching snow. *Journal of glaciology* Vol. 19, pp 357-363.

Henderson, F. M., 1966. *Open Channel Flow*, Macmillan, New York. pp 450.

Hildebrand, F. B., 1974. *Introduction to Numerical Analysis*. 2nd ed., McGraw-Hill.

Hoek, E. and Bray, J. V., 1977. *Rock Slope Engineering*. Inst. Min. Met., London, 309 pp.

Holmsen, P., 1953. Landslip in Norwegian quick- clays. *Geotechnique*, Vol, 3, pp 187-194.

Howard, K., 1973. Avalanche mode of motion: implication from lunar examples. *Science*, Vol. 180, pp 1052-1055.

Hsu, K. J., 1975. Catastrophic debris streams (sturzstorms) generated by rockfalls. *Bull., Geol. Soc. of Am.*, Vol. 86, pp 129-140.

Hsu, K. J. 1978. Albert Heim, Observations on landslides and relevance to modern interpretations. In *Rockslides and Avalanches*, Voight, B., Ed., Elsevier,, Vol. 1, pp 71-92.

Huder, J., 1976. Creep in Bundner Schist. *Laurits Bjerrum Memorial Volume*, Oslo, pp 125-153.

Hutchinson, J. N., 1961. A landslide on a thin layer of quick clay at Furre, central Norway. *Geotechnique*, Vol 11, pp 69-94.

Hutchinson, J. N., 1968. Mass Movement. *The Encyclopedia of Geomorphology*. R. W. Fairbridge, Ed., Reinold, pp 688-695.

Hutchinson, J. N., 1970. A coastal mudflow on the London Clay cliffs at Beltinge, North Kent. *Geotechnique*, Vol, 20, pp 412-438.

Hutchinson, J. N. and Bhandari, R. K., 1971. Undrained loading, a fundamental mechanism of mudflow and other mass movements. *Geotechnique*, Vol. 21, pp 353-358.

Hutchinson, J. N., Prior D. B. and Stephens, N., 1974. Potentially dangerous surges in an Antrim mudslide. *Quart. Journ. Eng. Geol.*, Vol. 7, pp 363-376.

Hutchinson, J. N. and Bromhead, J., 1981. A method of calculation of the velocity and reach of flow slides. (Unpublished)

Hvorslev. M. J., 1939. Torsion shear tests and their place in the determination of the shearing resistance of soils. *Proc., Am. Soc. Testing Mat.*, Vol. 39, pp 999-1022.

Jackson, L. E., 1979. A catastrophic glacial outburst flood (jokulhlaup) mechanism for debris flow generation at the Spiral Tunnels, Kicking Horse River basin, B. C., *Canadian Geotech. Journ.*, Vol. 15, pp 806-813.

Jaeger, C., 1979. *Rock Mechanics and Engineering.* Cambridge University Press, 2nd. Ed., 523 pp.

James, P. M., 1971. The role of progressive failure in clay slopes. *Proc., 1st Australia-New Zealand Conference on Geomechanics*, Vol. 1, pp 344-349.

Jeyapalan, K., 1980. Analyses of flow failures of mine tailings impoundments. Ph. D. thesis, U. of California, Berkeley.

Johnson, A. M., 1970. *Physical Processes in Geology*. Freeman- Cooper, San Franccisco, 577 pp.

Johnson, A. M. and Rahn, P. H., 1970. Mobilization of debris flows. In *New Contributions to Slope Evolution*, Zeitschrift fur Geomorphologie, Supplement 9, pp 168-186.

Johnson, B., 1978. Blackhawk Landslide, California. In *Rockslides and Avalanches*, Voight, B., Ed., Elsevier,, Vol. 1, pp 481-504.

Kaiser, P., 1978. Analysis of Rubble Creek Debris Flow. Report in Vol. III of Hardy et al, 1978.

Kaiser, P., 1980. Unpublished field observations from the Mackenzie Mountains.

Keefer, D. K., 1977. Earthflow. Ph. D. thesis, Stanford U.

Kellerhals, R. and Bray, D. I., 1971. Sampling procedures for coarse fluvial sediments. *ASCE Journ. Hydraulics Div.*, Vol. 97, pp 1165-1180.

Kennedy, B. A. and Niermeyer, K. E., 1971. Slope monitoring systems used in the prediction of major slope failure at the Chiquicamata Mine, Chile. *Planning Open Pit Mines*, Johannesburg Symp., pp 215-225.

Kenney, T. C., 1967. The influence of mineral composition on residual strength of natural soils. Proc., Geotech. Conf. Oslo, Vol. 1, pp 123-129.

Kenney, T. C., 1967. Slide behaviour and shear resistance of a quick clay determined from a study of the landslide at Selnes, Norway. Proc., Geotech. Conf. Oslo, Vol. 1, pp 57-64.

Kenney, T. C., 1967. Stability of the Vaiont- Valley Slope. *Rock Mech. and Eng. Geol.*, Vol. 5, pp 10-16.

Kent, P. E., 1966. The transport mechanism in catastrophic rock falls. *Journ. of Geology*, Vol. 74, pp 79-83.

Keulegan, K. H., 1949. Interfacial mixing and instability in stratified flows. *U. S. Nat'l Standards Journ. of Research*, Vol. 43, pp 487-500.

Kirkby, M. J., 1967. Measurement and theory of soil creep. *Journ. of Geology*, Vol. 75, pp 359-378.

Kirkby, M. J. and Statham, I., 1975. Surface stone movement and talus formation. *Journ. of Geology*, Vol. 83, pp 349-362.

Koerner, H. J., 1976. Reichweite und Geschwindigkeit von Bergsturzen und Fliesschneelawinen. *Rock Mechanics*, Vol. 8, pp 225-256.

Koerner, H. J., 1977. Flow mechanisms and resistances in the debris streams of rock slides. *Bull., Int. Assoc. Eng. Geol.*, No. 16, pp 101-104.

Kojan, E., 1968. Mechanics and rates of natural soil creep. *Proc., 1st Session of the Int. Assoc. Eng. Geol.*, Prague, pp122-154.

Kojan, E. and Hutchinson, J. N., 1978. Mayunmarca rockslide and debris flow, Peru. In *Rockslides and Avalanches*, Voight, B., Ed., Elsevier,, Vol 1, pp 315-361.

Koppejan, A. W., Wamelen, B. M. and Weinberg, L. J., 1948. Coastal flowslides in the Dutch province of Zeeland. *Proc., Int. Conf. Soil Mech. Found. Eng.*, Rotterdam, Vol, 5 pp 89-96.

Krahn, J. 1974. Rock slope stability with emphasis on the Frank Slide. Ph. D. thesis, U. of Alberta.

Krahn., J. and Morgenstern, N. R., 1979. The ultimate frictional resistance of rock discontinuities. *Int. Journal Rock Mech. Min. Sci. & Geomech. Abstr.*, Vol. 16, pp 127-133.

Krsmanovic, D., 1967. Initial and residual shear strength of hard rocks. *Geotechnique*, Vol. 17, pp 145-160.

Kuenen, P. H., 1952. Estimated size of the Grand Banks turbidity current. *Am. Journ. of Science*, Vol. 250, pp 874-884.

Kunii, D. and Levenspiel, O., 1969. *Fluidization Engineering*, John Wiley, New York, 534 pp.

Kutter, H. K., 1974. Rotary shear testing of rock joints. *Proc., 3rd Congress ISRM*, Denver, Vol. II-A, pp 254-262.

Lachenbruch, A. H., 1980. Frictional heating, fluid pressure and the resistance to fault motion. *Journ. of Geophysical Research*, Vol. 85, pp 6097-6112.

Ladd, G. E., 1935. Landslides, subsidences and rockfalls. *Proc., Amer. Railway Eng. Assoc.* , Vol. 36, pp 1091-1162.

Ladanyi, B., Morin, J. P. and Pelchat, C., 1968. Post- peak behaviour of sensitive clays in undrained shear. *Canadian Geotech. Journ.*, Vol. 5, pp 59-68.

Lambe, T. W. and Whitman, R. V., 1979. *Soil Mechanics; SI Version*. Wiley, 553 pp.

Lewis, T. B. and Nielsen, L. E., 1968. Viscosity of dispersed and aggregated suspensions of spheres. *Trans. Soc. of Rheology*, Vol. 12, pp 421-443.

Lied, D., 1977. Rockfall problems in Norway. In *Rockfall Dynamics and Protective Works Effectiveness* ISMES Publication No. 90, pp 51-54, Bergamo, Italy.

Lo, K. Y. and Lee, C. F., 1973. Analysis of progressive failure in clay slopes. *Proc., Int. Conf. Soil Mech. Found. Eng.*, Moscow, Vol. 1.1, pp 251-258.

Lo, K. Y., 1972. An approach to the problem of progressive failure. *Canadian Geotech. Journ.*, Vol. 9, pp 407-429.

Lowe, D. R., 1975. Water escape structures in coarse-grained sediments. *Sedimentology*, Vol. 22, pp 157-204.

Lowe, D. R., 1976. Grain flows and grain flow deposits. *Journ. Sed. Petrol.*, Vol. 46, pp 188-199.

Lowe, D. R., 1976. Subaqueous liquefied and fluidized sediment flows and their deposits. *Sedimentology*, Vol. 23, pp 285-308.

Lucchitta, B. K., 1978. A large landslide on Mars. *Bull., Geol. Soc. of America* ,Vol. 89, pp 1601-1609.

Lumb, P., 1975. Slope failures in Hong-Kong. *Quart. Journ. Eng. Geol.*, Vol. 8, pp 31-65.

Marangunic, C., 1972. Effects of a landslide on Sherman Glacier, Alaska. Institute of Polar Studies Report No. 30, Ohio State University, Columbus, Ohio.

Massey, B. S., 1970. *Mechanics of Fluids.* Van Nostrand Reinhold, London, 507 pp.

Mathews, W. H. and McTaggart, K. C., 1969. The Hope Landslide, B. C. *Proc., Geolog. Assoc. Canada*, Vol. 20, pp 65-75.

McConnell, R. G. and Brock, R. W., 1904. The great landslide at Frank, Alberta, *Canadian Parliament Sessional Paper*, No. 25, Dept. of the Interior, 1904.

McRoberts, E. C. and Morgenstern, N. R., 1979. Stability of slopes in frozen soil, Mackenzie Valley. *Canadian Geotech. Journ.*, Vol. II, pp 554-573.

McRoberts, E. C., 1975. Some aspects of a simple secondary creep model for deformations in permafrost slopes. *Canadian Geotech. Journ.*, Vol. 12, pp 98-105.

McRoberts, E. C. and Nixon, J. F., 1976. A theory of soil sedimentation. *Canadian Geotech. Journ.*, Vol. 13, pp 294-310.

McSaveney, M. J., 1975. The Sherman glacier rock avalanche of 1964: its emplacement and subsequent effects. Ph. D. thesis, Ohio State U.

McSaveney, M. J., 1978. Sherman Glacier rock avalanche, Alaska. In *Rockslides and Avalanches*, Voight, B., Ed., Elsevier,, Vol. 1, pp 197-258.

Mears, A. I., 1979. Flooding and sediment transport in a small alpine drainage basin in Colorado. *Geology*, Vol. 7, pp 53-57.

Menard, H. W., 1964. *Marine Geology of the Pacific*. Mc Graw-Hill, New York, 271 pp.

Metzner, A. B. and Whitlock, M., 1958. Flow behaviour of concentrated (dilatant) suspensions. *Trans. Soc. Rheol.*, Vol. 2, pp 239-254.

Meyerhof, G. G., 1957. The mechanism of flow slides in cohesive soils. *Geotechnique*, Vol. 7, pp 41-49.

Melosh, H. J., 1979. Acoustic fluidization: a new geologic process? *Journ. Geophys. Res.*, Vol. 84, pp 7513-7520.

Mencl, V., 1966. Mechanics of landslides with non- circular slip surfaces with special reference to the Vaiont slide. *Geotechnique*, Vol 16, pp 329-337.

Michaels, A. S. and Bolger, J. C., 1962. The plastic flow behaviour of flocculated kaolin suspensions. *Industrial and Eng. Chemistry Fundamentals*, Vol. 1, pp 153-162.

Middleton, G. V., 1966. Experiments on density and turbidity currents, I, motion of the head. *Can. Journ. Earth Sci.*, Vol. 3, pp 523-546.

Middleton, G. V., 1966. Experiments on density and turbidity currents, II, uniform flow of density currents. *Can. Journ. Earth Sci.*, Vol. 3 pp 627-637.

Middleton, G. V., 1970. Experimental studies related to the problems of flysch sedimentation. *Geol. Assoc. of Canada, Spec. Paper* No. 7, pp 253-269.

Middleton, G. V. and Hampton, M. A., 1976. Subaqueous sediment transport and deposition by sediment gravity flows. In *Marine Sediment Transport and Environmental Management*, Stanley, D. J. and Swift, D. J., Eds., Wiley-Interscience, pp 197-220.

Mitchell, R. J. and Eden, W. J., 1972. Measured movements of clays in the Ottawa area. *Can. Journ. Earth Sci.*, Vol. 9, pp 1001-1013.

Mitchell, R. J. and Markell, A. R., 1974. Flowsliding in sensitive soils. *Canadian Geotech. Journ.*, Vol. 11, pp 11-31.

Mitchell, J. K., 1976. *Fundamentals of Soil Behaviour.* Willey, New York.

Mogami, T. and Kubo, K., 1953. The behaviour of soil during vibration. *Proc., Int. Conf. Soil Mech. Found. Eng.*, Zurych, Vol. 1, pp 152-155.

Mollard, J. D., 1977. Regional landslide types in Canada. In *Landslides*, Coates, D. R., Ed., Reviews in Eng. Geol. III, Geol. Soc. of Am., pp 29-56.

Morgenstern, N. R., 1967. Submarine slumping and the initiation of turbidity currents. In *Marine Geotechnique*, A. F. Richards, ed., Univ. of Illinois Press, pp 189-220.

Morgenstern, N. R., 1978. Mobile soil and rock flows. *Geotechnical Engineering*, Vol. 9, pp 123-141.

Morgenstern, N. R. and Tchalenko, J. S., 1967. Microstructural observations on shear zones from slips in natural clays. Proc., Geotech. Conf. Oslo, pp 147-152.

Morton, D. M. and Campbell, R. H., 1974. Spring mudflows at Wrightwood, S. California. *Quart. Journ. Eng. Geol.*, Vol. 7, pp 377-384.

Mueller, L., 1964. The Rock Slide in the Vaiont Valley. *Felsmechanik und Eng. Geol.* , Vol. 2, pp 1489-212.

Mueller, L., 1968. New Consideration on the Vaiont Slide. *Felsmechanik und Ing. Geol.* , Vol. 6, pp 1-91.

Nascimento, U. and Texeira, H., 1971. Mechanisms of internal friction in soils and rocks. *Proc., Internat. Symp. on Rock Fracture*, Nancy, Paper II-3.

Nasmith, H. W. and Mercer, A. G., 1979. Design of dykes to protect against debris flows at Port Alice, British Columbia. *Canadian Geotech. Journ.*, Vol. 16, pp 748-757.

Neal, V. E., 1976. Lahars as major geological hazards. *Bull., Int. Assoc. Eng. Geol.*, No. 14, pp 233-240.

Nemcok, A., Pasek, J. and Rybar, J., 1972. Classification of landslides and other mass movements. *Rock Mechanics*, Vol. 4, pp 71-78.

Nisbet, R. M., 1973. Energy considerations and movements of landslips with special reference to post- rupture analysis. M. Sc. thesis, Imperial College, London.

Novosad, J., 1964. Studies on granular materials II. *Colln. Czech. Chem. Commun.* , Vol. 29, p 2697.

Noren, C. H. and Porter, D. D., 1974. A comparison of theoretical explosive energy with measured rock fragmentation. *Proc., 3rd Congress ISRM*, Denver, Vol. II-B, pp 1371-1375.

Palmer, L., 1977. Large rockslides of the Columbia River gorge, Oregon & Washington. In *Landslides*, Coates, D. R., Ed., Reviews in Eng. Geol. III, Geol. Soc. of Am., pp 69-83.

Pautre, A. F., Sabarly, F. and Schneider, B., 1974. L'effet d'echelle dans les ecroulements de falaise. *Proc., 3rd Congress ISRM*, Denver, vol. II-B, pp 859-864.

Peck, R. B. and Kaun, W. V., 1948. Description of a flow slide in loose sand. *Proc., Int. Conf. Soil Mech. Found. Eng.*, Rotterdam, Vol. 2, pp 31-33.

Peckover, F. L. and Kerr, J. W. G., 1977. Treatment and maintenance of rock falls on transportation routes. *Canadian Geotech. Journ.*, Vol. 14, pp 487-507.

Petley, D. I., 1966. The shear strength of soils at large strains. Ph. D. thesis, University of London.

Pierson, T. C., 1980. Erosion and deposition by debris flows at Mt. Thomas, North Canterbury, New Zealand. *Earth Surface Processes*, Vol. 5, pp 227-247.

Piteau, D. R. and Clayton, R., 1972. Discussion of paper: Computerized design of rock slopes using interactive graphics for the input and output of geometrical data by Cundall, M. D. et al. in *Proc., 16th Symposium on Rock Mechanics*, C. Fairhurst, Ed., Minneapolis, Minn., pp 62-63.

Piteau, D. R., Mylrea, F. H. and Blown, I. G., 1978. Downie Slide, Columbia River, British Columbia. In *Rockslides and Avalanches*, Voight, B., Ed., Elsevier,, Vol. 1 pp 365-392.

Plafker, G. and Ericksen, G. E., 1978. Nevados Huascaran avalanches, Peru. In *Rockslides and Avalanches*, Voight, B., Ed., Elsevier,, Vol. 1, pp 277-314.

Radbruch-Hall, D. H. and Varnes, D. J., 1976. Landslides-causes and effects. *Bull., Int. Assoc. Eng. Geol.*, No. 14, pp 205-216.

Radbruch-Hall, D. H., 1978. Gravitational creep of rock masses on slopes. In *Rockslides and Avalanches*, Voight, B., Ed., Elsevier,, Vol. 1, pp 607-658.

Radley Squier, L. and Versteeg, J. H., 1971. The history and correction of the Omsi-Zoo landslide. *Proc., 9th Annual Eng. Geol. and Soil Mechanics Symp.* , Boise, Idaho, pp 237-256.

Rapp, A., 1960. Recent development of mountain slopes in Karkevagge and surroundings, northern Scandinavia. *Geogr. Annaler*, Vol 42, pp 65-200.

Reik, G. and Hesselman, F. J., 1977. A study of kinematic and dynamic aspects of rock slides. In *Rockfall Dynamics* *and Protective Works Effectiveness*, ISMES Publication No. 90, pp 97-122, Bergamo, Italy.

Richardson, A. M. and Whitman, R. V., 1963. Effect of strain rate upon undrained shear resistance of a saturated remolded fat clay. *Geotechnique*, Vol. 13, pp 310-324.

Richardson, V. F. and Zaki, W. N., 1954. Sedimentation and fluidization, Part I. *Trans. Inst. Chem. Eng.* , Vol, 32, pp 35-53.

Ritchie, A. M., 1963. Evaluation of rockfall and its control. *Higway Research Record*, Vol. 17, pp 13-28.

Roberts, J., 1969. An investigation of the gravity flow of noncohesive granular material through discharge chutes. *Trans., ASME, Journ. Eng. Ind.*, Vol. 91, pp 373-381.

Rodine, J. D., 1975. Analysis of the mobilization of debris flows. Ph. D. thesis, Stanford U.

Romero, S. U. and Molina, R. 1974. Kinematic aspects of Vaiont Slide. *Proc., 3rd Congress ISRM*, Denver, Vol. II-B, pp 865-870.

Rowe, P. W., 1962. The stress-dilatancy relation for static equilibrium of an assembly of particles in contact. *Proc., Royal Soc. of London*, Vol. 269. Ser. A, pp 500-527.

Saito, M. 1965. Forecasting the time of occurrence of a slope failure. *Proc., Int. Conf. Soil Mech. Found. Eng.*, Montreal, Vol. 6, pp 537-541.

Salm, B., 1966. Contribution to avalanche dynamics. *Int. Assoc. Sci. Hydrology, Publ.* , pp. 199-214.

Salm, B., 1968. On nonuniform steady flow of avalanching snow. *Int. Assoc. Sci. Hydrology, Publ.* , 79, pp 19-29.

Savage, J., 1979. *Fluid Mechanics*

Savigny, K. V., 1980. In situ analysis of naturally occurring creep in ice- rich permafrost. Ph. D. thesis, U. of Alberta.

Scarlett, B. and Todd, A. C., 1969. The critical porosity of free- flowing solids. *Trans., ASME, Journ. of Eng. Ind.* , Ser. A, Vol. 91, Pt 1.

Schaerer, P. A., 1975. Friction coefficients and speed of flowing avalanches. *Int. Assoc. Sci. Hydrology, Publ. 114*, pp 425-432.

Sheidegger, A. E., 1973. On the prediction of the reach and velocity of catastrophic landslides. *Rock Mechanics*, Vol. 5, pp 231-236.

Scheidegger, A. E., 1975. *Physical aspects of natural catastrophes*. Elsevier Sci. Publ. Co., New York, 289 pp.

Schmincke, H. U., 1967. Graded lahars in the type section of the Ellensburg formation, South- Central Washington. *Journ. Sed. Petrol.*, Vol. 37, pp 438-448.

Schmitt, H. H., 1973. Apollo 17 report on the valley of Taurus- Littrow. *Science*, Vol. 182, pp 681-690.

Schneider, H., 1976. Shear rate and friction of rock joints. *Bull., Int. Assoc. Eng. Geol.*, No. 13, pp 109-112.

Schofield, A. and Wroth, P., 1968. *Critical State Soil Mechanics*, Mc Graw-Hill, London, 310 pp.

Schumm, S. A., 1966. Rates of surficial rock creep on hillslopes in Western Colorado. *Science*, Vol. 155, pp 560-561.

Schumm, S. A. and Chorley, R. J. 1964. The fall of Threatening Rock. *American Journ. of Science*, Vol. 262, pp 1041-1054.

Schuster, R. L., 1978. Introduction to *Landslides Analysis and Control*, Transportation Research Board Special Report 176, Washington, pp 1-10.

Searle, A. B. and Grimshaw, R. W., 1959. *The Chemistry and Physics of Clays and Other Ceramic Materials*. Interscience Publishers, Inc., 942 pp.

Seed, H. B., 1968. Landslides during earthquakes due to soil liquefaction. *Journ. ASCE, Soil Mech. and Found. Eng. Div.*, Vol. 94, SM 5, pp 1053-1122.

Seed, H. B. and Wilson, S. D., 1967. The Turnagain Hts. landslide, Alaska. *Journ. ASCE, Soil Mech. and Found. Eng. Div.*, Vol 93, pp 325-353.

Sevaldson, R. A., 1956. The slide at Lodalen, Oct. 6th, 1954. *Geotechnique*, Vol. 6, pp 1-16.

Sharp, R. P., 1942. Mudflow levees. *Journ. of Geomorphology*, Vol. 5, pp 222-227.

Sharp, R. P. and Nobles, L. H., 1953. Mudflow of 1941 at Wrightwood, Southern California. *Bull., Geol. Soc. of Am.*, Vol. 64, pp 547-560.

Sharpe, C. F. S., 1938. *Landslides and Related Phenomena*, Columbia University Press, New York. 137 pp.

Sharpe, C. F. S. and Dosch, E. F., 1942. Relation of soil creep to earthflow in the Appalachian Plateau. *Journal of Geomorphology*, Vol. 5, pp 132.

Shreve, R. L., 1966. Sherman Landslide, Alaska. *Science*, Vol. 154, pp 1639-1643.

Shreve, R. L., 1968. The Blackhawk Landslide. *Geological Soc. of America, Special Paper* No. 108.

Shreve, R. L., 1968a. Leakage and Fluidization in Air-Layer Lubricated Avalanches. *Bull., Geol. Soc. of Am.*, Vol. 79, pp 653-658.

Simmons, J. V., 1981. Ph. D. thesis, U. of Alberta.

Simmons, J. V. and Cruden, D. M., 1980. A rock labyrinth in the Front Ranges of the Rockies, Alberta. *Canadian Geotech. Journ.*, Vol. 17, pp 1300-1309.

Skempton, A. W., 1964. Long-term stability of clay slopes. 4th Rankine Lecture, *Geotechnique*, Vol. 14, pp 77-102.

Skempton, A. W., 1966. Bedding plane slip, residual strength and the Vaiont Landslide. Correspondence, *Geotechnique*, vol. 16, pp 82-84.

Skempton, A. W. and Hutchinson, J., 1969. Stablility of natural slopes and embankment foundations. *Proc., Int. Conf. Soil Mech. Found. Eng.*, Mexico, State- of- the-Art volume, pp 291-340.

Solonenko, V. P., 1977. Landslides and collapses in seismic zones and their prediction. *Bull., Int. Assoc. Eng. Geol.*, No. 15, pp 4-8.

Spurek, M., 1972. Historical catalogue of slide phenomena. *Studia Geographica*, Brno, Col. 19, 178 pp.

Statham, I., 1976. A simple slope rockfall model. *Earth Surface Processes*, Vol. 1, pp 43-62.

Stroganov, A. S., 1961. Visco- plastic flow of soils. *Proc., Int. Conf. Soil Mech. Found. Eng.*, Paris, Vol. 2, pp 721-726.

Suklje, L., 1961. A landslide due to long term creep. proc., *Proc., Int. Conf. Soil Mech. Found. Eng.*, Paris, Vol. pp 727.

Suwa. H. Okuda, S. and Yokoyama, K., 1973. Observation system on rocky mudflow. *Bull. Disaster Prevention Inst.*, Kyoto Univ., Vol. 23, Parts 3-4, pp 59-73.

Suzuki, A. and Tanaka, T., 1971. Measurement of flow properties of powders along an inclined plane. *Ind. Chem. Fundam.*, Vol. 10, pp 84-91.

Takahashi, K., 1937. On the dynamical properties of granular masses. *Geophysical Magazine*, Vol. 11, pp 165-175.

Tavenas, F., Chagnon, J. Y. and la Rochelle, P., 1971. The Saint-Jean Vianney landslide: observations and eyewitness accounts. *Canadian Geotech. Journ.*, Vol. 8, pp 463-478.

Takahashi, T., 1978. Mechanical characteristics of debris flow. *Journ. ASCE, Hydraulics Div.*, Vol. 104, pp 1153-1169.

Takahashi, T., 1980. Debris flow on prismatic open channel. *Journ. ASCE, Hydraulics Div.*, Vol. 106, pp 381-396.

Taylor, D. W., 1948. *Fundamentals of Soil Mechanics*. Wiley, New York.

Ter-Stepanian, G., 1963. On the long-term stability of slopes. *NGI Publication* No. 52, Oslo.

Ter-Stepanian, G., 1965. In-Situ determination of the rheological characteristics of soils on slopes. *Proc., Int. Conf. Soil Mech. Found. Eng.*, Montreal, Vol. 6, pp 575-577.

Ter-Stepanian, G., 1967. Types of depth creep of slopes in rock masses. *Proc., 1st Congress ISRM*, Lisbon, Vol. 2, pp 157-160.

Terzaghi, K., 1950. Mechanics of landslides. *Berkey Volume*, New York. pp 83-124.

Terzaghi, K., 1957. Varieties of submarine slope failures. Reprint in *NGI Publication*, No. 25.

Terzaghi, K. and Peck, R. B., 1948. *Soil Mechanics in Engineering Practice*. Willey, New York.

Thomson, S. and Hayley, D. W., 1975. The Little Smoky Landslide. *Canadian Geotech. Journ.*, Vol. 12, pp 379-392.

Thomson, S. and Tweedie, R. W., 1979. The Edgerton landslide. *Canadian Geotech. Journ.*, Vol. 15, pp 510-521.

Twidale, C. R., 1968. Singing Sands. *Encyclopedia of Geomorphology*, R. W. Fairbridge, Ed., Reionhold, pp 994-995.

Vargas, M. and Pichler, E., 1957. Residual soil and rock slides in Santo, Brazil. *Proc., Int. Conf. Soil Mech. Found. Eng.*, London, Vol. II, pp 394-398.

Varnes, D. J., 1978. Slope movement types and processes. in *Landslides, Analysis and Control*, Schuster, R. L. and Krizek, R. J. Eds., Transportation Res. Board Spec. Report 176, Washington.

Voellmy, A., 1955. Uber die Zerstorungskraft von Lawinen. *Schweiz. Bauzeitung*, Vol. 73, pp 159-165, 212-217,. 246-249, 280-285.

Voight, B., 1978. Lower Gros Ventre Slide, Wyoming. In *Rockslides and Avalanches*, Voight, B., Ed., Elsevier,, Vol. 1, pp 113-166.

Voight, B. and Kennedy, B. A., 1978. Slope failure of 1967-1969 , Chiquicamata Mine, Chile. in *Rockslides and Avalanches*, Voight, B., Ed., Elsevier, Vol. 2, pp 595-632.

Watson, R. A. and Wright, H. E., 1967. The Saidmarreh Landslide, Iran. *Geol. Soc. of Am. Spec. Paper* 123, pp 115-139.

Whitman, R. V., 1957. The behaviour of soils under transient loadings. *Proc., Int. Conf. Soil Mech. Found. Eng.*, London, Vol. 1, pp 207-210.

Whitman, R. V. and Healy, K. A., 1962. Shear strength of sands during rapid loading. *Journ. ASCE, Soil Mech. and Found. Eng. Div.*, Vol. 88, No. SM2. pp 99-132.

Wilkes, P. F., 1972. An induced failure at a trial embankment at King's Lynn, Norfolk, England. In *Performance of Earth and Earth- Supported Structures*, ASCE, Vol. 1, part 1, pp 29-64.

Williams, G. P. and Guy, H. P., 1971. Erosional and depositional aspects of the hurricane Camille in Virginia. *U. S. Geol. Survey Prof. Paper* No. 804, 80 pp.

Wilson, S. D., 1970. Observational data on ground movements related to slope instability. *Journ. ASCE, Soil Mech.. and Found. Eng. Div.*, Vol. 96, No. SM5.

Yano, K. and Daido, A., 1965. Fundamental study on mudflow. *Bull., Disaster Prevention Inst., Kyoto Univ.* Vol. 14, Part 2, pp 69-83.

Yen, B. C., 1969. Stability of slopes undergoing creep deformation. *Journ. ASCE, Soil Mech. and Found. Eng. Div.*, Vol. 95, No. SM4, pp 1075-1096.

Zacas, M., 1977. Creep behaviour of a slope in schistose rocks. In *The Geotechnics of Structurally Complex Formations*, Capri, pp 469-470.

Zaruba, Q. and Mencl, V., 1969. *Landslides and their Control*. Elsevier, Amsterdam, 205 pp.

Zischinski, U., 1966. On the deformation of high slopes. *Proc., 1st Congress ISRM*, Lisbon, Vol. 2, pp 179-185.

15. APPENDIX A, METHOD OF GRAIN SIZE ANALYSIS USED FOR FRANK SLIDE DEBRIS

Since the landslide debris contains grain sizes ranging from silt to boulders several meters in diameter, a special technique of grain size analysis had to be developed. Shreve (1968) used a grid method to sample the debris of Blackhawk slide and found it somewhat biased against fine particles. He was not, furthermore, facing quite as large a range of sizes. The author decided to make use of the "area- by- number" method (Kellerhals and Bray, 1971), combined with conventional sieve analysis of the finer fraction.

The "area- by- number" method accepts a suitably large surface area of the outcrop as a sample. Size categories are defined, and a count is taken of all the particles of each category lying on the surface of the outcrop within the sample area. The percentage count can then be coverted into percentage by volume, when it is multiplied by the geometric mean size of the particular category. According to Kellerhals and Bray (1971) this method yields consistent results when compared to other methods, including grid- by- number and, presumably, the conventional percentage by weight.

The method is exceptionally well suited to the use of photographs. Grain size analysis methods using photography have been utilized in blasting fragmentation studies (e.g. Noren & Porter, 1974).

The sample area had to be relatively large, in view of the large size of some of the fragments. A 4 by 4 m square reference grid frame was taken to the site. This was placed on a well exposed and relatively planar area on the face of the cut and a photograph was taken (Fig. 10.9). Ideally, the area should be photographed from a perpendicular direction. This was not possible in this case, since the camera would have to be stationed 8 to 15 m above ground (see Fig. 10.8). Thus, all the photographs were taken from the base of the cut and include significant perspective distortion. The presence of the reference frame allows this to be taken into consideration. The sides of the frame are marked at 20 cm intervals. Each photograph was covered with a transparent sheet and the 20 cm marks were connected to generate a trapezoidal grid of 400 elementary areas (Fig. A.1a). Each of these areas was then examined with a magnifying glass and two pieces of information were collected from it:

a. A count of all particles larger than 5 cm was taken and placed into categories 5- 10- 20- 40- 80 and 160 cm. The particle size was estimated, in perspective, by comparison to the nearest side of the elementary trapezoid. I.e. particles covering one- quarter to one- half the side would belong to the 5- 10 cm category, one- half to one to the 10- 20 cm category and so on. The shorter axis of the particle projection was considered significant. Large particles overlapping several trapezoids were

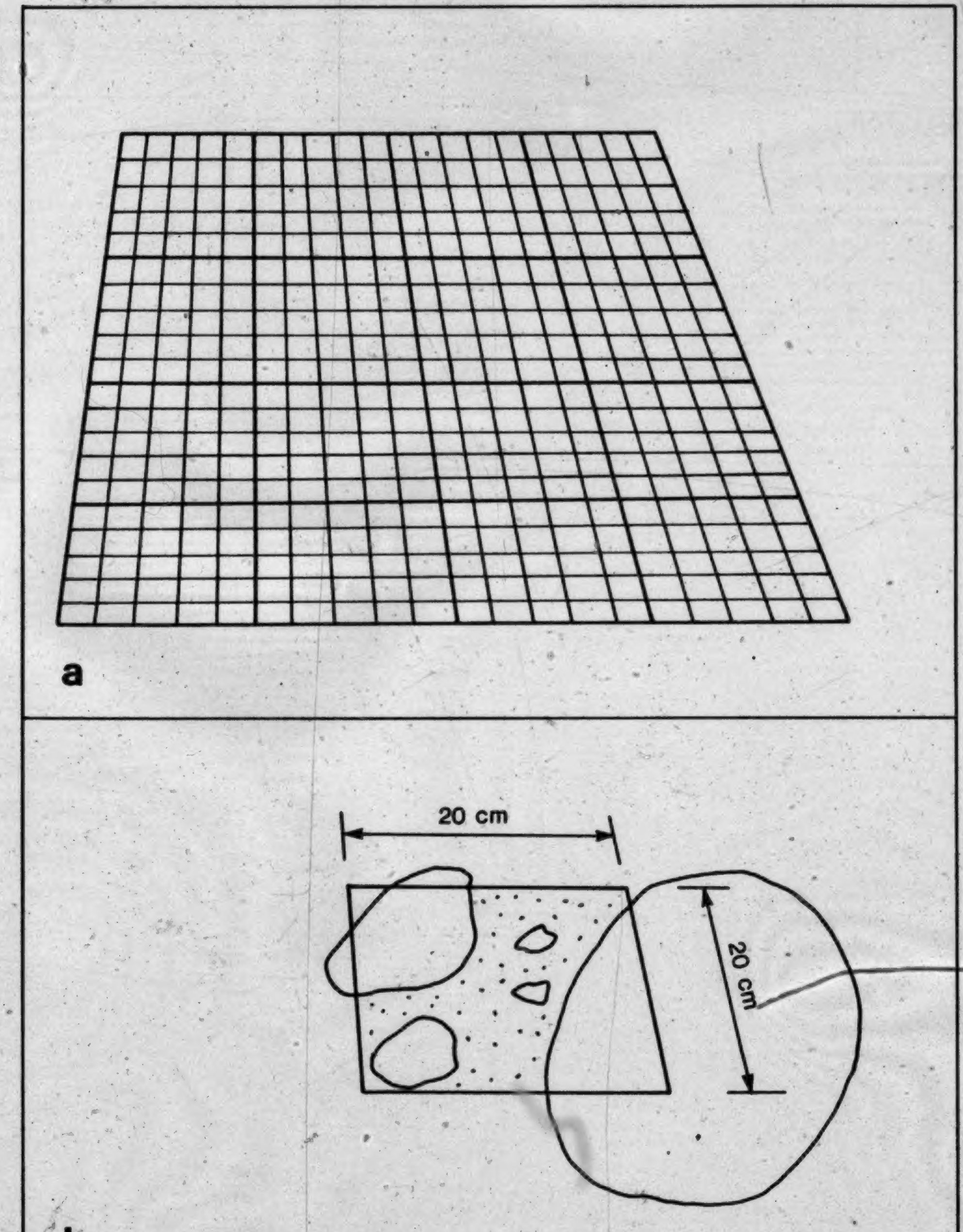
a
b
20 cm
20 cm

Figure B.1 (a) Reference grid in perspective view
(b) sample analysis of a single field

counted only once. Others, projecting outside the sample area, were counted in proportion to the area falling inside. Particles smaller than 5 cm were not counted, but were classified as "matrix".

b. A visual estimate was made of the areal proportion of matrix in each of the elementary trapezoids. For example, the elementary area shown in Fig. A.1b would be analyzed as follows: 1 particle in the 5-10 cm category, 1 in the 10- 20 cm category, 40 percent matrix. The large particle on the right hand side would be counted in the neighbouring area, where its center is located. The two small particles would be included with the matrix.

The average of the matrix percentages over all 400 elementary areas would yield an estimate of the matrix content by volume. This was converted into percentage by weight, when multiplied by the ratio of the bulk unit weight of the matrix to the unit weight of the rock in the large particles (equal to 2.0/2.7). The large particle counts were converted into percentages by weight by the previously described conversion. The curves representing both the coarse (larger than 5 cm) and fine fraction were then joined together to yield the complete grain size curve for each sample, as shown in Fig. 10.10. The curves show relatively constant slope through the point where they are joined, indicating that the two methods of analysis used are mutually compatible.

Sample 10 is not representative of the coarse surface material. A representative sample would require a low- level air photograph. The grain size curve for this sample is therefore only a rough estimate. The distortion of the frame at Sample 7 was not corrected since this was a dangerous location, on a steep angle and surrounded by precariously perched boulders. A correction was made in drawing the grid.

Sample locations were selected so as to include no talus or disturbed material. The material lying in the original position could by easily distinguished, being relatively dense, slightly cemented, completely unsorted on the small scale, standing at a steep angle of some 44 deg.

16. APPENDIX B, FRICTIONAL ENERGY BALANCE OF LANDSLIDE

Potential energy is lost during a landslide. It is partly converted into heat and new surface energy near the sliding plane. another part is radiated in the form of seismic and sound wawes. Some authors have estimated the relative importance of each of these basic energy sinks (e.g. Mathews and McTaggart, 1969). The estimates, supported also by calculations made by this author, indicate that heat accounts for perhaps 95 percent of the energy loss.

But this type of energy partition yields no means of estimating landslide mobility and different divisions are therefore of interest. The simplest use of the energy balance concept can be made in connection with the frictional (Coulomb) model, described at the start of Section 10.3. It is described there that the assumption of all the potential energy being spent in doing work against the *external* frictional forces results in equating the mean travel angle and the dynamic friction angle of the sliding surface.

But energy is lost not only at the base of the sliding mass; also by internal shearing which distorts the mass permanently, and by vibration which causes transient distortion. The following simple two- dimensional model estimates the role of internal shearing:

A mass moves down the slope along a curved sliding surface, while spreading in the longitudinal direction along a series of oblique shear zones (Fig. B.1a). The work done by internal shearing can be estimated separately, with reference to the diagram in Fig. B.1b. In an analogy to the derivation of the rigid block sliding equation (Eqn. 10.5), the following development considers only the horizontal components of both the path and the shear force. This greatly simplifies the mathematics, yet produces an exact result. This is because a projection of both the force and the path to the horizontal does not affect the work formula; the cosine of path inclination cancels out. The moving volume decreases, as material is being left behind, according to the equation:

Eqn. (B.1) $V_m = ab - \frac{hb}{2} - hx$

the dimensions being defined in the diagram. The horizontal component of the shear force on the series of shear planes consumes the energy:

$$W_i = \int_0^{l-b} \gamma f V_m \, dx$$

Eqn. (B.2)

where γ is the mass density and f the average friction coefficient of the shear planes. Assuming that ab=hl in neglect of bulking, the solution of the integral is:

$$W_i = \gamma f \frac{ab}{2} (l-b)$$

Eqn. B.3

The horizontal displacement of the centre of gravity due to the spreading equals (l-b)/2. In addition, the mass displaces horizontally due to the sliding on the basal

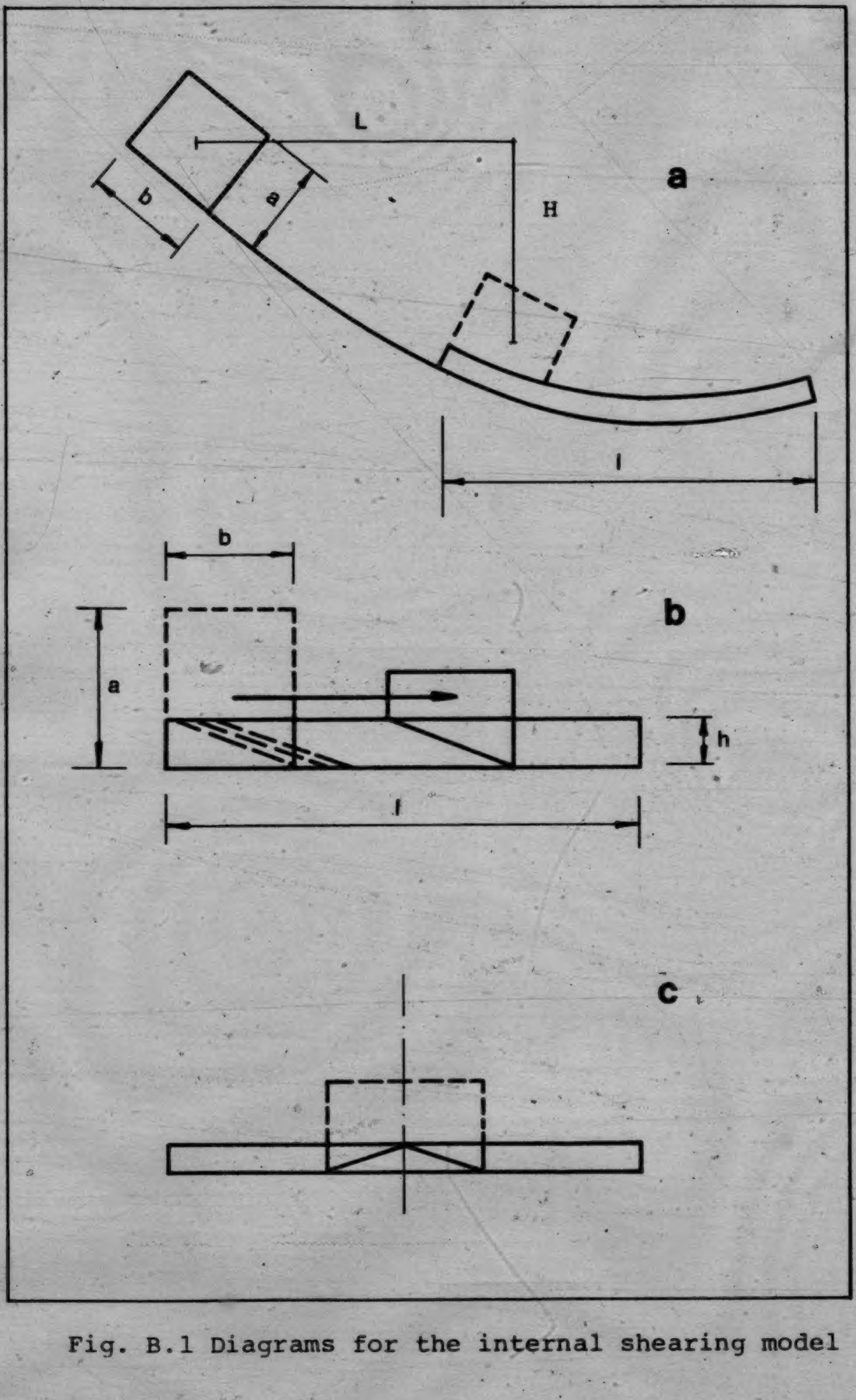
L
a
H
b
a
l
b
b
a
h
l
c

Fig. B.1 Diagrams for the internal shearing model

plane, by the amount L (Fig. B.1a). The work done by this displacement equals:

$$W_e = \gamma f abL$$

Eqn. (B.4)

The potential energy loss is approximately:

$$\Delta E_p = \gamma f abH$$

Eqn. (B.5)

which neglects the potential energy lost in spreading.

Equating the potential energy loss with the two types of frictional work done, one obtains:

$$f = \frac{H}{L+0.5(l-b)}$$

Eqn. (B.6)

This equation represents the ratio of vertical to horizontal displacement of the center of gravity of the mass. The conclusion is, therefore, that the inclusion of longitudinal internal shearing in the energy balance does not change the validity of Heim's model, as represented by Eqn. (10.5).

But the situation is different when internal shearing produces lateral spreading. The internal shearing work is in this case expended in the direction perpendicular to the motion, ands makes no contribution to the displacement of the center of gravity. One could visualize a model similar to Fig. B.1c, where the movement direction is perpendicular to the paper. Eqn. (B.6) still applies in this case, but L is now equal to the total horizontal displacement of the center of gravity. The displacement is seen to be reduced as more spreading occurs, for the same friction angle.

Similar "unproductive" expenditure of energy occurs when the slide mass vibrates normal to the sliding plane. This is, however, difficult to quantify. The indication from seismic observations made during the Hope Slide is that the vibrational energy production amounts to less than 1 percent of the total potential.